RICE UNIVERSITY

Study of Foam Mobility Control in Surfactant Enhanced Oil Recovery Processes in 1-D, Heterogeneous 2-D, and Micro Model Systems

by

Robert F. Li

A THESIS SUBMITTED
IN PARTIAL FULFILLMENT OF THE
REQUIREMENTS FOR THE DEGREE

Doctor of Philosophy

APPROVED, THESIS COMMITTEE

Dr. George J. Hirasaki, Co-Chair,
A. J. Hartsook Professor of Chemical and Biomolecular Engineering

Dr. Clarence A. Miller, Co-Chair,
Louis Calder Professor Emeritus of Chemical and Biomolecular Engineering

Dr. Sibani Lisa Biswal, Assistant Professor of Chemical and Biomolecular Engineering

Dr. Mason B. Tomson, Professor of Civil and Environmental Engineering

HOUSTON, TEXAS
April 2011

Abstract

Study of Foam Mobility Control in Surfactant Enhanced Oil Recovery Processes in 1-D, Heterogeneous 2-D, and Micro Model Systems

by

Robert F. Li

The focus of this thesis was conducting experiments which would help in understanding mechanisms and in design of surfactant enhanced oil recovery (EOR) processes in various scenarios close to reservoir conditions such as heterogeneity, effects of crude oil, wettability, etc.

Foam generated in situ by surfactant alternating gas injection was demonstrated as a substitute for polymer drive in a 1-D EOR process. It was effective in a similar process for a 266 cp crude oil even though the system did not have favorable mobility control.

Foam enhanced sweep efficiency in a layered sandpack with a 19:1 permeability ratio. Foam diverted surfactant from the high- to the low-permeability layer. Ahead of the foam front, liquid in the low-permeability layer crossflowed into the high-permeability layer. Foam completely swept the system in 1.3 TPV (total pore volume) fluid injection while waterflood required 8 TPV.

When the same 2-D system was oil-wet, the recovery by waterflood was only 49.1% of original oil-in-place (OOIP) due to injected water flowing through high-permeability zone leaving low-permeability zone unswept. To improve recovery, an anionic surfactant

blend (NI) was injected that altered the wettability and lowered the interfacial tension (IFT) and consequently enabled gravity and capillary pressure driven vertical counter-current flow to occur and exchange fluids between layers during a 42-day system shut-in. Cumulative recovery after a subsequent foamflood was 94.6% OOIP.

The addition of lauryl betaine to NI at a weight ratio of 2:1 made the new NIB a good IFT-reducing and foaming agent with crude oil present. It showed effectiveness in water-wet homogeneous and oil-wet heterogeneous sandpacks.

The unique attribute of foam with higher apparent viscosity in high- than in low-permeability regions makes it a better mobility control agent than polymer in heterogeneous systems. One single surfactant formulation such as NIB in this study that can simultaneously reduce IFT and generate foam will improve the microscopic displacement and sweep efficiency from the beginning of a chemical flooding process.

Foam generation mechanisms, alkaline/surfactant processes, and foam stability in presence of crude oil were investigated in a glass micro model.

Total acid number measurement with spiking method was discussed.

Acknowledgments

I would like to express my thankfulness to my thesis advisors Dr. George J. Hirasaki and Dr. Clarence A. Miller for their seasoned guidance in my research. Their wisdom, broad knowledge, valuable experience, as well as their insightful advice and scientific attitude towards research have inspired me and helped me grow from a college graduate to a more independent researcher.

I would like to thank Dr. Maura Puerto for her help in constructing the 2-D stainless steel sandpack, and her tips on laboratory experiments. I would like to thank Mr. Leyu Cui and Mr. John Chapman for their contribution in 1-D foam evaluations and in micro model studies. I also express my thankfulness to the rest of the EOR group.

I would like to thank Dr. Sibani Lisa Biswal for providing me with the access to use her laboratory space and equipment including the stereo microscope and the KSV contact angle measurement instrument. Dr. Biswal and Dr. Mason B. Tomson are acknowledged for serving as my thesis committee members.

The financial support from Shell International E&P B.V. is gratefully acknowledged. I appreciate the discussion and helpful ideas from Dr. Shehadeh K. Masalmeh, and Dr. Lingli Wei who taught me reservoir simulation techniques using MoRes. Shell is also acknowledged for the donation of the 2-D stainless steel sandpack and the glass micro model. The financial support of US Department of Energy Grant DE-FC26-03NT15406 and the Rice University Consortium on Processes in Porous Media is gratefully acknowledged.

Table of Contents

List of Figures

List of Tables

Chapter 1

INTRODUCTION

1.1 Enhanced Oil Recovery (EOR)

An oil recovery process from a petroleum reservoir can be divided into three classes: primary, secondary and EOR. Primary recovery refers to the utilization of energy present in the reservoir such as solution-gas drive, gas-cap drive, natural water drive, fluid and rock expansion, and gravity drainage [Green and Willhite, 1998]. From U.S. oil fields, primary recovery typically produces about 10% of the original oil-in-place [NETL-DOE]. Secondary recovery can refer to gas or water injection for pressure maintenance, but nowadays it mostly refers to water flooding, resulting in the recovery of 20-40% [US DOE] of the original oil-in-place. EOR, sometimes a synonym for tertiary recovery, refers to processes beyond primary and secondary recovery. An EOR process usually involves injection of fluids such as steam, CO_2, hydrocarbon gases, surfactant solutions, polymers, microorganisms, nutrients, etc., or the use of thermal energy. Currently, EOR recovers 5-30% of the original oil-in-place [NETL-DOE], and some EOR processes are still in research and development phase whereas others such as steam, CO_2, polymer flooding, etc, are being applied now in some fields. Figure 1-1 illustrates the oil production and the target for EOR in the United States. The target for EOR in the U.S. is 377 billion barrels which accounts for nearly 60% of the 649 billion barrels original oil-in-place.

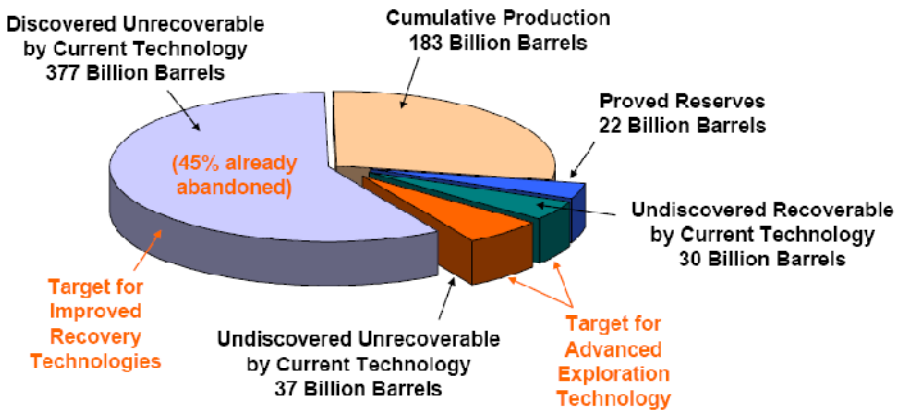

Figure 1-1 Oil production and target for EOR in US. Total 649 billion barrels original oil-in-place [Lake, 2006 (after NETL-DOE, 2005)].

EOR methods can be classified into four categories: chemical recovery, thermal recovery, gas injection recovery, and microbial recovery.

Chemical recovery involves injection of liquid chemicals which lower the interfacial tension (IFT) between injected fluids and oil, or provide effective mobility control. Chemical recovery can be again divided into three subdivisions: polymer flooding, surfactant/polymer flooding and alkaline/surfactant/polymer flooding. Polymer flooding is used as mobility control to augment water flooding sweep efficiency because of its high apparent viscosity and retention in porous media. The retention is a result of adsorption or trapping of macromolecules in pores, which reduces effective permeability. Surfactant/polymer flooding, also known as micellar/polymer (MP) flooding, injects a mixture of liquid chemicals including surfactants, cosurfactants, alcohol, brine and oil, recovering trapped oil in the rock. Surfactant/polymer has so far been proven to be the most efficient, but also the most costly EOR method. In alkaline/surfactant/polymer flooding, in addition to surfactant/polymer flooding mentioned above, the injected alkali reacts with acidic hydrocarbons in crude oil to produce soap -- a natural surfactant to help

reduce interfacial tension, and reduce adsorption of anionic surfactants on sandstones [Liu *et al.,* 2008]. It also helps change the wettability of the rock surface or cause spontaneous emulsification. Alkaline/surfactant/polymer/foam is a combined chemical recovery method which may be less costly than surfactant/polymer flooding [NETL-DOE]. Synthetic surfactants are added in addition to natural soap formed by alkali injection so as to achieve optimal condition of low tension [Nelson *et al.*, 1984]. Polymer and foam act as mobility control agents. Figure 1-2 illustrates the history of chemical recovery projects and production in the United States.

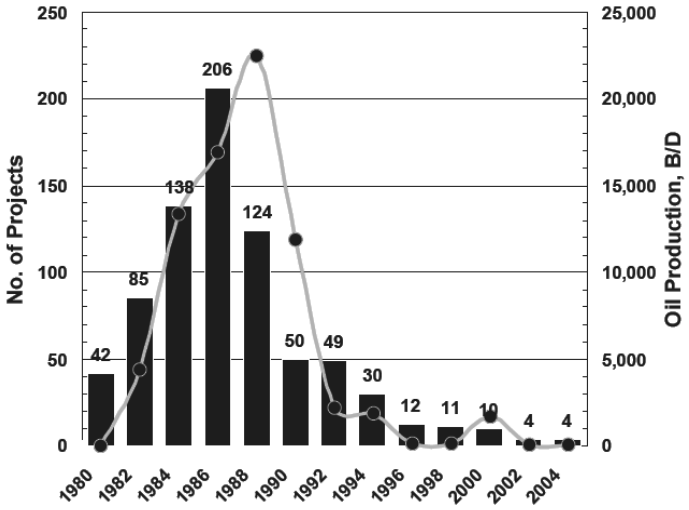

Figure 1-2 Chemical recovery projects and production in the U.S. [Thomas, 2006].

Thermal recovery methods include steam flooding, cyclic steam stimulation, and in-situ combustion. Basically, these methods reduce viscosity of heavy oils by heating them at high temperature.

Miscible recovery includes CO_2 flooding, cyclic CO_2 stimulation, nitrogen flooding, nitrogen-CO_2 flooding, and in some cases, light hydrocarbons as miscible solvents. These methods have a common objective that is to displace oil with a fluid that is multi-contact

miscible with the oil at the conditions existing at the interface between the injected fluid and the oil bank being displaced [Green and Willhite, 1998].

Microbial recovery is operated by injecting microorganisms and nutrients. Upon metabolism, various chemicals are produced by these microorganisms such as surfactants, acids, hydrogen, carbon dioxide, etc. These chemicals then react and recover the oil-in-place in various ways. However, the principal mechanism of this method still remains unknown and success has, at best, been quite limited.

1.2 EOR in an Oil-Wet Layered Heterogeneous System

In a layered reservoir with large permeability contrast that is preferentially oil-wet, the recovery factor is low because injected water sweeps only the high-permeability layer, leaving the low-permeability layer unswept. When capillary communication is allowed between the two layers, water injected into the low-permeability zone will quickly bypass oil there by crossflow into the high-permeability layer [Masalmeh and Wei, 2009].

In order to improve oil recovery in such a reservoir, it is desired to develop a chemical formulation that can alter the wettability from preferentially oil-wet to preferentially water-wet and/or reduce IFT such that the effect of capillarity retaining oil can be overcome and gravity-driven crossflow can exchange liquids between the high- and the low-permeability layers. Spontaneous imbibition occurs when the wettability is altered to preferentially water-wet [Austad *et al.* 1997; Chen *et al.* 2000]. With IFT reduction, especially to ultra-low values, capillarity-induced spontaneous imbibition may be insignificant because capillary pressure may become negligible. However, buoyancy,

independent of wettability, will float oil upward and draw in injected chemicals to replace the oil that has been displaced, and therefore becomes a dominant force [Hirasaki and Zhang, 2004]. If surfactant becomes depleted due to adsorption or dilution by connate water, diffusion may become an important factor [Masalmeh and Oedi, 2009]. The injected chemicals can be introduced into the lower permeability zones not only by spontaneous imbibition, but also by foam that diverts the liquid into the lower permeability layer [Li *et al.*, 2010].

1.3 Foam for Mobility Control in Surfactant EOR

Foam as a means for mobility control of surfactant flooding was introduced 28 years ago by Lawson and Reisberg (1980). This concept was not adopted immediately because of the lack of understanding of the mechanism of mobility control with foam. Since that time, there have been many advances in the understanding of foam mobility control. There have been many field tests of steam foam [Hirasaki, 1989; Patzek, 1996] and CO_2 foam. One of the most successful field demonstrations of foam mobility control was in the Snorre field [Blaker *et al.*, 2002]. Foam was used as mobility control for surfactant aquifer remediation at Hill Air Force Base in Utah [Hirasaki *et al.*, 1997, 2000]. Foam was used as mobility control for alkaline surfactant flooding in China [Zhang *et al*., 2000; Wang *et al.*, 2001].

The most important advance in understanding that has made foam mobility control practical is the understanding of the condition necessary to generate strong foam. There is a critical pressure gradient that must be exceeded to generate strong foam during the flow of surfactant solution and gas through homogeneous porous media [Falls *et al.*, 1988;

Gauglitz *et al.*, 2002; Kam and Rossen, 2003; Rossen, 1996; Rossen and Bruining, 2007; Tanzil, 2002a]. Below this pressure gradient, gas may flow as a continuous phase with only modest mobility reduction. Above this pressure gradient, stationary bubbles are mobilized such that bubble trains have multiple branch points. A flowing bubble divides into two bubbles at each branch point and thus regenerates bubbles that are lost to coalescence. Foam bubbles can also be regenerated (independent of pressure gradient) when gas and surfactant solution flow across a step increase in permeability with a ratio greater than 4 [Falls *et al.*, 1988; Tanzil *et al.*, 2002b]. If one recognizes the critical pressure gradient necessary for strong foam, experiments can be conducted at high enough flow rate or pressure drop such that the critical pressure gradient is exceeded.

The other important advance in understanding is the observation that, when the foam is flowing with conditions where it is regenerated in situ, the gas mobility is determined by a limiting capillary pressure, above which the lamellae become unstable and bubbles coalesce [Khatib *et al.*, 1988]. This understanding explains why, in this regime, the pressure gradient is a function of the liquid-flow rate but is independent of the gas-flow rate. Also, foam mobility can be modeled by fractional-flow theory in this flow regime [Gauglitz *et al.*, 2002; Rossen, 1996]. In this regime, gas mobility increases with increasing gas fractional flow and decreasing permeability. This permeability dependence makes foam especially useful for improving sweep in layered systems [Heller, 1994; Bertin *et al.*, 1999; Kovscek and Bertin, 2002]. The dependence of foam mobility on fracture aperture has been demonstrated to be beneficial in the sweep of fracture systems [Yan *et al.*, 2006]. Foam propagation in layered flow models with permeability contrast has been investigated with and without crossflow [Bertin *et al.*, 1999; Nguyen *et al.*, 2005]

and in foam-induced acid diversion [Gdanski, 1993; Zhou and Rossen, 1994]. In a layered system where capillary communication is allowed and crossflow is present, foam propagates almost simultaneously in both high- and low-permeability layers; whereas, in a system with isolated layers where capillary communication is prohibited, foam forms in the high-permeability layer and diverts more injected liquid and gas down to the low-permeability layer, resulting in a faster advancing foam front in the low-permeability layer.

It is generally recognized that oil tends to destabilize foam. However, the amount of destabilization depends on oil-, surfactant-, and aqueous-phase compositions. To destabilize a foam lamella, an oil drop must first overcome electrostatic or steric interactions in the aqueous pseudoemulsion film, which forms as the drop approaches the gas/water interface [Nikolov *et al.*, 1986; Manlowe and Radke, 1990]. Then, provided that the aqueous phase does not spread at the gas/oil interface so formed, the oil forms a lens that can destabilize the lamella by spreading along the gas/water interface [Lau and O'Brien, 1988], by bridging [Garrett, 1992], or by some combination of the two. It is a common observation during phase behavior of oil/water/surfactant systems that foam is more stable with Winsor I phase behavior and more unstable with Winsor II or III phase behavior.

1.4 Thesis Structure

Chapter 1 is the introduction.

Chapter 2 provides the readers with technical background related to topics discussed in this thesis.

Chapter 3 presents the experimental results of the processes in 1-D homogeneous sandpacks.

Chapter 4 presents the experimental results of the processes in 2-D heterogeneous sandpacks.

Chapter 5 demonstrates the micro model studies with microscopic videos in the accompanying CD.

Chapter 6 discusses total acid number measurements using the spiking method.

Chapter 7 concludes the thesis and gives suggestions on future work.

1.5 References

Austad, T. and Milter, J.: "Spontaneous Imbibition of Water Into Low Permeable Chalk at Different Wettabilities Using Surfactants," paper SPE 37236 presented at the 1997 SPE International Symposium on Oilfield Chemistry, Houston, 18–21 February.

Bertin, H.J., Apaydin, O.G., Castanier, L.M., and Kovscek, A.R. 1999. "Foam Flow in Heterogeneous Porous Media: Effect of Cross Flow," *SPE J.* 4 (2): 75–82. SPE-56009-PA. doi: 10.2118/56009-PA.

Blaker, T., Aarra, M.G., Skauge, A., Rasmussen, L., Celius, H., Martinsen, H.A., and Vassenden, F. 2002. "Foam for Gas Mobility Control in the Snorre Field: The FAWAG Project," *SPE Res Eval & Eng* **5** (4): 317–323. SPE-78824-PA. doi: 10.2118/78824-PA.

Chen, H.L. *et al.*: "Laboratory Monitoring of Surfactant Imbibition Using Computerized Tomography," paper SPE 59006 presented at the 2000 SPE International Petroleum Conference and Exhibition, Villahermosa, Mexico, 1–3 February.

Falls, A.H., Hirasaki, G.J., Patzek, T.W., Gauglitz, P.A., Miller, D.D., and Ratulowski, J. 1988. "Development of a Mechanistic Foam Simulator: The Population Balance and Generation by Snap-Off," *SPE Res Eng* 3 (3): 884–892. SPE-14961-PA. doi: 10.2118/14961-PA.

Garrett, P.R. ed. 1992. *Defoaming: Theory and Industrial Applications*, Vol. 45. Boca Raton, Florida: Surfactant Science Series, CRC Press.

Gauglitz, P.A., Friedmann, F., Kam, S.I., and Rossen, W.R. 2002. "Foam generation in homogeneous porous media," *Chemical Engineering Science* 57 (19): 4037–4052. doi: 10.1016/S0009-2509(02)00340-8.

Gdanski, R.D. 1993. "Experience and Research Show Best Designs for Foam-Diverted Acidizing," *Oil & Gas Journal* 91 (36): 85-89.

Green, D.W., and Willhite, G.P., Enhanced Oil Recovery, SPE textbook seires vol.6, pp.166, 1998

Heller, J.P. 1994. CO2 Foam in Enhanced Oil Recovery. In *Foams: Fundamentals and Applications in the Petroleum Industry*, ed. L.L. Schramm, No. 242, 201–234. Washington, DC: Advances in Chemistry Series, American Chemical Society.

Hirasaki, G.J. 1989. "The Steam-Foam Process," *J Pet Technol* 41 (5): 449–456. SPE-19505-PA. doi: 10.2118/19505-PA.

Hirasaki, G.J., Jackson, R.E., Jin, M., Lawson, J.B., Londergan, J., Meinardus, H., Miller, C.A. *et al*. 2000. "Field Demonstration of the Surfactant/Foam Process for Remediation of a Heterogeneous Aquifer Contaminated with DNAPL," In *NAPL Removal: Surfactants,*

Foams, and Microemulsions, ed. S. Fiorenza, C.A. Miller, C.L. Oubre, and C.H. Ward, Part 1, 3–163. AATDF monograph series, Boca Raton, Florida, USA: Lewis Publishers, CRC Press.

Hirasaki, G.J., Miller, C.A., Szafranski, R., Tanzil, D., Lawson, J.B., Meinardus, H., Jin, M., Londergan, J.T., Jackson, R.E., Pope, G.A., and Wade, W.H. 1997. "Field Demonstration of the Surfactant/Foam Process for Aquifer Remediation," SPE 39292 prepared for presentation at the SPE Annual Technical Conference and Exhibition, San Antonio, Texas, USA, 5–8 October. doi: 10.2118/39292-MS.

Hirasaki, G.J., Zhang D.L.: "Surface Chemistry of Oil Recovery From Fractured, Oil-Wet, Carbonate Formations," *SPEJ*., (June 2004) SPE 88365-PA

Kam, S.I. and Rossen, W.R. 2003. "A Model for Foam Generation in Homogeneous Porous Media," *SPE J.* 8 (4): 417–425. SPE-87334-PA. doi: 10.2118/87334-PA.

Khatib, Z.I., Hirasaki, G.J., and Falls, A.H. 1988. "Effects of Capillary Pressure on Coalescence and Phase Mobilities in Foams Flowing Through Porous Media," *SPE Res Eng* 3 (3): 919–926. SPE-15442-PA. doi: 10.2118/15442-PA.

Kovscek, A.R. and Bertin, H.J. 2002. "Estimation of Foam Mobility in Heterogeneous Porous Media," Paper SPE 75181 presented at the SPE/DOE Improved Oil Recovery Symposium, Tulsa, 13–17 April. doi: 10.2118/75181-MS.

Lake L., speaker presentations, 15th SPE/DOE Improved Oil Recovery Symposium, Tulsa, OK, April, 2006, data after NETL-DOE, 2005

Lau, H.C. and O'Brien, S.M. 1988. "Effects of Spreading and Non-spreading Oils on Foam Propagation through Porous Media," *SPE Res Eng* 3 (3): 893–896. SPE-15668-PA. doi: 10.2118/15668-PA.

Lawson, J.B. and Reisberg, J. 1980. "Alternate Slugs of Gas and Dilute Surfactant for Mobility Control During Chemical Flooding," Paper SPE 8839 presented at the SPE/DOE Enhanced Oil Recovery Symposium, Tulsa, 20–23 April. doi: 10.2118/8839-MS.

Li, R.F., Yan, W., Liu, S., Hirasaki, G.J., and Miller, C.A.: "Foam Mobility Control for Surfactant Enhanced Oil Recovery," *SPE J*. (December 2010) SPE-113910-PA.

Liu, S., Zhang, D.L., Yan, W., Puerto, M., Hirasaki, G.J., and Miller, C.A. 2008. "Favorable Attributes of Alkali-Surfactant-Polymer Flooding," *SPE J.* 13 (1): 5–16. SPE-99744-PA. doi: 10.2118/99744-PA.

Manlowe, D.J., and Radke, C.J. 1990. "A Pore-Level Investigation of Foam/Oil Interactions in Porous Media," *SPE Res Eng* 5 (4): 495–502. SPE-18069-PA. doi: 10.2118/18069-PA.

Masalmeh, S.K., Oedai, S., "Surfactant Enhanced Gravity Drainage: Laboratory Experiments and Numerical Simulation Model," SCA2009-06, presented at the International Symposium of the Society of Core Analysts, September, 2009.

Masalmeh, S.K., Wei, L.: "EOR Option for a Heterogeneous Carbonate Reservoirs with Complex Waterflood Performance," 15th European Symposium on Improved Oil Recovery, April 2009.

Nelson, R.C., Lawson, J.B., Thigpen, D.R., and Stegemeier, G.L., "Cosurfactant-enhanced alkaline flooding," SPE/DOE preprint 12672, presented at 4th symposium on EOR, Tulsa, OK, April, 1984

NETL-DOE: Natianal Energy Technology Laboratory: http://www.netl.doe.gov.

Nguyen, Q.P., Currie, P.K., and Zitha, P.L.J. 2005. "Effect of Capillary Cross-Flow on Foam-Induced Diversion in Layered Formations," *SPE J.* 10 (1): 54–65. SPE-82270-PA. doi: 10.2118/82270-PA.

Nikolov, A.D., Wasan, D.T., Huang, D.W., and Edwards, D.A. 1986. "The Effect of Oil on Foam Stability: Mechanisms and Implications for Oil Displacement by Foam in Porous Media," Paper SPE 15443 presented at the SPE Annual Technical Conference and Exhibition, New Orleans, 5–8 October. doi: 10.2118/15443-MS.

Patzek, T.W. 1996. "Field Applications of Steam Foam for Mobility Improvement and Profile Control," *SPE Res Eng* 11 (2): 79–86. SPE-29612-PA. doi: 10.2118/29612-PA.

Rossen, W.R. 1996. Foams in Enhanced Oil Recovery. In *Foams: Theory, Measurements and Applications*, ed. R.K. Prud'Homme and S. Khan, 413–464. New York: Marcel Dekker.

Rossen, W.R. and Bruining, J. 2007. "Foam Displacements With Multiple Steady States," *SPE J.* 12 (1): 5–18. SPE-89397-PA. doi: 10.2118/89397-PA.

Tanzil, D., Hirasaki, G.J., and Miller, C.A. 2002a. "Conditions for Foam Generation in Homogeneous Porous Media," Paper SPE 75176 presented at the SPE/DOE Improved Oil Recovery Symposium, Tulsa, 13–17 April. doi: 10.2118/75176-MS.

Tanzil, D., Hirasaki, G.J., and Miller, C.A. 2002b. "Mobility of Foam in Heterogeneous Media: Flow Parallel and Perpendicular to Stratification," *SPE J.* 7 (2): 203–212. SPE-78601-PA. doi: 10.2118/78601-PA.

Thomas, S. "Chemical EOR: The Past - Does It Have a Future?," This presentation was an SPE Distinguished Lecture during 2005-2006 doc number: 108828-DL, 2006

US DOE: http://www.fossil.energy.gov/programs/oilgas/eor/index.html

Wang, D., Cheng, J., Yang, Z., Li, Q., Wu, W., and Yu, H. 2001. "Successful Field Test of the First Ultra-Low Interfacial Tension Foam Flood," Paper SPE 72147 presented at the SPE Asia Pacific Improved Oil Recovery Conference, Kuala Lumpur, 6–9 October. doi: 10.2118/72147-MS.

Yan, W., Miller, C.A., and Hirasaki, G.J. 2006. "Foam Sweep in Fractures for Enhanced Oil Recovery," *Colloids and Surfaces A: Physicochem. Eng. Aspects* 282–283: 348–359. doi: 10.1016/j.colsurfa.2006.02.067.

Zapata, V.J. and Lake, L.W. 1981. "A Theoretical Analysis of Viscous Crossflow," Paper SPE 10111 presented at the SPE Annual Technical Conference and Exhibition, San Antonio, Texas, USA, 5–7 October. doi: 10.2118/10111-MS.

Zhang, Y., Yue, X., Dong, J., and Liu, Y. 2000. "New and Effective Foam Flooding To Recover Oil in Heterogeneous Reservoir," Paper SPE 59367 presented at the SPE/DOE Improved Oil Recovery Symposium, Tulsa, 3–5 April. doi: 10.2118/59367-MS.

Zhou, Z.H. and Rossen, W.R. 1994. "Applying Fractional-Flow Theory to Foams for Diversion in Matrix Acidization," *SPE Prod & Fac* 9 (1): 29–35; *Trans.,* AIME, 297. SPE-24660-PA. doi: 10.2118/24660-PA.

Chapter 2

TECHNICAL BACKGROUND

2.1 Recovery Efficiency of an Enhanced Oil Recovery (EOR) Process

The overall recovery efficiency of any oil recovery including EOR process can be expressed as follows:

$$E = \frac{Oil\ Recovered\ by\ the\ Process}{Oil\ Present\ before\ the\ Process} \quad \text{Equation 2-1}$$

The total recovery is a product of microscopic displacement efficiency and macroscopic

$$E = E_D E_V \quad \text{Equation 2-2}$$

E_D is the microscopic displacement efficiency that measures the effectiveness of the displacing fluid in mobilizing the oil at the local pore level where the displacing fluid contacts the oil, *i.e.*

$$E_D = \frac{S_{oi} - S_{or}}{S_{oi}} \quad \text{Equation 2-3}$$

where S_{oi} is the initial oil saturation, and S_{or} is the residual oil saturation. E_v is the sweep efficiency that measures the effectiveness of the displacing fluids sweeping out the reservoir in a volumetric sense. It is also called volumetric displacement efficiency.

The EOR processes in this thesis are surfactant EOR processes which are alkaline/surfactant/polymer (ASP), alkaline/surfactant/polymer/foam (ASPF), and alkaline/surfactant/foam (ASF) processes. Alkali and surfactants were used to cause spontaneous emulsification, to lower interfacial tension and/or viscosity, etc., so as to improve E_D. Polymer or foam was used for mobility control in order to improve the volumetric sweep efficiency E_v.

2.2 Surfactant

"Surfactants" or "surface active agents" are a type of substance that is active or highly enriched at the surface or interface between phases [Miller and Neogi, 1985]. A surfactant molecule is usually comprised of two moieties: a hydrophilic head and a hydrophobic tail. Owning to their amphiphilic nature, surfactant molecules tend to accumulate and form a monolayer at surfaces or interfaces (Figure 2-1.) with the hydrophilic moiety residing in the polar medium (water) and the hydrophobic hydrocarbon chain residing in the non-polar medium (oil or air). This energetically favorable orientation of surfactant molecules with each moiety staying in the environment with which it has the greatest affinity can reduce the interfacial tension between two phases.

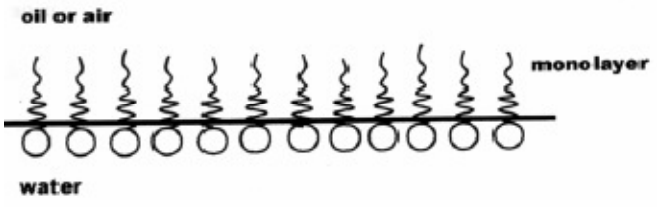

Figure 2-1 Surfactant monolayer at the interface.

Surfactants are classified into four categories with respect to the hydrophilic (polar) moiety of the molecule. They are: anionic, cationic, non-ionic, and zwitterionic (amphoteric) as shown in Table 2-1.

Table 2-1 Classification of surfactants [Akstinat, 1981]

Class	Examples	Structures
Anionic: negatively charged head group	Sulfonates Sulfates Carboxylates Phosphates	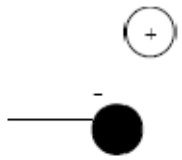
Cationic: positively charged head group	Quanternary ammonium organics, amines, pyridinum, imidazolinium, piperidinium, sulfonium compounds	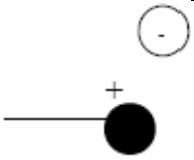
Non-ionic: molecule does not ionize	Alkyl-, Alkyl- aryl-, acyl-, acylamindo-, acyl- aminepolyglycol polyol ethers Alkanolamides	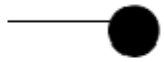
Zwitterionic: with two or more of the other classes	Aminocarboxylic acids, Betaine surfactants	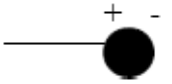

At low concentrations in aqueous solution, surfactants act not much differently than dispersed monomers. But at high concentrations, instead of being dissolved as individual molecules, a number of surfactant molecules form an organized aggregate called a micelle. In this structure, the hydrophobic chains associate in the interior of the aggregate and the hydrophilic head groups face the polar aqueous media, so that both moieties avoid energetically unfavorable contact (Figure 2-2).

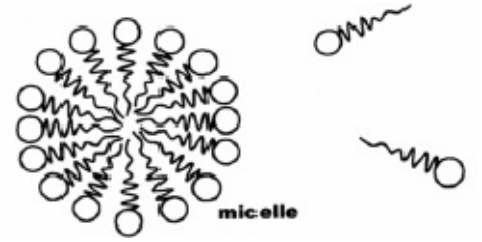

Figure 2-2 Surfactant molecules form a micelle above CMC.

The critical concentration of the surfactant to form significant micelles is called the critical micelle concentration (CMC). Some typical values of CMC at room temperature are listed in the table below:

Table 2-2 Typical values of CMC at room temperature [Schramm, 2005]

Surfactant Class	Non-ionics	Anionics	Zwitterionics
CMC (mol/L)	10^{-5}-10^{-4}	10^{-3}-10^{-2}	10^{-3}-10^{-1}

CMC is important in that below CMC, interfacial tension decreases markedly with increasing surfactant concentration but hardly changes above CMC, where the increase in surfactant concentration will only result in further micelles [Miller and Neogi, 1985] rather than significantly reduce the interfacial tension. However, above CMC, since the hydrophobic chains associated in the interior of the micelles behave much as liquid hydrocarbon, each micelle is able to solubilize more non-polar molecules such as oil, which greatly increases the apparent solubility of such substances [Schramm, 2005].

Surfactant as a foaming agent stabilizes thin liquid films in gas. In addition, certain types of surfactant adsorbed at the interface can also increase the interfacial viscosity, which stabilizes the foam as well. Foam is more stable above CMC. Ionic surfactants are better foaming agents because the electrostatic repulsion between the two sides of the foam lamella makes it more stable [Rosen, 2000]. Also, in general, foam stability increases with longer alkyl chain in the hydrophobic moiety and decreases with branching because close-packed alkyl chains not only stabilize foam but also increase the surface viscosity [Schramm, 2005].

2.3 Fundamentals of Flow in Porous Media

2.3.1 Viscous Forces and Darcy's Law

Viscous forces and capillary pressure are the two most important physical phenomena in flow through porous media. This combination makes reservoir engineering different from most other engineering subjects. Viscous forces in a porous medium are reflected in the magnitude of the pressure drop that occurs as a result of flow of a fluid through the medium. It can be expressed by Darcy's law. In 1855 and 1856, Henri d'Arcy developed a flow experiment through vertical sand column, which is known today as Darcy's law.

Darcy's law for a single-phase flow with low Reynolds number in a homogeneous porous medium can be described as

$$\vec{u} = -\frac{k}{\mu}(\nabla p - \rho \vec{g}) \qquad \text{Equation 2-4}$$

In the above equation, $\vec{u}$ is the superficial velocity and is also called Darcy velocity. It is the ratio of volumetric flow rate to the cross sectional area of the porous medium: $\vec{u} = \frac{\vec{q}}{A}$.

The superficial velocity $\vec{u}$ is related to $\vec{v}$, the average velocity of the fluid in the pores by $\vec{u} = \vec{v}\phi$. ϕ is porosity which is the fraction of void pore space in a porous medium. In Equation 2-4 k is permeability; it is a property of the porous medium. μ is viscosity; it is a property of the fluid. The ratio $\lambda = k/\mu$ is defined as the fluid mobility in porous medium.

Darcy's law for a multiphase flow can be described as

$$\vec{u}_j = -\lambda_j \left(\nabla p_j - \rho_j \vec{g}\right) \qquad \text{Equation 2-5}$$

In the above equation, the mobility of phase *j* is defined by

$$\lambda_j = \frac{k \cdot k_{rj}(S_j)}{\mu_j} \qquad \text{Equation 2-6}$$

where k_{rj} is the relative permeability which is a function of fluid saturation S_j.

2.3.2 Interfacial Tension and Capillary Pressure

Capillarity is another important physical phenomenon besides Darcy's law in flow through porous media. Most EOR processes involve immiscible fluids. The co-existence of immiscible phases at the pore level results in curvature at the interface between any two phases. There is a tension between any two phases due to the dissimilarity of the intermolecular forces between the molecules comprising the phases. These molecular interactions create a force that tends to contract the interface to a smaller area, which creates a tension that is dependent only on the presence of the interface. Interfacial tension (when both phases are liquid, such as crude oil and brine), expressed as energy per unit area or force per unit length is used to describe such a force. When one of the phases is gas or vapor, it is called surface tension.

Each immiscible phase has an individual pressure that is distinctive from other phases because of the curvature at the interface. The pressure difference between two phases is called capillary pressure. In reservoir engineering, it is usually expressed as a function of saturation of one phase.

The IFT and capillary pressure can be related by Young-Laplace equation:

$$\Delta p = 2H\sigma \qquad \text{Equation 2-7}$$

where Δp is the pressure difference across the interface; H is the mean curvature; and σ is the interfacial or surface tension.

2.3.3 Wettability

Fluid distributions in porous media are affected not only by the forces at fluid/fluid interfaces, but also by forces at fluid/solid interfaces. Wettability is the tendency of one fluid to spread on or adhere to a solid surface in the presence of a second fluid [Green and Willhite, 1998]. When two immiscible phases are placed in contact with a solid surface, one phase usually is attracted to the solid more strongly than the other phase. The more strongly attracted phase is called the wetting phase. Wettability can be categorized as water-wet, intermediate-wet, and oil-wet by contact angle measurement. According to Morrow (1990) when $0°<\theta<75°$ a surface is preferentially water-wet, when $75°<\theta<115°$ it is intermediate-wet, and when $115°<\theta<180°$ it is preferentially oil-wet, where θ is the water-advancing contact angle.

When a wetting-phase is displaced by a non-wetting phase, the trapped wetting phase usually coats the solid rock surfaces or resides in smaller pore spaces such as in pore throats, and the trapped wetting phase in these regions is usually continuous as an inter-connected thin layer. When a non-wetting phase is displaced by a wetting phase, at the residual condition, it usually resides in larger pore spaces such as in pore bodies, and the trapped non-wetting phase usually takes form of disconnected drops that are held by strong capillary forces which cannot be overcome by the relatively small viscous forces.

2.3.4 Capillary Number

The competition between viscous forces and capillary forces casts a direct influence on residual phase saturation. The capillary number, a dimensionless group is then defined to relate these two forces. It is also called viscous to capillary ratio.

$$N_{vc} = \frac{u\mu}{\sigma} \qquad \text{Equation 2-8}$$

where u is the superficial velocity, μ is the fluid viscosity, σ is the interfacial tension or surface tension. When the driving force is gravity, *i.e*. buoyancy, the dimensionless group becomes the Bond number:

$$N_B = \frac{\Delta\rho L^2 g}{\sigma} \qquad \text{Equation 2-9}$$

where $\Delta\rho$ is the density deference between the drop and surrounding phase, L is the characteristic length, g the gravitational acceleration constant.

Figure 2-3 is a capillary desaturation curve. It correlates capillary number and residual oil saturation in sandstone cores.

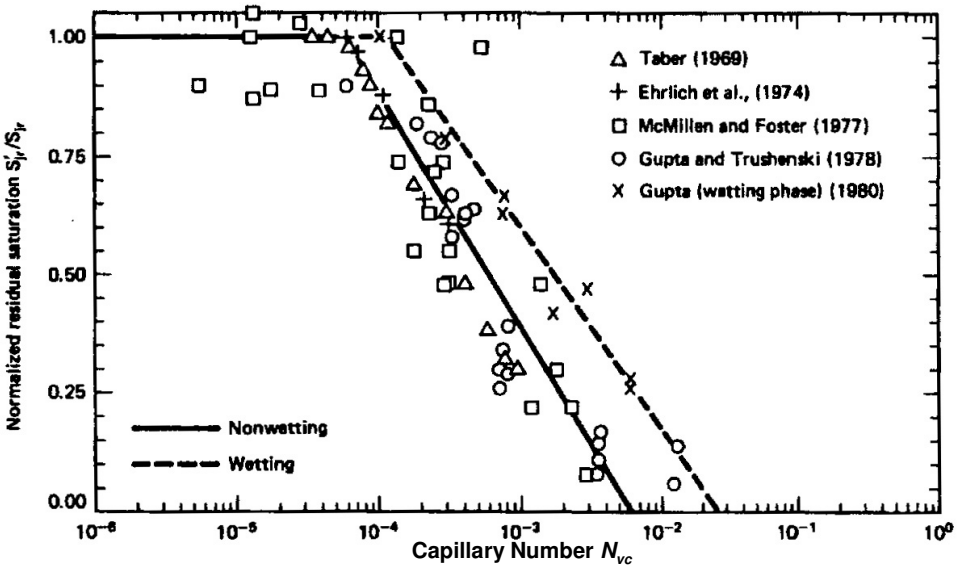

Figure 2-3 Capillary desaturation curves [Lake, 1989 (Camilleri, 1983)].

The capillary number needs to be greater than 10^{-3} to reach near zero residual oil saturation. While it appears to be hard to increase injection pressure gradient by several orders of magnitude, it is, however, possible to reduce IFT by several orders of magnitude. This is where surfactant EOR plays an important role. Surfactants can reduce the oil/water IFT from typically 20-30 mN/m to ultra low value of 10^{-3} mN/m.

2.4 Foam Flow in Porous Media

Foam in porous media is defined as "a dispersion of gas in liquid such that the liquid phase is continuous (*i.e.* connected) and at least some part of the gas phase is made discontinuous by thin liquid films called lamellae [Hirasaki, 1989]." Gas phase is flowing in the continuous phase, but it can be either flowing or trapped in the discontinuous phase (Figure 2-4).

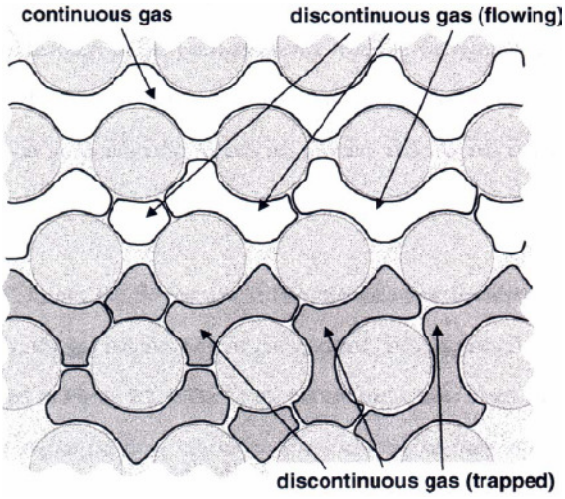

Figure 2-4 Pore level schematic of foam flow in porous media [Radke and Gillis, 1990].

Foam is useful in EOR as a mobility control agent because its resistance to flow is usually significantly higher than that of either phase that makes up the foam. The reduced

mobility ($\lambda = k / \mu$) comes from: 1) reduction of gas relative permeability, 2) rise in apparent viscosity.

As shown in Figure 2-4, some pore space is occupied by trapped gas, which blocks the gas pathway and reduces the effective gas permeability. Increased viscosity is not only a result from viscous shear stresses in thin films between the pore walls and the gas liquid interface, but also a result of forces required to push lamellae through constricted pore throats [Falls *et al.*, 1989]. It is notable that either trapped or moving gas bubbles exist only in a time-averaged sense. As flow path changes, gas bubbles can switch between moving and blocking as a result of the liquid lamellae mobilization. Furthermore, increased pressure gradient will mobilize trapped gas bubbles and will hence open new flow channels. Foam, therefore, is non-Newtonian and shear thinning [Hirasaki and Lawson, 1985; Falls *et al.*, 1989].

When gas phase is continuous, foam is weak because it does not significantly reduce the mobility. In contrast, gas bubbles in strong foam encounter much more resistance and flow in a so-called "bubble train" as shown in the center Figure 2-4. Strong foam has much higher apparent viscosity than weak foam as shown in the experimental sections of this thesis.

Among factors that govern the process of foam trapping and mobilization (*e.g.* pressure gradient, geometry of the flow system, foam texture, bubble-train length, and gas velocity), foam texture (lamella density or bubble size) is the most important parameter to determine gas mobility in the porous medium. There exists a critical pressure gradient [Rossen, 1988] $\nabla p^{\min}$ above which strong foam can be formed. There is also a minimum pressure gradient to mobilize a discontinuous bubble-train. In this case

∇p^{min} is determined by lamella density: the higher the density, the larger the ∇p^{min} required [Alvarez, 1998].

2.4.1 Mechanisms for Foam Generation

Three mechanisms account for foam generation: snap-off (Figure 2-5), lamella division (Figure 2-6), and leave-behind (Figure 2-7). Snap-off and lamella division create strong foam while leave-behind mechanism only leads to weak foam.

Snap-off is a mechanical process. It occurs during multiphase flow in porous media regardless of the presence of surfactant. As a gas finger passes through the pore throat into the pore body which is initially filled with liquid, the leading surface expands. The reduced curvature on the leading surface will then build a pressure gradient forcing liquid to flow from the pore body towards the pore throat. As liquid accumulates in the pore throat, it finally pinches off a small gas bubble from the initial one and creates a new lamella.

Capillary pressure plays an important role for a snap-off to take place. First of all, the capillary pressure must be equal or greater than the capillary entry pressure P_c^e for

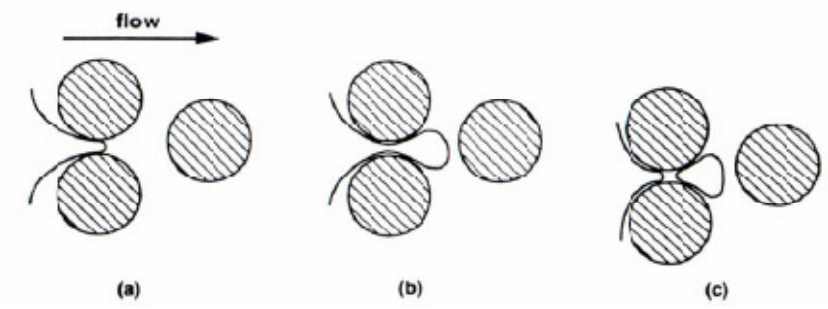

Figure 2-5 Schematic of capillary snap-off mechanism showing (a) gas enters liquid filled pore throat (b) leading surface expands (c) accumulated liquid snaps off a small gas bubble from the original one. [Kovscek and Radke, 1994].

gas to enter the pore throat. Then, it must drop below a critical value of $P_c^{sn} \approx\sim 0.5 P_c^e$ for snap-off to occur [Falls *et al.*, 1988]. Snap-off also depends on pore geometry, liquid saturation, and heterogeneity. When gas flows from a low permeability zone into a high permeability zone with a permeability contrast at least 4:1, snap-off will occur due to reduced capillary pressure [Tanzil, 2002].

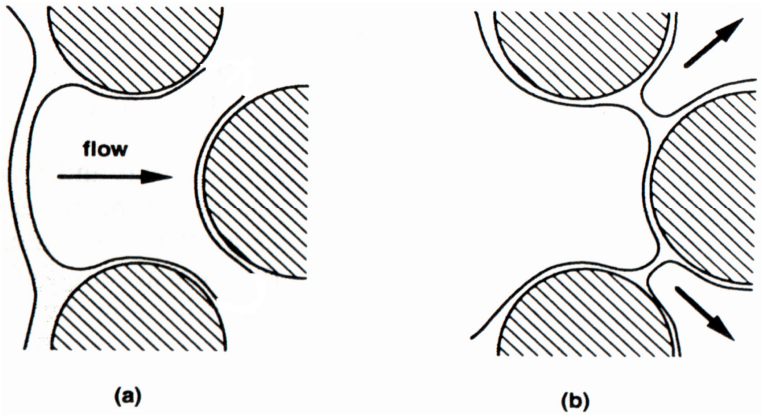

Figure 2-6 Schematic of lamella division mechanism. (a) Flow encounters branching point (b) A lamella flows into both directions and splits into two [Kovscek and Radke, 1994].

When a mobilized liquid lamella encounters a branch, it may flow in both directions and the original lamella will split into two lamellae as shown in Figure 2-6. The created lamellae are perpendicular to the flow directions. Therefore, they will increase the number of flowing lamellae and raise the flow resistance. So lamella division also generates strong foam. For lamella division to take place, the pressure gradient must exceed a certain value such that the lamellae are mobilized. Also, the moving gas bubble must be larger than the pore throat; otherwise the bubble would flow through either throat without splitting the liquid lamella.

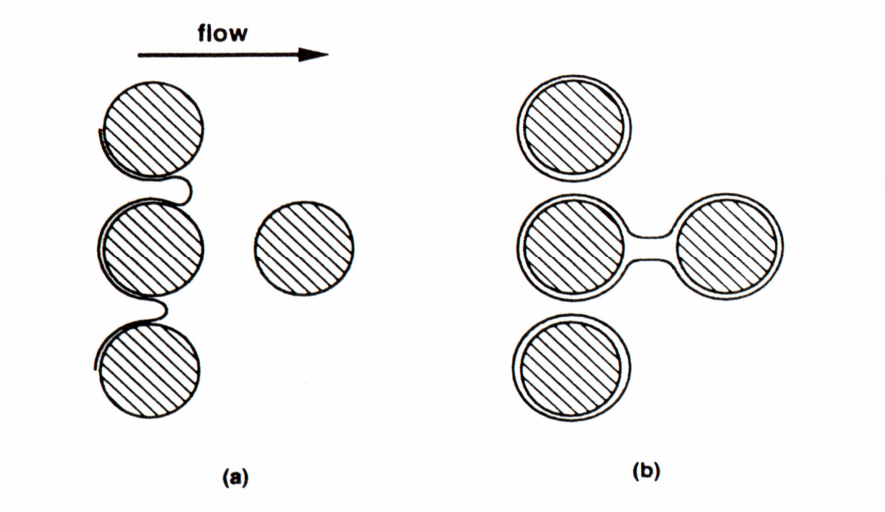

Figure 2-7 Schematic of leave-behind mechanism. (a) Two gas fingers enter adjacent pore throats. (b) A lens is left behind [Kovscek and Radke, 1994].

As two gas fingers enter adjacent pore throats and converge downstream at low capillary pressure (high liquid saturation) and low pressure gradient, a lamella is then left behind. This left-behind lamella is parallel to the flow direction as shown in Figure 2-7, which does not result in much resistance. Leave-behind mechanism only forms weak foam.

2.4.2 Mechanisms for Foam Destruction

Lamella destruction has an important role in controlling gas mobility. Liquid lamellae can be destroyed in two ways: capillary suction coalescence and gas diffusion, of which the former is more important with respect to foam in porous media.

Liquid film between two gas bubbles undergoes a thinning process, which will eventually cause the foam to rupture. Gravity always tends to force liquid to flow down through well-connected network of liquid films. In bulk foam, as liquid film is being drained, the shape of a gas bubble will be more close to a polyhedron rather than a perfect

sphere, and the liquid lamella in between is relatively planar. As shown in Figure 2-8, at the borders, the gas liquid interface is quite curved, generating low pressure. The interface along the flat lamella is quite flat, so higher pressure resides there. This pressure gradient forces flow towards the borders causing film thinning. Besides pressure gradient as a driving force of film thinning, van der Waals attractive forces also cause film thinning.

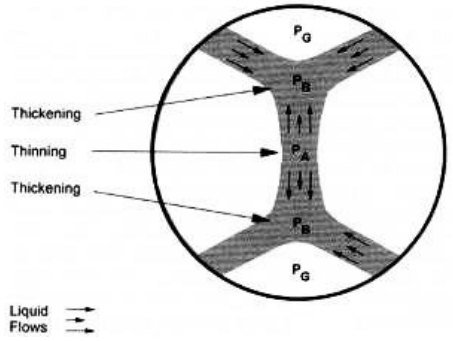

Figure 2-8 Pressure gradient as a driving force during film thinning [Schramm, 2005].

However, some other factors counteract the film thinning process. These include surface elasticity, surface viscosity, steric interactions, and repulsive force of electric double layer. Surface elasticity is a resistant property which contributes to lamellae stabilization. As a liquid film expands, the thinning process tends to rupture the film, but the increased surface area results in locally lower surfactant concentration, *i.e.*, higher surface tension. This surface tension gradient will draw more liquid from neighboring area, which tends to thicken the liquid film. Surface viscosity is greatly increased by suitable surfactants, which hampers the film drainage rate. The repulsive force is of most importance. When ionic surfactant molecules are adsorbed on both sides of the gas liquid interfaces of a lamella, an electric double layer will form. As two interfaces of a lamella approach each other, repulsive force will increase and resist thinning. In order to describe

liquid film stability, the film disjoining pressure Π is introduced as a function of film thickness h. The condition for foam rupture is given by [Scheludko, 1967]:

$$\frac{dP_c}{dh} + \frac{d\Pi}{dh} = 0 \qquad \text{Equation 2-10}$$

In a porous medium, the capillary pressure increases as liquid saturation reduces, and film thickness decreases accordingly. As shown in Figure 2-9, when the film thickness reduces to a critical value h_{cr} and continues to decrease, the capillary pressure will exceed the maximum stable disjoining pressure Π_{max} and the static film ruptures.

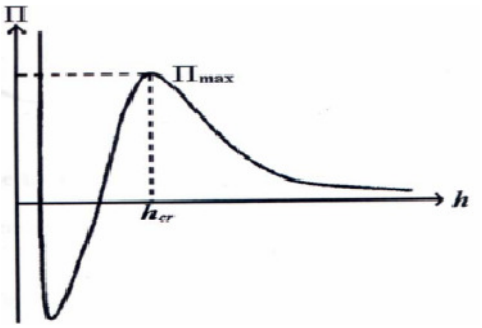

Figure 2-9 Disjoining pressure curve governs the stability of a thin film

In the case of a moving lamella, its thickness oscillates due to the geometry of the porous media. As shown in Figure 2-10, a moving lamella undergoes stretching or squeezing. When it is being stretched, if the film thickness falls below h_{cr}, the lamella will break.

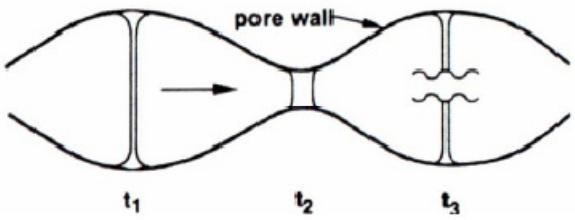

Figure 2-10 A moving lamella undergoes stretching or squeezing with different pore size [Kovscek and Radke, 1994]

The driving force for gas diffusion across a curved lamella is the gradient of chemical potential caused by the pressure difference across the lamella. It directs the mass transfer from the concave side to the convex side through a liquid film. Besides pressure difference, the curvatures are also affected by pore structures and flow properties, etc. It is important to distinguish between gas diffusion by mass transfer and by phase transfer. The latter is a result of gas condensation (as in the steam foam) and liquid film evaporation. In general, the consequence of gas diffusion is that large bubbles grow while small bubbles shrink and disappear. This phenomenon is not as important for foam in porous media as for bulk foam, with the exception of steam foam. Because of the pore structure, coarsening can be halted when a lamella reaches a stable position as in a pore throat.

2.4.3 Foam Stability in Presence of Crude Oil

It is well-known that crude oils often destabilize foam and widely believed that light crude oils are more effective defoaming agents. The mechanisms have been extensively investigated [Garrett, 1993; Aveyard, 1994; Zhang *et al*., 2003; Schramm, 2005]. Garrett summarized three coefficients, namely entry coefficient E, spreading coefficient S, and bridging coefficient B, that are important in interpreting the mechanisms of oil destabilizing foam. These coefficients are defined as follows:

$$E = \gamma_{AW} + \gamma_{OW} - \gamma_{AO} \qquad \text{Equation 2-11}$$

$$S = \gamma_{AW} - \gamma_{OW} - \gamma_{AO} \qquad \text{Equation 2-12}$$

$$\mathrm{B} = \gamma_{AW}^2 + \gamma_{OW}^2 - \gamma_{AO}^2 \qquad \text{Equation 2-13}$$

where, γ_{AW}, γ_{OW}, γ_{AO} stand for air/water, oil/water, and air/oil interfacial tensions. To break a foam lamella, an oil drop must enter the air/water surface, *i.e.* $E>0$. In order to enter the air/water surface, the oil drops must first overcome the repulsive forces caused by the pseudoemulsion films separating these drops from the air/water interface [Nikolov *et al.*, 1986; Manlowe and Radke, 1990; Basheva, *et al*., 2000]. Once an oil drop enters, it may spread at the air/water interface *i.e.* $S\geq 0$, leading to foam lamella rupture. When $S\leq 0$ an oil drop forms a lens on one side of the air/water interface and may reach the other side as the foam film thins, thus forming a bridge. If $B>0$, the bridge is unstable and the film breaks. By understanding these mechanisms, surfactants that can stabilize foam in presence of oil – foam 'boosters' – can be designed.

2.5 References

Alvarez, J.M. "Foam Flow Behavior in Porous Media: Effects of Flow Regime and Porous Medium Heterogeneity," Ph.D. dissertation, The University of Texas at Austin, 1998.

Akstinat, M.H. "Surfactants for EOR Process in High-Salinity Systems: Product Selection and Evaluation," in Enhanced Oil Recovery, F.J. Fayers (ed.), Elsevier: New York, 1981.

Aveyard, R., Binks, B.P., Fletcher, P.D.I., Peck, T.G., Rutherford, C.E., *Advanced Colloid Interface Science, 48* (1994) 93.

Basheva, E.S., Ganchev, D., Denov, N.D., Kasuga, K., Satoh, N., Tsujii, K. 2000. "Role of Betaine as Foam Booster in the Presence of Silicone Oil Drops," *Langmuir, Vol. 16*, 1000-1013.

Camilleri, D., "Micellar/Polymer Flooding Experiments and Comparison with an Improved 1-D Simulator," M.S. thesis, The University of Texas at Austin, 1983.

Falls, A.H., Hirasaki, G.J., Patzek, T.W., Gauglitz, D.A., Miller, D.D., and Ratulowski, T. "Development of a Mechanistic Foam simulator: The Population Balance and Generation by Snap-off," SPE Reservoir Engineering, August 1988, 884-892.

Falls, A.H., Musters, J.J., and Ratulowski, J. "The Apparent Viscosity of Foams in Homogeneous Bead Packs," SPE Reservoir Engineering, May 1989, 155-164.

Garrett, P.R., "The Mode of Action of Antifoams," in *Defoaming: Theory and Industrial Applications*, edited by P.R. Garrett, Marcel Dekker, New York, 1993, p. 14.

Green, D.W., and Willhite, G.P., *Enhanced Oil Recovery*, SPE textbook seires vol.6, pp.166, 1998

Hirasaki, G.J. and Lawson, J.B. "Mechanisms of Foam Flow in Porous Media: Apparent Viscosity in Smooth Capillaries," SPE J., April 1985, 176-190.

Hirasaki, G.J. "The Steam-foam Process," JPT, May 1989, 449-456. The full-length article is available as paper SPE 19518, 1989.

Kovscek, A.R. and Radke, C.J. "Fundamentals of Foam Transport in Porous Media," in Foams: Fundamentals and Applications in the Petroleum Industry, L.L. Schramm (ed.), American Chemical Society, Washington, DC, 1994.

Lake, L. W., *Enhanced Oil Recovery*, Prentice-Hall, Englewood Cliffs, NJ, 1989.

Miller, C.A. and Neogi, P. Interfacial Phenomena: Equilibrium and Dynamic Effects, Marcel Dekker: New York, 1985.

Morrow, N.R.: "Wattability and Its Effect on Oil Recovery," JPT, (December 1990) 1476-1484.

Nikolov, A.D., Wasan, D.T., Huang, D.W., Edwards, D.A. 1986. "The Effect of Oil on Foam Stability: Mechanisms and Implications for Oil Displacement by Foam in Porous Media," SPE 15443 presented at the SPE ATCE, 5-8 October, New Orleans, Louisiana.

Radke, C.J. and Gillis, J.V. "A Dual Tracer Technique for Determining Trapped Gas Saturation during Steady Foam Flow in Porous Media," paper SPE 20519, 1990.

Rosen, M.J. and Dahanayake, M. Industrial Utilization of Surfactants, AOCS Press: Champaignm Illinois, 2000.

Rossen, W.R. "Theories of Foam Moblilization Pressure Gradient," SPE 17358, Soc. Petr. Eng./DOE Symp. on Enhanced Oil Recovery, Tulsa, 1988

Scheludko, A. "Thin Liquid Films," Advance. Coll. Interface Sci., 1, 391-432, 1967.

Schramm, L.L. Emulsions, Foams, and Suspensions: Fundamentals and Applications, Wiley-VCH: Weinheim, 2005.

Tanzil, D., Hirasaki, G.J., and Miller, C.A. "Conditions for Foam Generation in Homogeneous Porous Media," paper SPE 75176, 2002.

Zhang, H., Miller, C.A., Garrett, P.R., Raney, K.H., *Journal of Colloid and Interface Science, 263* (2003) 633-644.

Chapter 3

PROCESSES IN 1-D HOMOGENEOUS SANDPACKS

In this chapter, foaming surfactants were first evaluated with and without the presence of crude oil in 1-D homogenous silica sandpacks. Next, foam stability as well as tertiary oil recovery with alkaline/surfactant/polymer/foam (ASPF) and alkaline/surfactant/foam (ASF) processes will be discussed.

3.1 Experimental

3.1.1 Materials

The following surfactants or their blends were used: Neodol 67-7PO (ammonium C16-17 7PO sulfate, Stepan); IOS 15-18 (sodium 15-18 internal olefin sulfonate, Shell); AOS 16-18 (sodium 16-18 alpha olefin sulfonate, Stepan); N25-7EO glycidyl sulfonate (Shell); N67-9EO glycidyl sulfonate (Enordet A092, Shell); Avanel surfactants S150, S70, and S74 (BASF); Triton X-200 (C9-ph, 3EO, sulfonate, Dow); Dowfax 8390 (Dow); lauryl betaine (Rhodia). NI is a blend of 4:1 (wt/wt) Neodol 67-7PO and IOS 15-18. NIB is a blend of 4:1:10 (wt/wt/wt) Neodol 67-7PO, IOS 15-18 and lauryl betaine unless otherwise stated. IB is a blend of IOS 15-18 and lauryl betaine. CTAB (hexadecyltrimethylammonium bromide, Matheson Coleman & Bell) was used for wettability alteration.

Three crude oils were used: SMY: Deepwater Gulf of Mexico [15 cp at 25°C, total acid number (TAN)=0.34 mg KOH/g]; Crude B: moderately viscous oil (266 cp at 25°C, TAN=4.8 mg KOH/g); SME (3.93 cp at 25°C, TAN=0.062 mgKOH/g).

Three silica sands from U.S. Silica Company were used in the flow experiments: Oil Frac 20/40 (100-200 darcy); F-42 (40 darcy); F-110 (4.8 darcy). Crushed limestone between sieve No. 20 and 40 (N20/40) from Nolanville TX was used.

Na_2CO_3 (anhydrous, certified American Chemical Society) and NaCl (biological certified) were both obtained from Fisher Scientific. SME brine had a composition of total dissolved solids 187,200 mg/L; sodium 49,933 mg/L; calcium 14,501 mg/L; magnesium 3,248 mg/L; chloride 111,810 mg/L; sulfate 234 mg/L; and no bicarbonate. Flopaam 3330S (SNF Floerger) is a partially hydrolyzed polyacrylamide, $Mw \approx 8 \times 10^6$.

3.1.2 Equipment

The 1D system was a 1-ft-long glass column with 1-in. inner diameter packed with sand. All columns were dry packed unless otherwise stated, and were tightly packed by continuously tapping the glass wall during packing to induce mixing and settling. Each end was sealed by a rubber stopper, and a metal screen was put between the rubber and the sand.

Porosity was measured using the following procedure. The sand column was first flushed with CO_2 under mild pressure (~2.5 psig) for 30 minutes to purge trapped air in the pores. The column was then filled and flushed with approximately five pore volumes (PV) of distilled water to make sure water dissolved CO_2 and occupied all the pore space. The pore volume equals the total volume of water in the sandpack. The total volume of

the porous medium equals the product of the distance between two ends times the cross-sectional area. Then the porosity ϕ is given by

$$\phi = \frac{V_{H_2O}}{\frac{\pi D^2}{4} L} \qquad \text{Equation 3-1}$$

where *D* is the inner diameter of the glass column and *L* is the distance between two ends of the sand, which is the distance between the two rubber stoppers. The measured porosity was 0.39 for Oil Frac 20/40, and 0.37 for F-110. Theoretically, porosity of randomly packed spherical sand grains with equal diameter is 0.40. The measured porosity is lower than theoretical value because of grain size distribution.

Permeability *k* was calculated from single-phase Darcy's law

$$\vec{u} = -\frac{k}{\mu}(\nabla p - \rho \vec{g}) \qquad \text{Equation 3-2}$$

where *u, μ, ρ* are the superficial velocity, viscosity, and density of injected brine. *k* values can be obtained by measuring water flow rate and pressure gradient across the sandpack. In a horizontal experiment, the gravity term is neglected, and Equation 3-2 is reduced to

$$u = \frac{k}{\mu} \cdot \frac{\Delta p}{L} \qquad \text{Equation 3-3}$$

where *Δp* is the pressure difference and *L* is the distance between inlet and outlet. I further assume the outlet pressure to be atmospheric pressure. A high-pressure liquid chromatography (HPLC) pump (ISCO Model 2350) and a syringe pump (Harvard Apparatus) were used for fluid injection. Pressure was measured and recorded by a pressure transducer (Validyne, Northridge) connected to a computer. Figure 3-1 is a schematic of the experimental setup.

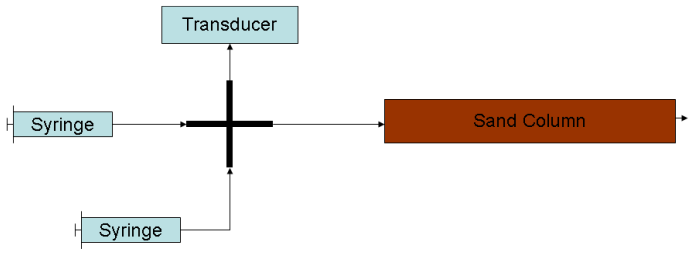

Figure 3-1 Experimental setup in 1-D sand columns.

The ASPF experiments were conducted with vertical, upward flow direction, unless otherwise stated. For constant-rate injection, liquid was injected by an HPLC pump and gas (air) was injected by a syringe pump specified at a certain volumetric flow rate. For constant-pressure injection, liquid and gas were injected manually by monitoring the pressure so that it was maintained within ±10% of the specified value. Liquid and gas rates reported for constant-pressure injection were averaged values of slug volume divided by injection time. All experiments were conducted at ambient room temperature.

A foam generator was made of a 1-in. I.D. x 1.5-in. long stainless steel chamber with a porous ceramic plate, a frit, inside.

3.2 Results and Discussion

3.2.1 Evaluation of Foaming Surfactants in Oil-Free 1-D Homogeneous Sandpacks

During foam flow in a homogeneous sandpack, there is a critical pressure gradient above which strong foam can be generated. This critical pressure gradient exists in both surfactant solution and gas co-injection scheme [Rossen and Gauglitz, 1990], and surfactant alternating gas injection (SAG) scheme [Szafranski, 1997]. This critical pressure gradient is a criterion for strong foam generation and needs to be determined experimentally with different surfactant formulations, sandpacks, cores, or permeability.

Unless otherwise stated, the surfactant formulation used in this section was comprised of 0.2% (w/w, active) AOS 16-18 in 2% NaCl and 1% Na_2CO_3.

Critical pressure gradient was found in surfactant/air co-injection and alternating injection schemes. In co-injection scheme, surfactant solution and air were co-injected into the 88.8 darcy sand column initially filled with brine at constant rate with a liquid to gas ratio of 1:1 (or f_g=1/2). *fg* stands for gas fraction. Figure 3-2 shows the pressure history during co-injection scheme. In Figure 3-2, a first rapid increase in pressure drop was observed at 0.5 PV with all curves. Then a second rapid increase in pressure drop was observed after 1 PV except for 10 ft/D. The critical pressure gradient was found to be $\nabla p^* = 1.1 psi/ft$. ∇p^* was chosen according to the second sudden increase in pressure drop after 1 PV except for 10 ft/D. This is because, with less than 0.5 PV fluid injected, foam had not yet formed throughout the entire sand column that was initially saturated with brine. ∇p might not be uniform in this case. Rossen and Gauglitz found this critical pressure gradient is inversely proportional to the permeability [Rossen and Gauglitz, 1990]. Tanzil further defined a dimensionless pressure gradient $N_{\nabla p} = \frac{\Delta p}{\sigma L}\frac{k}{\phi}$, [Tanzil, 2002a]. In my experiments shown in Figure 3-2, σ=30 mN/m, L=30 cm, ϕ=0.4. With Δp=1.1 psi chosen slightly higher than the inflection point in Figure 3-2, $N_{\nabla p}$ was found to be $N_{\nabla p}$ ~1.84×10^{-4}. At steady state after strong foam was formed, at 1 ft/D, Δp=1.7 psi, $N_{\nabla p}$ was found to be $N_{\nabla p}$ ~2.85×10^{-4}. This was close, at least in the same order of magnitude, to Gauglitz and Rossen's finding of $N_{\nabla p} \sim 2.6\times10^{-4}$. $N_{\nabla p} \sim 2.95\times10^{-4}$ or ∇p^*=1.7 psi/ft is an upper bound of the critical pressure gradient in the range of injection

velocities studied, since we do not know how much lower the injection velocity needs to be to reach a situation where strong foam does not form. Blue curve in Figure 3-5 of foam apparent viscosity was calculated by the steady state pressure from Figure 3-2. These large values of viscosity also indicate that strong foam was formed in the range of injection velocities studied.

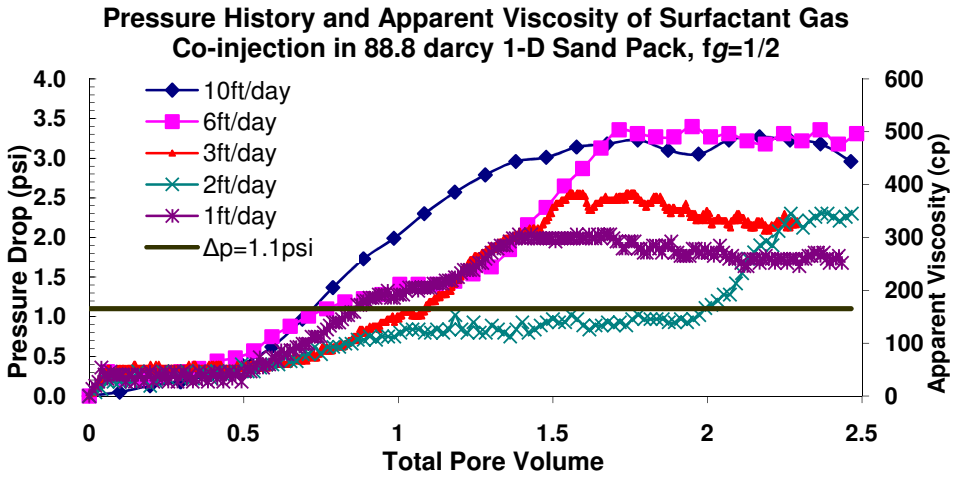

Figure 3-2 Pressure history during surfactant air co-injection: $\nabla p^* = 1.1 psi / ft$.

In SAG scheme, surfactant and gas slugs were injected into the sandpack one after another with a liquid slug size of 0.1 PV (pore volume) and f_g=2/3. Figure 3-3 shows the pressure history of injection of surfactant solution and air into a sand column which was initially filled with brine. Figure 3-4 shows the pressure history of injection of surfactant and air into a sand column in which foam was already developed. The critical pressure gradient was again chosen at the inflection point of the pressure curves in Figure 3-3 where the second derivative was zero. The critical pressure gradient was found to be ∇p^* 1.0 psi/ft. In Figure 3-3, strong foam formed at fewer PV's with higher injection velocity. In the case of 20 ft/D injection, a rapid increase in pressure drop took place as early as 1

PV. This was in accordance with previous findings in my group [Szafranski, 1997]. However, due to the fluctuation in pressure drop during gas and liquid injection, ∇p^* was chosen in a conservative way to ensure strong foam formation for all injection velocities studied. Again, this appears to be an upper bound, assuming only strong foam was formed.

These ∇p^* values with different injection scheme are close to each other. It is the minimum pressure gradient used in later experiments to generate strong foam.

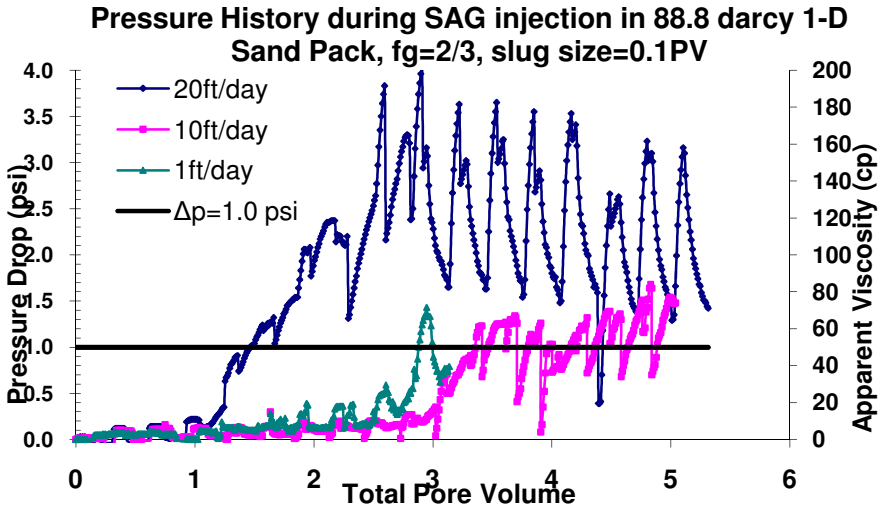

Figure 3-3 Pressure history during SAG injection: $\nabla p^* = 1.0 psi / ft$.

Various surfactants or their blends were evaluated in terms of the ability to generate strong foam by comparing foam apparent viscosities. These surfactants were: AOS 16-18; IOS 15-18; BASF Avanel S150, S74, S70; Triton X-200; DowFax 8390; N67-9EO-GS, N25-3EO-GS. If foam was treated as a single-phase, its apparent viscosity was calculated from single-phase Darcy's law $\mu_{app} = -\frac{k}{uL}(P - P_{static})$, where k was the measured permeability of the sanpack; u was the superficial injection velocity; L was the length of the sandpack; and (P-P_{static}) was the pressure difference across the sandpack. Foam was

generated using SAG injection with *fg*=2/3 and liquid slug size of 0.1 PV. All experiments were performed in horizontal clean silica sandpacks. Figures 3-5 to 3-12 show foam apparent viscosity at different injection rates. The apparent viscosity during liquid injection appeared to be higher than that during gas injection. Injecting liquid made the system wetter (decreased foam quality) corresponding to higher liquid flow rate than that of gas. In the high-quality regime [Osterloh and Jante, 1992] given fixed total injection rate, pressure gradient and hence apparent viscosity became higher as a result of decreased foam quality. Triton X-200, AOS16-18, IOS15-18, N25-7EO-GS, N67-9EO-GS were found to be good foaming agents at low salinity (1% Na_2CO_3, 2~3.5% NaCl). N25-7EO-GS was a good foaming agent in SME brine. BASF Avanel surfactants, NI [Yan, 2006], DowFax8390 were not good foaming agents. Triton X-200 may contain liquid crystalline structures. Its molecular structure is $C_9H_{19}(C_6H_4)$ $(EO)_3SO_3Na$. The hydrophobic tail has a benzene ring and an alkyl chain. Because of supramolecular interactions, benzene rings tend to stack on top of each other to share the π orbits known as π- π stacking. Subsequently, the alkyl chains are oriented in a way such that they stay together. Both π- π stacking and the alkyl chain orientation are entropically favorable, leading to an ordered structure of Triton X-200 surfactant's molecule. Therefore, crystals may form. Figure 3-13 is a microscopic picture of 28% active Triton X-200 under cross-polarized light. Color agglomerates indicate crystalline structures.

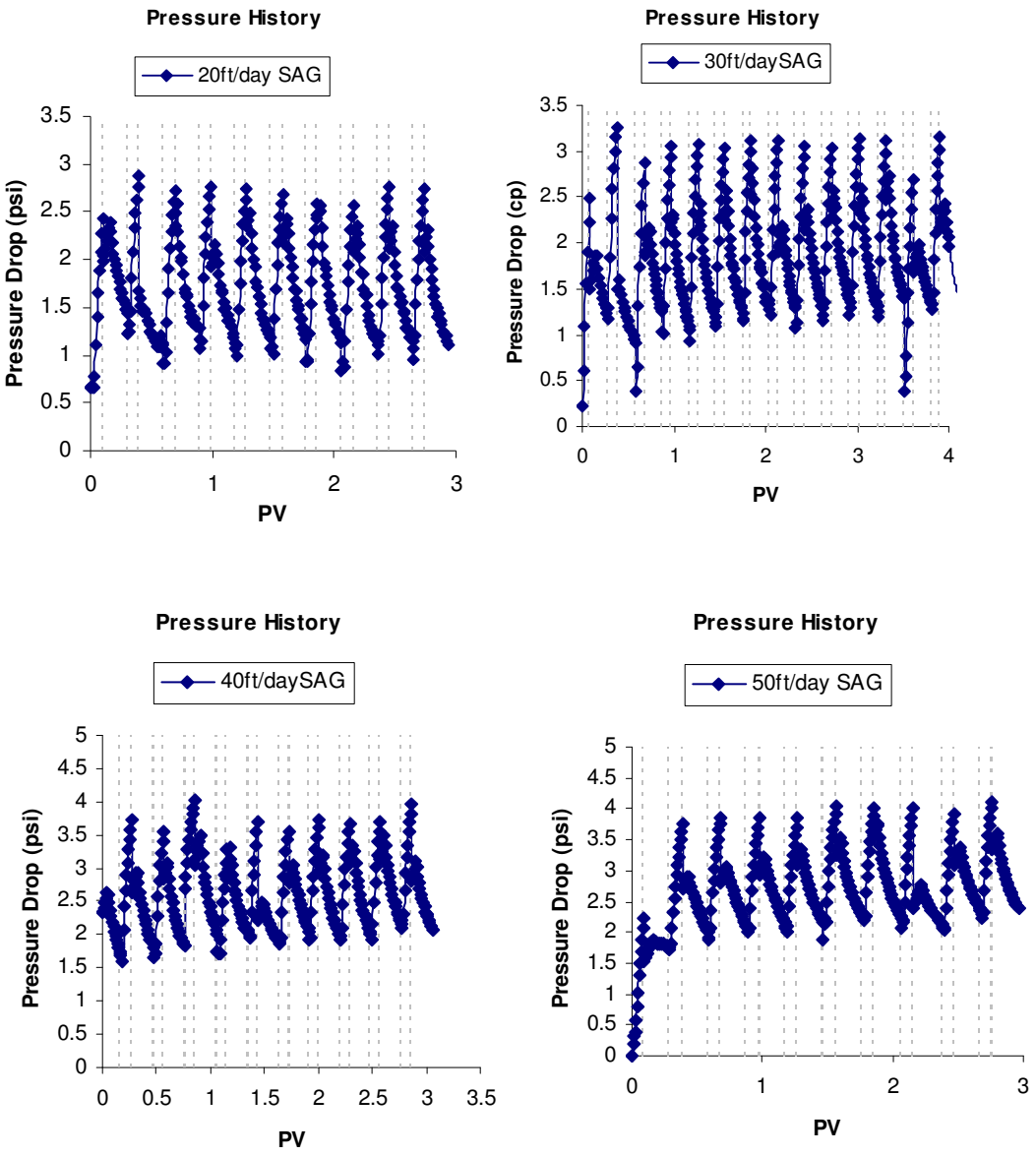

Figure 3-4 Pressure history during SAG injection after strong foam was generated in 88.8 darcy 1-D sand column, f_g=2/3.

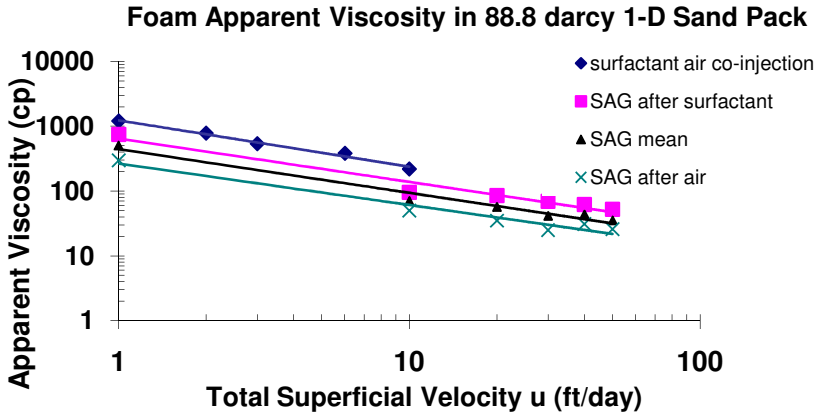

Figure 3-5 Foam apparent viscosity with AOS 16-18.

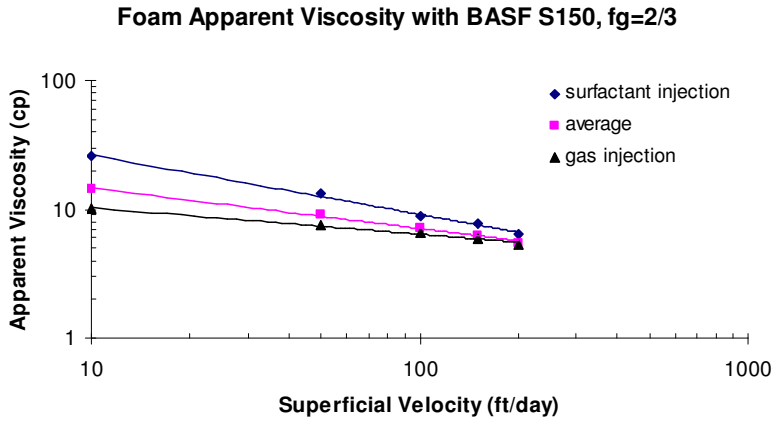

Figure 3-6 Foam apparent viscosity with BASF Avanel S150.

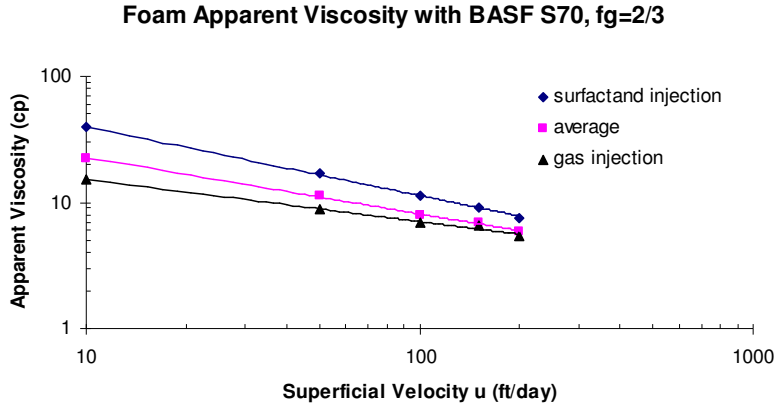

Figure 3-7 Foam apparent viscosity with BASF Avanel S70.

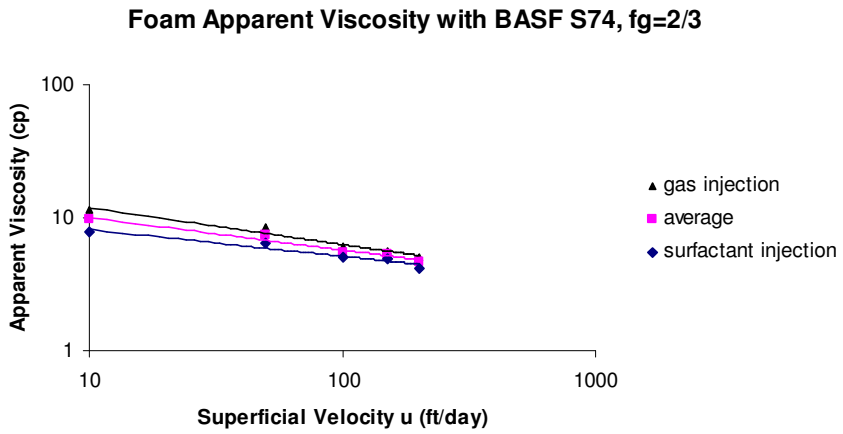

Figure 3-8 Foam apparent viscosity with BASF Avanel S74.

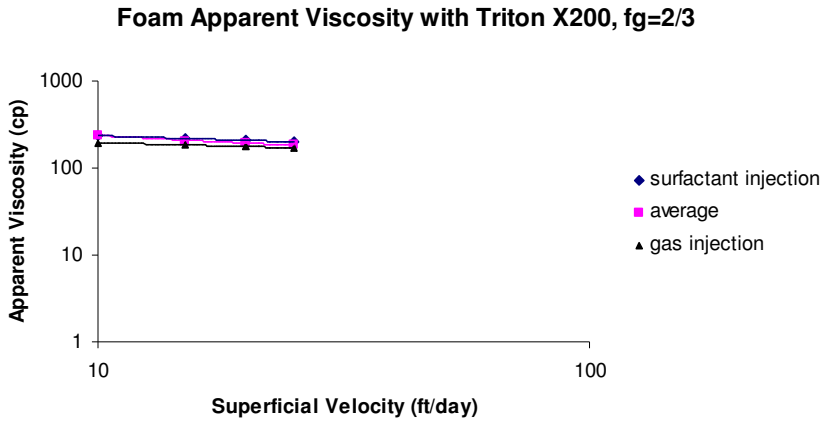

Figure 3-9 Foam apparent viscosity with Triton X-200.

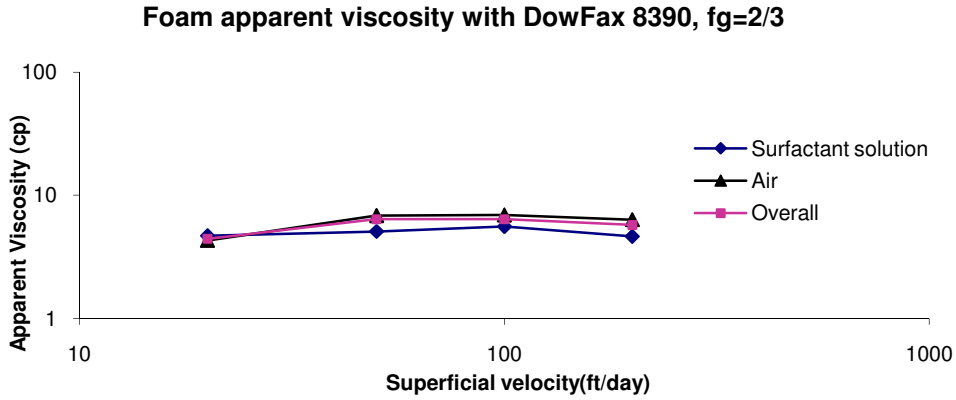

Figure 3-10 Foam apparent viscosity with DowFax 8390

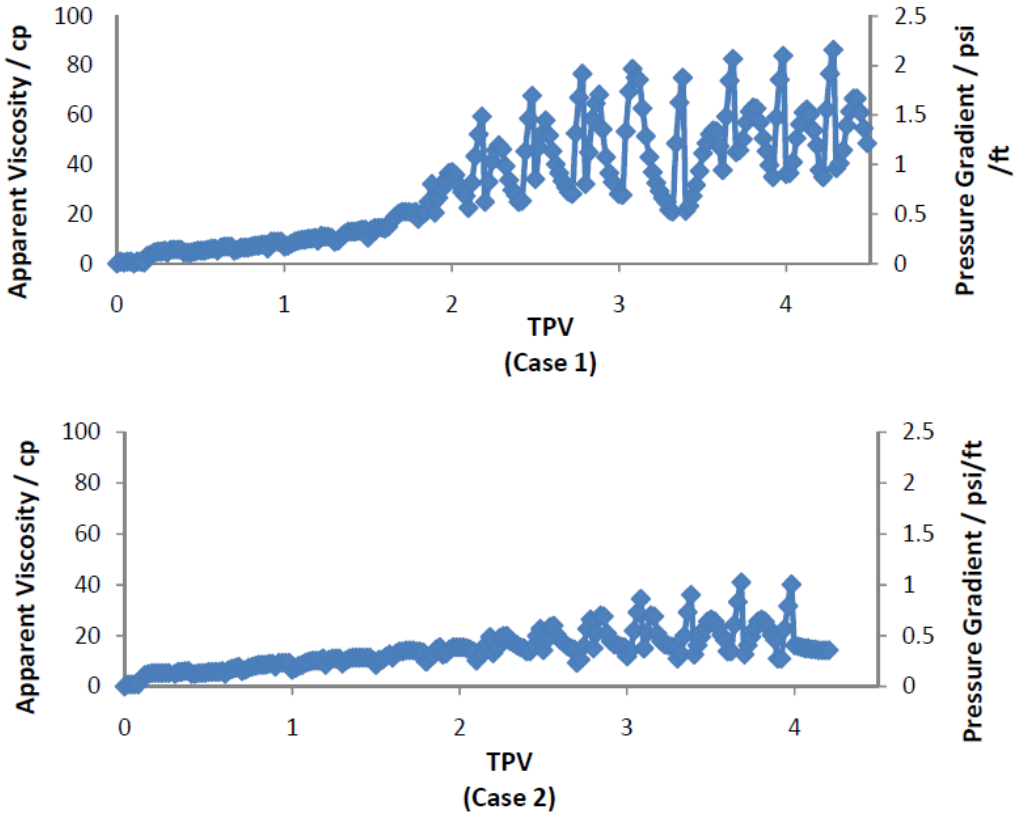

Figure 3-11 Foam apparent viscosity with 0.5% N67-9EO-GS. Case 1 was in low salinity; Case 2 was in SME brine.

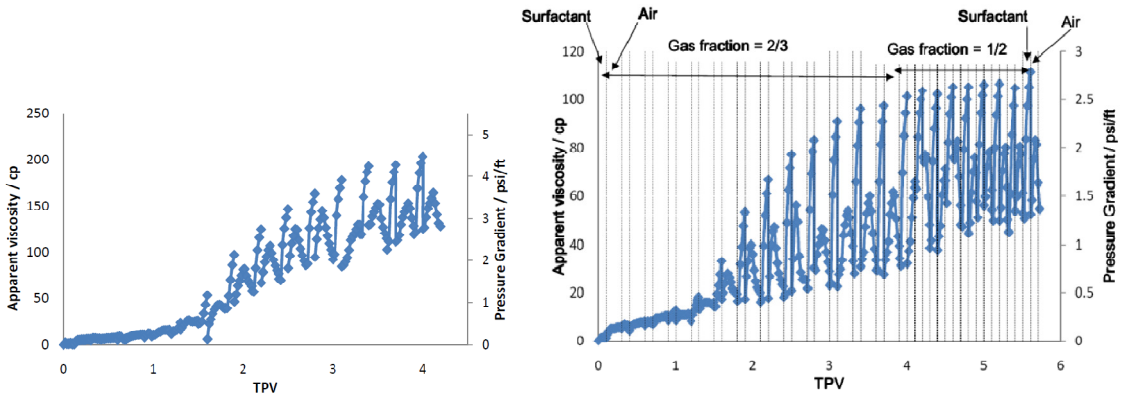

(Case 1) **(Case 2)**

Figure 3-12 Foam apparent viscosity with 0.5% N25-7EO-GS. Case 1 was in low salinity; Case 2 was in SME brine.

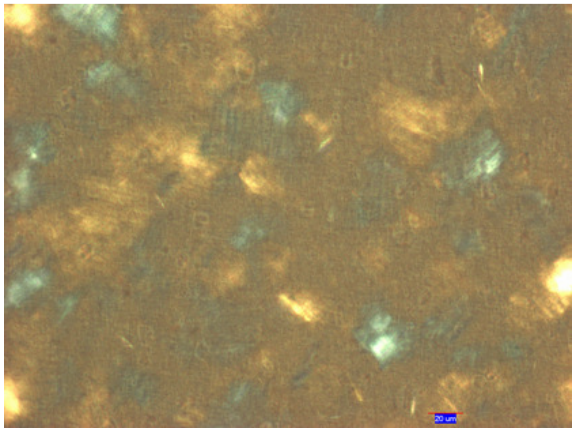

Figure 3-13 Microscopic pictures of Triton X-200 from its manufactured bottle (28% active) under cross-polarized light. Red bar indicates 20 microns.

3.2.2 Evaluation of Foaming Surfactant with the Presence of Crude Oil in 1-D Homogeneous Sandpacks

Strong foaming agents in oil-free systems were further evaluated in 1-D sandpacks with the presence of residual SME crude oil. SAG injection was used with *fg*=2/3, at 20 ft/D. None of the surfactant formulations tested would generate strong foam as shown in Figures 3-14 to 3-17. Compared with oil-free experiments, foam apparent viscosity with the presence of SME crude oil reduced by 1 or 2 orders of magnitude. The SME crude oil was extremely detrimental to foam generation.

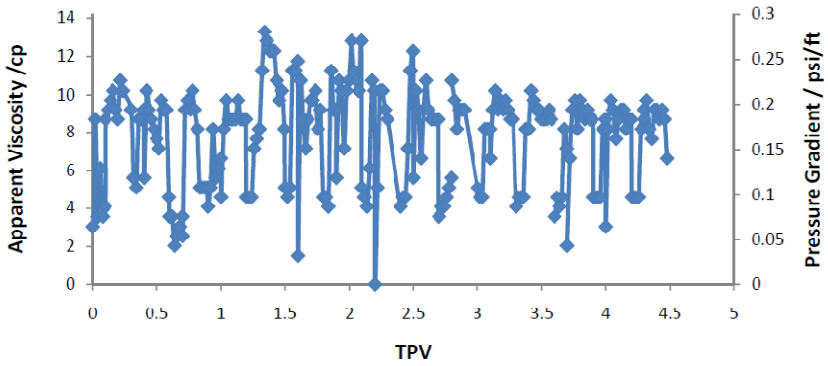

Figure 3-14 Foam apparent viscosity with 0.2% AOS16-18 (1% Na_2CO_3 and 2% NaCl) in presence of residual SME.

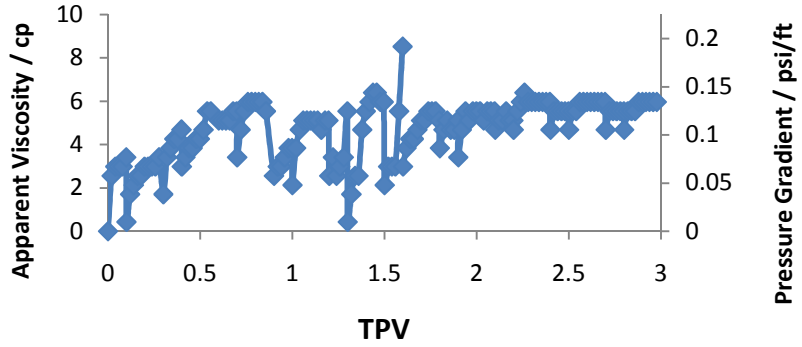

Figure 3-15 Foam apparent viscosity with 0.5% N25-7EO-GS (1% Na_2CO_3 and 3.5% NaCl) in presence of residual SME.

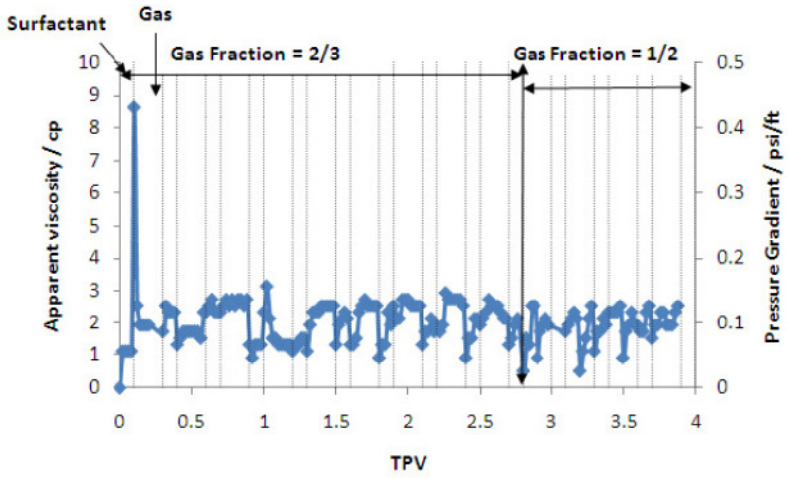

Figure 3-16 Foam apparent viscosity with 0.5% N25-7EO-GS (in SME brine) in presence of residual SME.

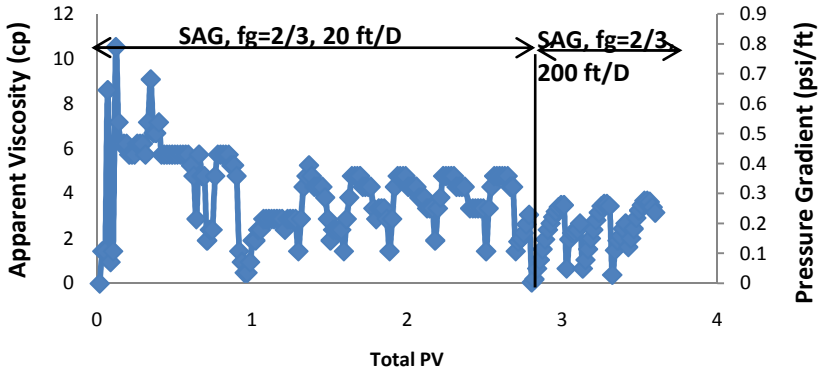

Figure 3-17 Foam apparent viscosity with 0.5% N67-9EO-GS (1% Na_2CO_3 and 3.5% NaCl) in presence of residual SME.

3.2.3 Phase Behavior of Crude Oils with NI

The phase behavior of the NI blend with different crude oils was investigated at room temperature. All systems had 1% Na_2CO_3. Salinity scans with increasing NaCl were conducted to determine the optimal salinity, expressed as wt% NaCl. Optimal salinities were estimated based on trends in solubilization and changes in color of the aqueous phase when the surfactant became preferentially oil soluble. Quantitative solubilization ratios could not be used to confirm these estimates because either surfactant concentration was too low or the phases were too dark (for Crude B) to measure these ratios. The optimal salinity for the three crude oils and NI are shown in Figure 3-18 as a function of the fraction, soap/(soap+surfactant) with soap content based on the amount of soap extracted from the crude oil for highly alkaline conditions as measured by aqueous phase titration [Liu, 2008a]. Arrows in this figure show the values of the soap fraction determined from the water/oil ratio corresponding to waterflood remaining oil saturation.

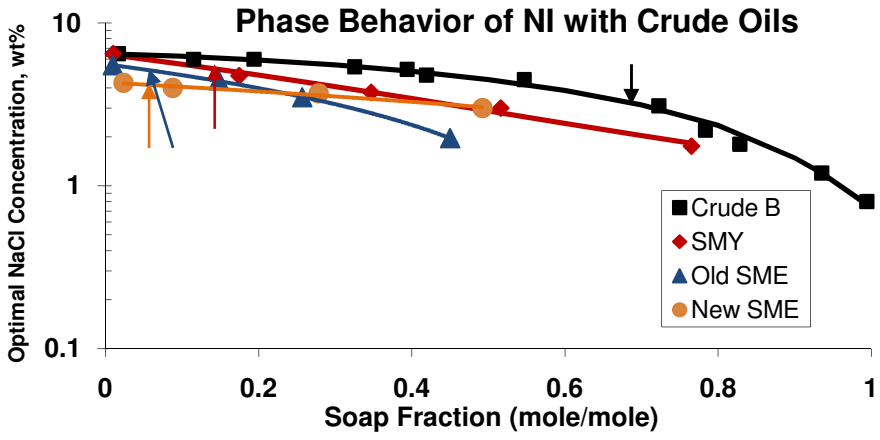

Figure 3-18 Phase behavior of Crude B, SME, Old and New SME with NI blend.

While it may appear favorable to inject the surfactant solution at the optimal salinity for minimum IFT, mobility control will be lost if the surfactant slug separates into surfactant-rich and polymer-rich phases [Liu, 2008b]. Previous sandpack experiments [Liu, 2008b] showed that when the salinity was 4% NaCl such that polymer and surfactant separated into different phases, poor sweep and high pressure gradients resulted. Thus injection compositions were designed such that the surfactant and/or polymer remained as a single, clear phase. The alkaline/surfactant slugs discussed below were injected at 2% NaCl for SMY crude oils, at 1% NaCl for Crude B, and at 2% or 3.5% NaCl for SME. A lower injected salinity was used for Crude B because its high acid number generated much more soap than the other crude oils. This formulation reduced oil/water IFT to the order of 10^{-3} mN/m, and had displaced oil successfully in previous ASP sandpack experiments [Liu, 2008b]. The phase behavior suggests that low IFTs and good oil displacement should be obtained for them and it is confirmed by sandpack experiments given in the following sections. Simulations indicate that high recovery is possible for a wide range of conditions with injection below optimal salinity of the surfactant owing to development of a gradient in soap fraction [Liu, 2008a].

3.2.4 Displacement of Moderately Light SMY Crude Oil by ASPF Process

The performance of the ASPF process displacing residual SMY crude oil (15 cp) was compared when injection was by either constant rate or constant pressure. The sandpack permeability was 79-98 darcy and the waterflood residual oil saturation was 23%-26%.

The brine was 2% NaCl throughout. The surfactant slug was 0.2% NI, 0.5% polymer, 1% Na_2CO_3, and 2% NaCl. The slug viscosity was about 47 cp. It was injected as 0.1 PV slugs alternating with 0.1 PV air, for 0.6 TPV. The drive was 0.5% IOS 15-18, 1% Na_2CO_3, and 2% NaCl, injected as 0.1 PV slugs alternating with 0.1 PV air. The constant rate experiment was 20 ft/D. The constant pressure experiment was 1.2 psi/ft.

The displacement profiles and pictures of effluent are shown in Figures 3-19 and 3-20 for the constant rate and constant pressure experiments, respectively. The recovery of the SMY residual oil and apparent viscosity are shown in Figures 3-21 and 3-22, respectively. The injection pressure gradient is shown in Figure 3-23.

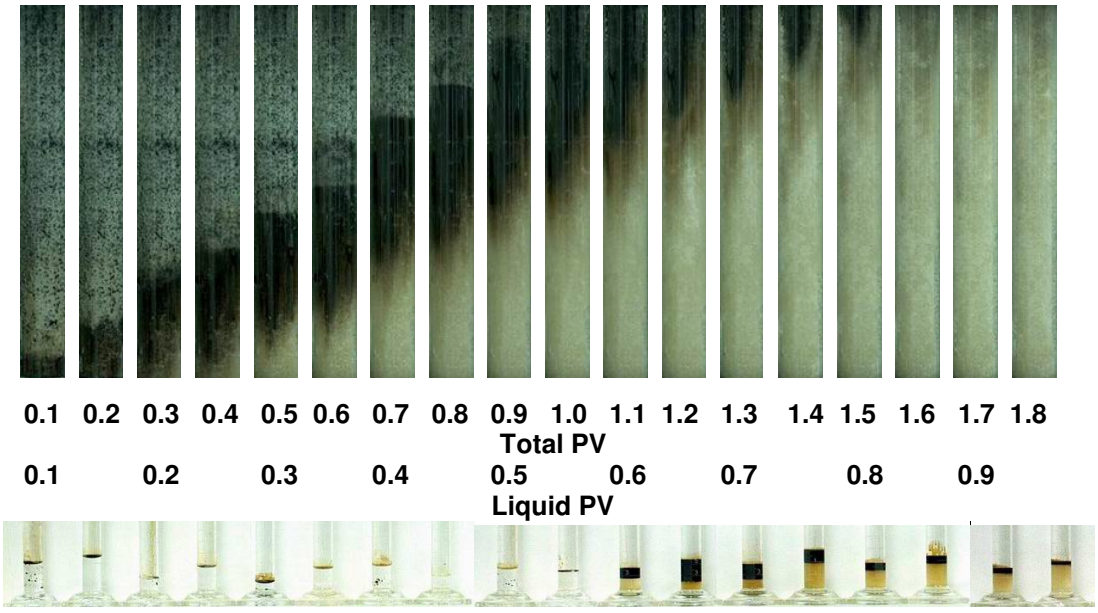

Figure 3-19 Displacement profiles and pictures of effluent for the displacement of SMY residual crude oil by ASPF with constant rate injection.

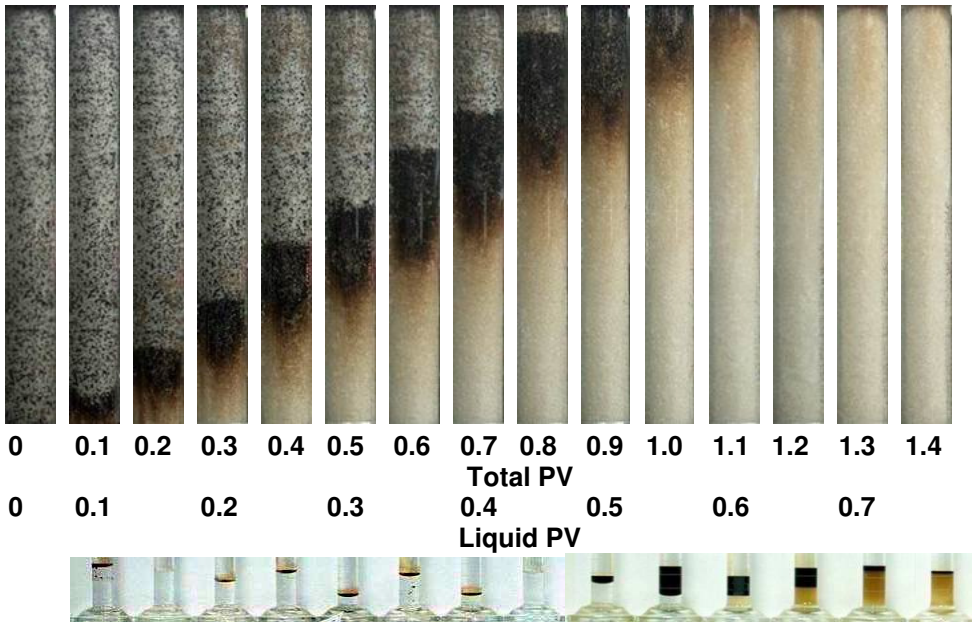

Figure 3-20 Displacement profiles and pictures of effluent for the displacement of SMY residual crude oil by ASPF with constant pressure injection.

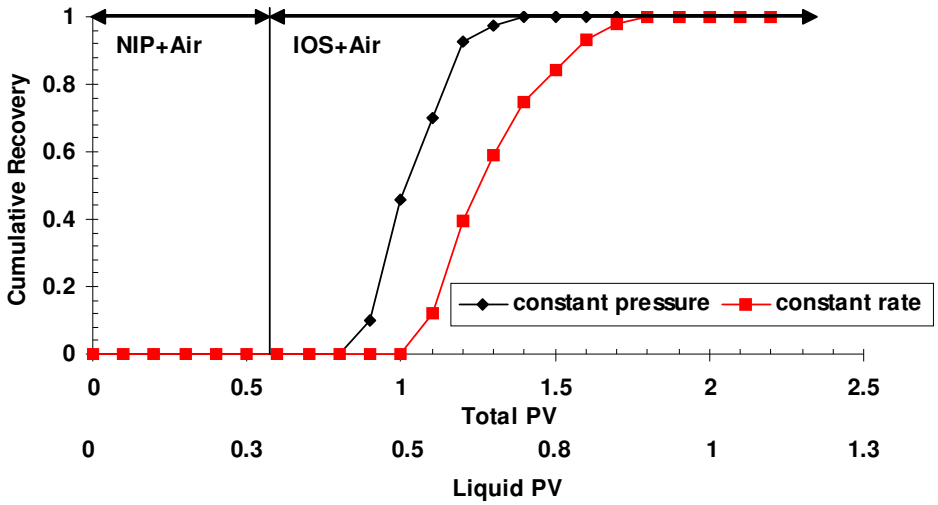

Figure 3-21 Recovery of SMY residual oil with ASPF, comparing constant pressure (1.2 psi/ft) and constant rate (20 ft/D).

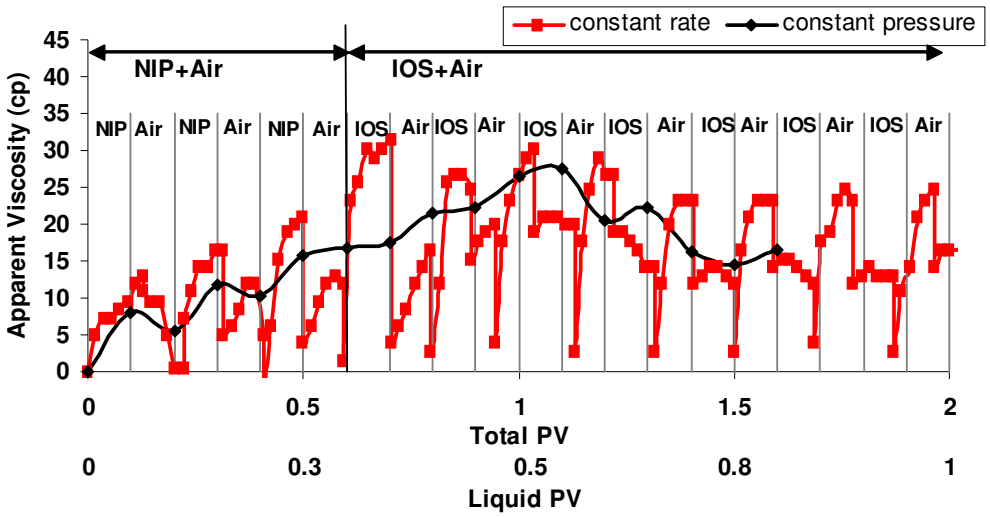

Figure 3-22 Apparent viscosity of ASPF displacing SMY crude oil, comparing constant pressure (1.2 psi/ft) and constant rate (20 ft/D). Apparent viscosity for the constant pressure injection had only one data point at the end of each fluid slug injection because only one averaged flow rate was measured during each slug injection.

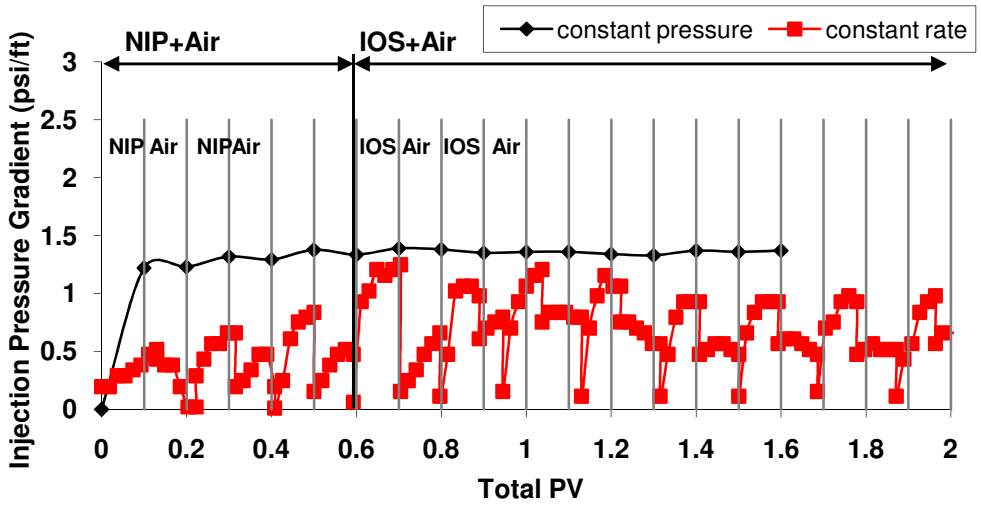

Figure 3-23 Pressure history of ASPF displacing SMY crude oil, comparing constant pressure (1.2 psi/ft) and constant rate (20 ft/D).

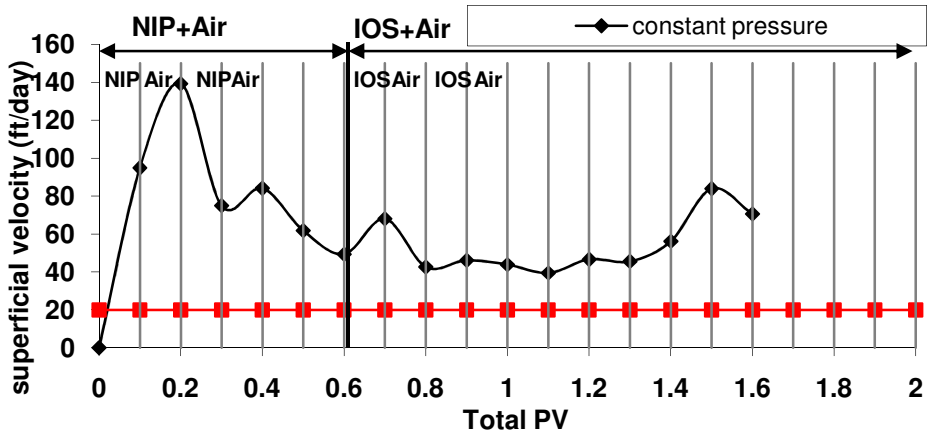

Figure 3-24 Injection rate during ASPF displacing SMY crude oil, comparing constant pressure (1.2 psi/ft) and constant rate (20 ft/D).

Comparison of the recovery curves in Figure 3-21 shows that the constant pressure experiment recovered oil earlier than the constant rate experiment. These experiments were conducted with the expectation that a critical pressure gradient had to be exceeded to generate strong foam. Firstly the pressure gradient during constant pressure injection was always higher than during the constant rate injection (Figure 3-23). It should be noted that the maximum pressure gradient in the constant rate experiment did not exceed 1.25 psi/ft. As a result, foam was generated faster with constant pressure injection. Secondly, gas was more compressed during constant pressure injection because of the higher pressure gradient. The gas expanded as it moved through the sandpack, resulting in earlier oil recovery. Figure 3-22 does not show a clear difference in foam strength (apparent viscosity) between the constant rate and constant pressure experiments Apparent viscosity for the constant pressure injection had only one data point at the end of each fluid slug injection because only one averaged flow rate was measured during each slug injection.

The critical pressure gradient was determined from oil-free foam experiments in 1-D sandpack such that there was a rapid rise in pressure drop (or apparent viscosity), as discussed in the beginning of this chapter and shown in Figures 3-2 and 3-3 Generally, it was the inflection point in the pressure versus PV curves. Figure 3-24 shows that constant pressure injection produced very high injection rate at the beginning. However, the rate was reduced after foam was formed.

3.2.5 Displacement of Moderately Viscous Crude B by ASPF Process

The ASPF process was used to displace Crude B, which has a viscosity of 266 cp. The remaining oil saturation was 36% after 6 PV of waterflood in a 106 darcy silica sandpack. The salinity was 1% NaCl throughout. A 0.3 PV ASP slug of 0.5% NI Blend, 0.5% polymer, 1% Na_2CO_3, and 1% NaCl was first injected at 1 ft/D. The viscosity of this slug was about 46 cp. A salinity of 1% NaCl was selected because of the high acid content of this crude oil, as indicated previously. Slugs of air (0.1 PV) were then injected alternating with 0.1 PV slugs of NIP to 0.8 TPV at 20 ft/D. Following this, the drive consisted of 0.1 PV slugs of 0.5% IOS 15-18, 1% Na_2CO_3, and 1% NaCl alternated with 0.1 PV slugs of air at 20 ft/D. The higher injection rate was to assure generating strong foam. The displacement profiles, oil recovery and oil cut, and apparent viscosity and pressure gradient are shown in Figures 3-25 through 3-27, respectively.

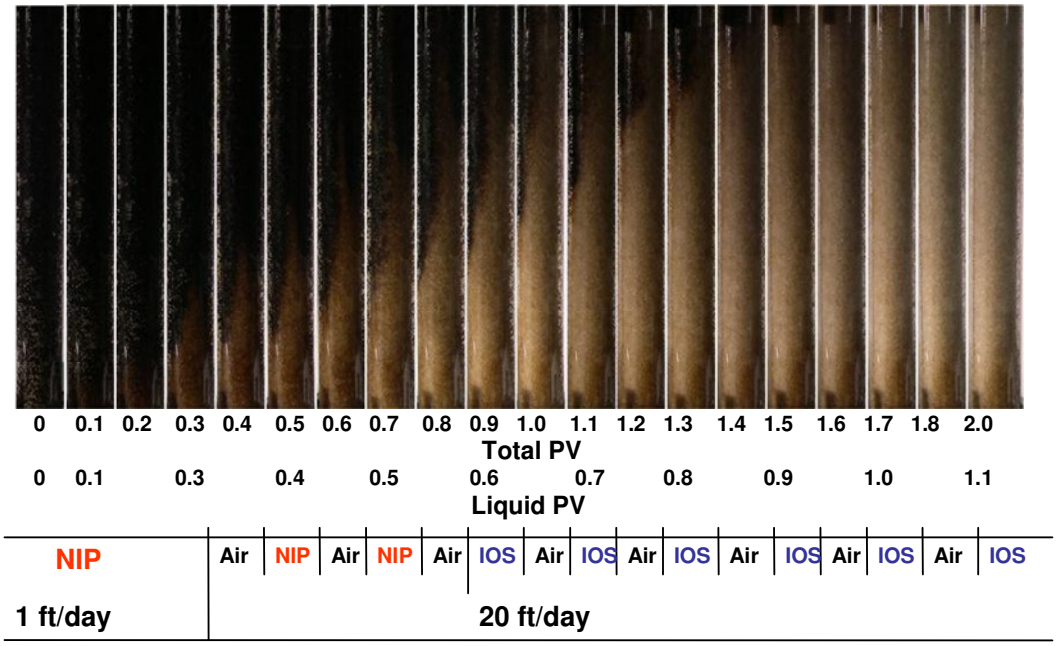

Figure 3-25 Profiles of the displacement of 266 cp Crude B with ASP and ASPF.

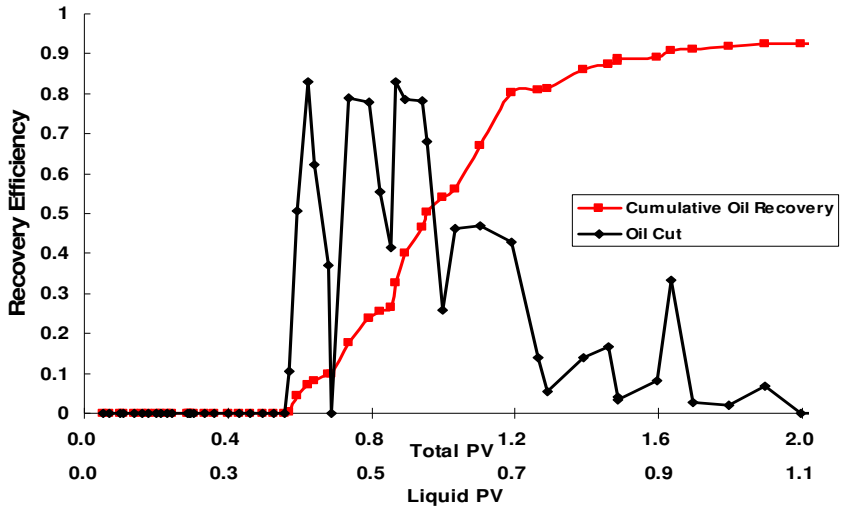

Figure 3-26 Recovery of waterflood remaining oil, 266 cp Crude B with ASP and ASPF. Oil-cut was the volume fraction of oil in the liquid effluent after each slug injection.

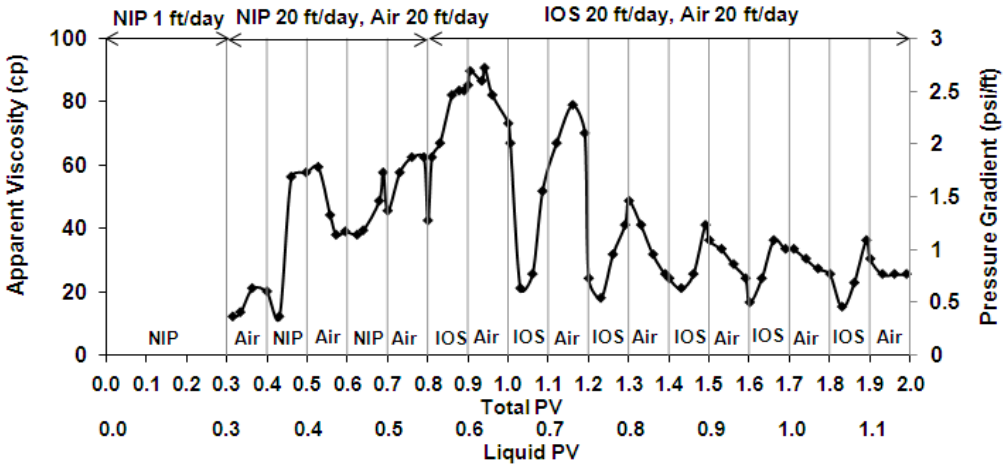

Figure 3-27 Apparent viscosity and pressure gradient of ASPF for Crude B. During first 0.3 PV NIP injection, because of very low rate and very high permeability, pressure was too low to be accurately measured.

The ASPF process recovered 93% of the waterflood remaining oil. The oil viscosity is 266 cp while the surfactant slugs with 0.5% polymer (NIP) had a viscosity of about 46 cp. This surfactant slug had a very unfavorable viscosity ratio with respect to the oil. The displacement profiles shown in Figure 3-25 (and visual observations) showed very little change in saturation during the ASP injection. Movement of oil became visible immediately upon injection of air. Oil breakthrough occurred at 0.6 TPV. The early oil production consisted of water-in-oil emulsion and free gas. Later, the oil was produced as oil-in-water emulsion and gas bubbles (foam). Emulsified oil was observed from effluent. Visual observation of the sandpack showed very little movement of oil during liquid injection but the oil appeared to move with passage of gas bubbles. The oil cut and apparent viscosity showed large changes as slugs of liquid and gas were alternated, Figures 3-26 and 3-27. A remarkable observation is that foam injection started at 0.3 PV and most of the oil was displaced by 1.3 TPV; almost piston-like displacement was observed during foam injection.

It appears that foam had a greater role than just mobility control. It is speculated that as gas/water interfaces advance through pore throats, the local capillary number (and pressure gradient) become large enough to also displace oil/water interfaces through neighboring pore throats and thus emulsify oil. This appears likely since the oil/water IFT is several orders of magnitude less than the gas/water surface tension. The gas bubbles thus displaced the viscous oil through attrition and dispersion as oil-in-water emulsion. The low IFT minimized trapping of oil during emulsion flow. This speculation is consistent with the observation that the apparent viscosity in Figure 3-27 is far less than the oil viscosity of 266 cp. Observation from glass micro model studies of displacement mechanism with NI and Crude B, as will be discussed in details in a separate chapter, showed that oil was emulsified and flowed as oil-in-water emulsion phase. Later when air was injected, oil drops tended to adhere to the liquid-gas interface. When this interface was advanced as gas flowed, the oil drops were mobilized at the same rate. The presence of high oil saturation destabilizes foam and the pressure gradient is focused at fewer advancing gas/water interfaces. A region where oil saturation is low has stable foam and its resistance diverts the injected fluids to regions of high oil saturation.

3.2.6 1-D ASF Processes with SME Crude Oil

3.2.6.1 With and Without Using Polymer

Displacement of SME crude from waterflooding residual condition in 1-D silica sandpacks will be discussed in this section. A successful ASPF process was first shown to have recovered nearly 100% of the residual SME with strong foam formed. These results are summarized in Table 3-1 and Figures 3-28 to 3-31.

Table 3-1 Summary of 1-D ASPF process with NI-blend, polymer, and IOS foam

	ASPF ***with polymer***	ASF ***without polymer***
Silica Sandpack	165.8 darcy	142.2 darcy
Flow Direction	Vertical	Vertical
Surfactant Concentration	0.2% NI, 0.5% IOS 15-18 in foam drive	0.2% NI, 0.5% IOS 15-18 in foam drive
Polymer Concentration	5000ppm	No polymer used
Viscosity of Slug	47 cp	~ 1 cp
Salinity	2%NaCl, 1% Na2CO3	2%NaCl, 1% Na2CO3
Temperature	20 C	20 ºC
Oil Viscosity (Old SME)	3.74 cp (25º)	3.74 cp (at 25 ºC)
Residual Oil Saturation after Waterflood	18.1%	26.4%
Surfactant Slug	0.3 PV	0.3 PV
Injection Pressure	~1.2 psi/ft	~1.2 psi/ft
Foam Generation	SAG	SAG
Oil Breakthrough	1.1 TPV	1.1 TPV
Foam Breakthrough	1.3 TPV	Gas broke through early
Cumulative Recovery	100% at 1.6 TPV (or 0.8 PV's of liquid)	98.6% at 2.3 TPV (or 1.2 PV's of liquid)

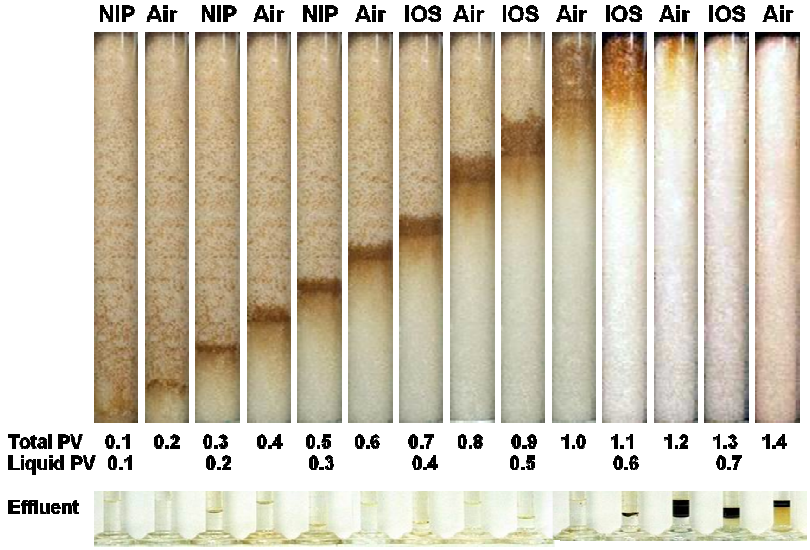

Figure 3-28 Displacement profiles and pictures of effluent during SME ASPF process under constant pressure gradient ~1.2 psi/ft

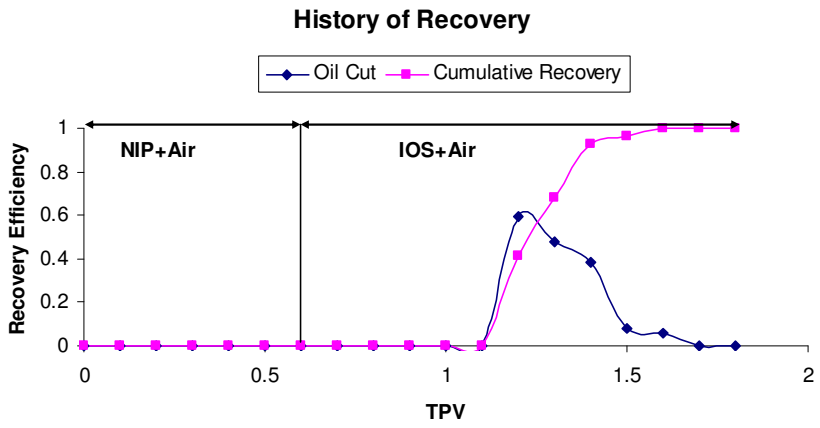

Figure 3-29 History of oil recovery efficiency.

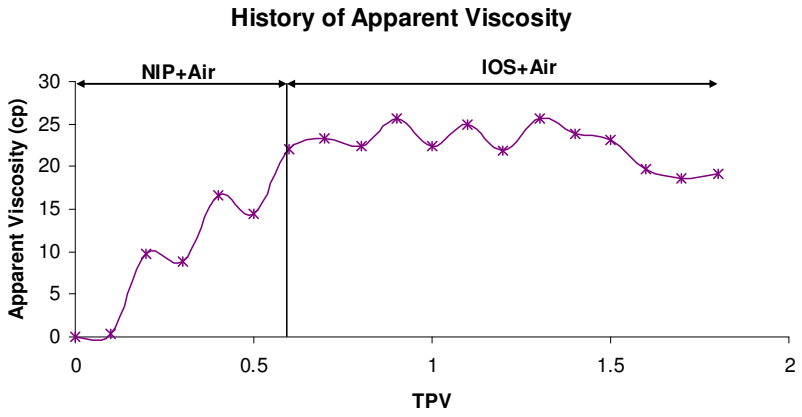

Figure 3-30 History of foam apparent viscosity.

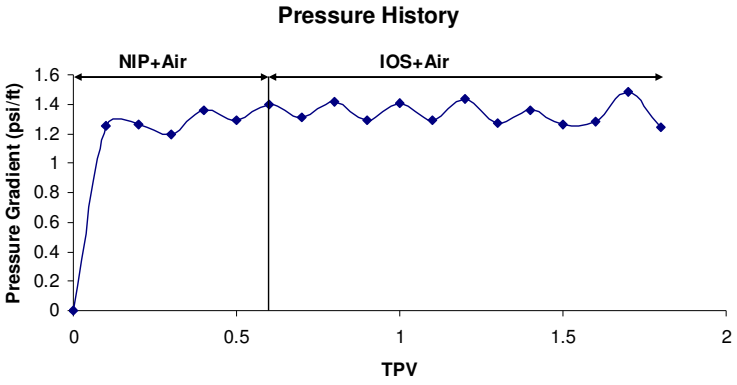

Figure 3-31 History of pressure gradient.

NIP (P stands for polymer) had a viscosity of 47 cp, much greater than the viscosity of crude oil 3.74 cp. As a result of favorable mobility ratio, the sweep efficiency was greatly improved along with ultra low IFT, and hardly any residual oil was left behind this ASP slug. Displacement profiles in Figure 3-28 show that the sand behind oil bank was as white as clean silica sand. Therefore strong foam would form in the absence of crude oil as in previous oil-free experiments. However, the application of polymer is limited under many reservoir conditions *e.g.* polymer will decompose at high temperature; cross-link when divalent or trivalent ions are present; will not transport in matrix pores whose sizes are smaller than the macromolecules, etc. Fortunately, these constraints can be overcome by using foam. One of the unique attributes of foam in heterogeneous systems that makes foam more favorable than polymers is that foam has higher apparent viscosity in high- than in low-permeability zones and therefore improves sweep [Heller 1994; *et al.* 1999; Kovscek and Bertin 2002; Nguyen *et al.* 2005; Li. *et al.*, 2010]. Unfortunately the SME crude oil studied here was a light crude (API=41.1°), and was extremely detrimental to foam stability. When polymer was omitted, the original NI slug was lacking mobility control. Consequently, the reduced sweep efficiency left much residual oil behind that was more than enough to destabilize foam in the drive that followed. These results are summarized and compared with the previous ASPF process in Table 3-1, and Figures 3-32 to 3-35. Because of no mobility control, no oil bank was formed as shown in Figure 3-32. Cumulative recovery was satisfactory (98.6% from residual oil) although it required more PV than ASPF. This may have been due to the fact that SAG generated foam in-situ. Although foam was broken by residual oil, transient gas bubbles still displaced oil by local pressure gradient and by attrition. Since strong foam

was not formed and injection was at constant pressure, the rate was in the magnitude of 10^2 ft/D. This abnormally high rate contributed to high capillary number and hence apparently good recovery.

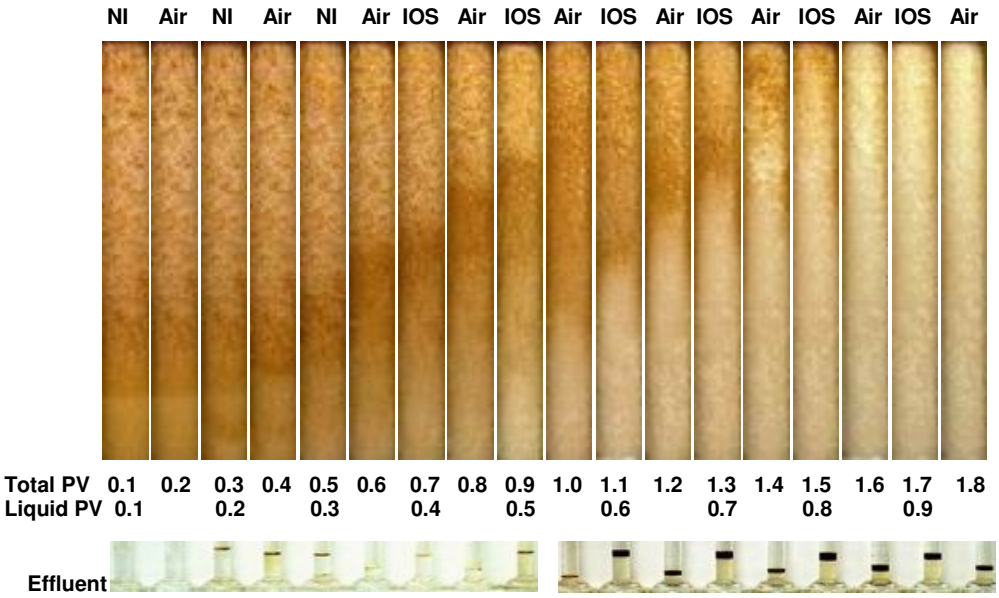

Figure 3-32 Displacement profiles and pictures of effluent during SME ASF process under constant pressure gradient ~1.2psi/ft. No polymer was used.

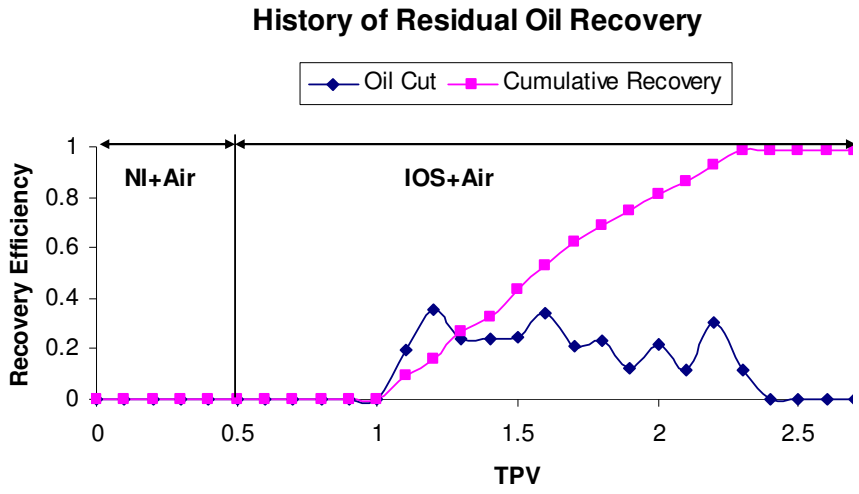

Figure 3-33 History of oil recovery efficiency.

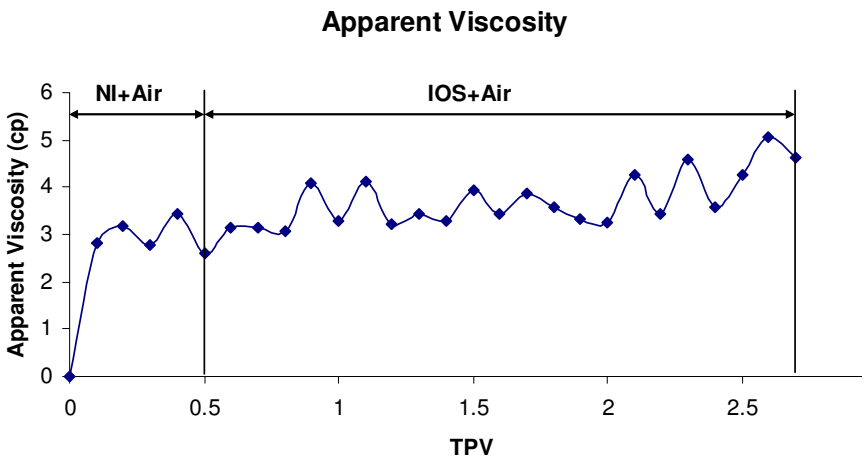

Figure 3-34 History of foam apparent viscosity.

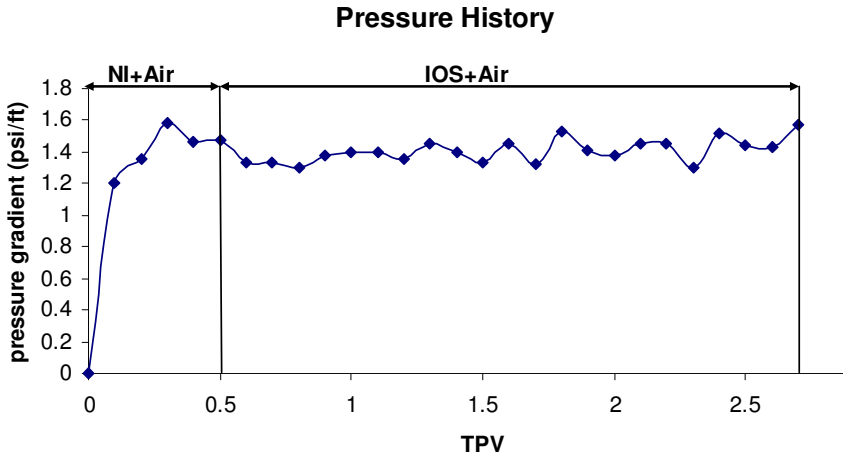

Figure 3-35 History of pressure gradient.

In order to generate strong foam in presence of SME without using polymer, several methods were designed and evaluated in forced displacement tests. These methods include: using pre-generated foam; incorporating dikes in the sandpack; adding a betaine surfactant as a foam booster. These cases will be discussed in the following individual sections.

3.2.6.2 Pre-Generated Foam

0.5% IOS15-18 in 2% NaCl and 1% Na_2CO_3, and air were co-injected into a foam pre-generator at 20 ft/D (10 ft/D for either fluid, thus *fg*=0.5). This experiment is summarized in Table 3-2. With pre-generated foam, there were noticeably two oil banks as shown in Figures 3-36 and 3-38. The first oil bank broke through at 0.9 TPV associated with the surfactant front, and the second bank broke through at 3.3 TPV associated with the strong foam front. Although the second oil bank had piston-like displacement front, air still broke through as if it was a 'leaky piston'. This may be one reason why the second oil bank advanced more slowly than the first oil bank. Another reason may be that gas was compressed as foam became stronger. Good recovery was a result of high capillary number which was due to very high foam apparent viscosity, as shown in Figure 3-37, although tension was not ultra low. IFT between this surfactant composition (*i.e.* 0.5% IOS 15-18 in 2% NaCl and 1% Na_2CO_3) and SME was 0.354 mN/m measured by spinning drop method. However this may not be desirable in a field application. Too high values of apparent viscosity would cause injectivity problems, and too many through-puts of chemical slug injection are not economical.

Table 3-2 Summary of 1-D ASF process with IOS15-18 pre-generated foam

Permeability	156 darcy
Flow Direction	Vertical
Surfactant Composition	0.5% IOS15-18 in 2% NaCl, 1% Na_2CO_3
Temperature	25 °C
Oil Viscosity (old SME)	3.74 cp
Waterflood Residual Saturation	25.6%
Surfactant Slug Size	0.1 PV increment
Injection Rate	20 ft/D
Foam Generation	Co-injection into a foam pre-generator
Oil Breakthrough	0.9 PV
Cumulative Recovery	99.3%

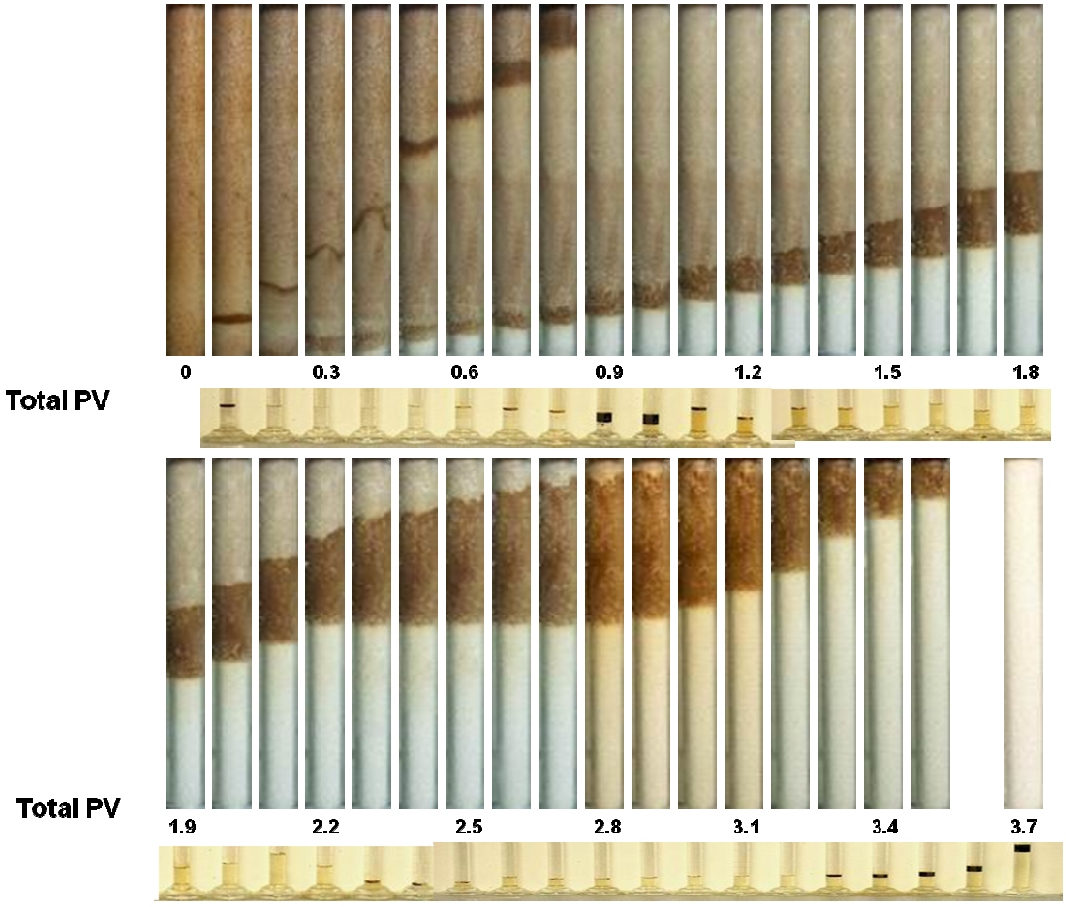

Figure 3-36 Sweep profiles. Syringe change due to surfactant refill at 2.3 PV.

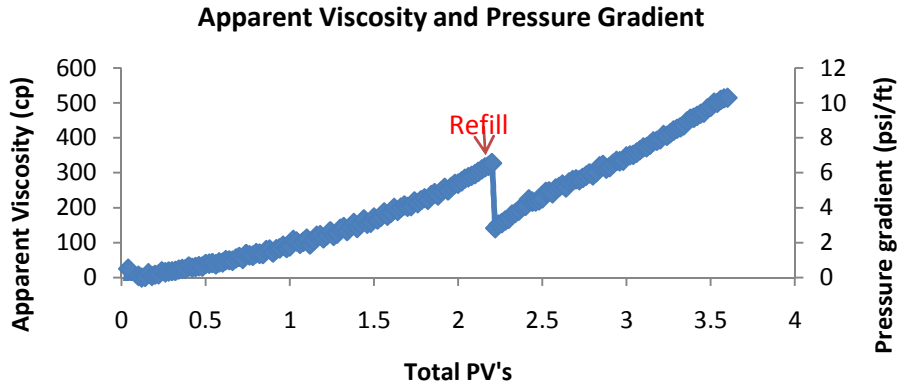

Figure 3-37 Foam apparent viscosity and pressure gradient. Red arrow indicates refilling surfactant solution in the syringe.

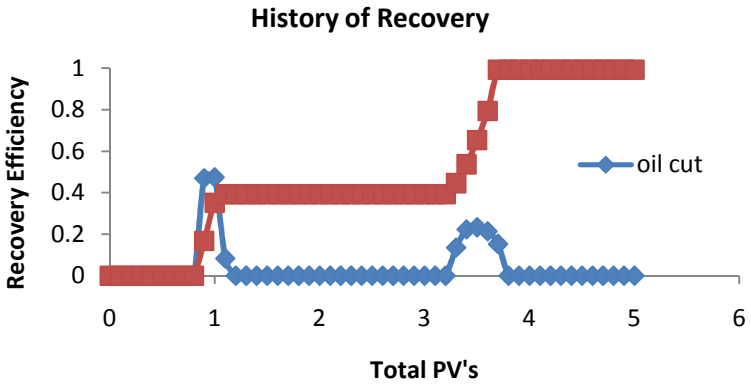

Figure 3-38 Oil cut and cumulative recovery.

3.2.6.3 Dikes to Enable Boundary Snap-off

Foam bubbles can be regenerated (independent of pressure gradient) when gas and surfactant solution flow across a step increase in permeability with a ratio greater than 4 [Falls *et al.* 1988; Tanzil *et al.* 2002b]. In order to generate foam in-situ by snap-off, 'dikes' were introduced in the original 1-D sandpack. Figure 3-39 shows a schematic of such a sandpack.

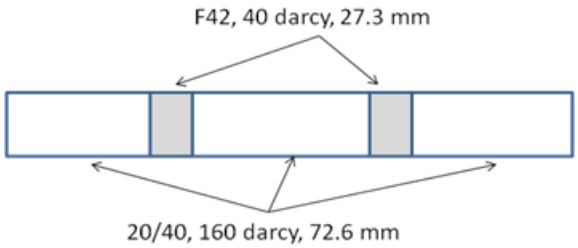

Figure 3-39 A 1-D Heterogeneous sandpack schematic with 'dikes'.

1-D silica sandpack was tightly packed with US OilFrac 20/40 (~160 darcy) and F-42 (~40 darcy) silica sands. Overall permeability is the harmonic average. $\bar{k} = \frac{\sum_{n=1}^{N} l_n}{\sum_{n=1}^{N} l_n / k}$,

where l_n is the length and k_n is the permeability of the n^{th} layer respectively, and N is the

number of layers. Theoretical overall permeability was 88 darcy, and the measured real permeability was 80 darcy. They agreed well.

Foam was first evaluated in such a diked sandpack without the presence of crude oil. Figure 3-40 is a comparison between an 80-darcy 1-D heterogeneous sandpack with dikes and an 88-darcy homogeneous sandpack. With AOS16-18 being a strong foaming agent, foam formed even faster and stronger in the diked column than the homogeneous column. This behavior was similar to pre-generated foam, in which small permeability 'dikes' served as in-situ foam generators.

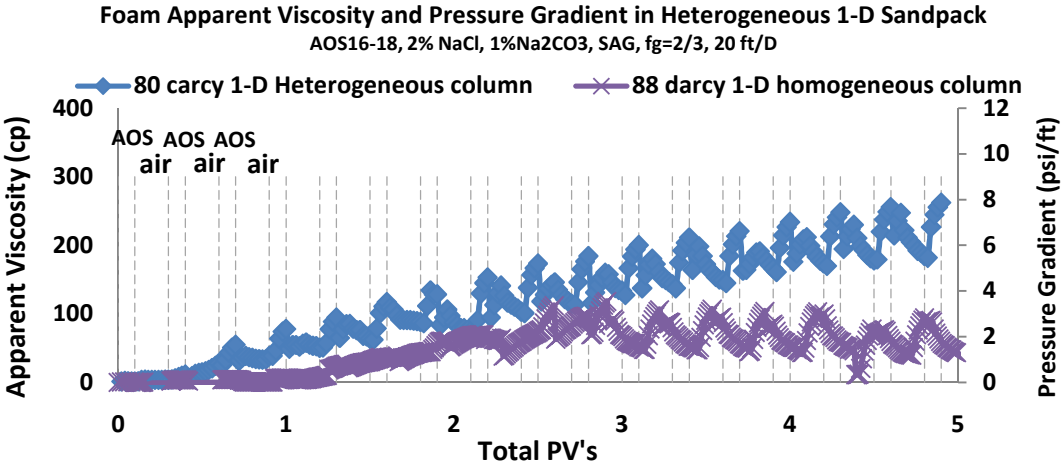

Figure 3-40 Comparison between hetero- and homogeneous 1-D columns.

Next, an ASPF forced displacement was done in such a sandpack with dikes. Table 3-3 is a summary of results. Displacement profiles and pictures of effluent were shown in Figure 3-41. Figure 3-42 shows foam apparent viscosity and pressure gradient. Data points after 1.9 TPV were not reliable due to pressure transducer malfunctioning. Figure 3-43 is a plot of oil recovery. This experiment recovered more residual oil and faster than previous homogeneous 1-D ASF experiment discussed in **3.2.6.1**. Strong foam was still not formed due to the presence of crude oil. Although foam was broken by oil, it still

formed transiently in-situ by snap-off mechanism at the permeability transition boundary, and this may be responsible for better and earlier recovery.

Table 3-3 Summary of results in a 1-D heterogeneous sandpack with dikes

Silica Sandpack	Overall 80 darcy with dykes.
Flow Direction	Vertical
Surfactant Concentration	0.5% NI; 0.2% AOS16-18 in foam drive
Salinity	4% NaCl, 1% Na2CO3 in NI 2% NaCl, 1% Na2CO3 in foam drive
Temperature	25 °C
Oil Viscosity	3.93 cp (25ºC)
Waterflood Residual Oil Saturation	19.4%
Total NI Slug	0.3 PV
Injection Rate	5 ft/D NIB (0-0.2TPV); 20ft/D from 0.3th TPV.
Slug Size	0.1 PV
Foam Generation	AOS 16-18 alternating air
Oil Breakthrough	0.9 TPV
Cumulative Recovery from Residual	87% at 1.7 TPV

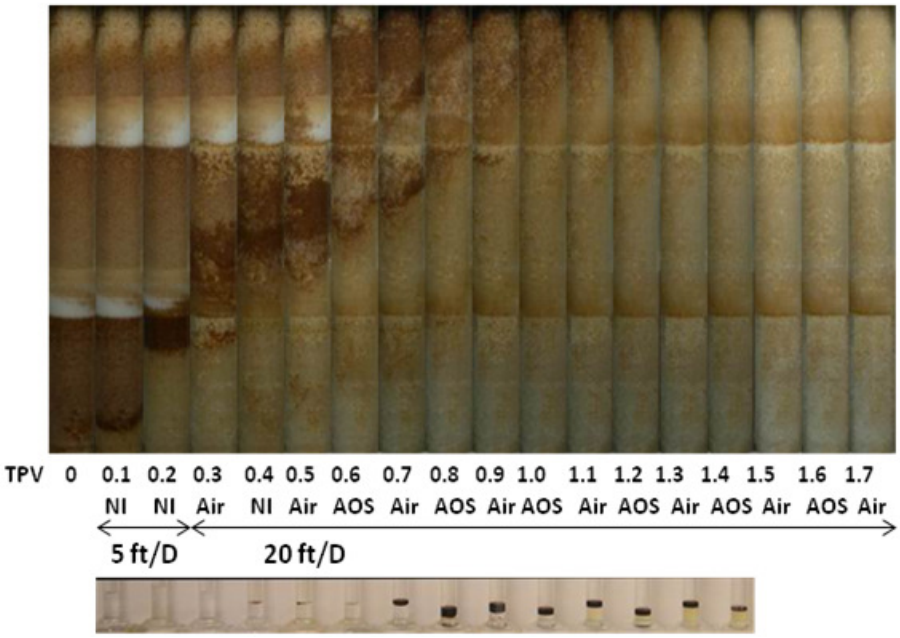

Figure 3-41 Displacement profiles and pictures of effluent during 1-D ASF process.

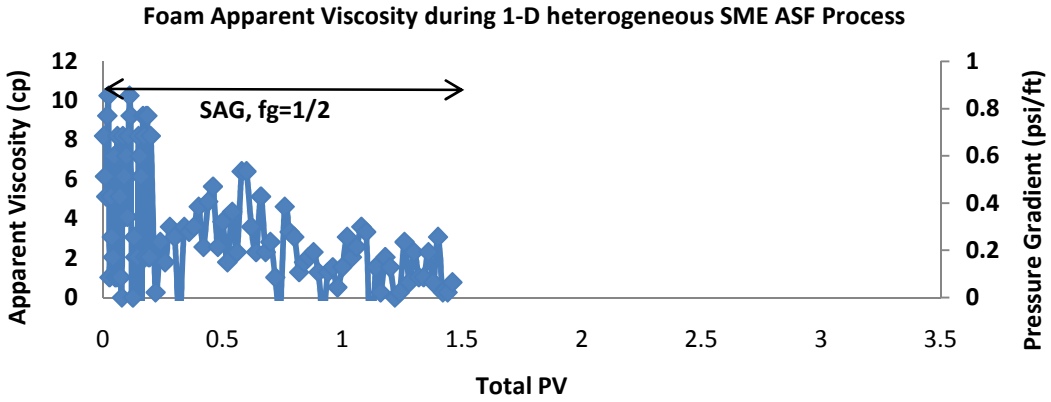

Figure 3-42 Foam apparent viscosity and pressure gradient. Data points after 1.9 TPV were not reliable due to transducer malfunctioning.

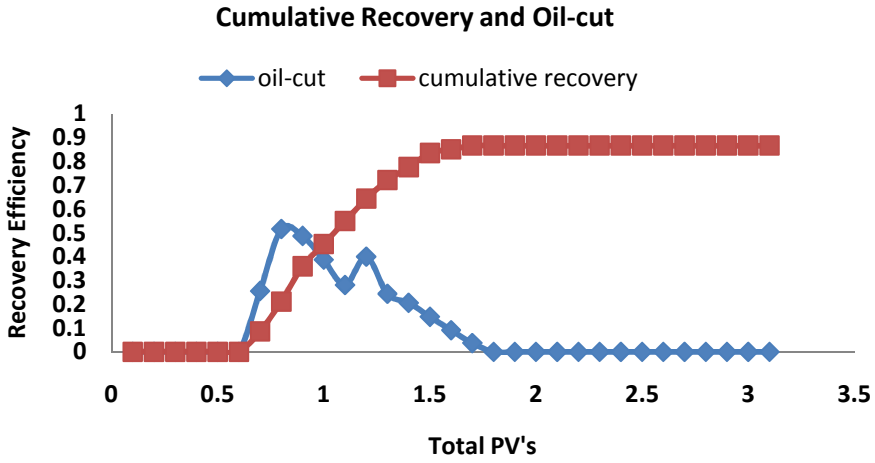

Figure 3-43 Plot of recovery from residual oil. Cumulative recovery was 87%.

3.2.6.4 Adding Lauryl Betaine as a Foam Booster

NI can reduce IFT to ultra low values, but it was a weak foaming agent even in the absence of crude oil. However, with the addition of lauryl betaine, a zwitterionic surfactant, at a weight ratio of 1:2 NI:B, the new NIB formulation became a good foaming agent, Figure 3-44.

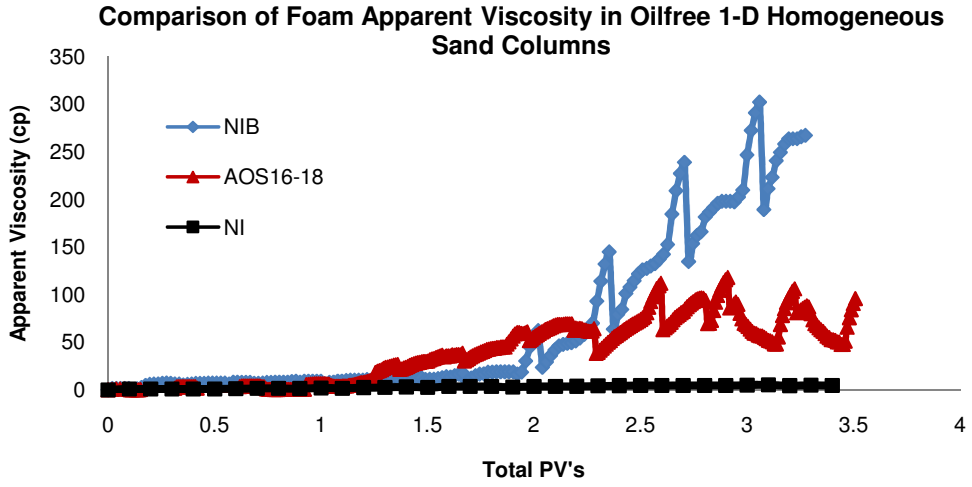

Figure 3-44 Comparison of foaming ability among NI, AOS 16-18, and NIB. NI foam was injected at 0.5 psi/ft with *fg*=0.5. NIB and AOS 16-18 was injected at 20 ft/D with *fg*=2/3.

The micro model picture shown in Figure 3-45 reveals that NI, being a weak foaming agent, did not stabilize foam lamellae in presence of SME. Air flowed in continuous gas channels. However, Figure 3-46 shows that NIB could stabilize foam lamellae. Trapped gas flowed as bubble chains even in the presence of oil, resulting in gas mobility reduction. The dark color on the contour of a bubble or a bubble chain indicates oil was in very close proximity to bubbles but did not break them. Since oil drops did not form lenses or rupture foam lamellae, it is possible that these drops could not reach the air-water interface through a pseudoemulsion film or could not enter the interface if they did reach it, *i.e., E≤0.*

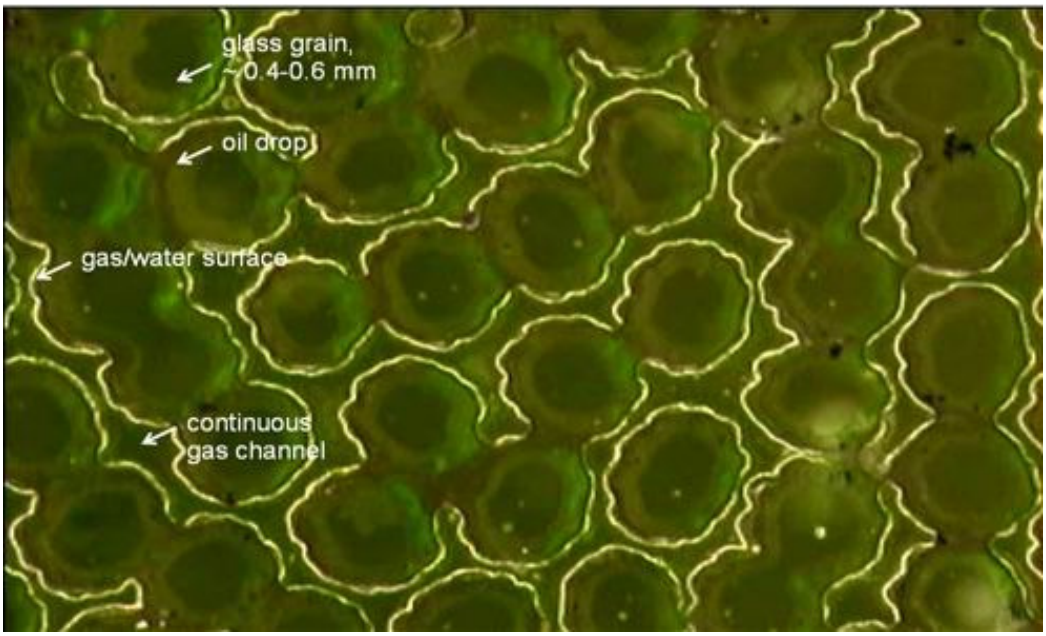

Figure 3-45 NI alone without lauryl betaine in presence of SME in a glass micro model.

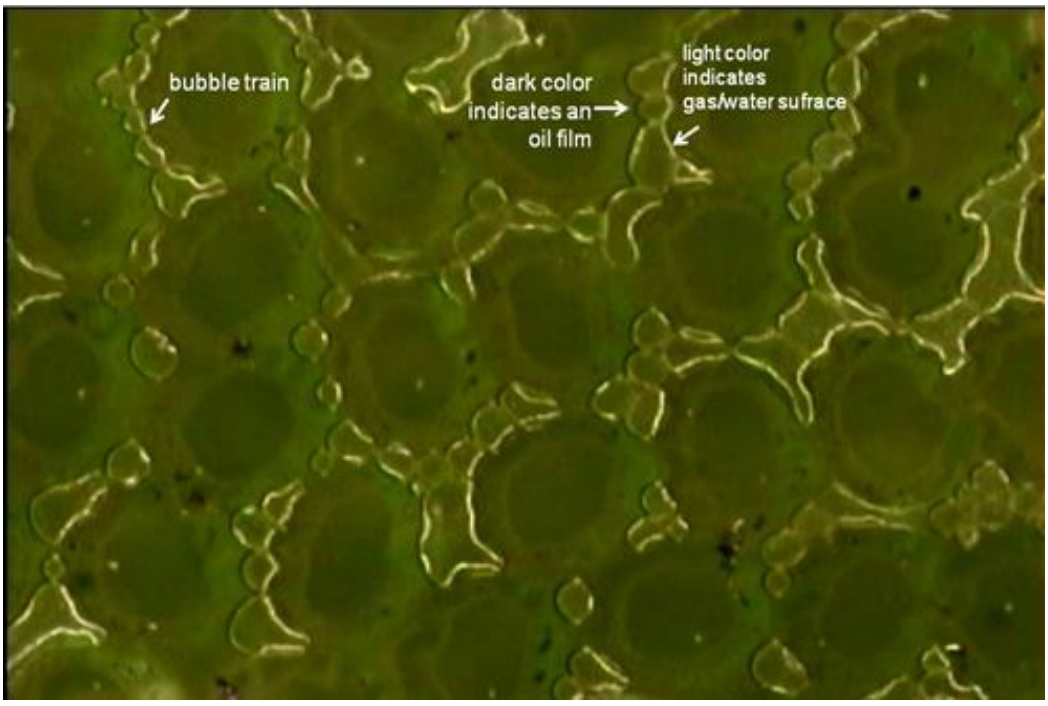

Figure 3-46 NIB (NI:lauryl betaine=1:2) in presence of SME in a glass micro model.

All experiments described below were ASF EOR processes at ambient temperature without using polymer. Foam in presence of oil was first evaluated in water-wet, 1-D

homogeneous sandpacks, then in a layered, oil-wet heterogeneous sand column with a permeability ratio of approximately 34:1.

The initial condition was waterflood residual oil condition. Foam was first evaluated as a drive behind NI or NIB slugs. It was generated by surfactant alternating air (SAG) injection at constant pressure gradient (1.2 ~1.5 psi/ft) using IOS 15-18 or IOS 15-18 and lauryl betaine blends (IB) at different ratios. These experiments are summarized in Table 3-4 and Figures 3-47 to 3-53.

Table 3-4 Summary of 4 experiments in 1-D homogeneous sandpacks

Experiments	(a)	(b)	(c)	(d)
Silica Sandpack	142.2 darcies	185 darcies	144 darcies	193 darcies
Flow Direction	Vertical	Vertical	Vertical	Vertical
Surfactant Concentration (wt%)	NI 0.16% N67-7PO 0.04% IOS15-18	NIB 0.4% N67-7PO 0.1% IOS15-18 0.02% betaine	NIB 0.4% N67-7PO 0.1% IOS15-18 0.02% betaine)	NIB 0.2% N67-7PO 0.05% IOS15-18 0.5% betaine
Foam Drive (wt%)	0.5% IOS 15-18	IB 0.5% IOS15-18 0.02% betaine	IB 0.5% IOS15-18 0.05% betaine	IB 0.5% IOS15-18 0.05% betaine
Salinity	1% Na_2CO_3 2%NaCl	1% Na_2CO_3 3.5% NaCl	1% Na_2CO_3 3.5% NaCl	1% Na_2CO_3 3.5% NaCl
Temperature	25 ºC	25 ºC	25 ºC	25 ºC
Oil Viscosity	3.74 cp (at 25 ºC)	3.92 cp (at 25 ºC)	3.92 cp (at 25 ºC)	3.92 cp (at 25 ºC)
Residual Oil Saturation after Waterflood	26.4%	20.0%	21.8%	20.9%
Surfactant Slug	0.3 PV NI	0.3 PV NIB	0.3 PV NIB	0.3 PV NIB
Injection Scheme	1.2 psi/ft	5 ft/D NIB (0-0.2TPV); 1.4 psi/ft from 0.3th TPV.	5 ft/D NIB (0-0.2TPV); 1.5 psi/ft from 0.3th TPV.	5 ft/D NIB (0-0.2TPV); 1.4 psi/ft from 0.3th TPV.
Foam Generation	SAG, *fg*=0.5	SAG, *fg*=0.5	SAG, *fg*=0.5	SAG, *fg*=0.5
Oil Breakthrough	1.1 PV	1.1 TPV	0.3 and 0.9 TPV	0.7 TPV
Cumulative Recovery from Residual	98.6% at 2.3 TPV	98% at 2.2 TPV	97.5% at 2.2 TPV	99.7% at 1.9 TPV

Experiment (a) to (d) show the successful progression in terms of cumulative recovery from residual oil (Figure 3-47) and foam apparent viscosity (Figure 3-48) as lauryl betaine was added to NI and IOS 15-18, and the ratios were optimized. Experimental (a) is the same ASF process discussed in **3.2.6.1** and it did not contain any betaine in either NI or IOS 15-18 slugs. Foam did not form due to the adverse effect of crude oil. There was not a distinctive oil bank (Figure 3-32), and foam apparent viscosity was low (Figure 3-48). Both indicate there was not effective mobility control. In experiment (b), lauryl betaine was added to both NI (NI:B=25:1) and IOS 15-18 (IOS:B=25:1) slugs (Figure 3-49). These ratios had not been optimized yet and foam was still weak (Figures 3-48). In experiment (c), NIB was kept the same as in (b), but the ratio between IOS 15:18 and lauryl betaine in IB was optimized to be 10:1. The ratio was so chosen because this IB had the highest viscosity while still remained as a clear single phase solution (Figure 3-52). This viscosity increase may be due to a sphere to rod micelle transition [Christov, *et al*., 2004]. One can see oil bank building up (Figure 3-50), and foam began to become stronger (Figure 3-48). In experiment (d), the ratio between NI and B was optimized to 1:2 in NIB, and the optimized 10:1 ratio in IB was maintained the same as in (c). The 1:2 ratio was so chosen because from qualitative bottle tests (Figure 3-53), foam was both stable with and without crude oil while minimizing the use of lauryl betaine. The NIB blends did not display significant viscosity dependence on blending ratio. With both NIB and IB optimized, one can see a distinctive oil bank forming and moving from the displacement profiles (Figure 3-51). Most residual oil was recovered by 1.0 TPV. Foam apparent viscosity was much higher compared with (a) – (b) (Figure 3-48). Foam did not break through oil bank as liquid fraction in the effluent

(Figure 3-51) remained nearly 100%. These all indicate that foam worked well as an effective mobility control agent.

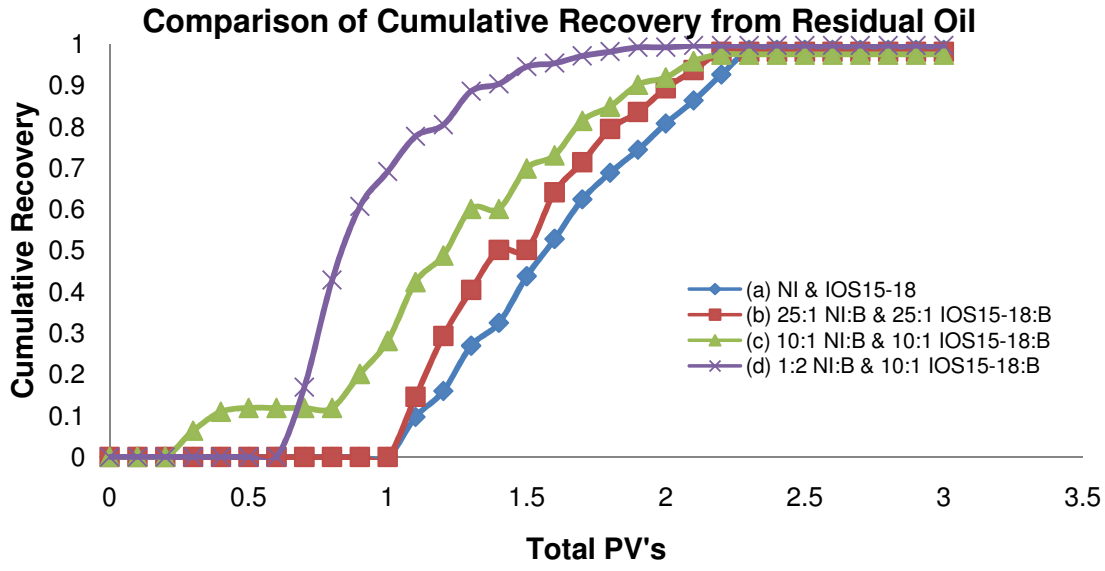

Figure 3-47 Cumulative recovery of waterflood residual oil in experiments (a), (b), (c), (d).

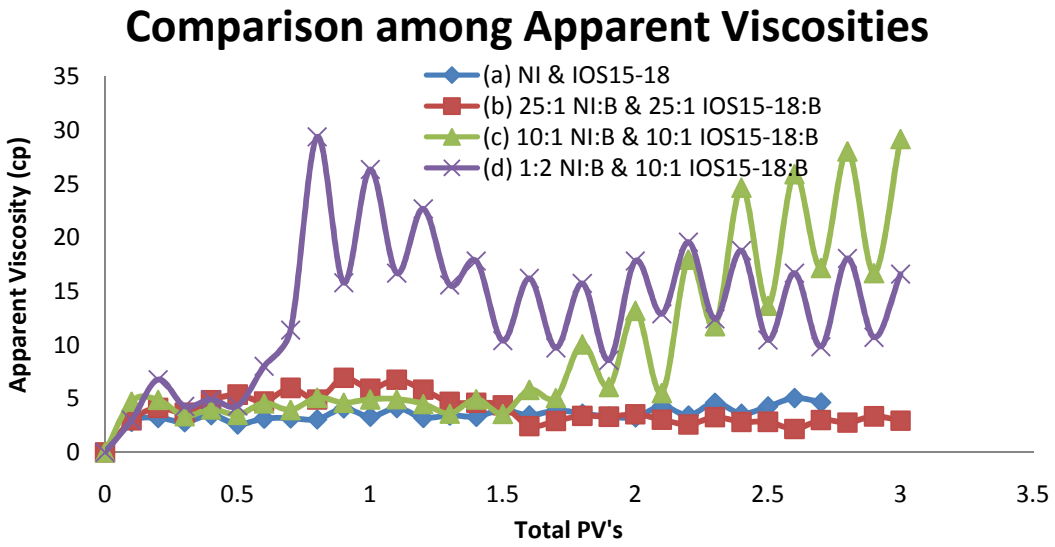

Figure 3-48 Foam apparent viscosity curves in experiments (a), (b), (c), (d).

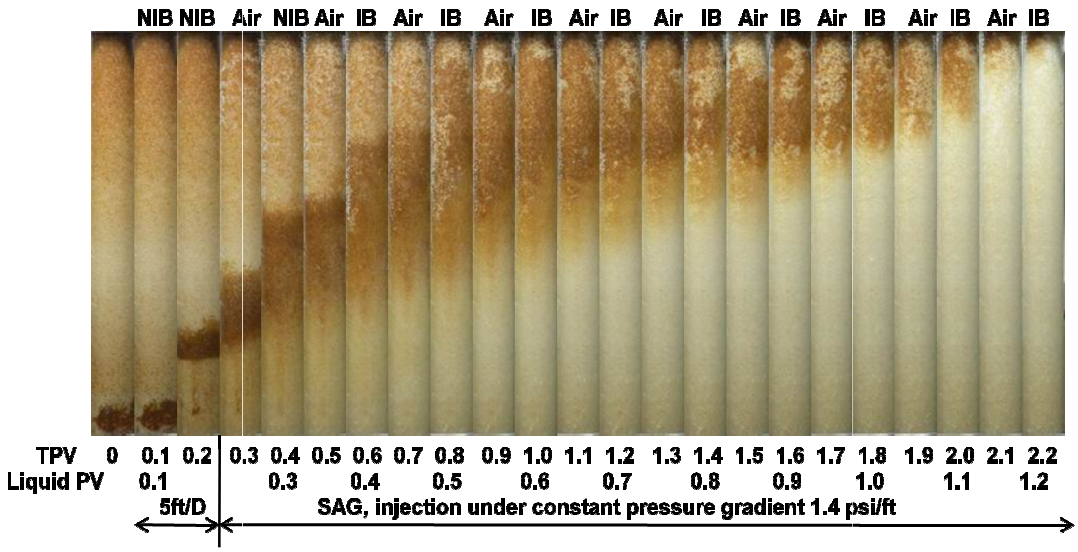

Figure 3-49 Displacement profiles in experiment (b).

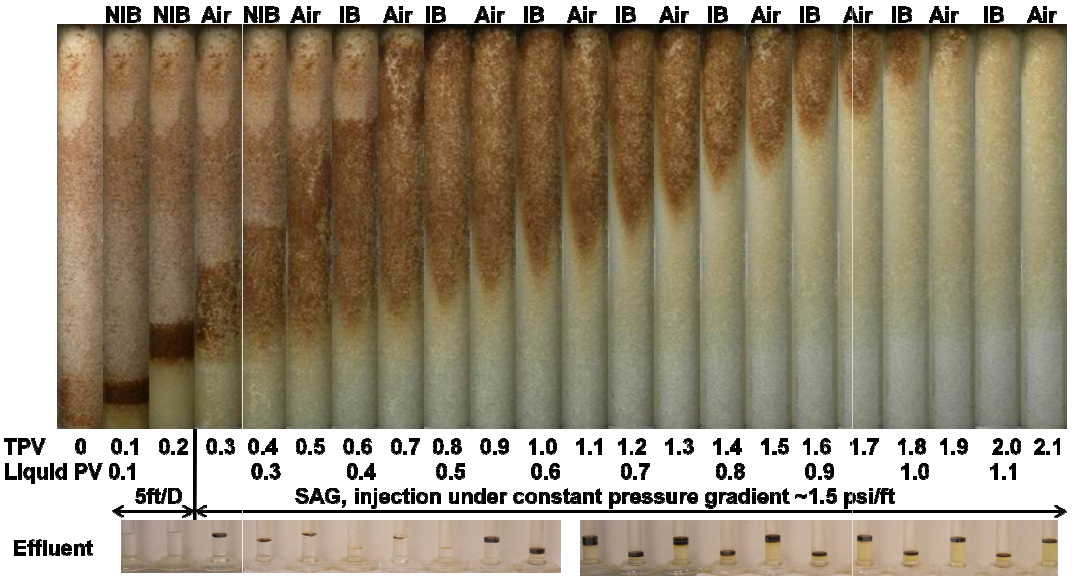

Figure 3-50 Displacement profiles and pictures of effluent in experiment (c).

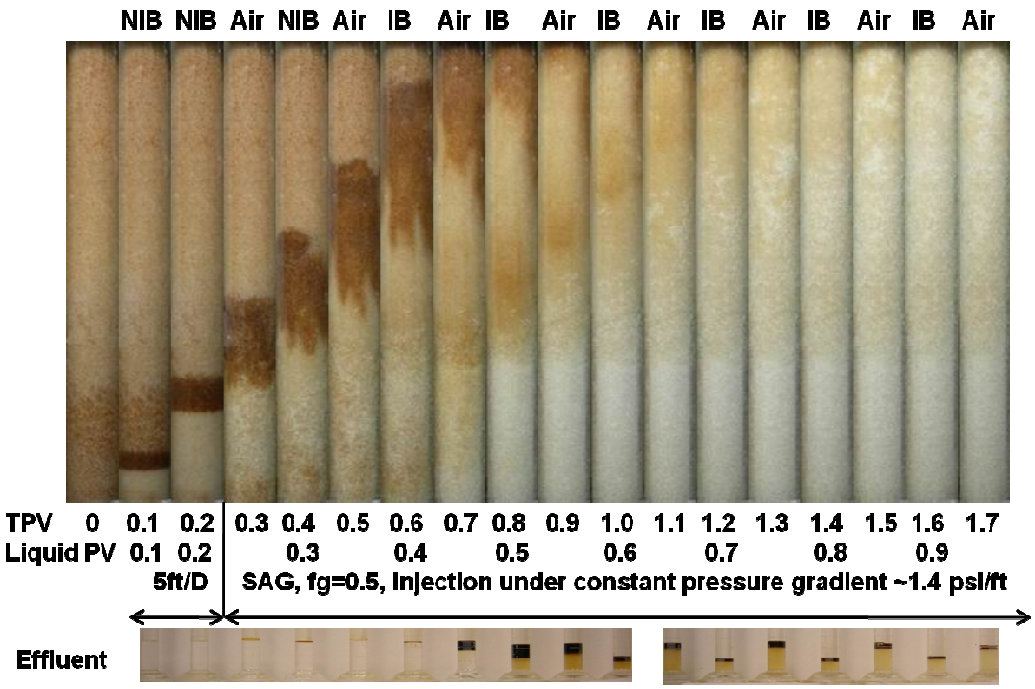

Figure 3-51 Displacement profiles and pictures of effluent in experiment (d).

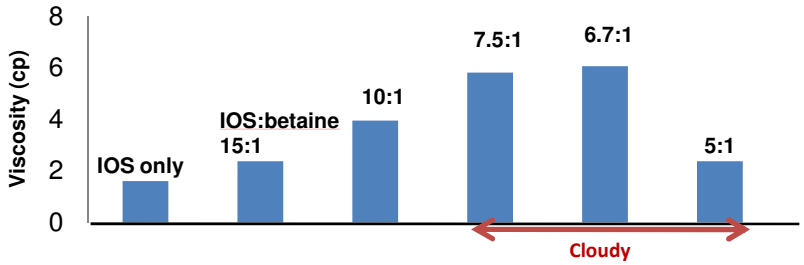

Figure 3-52 Viscosity with IOS15-18 and lauryl betaine blends in 1% Na_2CO_3 and 3.5% NaCl.

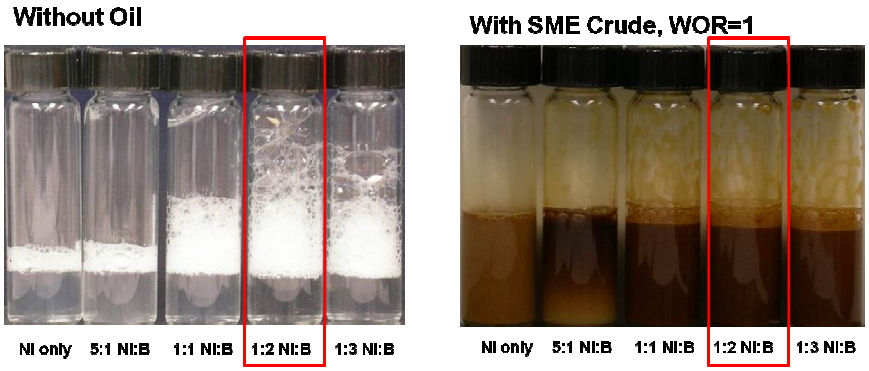

Figure 3-53 Qualitative foam stability test with NIB. All vials contain 0.5% lauryl betaine (except NI only) in 1% Na2CO3 and 3.5% NaCl.

3.2.6.5 NIB as One Formulation to Reduce IFT and Generate Foam for Mobility Control

It is commonly observed that for a given surfactant and oil, strong foam is generated at salinities far below optimum but not near the optimum, where IFT is minimized. This leads to a dilemma that a surfactant formulation that can reduce IFT to ultra low values is not a good foaming agent, and vice versa. As a consequence, in such a flooding process, foam is usually injected as a drive after the low-tension surfactant slug as the chapter has discussed so far. The disadvantage is that the low-tension surfactant slug is lacking mobility control, leading to poor sweep. It is ideal to develop a single surfactant formulation that can simultaneously reduce IFT to ultra low values and generate strong foam so that microscopic displacement as well as sweep efficiency will be greatly improved from the beginning of the chemical flooding process.

NIB by itself in a tertiary recovery process was evaluated as shown in Figures 3-54 to 3-57. Figure 3-54 shows there was a distinctive oil bank, and the oil bank was recovered within 1.1 TPV. It also shows gas did not break through the oil bank as the liquid fraction in the effluent was nearly 100%. Cumulative recovery from waterflood residual oil was 97% shown in Figure 3-55. Foam apparent viscosity was high (Figure 3-56) and injection rate was greatly reduced (Figure 3-57) once foamed was generated indicating favorable mobility.

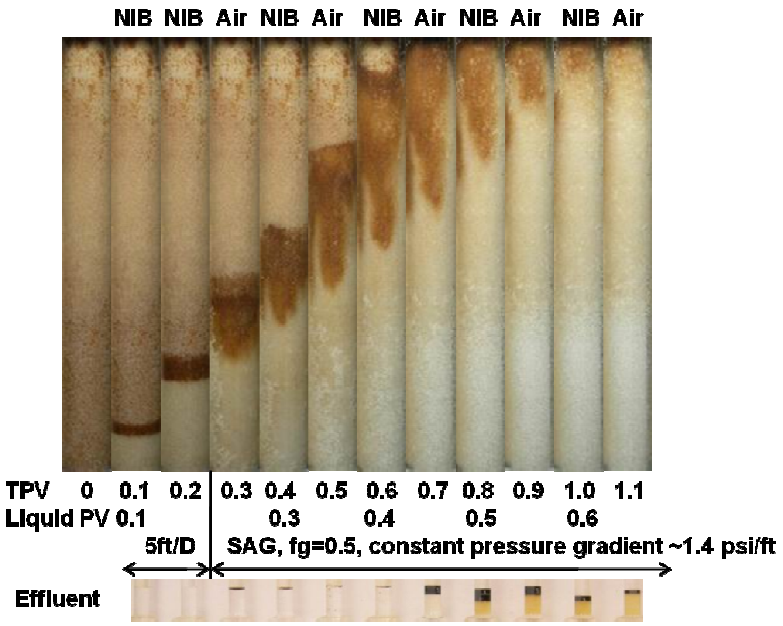

Figure 3-54 Displacement profiles and pictures of effluent in an ASF process using NIB alone.

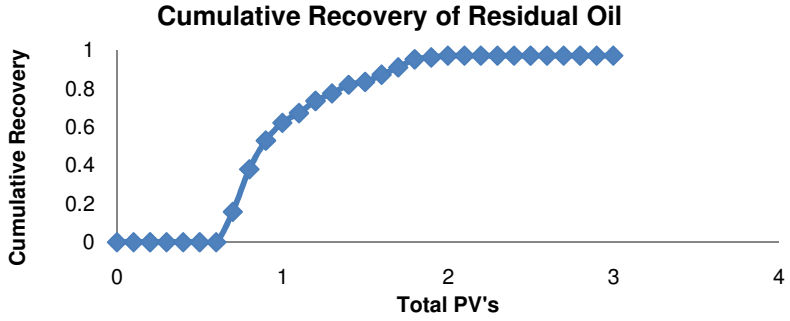

Figure 3-55 Cumulative recovery curves with NIB alone in a tertiary recovery process of residual SME.

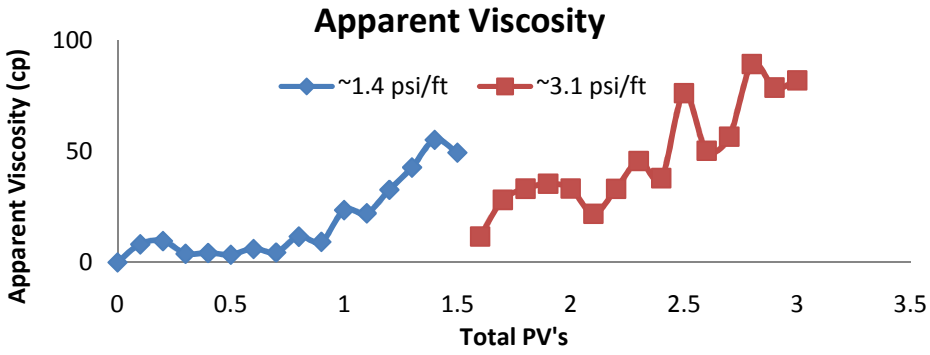

Figure 3-56 Foam apparent viscosity during the ASF process using NIB alone.

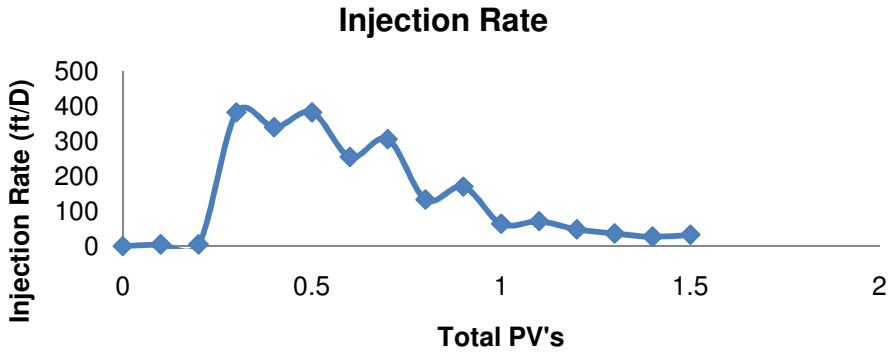

Figure 3-57 Injection rate during the ASF process using NIB alone.

From the displacement profiles in Figure 3-54, one can see there is a distinctive boundary in the middle of the sandpack below which foam was much dryer than above. Higher gas saturation resulted in stronger foam. This 'strong foam' front seemed to have stopped moving after 0.7 TPV. A higher pressure gradient may be needed to make strong foam propagate. Therefore, starting from the 1.6th TPV, fixed injection pressure was raised to 3.1 psi/ft. Figure 3-58 below shows comparison between 1.4 psi/ft and 3.1 psi/ft. Strong foam front did seem to propagate faster at higher pressure gradient.

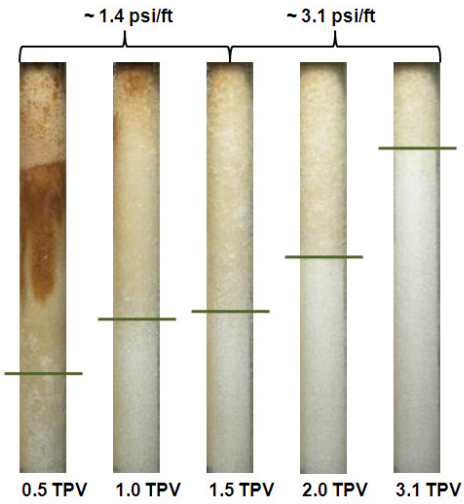

Figure 3-58 Propagation of 'strong foam' front. Green lines indicate the locations of the 'strong foam' front. Higher pressure gradient is needed in order for the strong foam to propagate.

3.2.6.6 NIB in Secondary Recovery of SME Crude

The formulation was then evaluated in a secondary recovery and its performance was compared with AOS 16-18 (Figures 3-59 to 3-61). Foam was not as strong as in the tertiary recovery case. This may have been due to the fact that oil saturation was much higher and it broke the foam. However, the cumulative recovery after 1.8 TPV was 99.6% from OOIP (Figure 3-61). This was much greater than 69% OOIP in the AOS 16-18 case, which was worse than waterflood because of air breaking through and flowing in continuous gas channels.

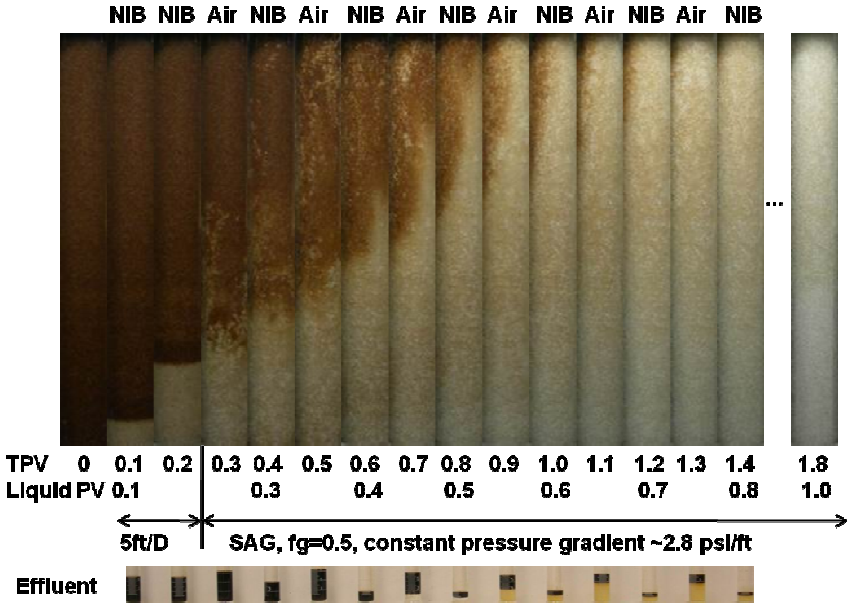

Figure 3-59 Foam using NIB alone in a secondary recovery. Flow direction was vertical.

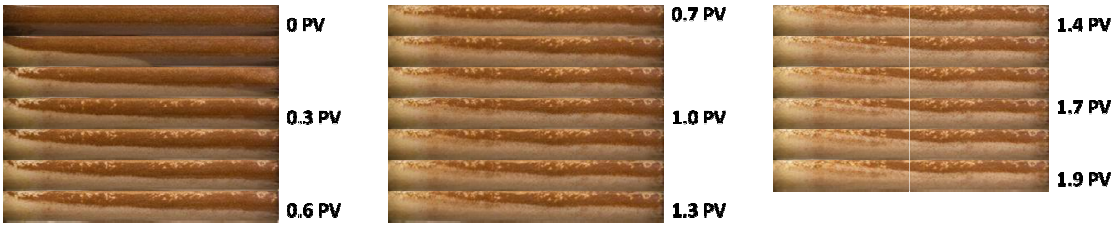

Figure 3-60 Foam using AOS 16-18 alone in a secondary recovery. Flow direction was horizontal.

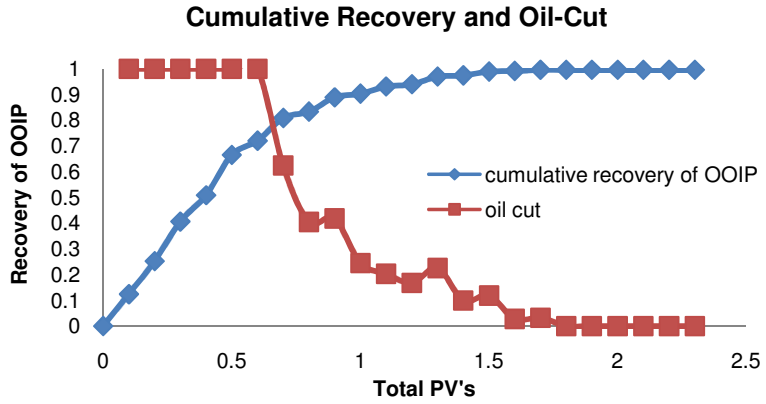

Figure 3-61 Cumulative recovery curves using NIB alone in a secondary recovery process of SME crude.

The oil bank observed during 0-0.2 TPV NIB injection in displacement profiles in Figures 3-51, 3-54, and 3-59 was a result of low IFT between SME and NIB. It happened during the first two slugs of NIB injection at a constant rate of 5 ft/D. There was a clear oil bank below which the residual oil saturation was near zero as the sand below the oil bank appeared to be the same color as clean silica sand. IFT can be estimated using a dimensionless trapping number which combines the capillary number and the bond number [Pope *et al.*, 2000]. The simplified trapping number in these 1-D homogeneous sandpacks becomes

$$N_T = \frac{k.(g.\Delta\rho+\nabla P)}{\sigma} \qquad \text{Equation 3-4}$$

In the experiment shown in Figure 3-54, for example, k the permeability was 174 darcy; g=9.8 m/s^2 is the gravitational acceleration constant; $\Delta\rho$ the density difference was 288 kg/m^3; ∇P the pressure gradient was 908 Pa/m (0.040 psi/ft). In order to reach near zero residual oil saturation, N_T needs to be greater than 10^{-3}. Consequently, IFT should be lower than 0.6 mN/m. The gravity term in this equation $g.\Delta\rho$ was more than three times

as big as the pressure gradient∇P. Buoyancy and high permeability can contribute to the displacement of trapped oil.

Gravity also improved sweep efficiency during early stage low-rate injection at 5 ft/D. A dimensionless gravity number in this 1-D experiment can be expressed as

$$N_g = \frac{kg\Delta\rho}{u\mu_o} \qquad \text{Equation 3-5}$$

where the oil viscosity μ_o was 3.93 cp. During 0-0.2 TPV, only NIB was injected at a low rate of 5ft/D. The calculated N_g=7.0, which is greater than unity. It indicates that, regardless of mobility ratio, a piston-like displacement front will always result [Hirasaki, 1975]. It accounts for the gravity-stabilized clear oil-bank in Figures 3-51, 3-54, and 3-59. Starting from 0.3th TPV, fluid was injected at a constant pressure (1.4 psi/ft), and injection rate was very high before strong foam was formed (Figure 3-57). At 0.3th TPV (air injection) and 0.4th TPV (NIB injection), the rate was 382 ft/D and 340 ft/D respectively. The calculated N_g=0.09, and N_g=0.10, respectively. N_g<<1 and slightly unfavorable mobility ratio explain the tailing effect behind the oil back after 0.3th TPV in Figure 3-54.

3.2.7 1-D ASF Processes in Water-Wet or Oil-Wet Crushed Limestone Sandpacks

NIB alone was evaluated in crushed limestone sandpacks. Experimental procedures were the same as in **3.2.6.5**, except for water-wet and oil-wet carbonate sand was used in lieu of silica sand. Carbonate sand was made to be oil-wet by first centrifuging to connate water saturation then aging in SME crude oil at 85°C for three weeks. These results are summarized in Table 3-5 and Figures 3-62 to 3-65. Figures 3-62 and 3-63 are displacement profiles and pictures of effluent. There was not a distinctive oil bank in

either cases. Figure 3-64 is cumulative recovery. Recovery from residual oil was 95.6% and 62.2% for water-wet and oil-wet carbonate sandpack respectively. Figure 3-65 is a plot of foam apparent viscosity. Strong foam was not formed.

Table 3-5 Comparison of silica and carbonate sandpacks using NIB

	Water-wet Silica	Water-wet $CaCO_3$	Oil-wet $CaCO_3$
Sandpack	174 darcy	162 darcy	180 darcy
Flow Direction	Vertical	Vertical	Vertical
Surfactant Formulation	NIB (0.2%N, 0.05%IOS, 0.5%betaine), 1.18 cp	NIB (0.2%N, 0.05%IOS, 0.5%betaine), 1.18 cp	NIB (0.2%N, 0.05%IOS, 0.5%betaine), 1.18 cp
Salinity	3.5% NaCl, 1% Na_2CO_3	3.5% NaCl, 1% Na_2CO_3	3.5% NaCl, 1% Na_2CO_3
Temperature	25 °C	25 °C	25 °C
Oil Viscosity	3.93 cp (25ºC)	3.93 cp (25ºC)	3.93 cp (25ºC)
Waterflood Residual Oil saturation	19%	12.4%	16.3%
Injection Rate/Pressure	5 ft/D NIB (0-0.2TPV); 1.4 psi/ft, 0.3-1.5TPV;	5 ft/D NIB (0-0.2TPV); 1.4 psi/ft, 0.3-1.5TPV	5 ft/D NIB (0-0.2TPV); 1.4 psi/ft, 0.3-1.5TPV
Slug Size	0.1 PV	0.1 PV	0.1 PV
Foam Generation	NIB alternating air; *fg*=0.5	NIB alternating air; *fg*=0.5	NIB alternating air; *fg*=0.5
Oil Breakthrough	0.7 TPV	1.1 TPV	0.3 then 0.9 TPV
Cumulative Recovery from Residual Oil	97%	95.6%	62.2%

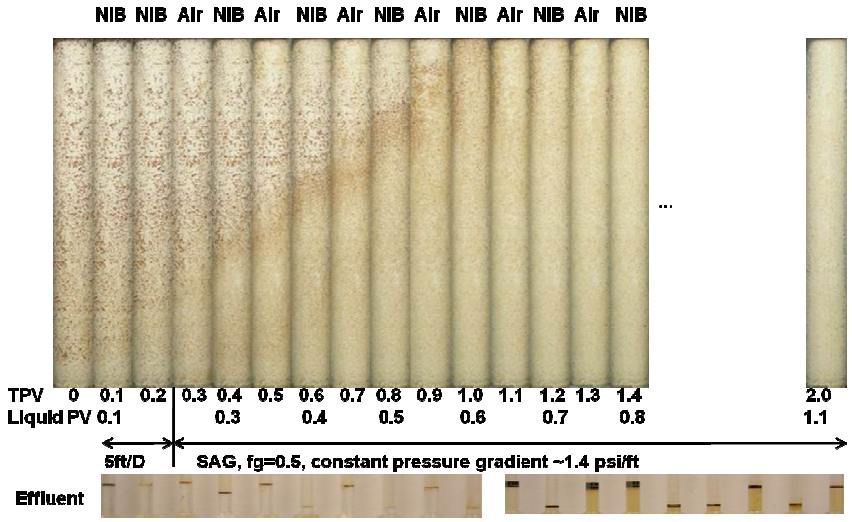

Figure 3-62 Displacement profiles and pictures of effluent using NIB (1:2) in an untreated water-wet carbonate sandpack.

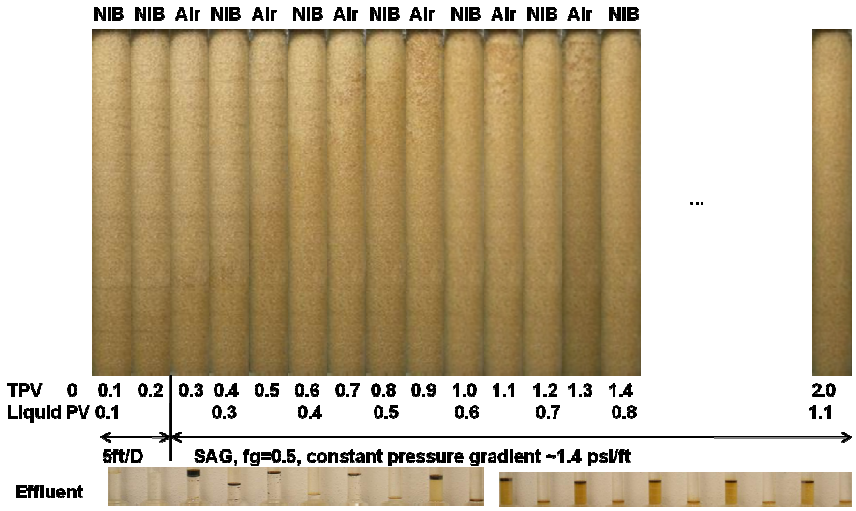

Figure 3-63 Displacement profiles and pictures of effluent using NIB (1:2) in an oil-wet carbonate sandpack.

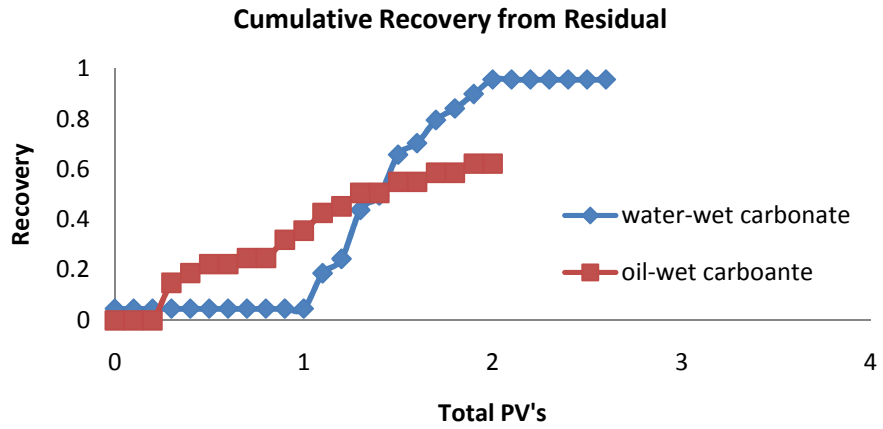

Figure 3-64 Comparison of cumulative recovery between two carbonate sandpack.

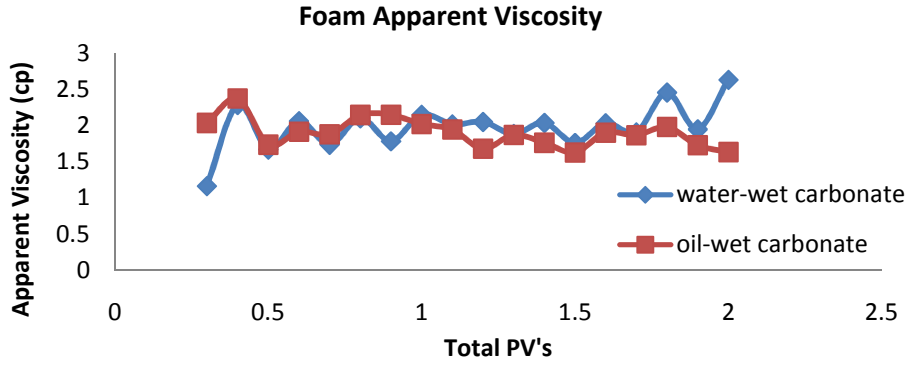

Figure 3-65 Comparison of foam apparent viscosity between two carbonate sandpack.

The oil and surfactant break-through was delayed in both carbonate sandpacks' experiment compared to that in the silica sandpack. This may have been due to surfactant adsorption on the carbonate mineral surface. Previous work in my group has suggested that 1% Na_2CO_3 was effective in reducing adsorption of NI in carbonates [Zhang, 2005; Liu, 2007], I suppose that either lauryl betaine was adsorbed or chromatographical separation among each component in NIB made the blending ratio deviate away from optimum. As a result, strong foam was not formed in either of the carbonate sandpacks.

3.3 Conclusions

In an oil-free system, Triton X-200, AOS16-18, IOS15-18, N25-7EO, N67-9EO were found to be good foaming agents at low salinity (1% Na_2CO_3, 2~3.5% NaCl). N25-7EO was a good foaming agent in SME brine. BASF Avanel surfactants, NI, DowFax8390 were not good foaming agents.

Without adding betaine at the optimal ratio, none of the surfactants or their blends would generate strong foam in the presence of residual SME crude oil.

A foam drive with surfactant SAG can be used as an alternative for polymer drive in ASP EOR. The apparent viscosity of SAG is a function of pressure gradient, permeability, and gas fraction. A moderately viscous (266 cp) oil was displaced successfully with ASP and SAG. The apparent viscosity of the displacement process was much less than that of the crude oil. The oil may have been dispersed by the foam as oil-in-water emulsion.

In 1-D forced displacement of residual SME crude oil, strong foam was formed in three cases: 1) with polymer, 2) with pre-generated foam, and 3) when betaine was added. Recovery was nearly 100% from residual oil in all cases, although it took many PV's for

the pre-generated foam. NI alone is not a good foaming agent. The addition of lauryl betaine made NIB a strong foaming agent with and without SME crude oil. NIB (NI:B=1:2) worked well in both secondary and tertiary recovery of residual SME in terms of reducing IFT and generating foam for mobility control in silica sandpacks.

NIB (NI:B=1:2) did not work in either water-wet or oil-wet carbonate sandpack due to possible surfactant adsorption.

3.4 References

Bertin, H.J., Apaydin, O.G., Castanier, L.M., and Kovscek, A.R. 1999. "Foam Flow in Heterogeneous Porous Media: Effect of Crossflow," *SPEJ,* (June 1999): 75-82.

Christov, N.C., Denkov, N.D., Kralchevsky, P.A., Ananthapadmanabhan, K.P., and Lips, A. 2004. "Synergistic Sphere-to-Rod Micelle Transition in Mixed Solutions of Sodium Dodecyl Sulfate and Cocoamidopropyl Betaine," *Langmuir, 20*, 565-571.

Kovscek, A.R. and Bertin, H.J. 2002. "Estimation of Foam Mobility in Heterogeneous Porous Media," SPE 75181 presented at the SPE/DOE Improved Oil Recovery Symposium, 13-17 April, Tulsa, Oklahoma.

Falls, A.H., Hirasaki, G.J., Patzek, T.W., Gauglitz, P.A., Miller, D.D., and Ratulowski, J. 1988. "Development of a Mechanistic Foam Simulator: The Population Balance and Generation by Snap-Off," *SPE Res Eng* **3** (3): 884–892. SPE-14961-PA. doi: 10.2118/14961-PA.

Heller, J.P. 1994. "CO_2 Foam in Enhanced Oil Recovery," in Schramm, L.L., *Foams: Fundamentals and Applications in the Petroleum Industry*, American Chemical Society, Washington, DC.

Hirasaki, G. J., "Sensitivity Coefficients for History Matching Oil Displacement Processes", *SPEJ* (February 1975), 39-50.

Li, R.F., Yan, W., Liu, S., Hirasaki, G.J., and Miller, C.A.: "Foam Mobility Control for Surfactant Enhanced Oil Recovery," *SPE J.* (December 2010) SPE-113910-PA.

Liu, S, Li, R.F., Miller, C.A., and Hirasaki, G.J. 2008a. "Alkaline/Surfactant/Polymer Processes: Wide Range of Conditions for Good Recovery," *SPE J.* **15** (2): 282-293. SPE-113936-PA.

Liu, S., Zhang, D.L., Yan, W., Puerto, M., Hirasaki, G.J., Miller, C.A. 2008b. "Favorable Attributes Of Alkaline-Surfactant-Polymer Flooding," *SPEJ,* (March, 2008b): **5-16**.

Liu, S., "Alkaline Surfactant Polymer Enhanced Oil Recovery Process," Ph.D. thesis, Rice University, Houston, TX, 2007

Nguyen, Q.P., Currie, P.K., Zitha, P.L.J. 2005. "Effect of Crossflow on Foam-Induced Diversion in Layered Formations," *SPEJ,* (March 2005): 54-65.

Osterloh, W.T. and Jante, M.J. 1992. "Effects of Gas and Liquid Velocity on Steady-State Foam Flow at High Temperature," SPE 24179, presented at the SPE/DOE Enhanced Oil Recovery Symposium, 22024 April, Tulsa, Oklahoma.

Pope, G.A., Wu, W., Narayanaswamy, G., Delshad, M., Sharma, M.M., Wang, P., 2000. "Modeling Relative Permeability Effects in Gas-Condensate Reservoirs with a New Trapping Model," *SPE Reservoir Eval. and Eng.* 2000 **3**(2) 171-178

Rossen, W.R., and Gauglitz, P.A., "Percolation Theory of Creation and Mobilization of Foam in Porous Media," *AICHE J.,* 36, 1176-1188, 1990

Szafranski, R. "Laboratory development of the surfactant/foam process for aquifer remediation," Ph.D. thesis, Rice University, Houston, TX, 1997

Tanzil, D., Hirasaki, G.J., and Miller, C.A. "Conditions for Foam Generation in Homogeneous Porous Media," paper SPE 75176, 2002a.

Tanzil, D., Hirasaki, G.J., and Miller, C.A. 2002b. Mobility of Foam in Heterogeneous Media: Flow Parallel and Perpendicular to Stratification. *SPE J.* **7** (2): 203–212. SPE-78601-PA. doi: 10.2118/78601-PA.

Yan, W. "Foam for mobility control in alkaline/surfactant enhanced oil recovery process",.Ph.D. thesis, Rice University, Houston, TX, 2005

Zhang, D., "Surfactant-Enhanced Oil Recovery Process For a Fractured, Oil-wet Carbonate Reservoir", .Ph.D. thesis, Rice University, Houston, TX, 2005

Chapter 4

PROCESSES IN 2-D HETEROGENEOUS SANDPACKS

In this chapter, alkaline/surfactant/foam (ASF) processes in 2-D heterogeneous sandpacks are experimentally demonstrated. These experiments included water-wet and oil-wet silica, and crushed limestone sandpacks. The permeability ratio of the 2-D system was 19:1 in silica sandpacks and 6.4~8.3:1 in crushed limestone sandpacks. Foam mobility control was first shown in two oil-free systems with or without inter-layer capillary communication. Surfactant alternating gas (SAG) injections at various pressure gradients and gas fractions were compared with waterflood and water alternating gas (WAG) injections. Two types of crossflows associated with foamflood were identified and their effect on fluid distribution was illustrated. Next, a successful surfactant-induced wettability alteration and gravity drainage tertiary recovery process was demonstrated in a CTAB-treated, oil-wet silica sandpack during a 42-day system shut-in and a subsequent foamflood. It was compared with an untreated silica sandpack which did not allow system shut-in. Last, similar processes were repeated using crushed limestone that was aged in crude oil either at environmental room temperature (37~42 °C), or at 85°C after initial water saturation was reduced by centrifuging.

4.1 Experimental

4.1.1 Materials

The following surfactants or their blends were used: Neodol 67-7PO (ammonium C16-17 7PO sulfate, Stepan); IOS 15-18 (sodium 15-18 internal olefin sulfonate, Shell); AOS 16-18 (sodium 16-18 alpha olefin sulfonate, Stepan); Lauryl betaine (Rhodia). NI is a blend of 4:1 (wt/wt) Neodol 67-7PO and IOS 15-18. NIB is a blend of 4:1:10 (wt/wt/wt) Neodol 67-7PO, IOS 15-18 and lauryl betaine unless otherwise stated. CTAB (hexadecyltrimethylammonium bromide, Matheson Coleman & Bell) was used for wettability alteration.

Crude oil used was SME [API=41.1°, 3.93 cp at 25°C, Total acid number (TAN) = 0.062 mgKOH/g].

Two silica sands from U.S. Silica Company were used in the flow experiments: Oil Frac 20/40 (100-200 darcy); F-110 (4.8 darcy). Silica flour (US Silica MIN-U-SIL 30) was used in the zeta potential measurements. Two crushed limestone carbonate sands from Nolanville, TX were used: N16/20 (219 darcy) and N40/120 (29 darcy).

Na_2CO_3 (anhydrous, certified American Chemical Society) and NaCl (biological certified) were both obtained from Fisher Scientific.

In oil-free experiments, aqueous solution was made green by dissolving 3 mL green food dye (water, propylene glycol, yellow 5, blue 1, purchased from Kroger) in 1000 mL brine.

4.1.2 Construction of the 2-D Heterogeneous Sandpack

The 2-D system was made of stainless steel with a glass observation window of 1.25 in. thickness in the front. The interior was a 20 in. by 3 in. by ¾ in. chamber. There were 21 ports with 60 and 200 mesh screens: 3 on the left, 3 on the right and 15 at the back.

The construction of the model is shown in Figure 4-1 [Szafranski, 1997]. The pressure ports were designed for pressure measurement during flow experiment. These inner pressure taps helped overcome end piece effects which could otherwise result in extra pressure drop.

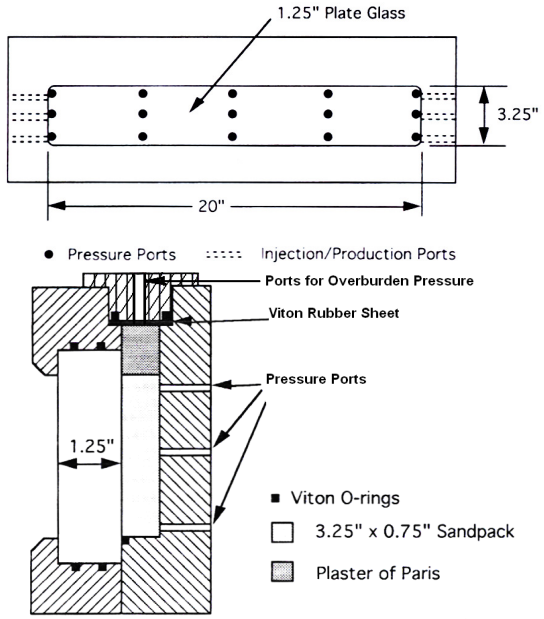

Figure 4-1 Front and side view of the 2-D model.

Take the silica sandpack for example. The model was packed with two layers of silica sand: Oil Frac 20/40 overlaying F-110. Of the top and bottom layers, the thickness ratio was 2:3 and the permeability ratio was 19:1 (90 and 4.8 darcy). The total pore volume (TPV) was 332.1 mL. The overall porosity was 0.381 and the measured overall permeability was 38.5 darcy. Overall permeability was measured by injecting water through a manifold as shown in Figure 4-2. Pressure drop across the entire sandpack was measured. Overall permeability was thence calculated using single-phase Darcy's law. Figure 4-2 is a photograph of the sandpack saturated with water.

Figure 4-2 Photograph of the 2-D heterogeneous sandpack. Arrows show direction of flow through manifolds.

4.1.3 Surface Properties Determination

The zeta potential of clean, CTAB-treated silica flour was measured by Beckman Instrument Coulter DELSA 440 (conductivity 2.37~2.46 mS/cm, 1% wt solid in 0.02 mol/L NaCl). An Olympus SZX12 stereo microscope equipped with a camera was used in taking microscopic pictures on the pore level. Water receding and advancing contact angles were measured by KSV Instrument with CAM2008 software. [Treiber *et al.* 1972; Hjelmeland *et al.* 1986; Yang *et al.* 2000]. Three types of microscopic glass slides with different surface properties were used:

1) Clean glass: to mimic the natural state of silica surface;

2) CTAB-treated glass: clean glass slides mentioned above were soaked in CTAB (~ ½ CMC) solution for 20 min, and rinsed with sufficient deionized water before use;

3) CTAB- then NI- treated glass: CTAB-treated glass slides as above were soaked in an aqueous solution of NI blend for 20 min and rinsed with sufficient deionized water before use.

Water receding contact angle: a drop of oil was carefully formed by gradually dispensing oil from the syringe to contact the glass surface. Water receding contact angle was measured when contact line appeared at equilibrium after about 5 minutes.

4.2 Results and Discussion

4.2.1 Overall Permeability

In permeability measurements, DI water was injected from all three inlets either at constant rate or constant pressure into the sandpack pre-saturated with DI water. Pressure drop was measured by inner pressure taps at the back of the model, which eliminated the end piece effect. Figure 4-3 is a schematic of the locations of the inner pressure taps where pressure transducers were connected. Volumetric flow rate of liquid and gas (before gas break-through) was determined by volume of effluent divided by duration of injection.

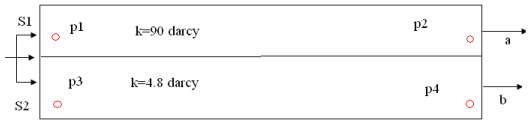

Figure 4-3 Position of inner pressure taps. Red circles show the positions of inner pressure taps. Black arrows show the flow direction. S1 and S2 are the cross sectional areas of upper and lower layer.

Theoretically, when flow is parallel to the bedding, the overall permeability of n parallel layers is the arithmetic average of each layer with permeability k_i thickness h_i.

$$k_{overall} = \sum_{i=1}^{n} k_i h_i / \sum_{i=1}^{n} h_i \qquad \text{Equation 4-1}$$

Let h be the height of the sand in the sandpack. Since the height ratio of upper layer coarse sand to lower layer fine sand is 2:3, from Equation 4-1, the overall permeability in the 2-D system

$$k_{overall} = \frac{88.8darcy \times 0.4h + 4.76darcy \times 0.6h}{0.4h + 0.6h} = 38.4darcy$$

Experimental measurements were carried out by injecting water either at constant rate or under constant pressure. The measured values as well as the calculated arithmetic average are listed in Figure 4-4 and Table 4-1. Experimental results agreed with theoretical calculation very well.

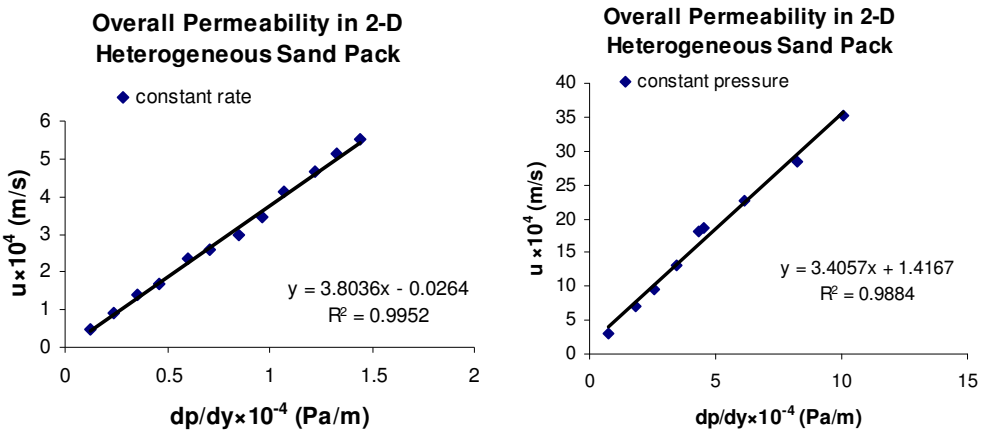

Figure 4-4 Measured overall permeability in the 2-D sandpack. *k*=38.5 darcy for injection at constant rate and *k*=34.5 darcy for injection at constant pressure.

Table 4-1 Overall permeability in the 2-D heterogeneous sandpack

Permeability	by calculation	constant rate	constant pressure
k (darcy)	38.4	38.5	34.5

4.2.2 Foam Mobility Control in an Oil-Free 2-D Heterogeneous Sandpack

In foam-aided sweep experiments, the sandpack was initially filled with green water. SAG injection scheme under constant pressure (4, 6, and 8 psig) was adopted with a liquid slug size of 0.1 pore volume (PV). Fluid was injected into all three inlets through a manifold. Pictures were taken at the end of each slug of fluid injection. Each picture was converted to a binary image, *i.e.,* green and non-green. Fraction of green area represents the residual saturation. Sweep efficiency can be calculated by

$$\text{Sweep Efficiency} = \frac{\text{Area of non-green}}{\text{Total Area}} \qquad \text{Equation 4-2}$$

After each experiment, the sandpack was thoroughly purged. First, it was washed with 10 PV's of water. Next it was purged with CO_2 at 10 psig for 30 minutes. Water flushing and CO_2 purging were repeated twice. Finally, it was washed with 10 PV's water.

In WAG experiments, procedures were similar to those of SAG experiments except in WAG, water was injected instead of surfactant solution. Water and gas were injected at 4 psig with various f_g (gas fraction) from 0 (water only) to 4/5.

4.2.2.1 Sweep with Water or WAG

Sweep of the layered sandpack with water only and with WAG is compared in Figure 4-5. The upper, high-permeability layer was quickly swept in either water only or WAG injection cases. However, multiple PV injection was required to sweep the lower-permeability layer. The injection volume is expressed as total fluid (liquid plus gas). Inspection shows that sweep of the low-permeability layer is a function only of the liquid volume, *i.e.*, independent of the volume of gas injected. This can be seen by comparing the sweep at 2, 4, and 6 TPV in Figure 4-5 for water only, f_g=1/2, and f_g=2/3, respectively.

4.2.2.2 Foam Mobility Control

Sweep with surfactant alternating with gas (SAG) is compared with water only in Figure 4-6. The surfactant solution was 0.2% AOS 16-18 in 1% Na_2CO_3 and 2% NaCl. The sandpack was completely swept with 1.3 TPV with the SAG process (f_g=1/3 at 6

psig). By comparison the low-permeability layer was only 1/3 swept with water only at the same injection volume.

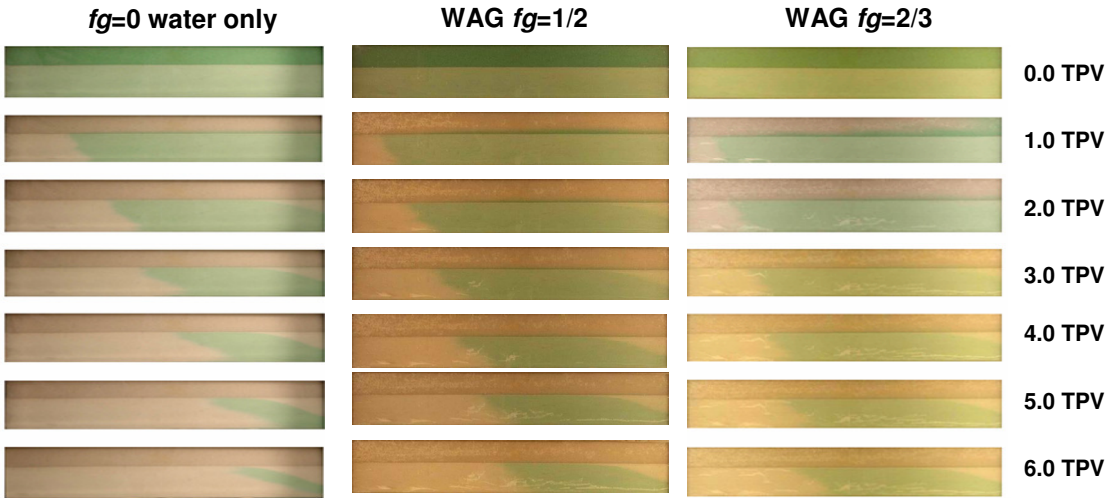

Figure 4-5 Profiles of sweep with waterflood or WAG in 19:1 permeability ratio sandpack.

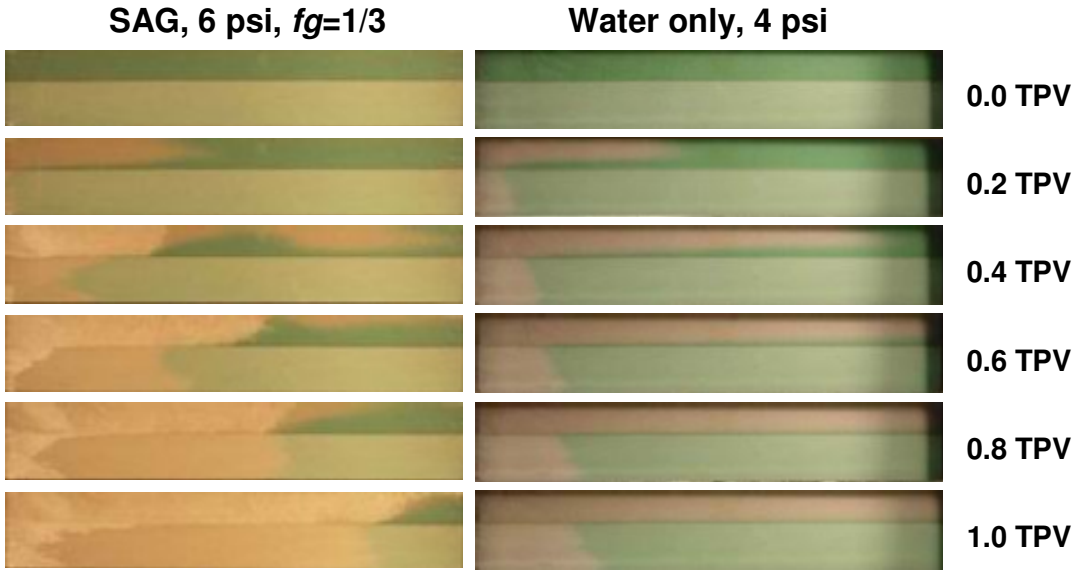

Figure 4-6 Comparison of SAG with waterflood in 19:1 permeability ratio sandpack.

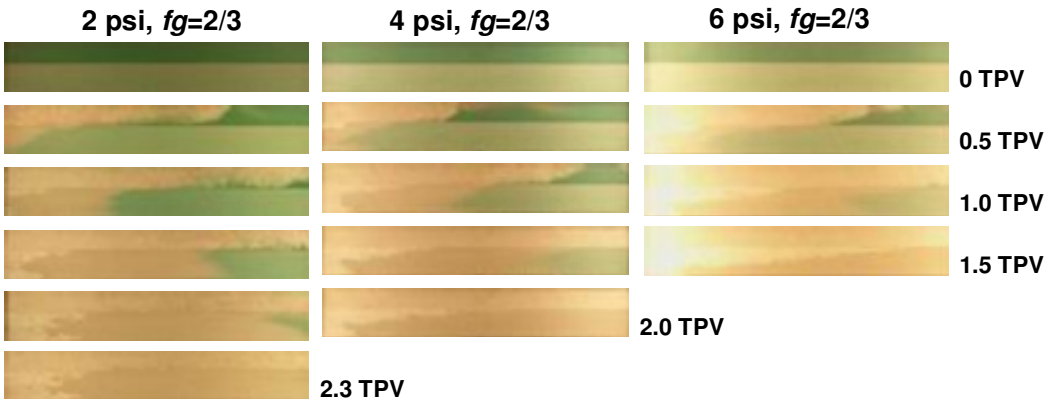

Figure 4-7 SAG injection at 2, 4, 6 psig with f_g=2/3. Injection at 8 psig did not differ much from 6 psig. Last photo in each column indicates 100% sweep efficiency.

Sweep with SAG of different injection pressures is compared in Figure 4-7. Sweep improved with increase in injection pressure from 2 to 6 psig. There was very little improvement with changing injection pressure to 8 psig. This is consistent with the interpretation that a critical pressure gradient must be exceeded to generate strong foam by bubble division.

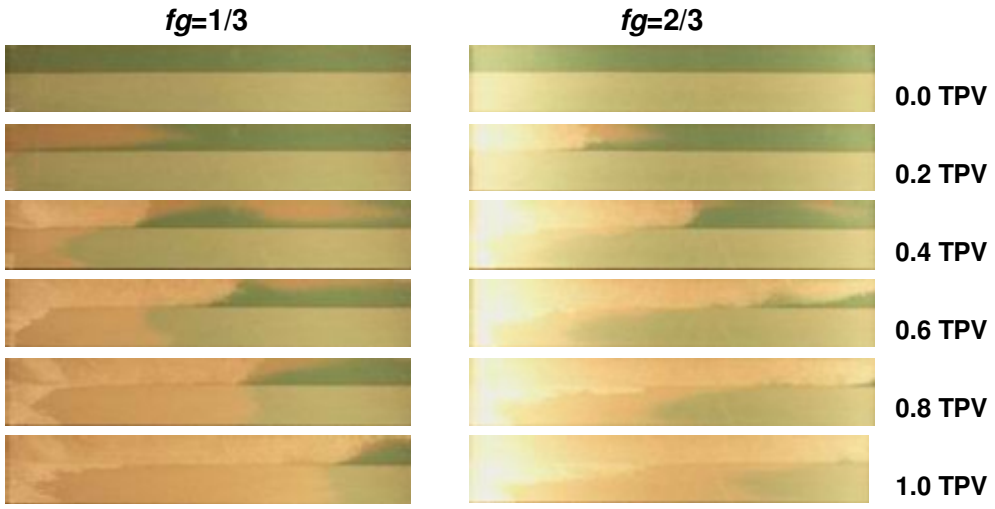

Figure 4-8 Comparison of SAG with f_g=1/3 and 2/3 at 6 psig injection pressure.

Sweep of SAG with different gas fractions at 6 psig injection pressure is compared in Figure 4-8. To achieve 100% sweep efficiency, it took 1.3 and 1.5 TPV for f_g=1/3 and 2/3, respectively. Expressed as liquid volume, it took 0.87 and 0.5 LPV, respectively.

In addition, 0.2% IOS 15-18 in brine as a foaming agent was compared with 0.2% AOS 16-18 in a foam-aided sweep as shown in Figure 4-9. Both surfactants could generate foam as effective mobility control, and behaved very similarly.

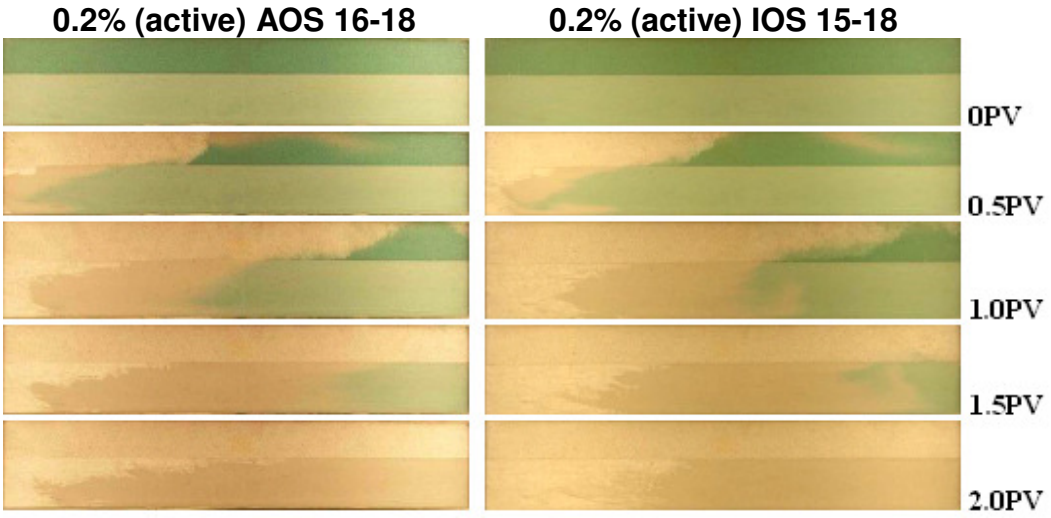

Figure 4-9 Foam-aided sweep with different surfactants. 4 psig, f_g=2/3, slug size=0.1 PV.

4.2.2.3 Sweep Efficiency

The sweep efficiency of all experiments is summarized in Figure 4-10. Here sweep is expressed as a function of liquid volume injected since this groups waterflood and WAG together. SAG clearly has better sweep efficiency in this system with a 19:1 permeability contrast.

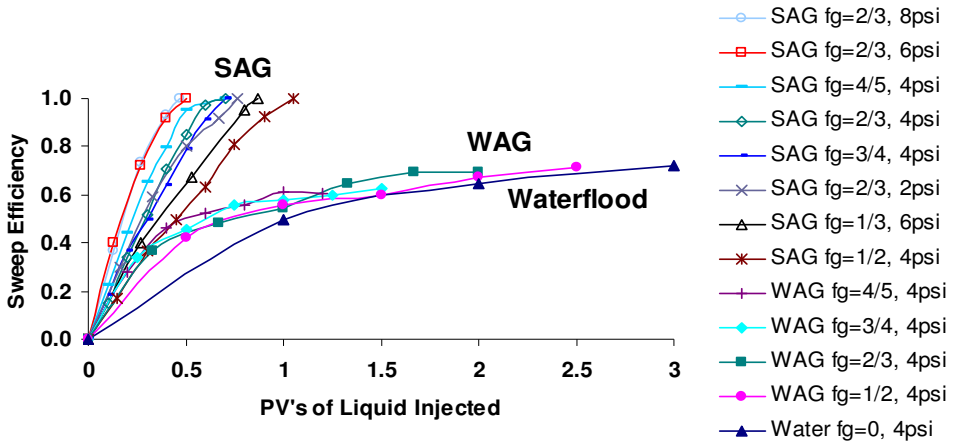

Figure 4-10 Sweep in 19:1 permeability contrast sandpack with SAG, WAG, and waterflood.

4.2.2.4 Description of the Crossflow

The crossflow associated with foam between the two layers had an important role in improving sweep efficiency. Two types of crossflow were identified as illustrated in Figure 4-11. The first type of crossflow occurred behind the foam front in the high-permeability layer, diverting surfactant solution into the low-permeability layer as shown in Figure 4-12. The second type of crossflow occurred from the low-permeability layer to the high-permeability layer, ahead of the foam front as shown in Figure 4-13.

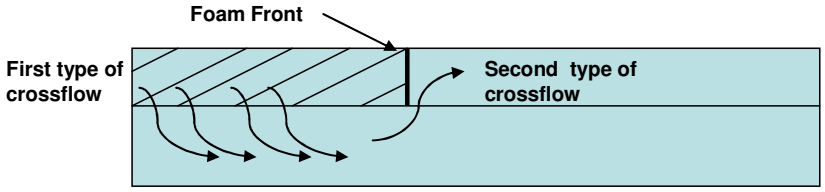

Figure 4-11 Schematic illustrating two types of crossflow during foam flooding.

Figure 4-12 Example of diversion by crossflow of liquid (colorless) behind foam front in high-permeability layer to the low-permeability layer. 0.8 TPV SAG with f_g=1/3, 6 psig injection pressure.

Figure 4-13 Example of crossflow of the second type: crossflow of green-dyed liquid from low-permeability to high-permeability ahead of the foam bank. 0.4 TPV, f_g=1/3, 6 psig injection pressure.

The diversion of liquid from foam in the high-permeability layer to the low-permeability layer is an important attribute of foam and required further study. After the green-dyed water was completely swept out of the sandpack at 1.3 TPV (f_g=1/3 experiment in Figure 4-6), the experiment was continued by injecting green-dyed surfactant-slugs alternating with gas as shown in Figure 4-14. At 1.3 TPV foam had entered only about 15% of the low-permeability layer. At 1.5 TPV the green color is apparent in the high-permeability layer and near the layer-boundary in the low-permeability layer. Subsequent photos show the green-dyed surfactant solution progressively sweeping out the low-permeability layer by the end of 2.1 TPV. Recall that the waterflood in Figure 4-5 had not completely swept the low-permeability layer after as much as 6 PV.

The crossflow mentioned here is a recognized attribute of favorable mobility ratio displacement in layered systems [Zapata, 1981]. In a layered system with large permeability contrast, with foam flow, the fluid that was diverted into the low-permeability layer was primarily the liquid component of foam, and foam is stronger in high permeability zones than in low permeability zones as will be discussed in the following section. Polymer or alkaline/surfactant/polymer (ASP) may only provide mobility control in each individual zone or in a homogenous system, because polymer solution of a given concentration has the same viscosity in all layers regardless of permeability difference.

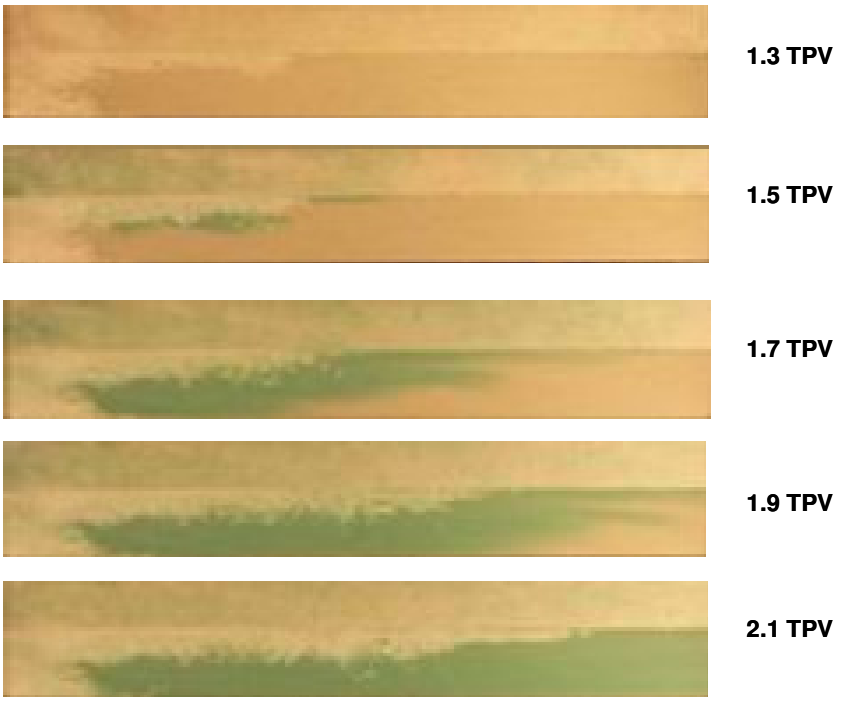

Figure 4-14 Diversion of green-dyed surfactant solution from high- to low-permeability layer**.**

4.2.2.5 Distribution of Produced Liquid

The distribution of produced liquid between the two layers was measured to interpret the mechanisms for the improved sweep with foam. Figure 4-15 shows the liquid produced from the upper, high-permeability and the lower, low-permeability layer during f_g=1/3 SAG injection at 20 ft/day after foam had been well established in the high-permeability layer. The production from individual layers was measured from the produced fluids from the top and bottom flow lines in Figure. 4-2. Figure 4-15 shows that nearly all of the liquid was produced from the low-permeability layer. During periods of gas injection, foam was produced from the high-permeability layer, but flow from the high-permeability layer stopped during liquid injection. Thus foam was successful in diverting nearly all of the liquid to the low-permeability layer even though the permeability contrast was 19:1.

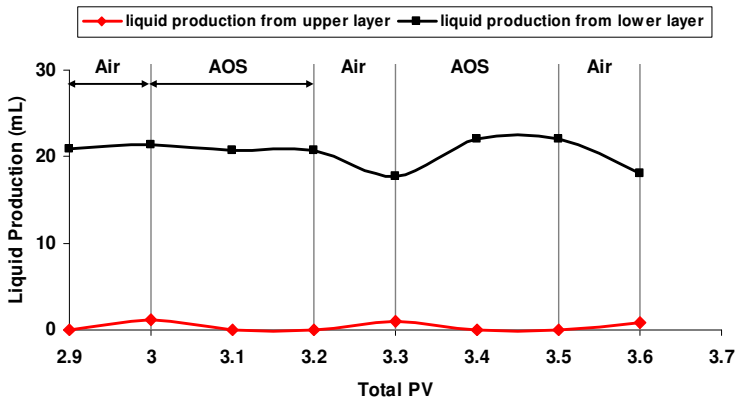

Figure 4-15 Liquid production from the upper and lower layers.

4.2.2.6 Apparent Viscosity with WAG and SAG

WAG apparent viscosity is shown in Figure 4-16. Foam (SAG) apparent viscosity based on averaged permeability of the 2-D sandpack is shown in Figure 4-17 and 4-18. If treated as single-phase flow, foam apparent viscosity was calculated from single-phase Darcy's law, $\mu_{app} = \frac{k}{uL}(P - P_{static})$, where k was the measured permeability of the sandpack, u was the superficial injection velocity, L was the length of the sandpack, and (P–P_{static}) was the pressure difference across the sandpack. For detailed description of Darcy's law, please refer to Chapter 2. Foam had much higher apparent viscosity than waterflood or WAG.

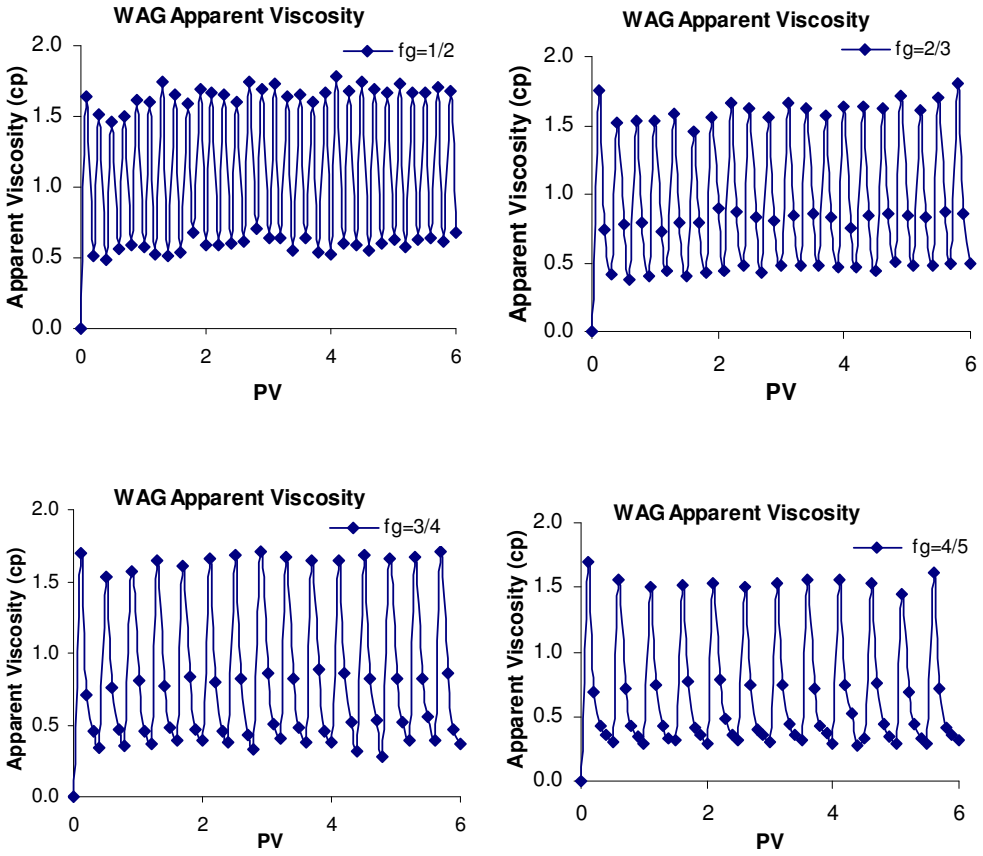

Figure 4-16 WAG apparent viscosity in the 2-D sandpack at 4 psig, 0.1 PV slug size. The top row indicates water injection, and lower rows indicate air injection.

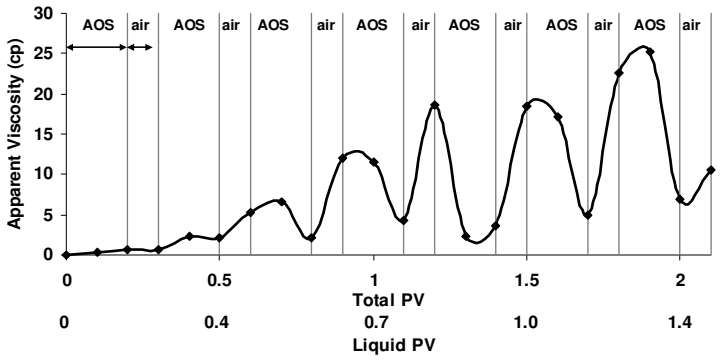

Figure 4-17 Apparent viscosity during SAG injection at 6 psig.

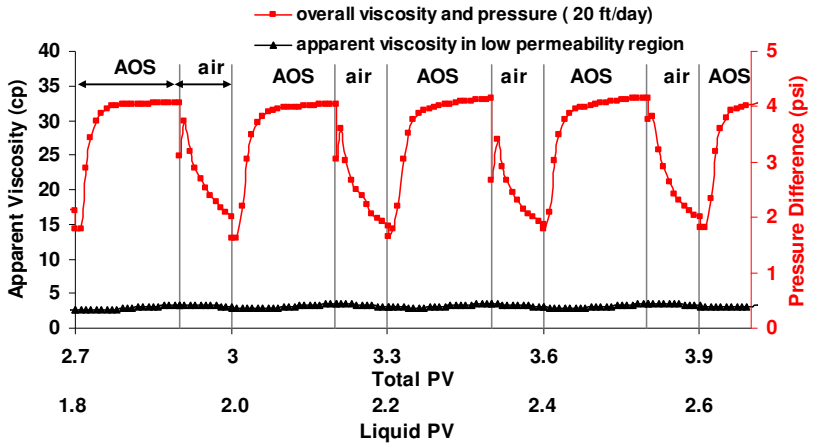

Figure 4-18 Apparent viscosity during SAG injection at 20 ft/day.

The apparent viscosity with constant pressure and constant rate injection are compared in Figure 4-17 and 4-18. It is remarkable that SAG injection at 6 psig had apparent viscosity increasing during gas injection and decreasing during surfactant injection while the constant rate experiment (at lower pressures) had the opposite trend. During constant pressure injection, the air injected needed to first overcome the yield stress associated with foam before it could enter and further create more foam lamellae. The yield stress is one of the characteristics of strong foam. The time caused for gas injection to overcome the foam yield stress reduced the average injection rate, and therefore, a higher apparent viscosity calculated from Darcy's law.

Figure 4-17 shows the apparent viscosity increasing gradually with continued SAG injection. The sandpack was initially filled with water (1 cp). SAG injection at 6 psig (3.6 psig/ft) was greater than the critical pressure gradient required for strong foam of about 1.5 psig/ft. The slow increase in apparent viscosity was not because of lack of generation of foam. Apparently the preferential flow of gas in the high-permeability layer and diversion of liquid to the low-permeability layer redistributed the flow as to have lower

apparent viscosity than in the 1-D experiments, as discussed in Chapter 3. This is consistent with observations of foam flow in a 3-D sandpack [Li, 2006].

It was mentioned earlier that only liquid was produced from the low-permeability layer. The apparent viscosity for flow in the low-permeability layer was computed using the flow from that layer, pressure drop across the internal pressure taps, and the permeability of the low-permeability layer. The apparent viscosity in the low-permeability layer was only slightly greater than that of water. This was the case when there was no gas in most of this layer and virtually all the injected liquid entered this layer not far from the injection point. Thus a combination of flow redistribution and permeability dependence of apparent viscosity compensates for the 19:1 permeability contrast.

4.2.3 Foam Mobility Control in Two Oil-Free Parallel 1-D Sand Columns

Crossflow as a result of capillary communication between two layers was discussed in the last section. Here, foam mobility control in a heterogeneous system where capillary communication was not allowed will be demonstrated in two isolated parallel sand columns. Figure 4-19 is a schematic of such a system. Both sandpacks had the same pressure drop. There was no cross flow. One sandpack was packed with US Oil Frac 20/40 (75 darcy), the other was packed with US Silica F-110 (8.9 darcy). Overall measured permeability was 41 darcy. Between two columns, thickness ratio was 1:1. Permeability ratio was 8:1.

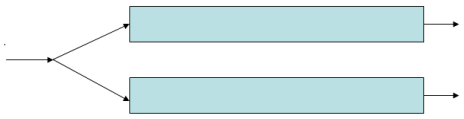

Figure 4-19 Schematic showing the system comprised of two parallel sand columns without crossflow.

Three experiments were carried out in this system: water only, WAG, SAG (foam). The injection pressure was maintained at a constant value, *i.e.* 4 psi. In WAG and SAG cases, f_g=2/3. The liquid slug size is 0.2 TPV in water only injection, 0.1 PV in WAG and SAG injection. In water only experiment, it took ~0.6 TPV to sweep out green water in high permeability region and ~3.0 TPV to sweep out the entire system as shown in Figure 4-20. In WAG injection experiment, it took ~1.2 TPV in high permeability region and after 1.5 TPV there was still over 80% left unswept in the low permeability region as shown in Figure 4-21. In SAG injection experiment, it took ~1.0 TPV to sweep out green water in high permeability region and 1.5 TPV to sweep out the entire system, as shown in Figure 4-22.

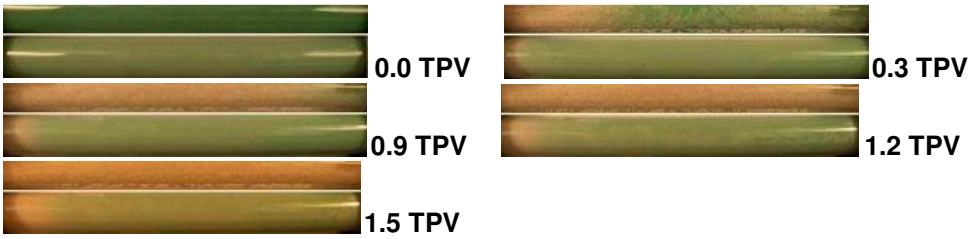

Figure 4-20 Profiles of WAG injection. Green water was first swept out in the high permeability column at ~1.2 TPV. At 1.5 PV, there was >80% green water left unswept in the low permeability region.

Apparent viscosity with these three cases was plotted in Figure 4-23. SAG injection had the highest apparent viscosity among all three injection schemes. In this parallel system, since the inlets were interconnected. Foam apparent viscosity should be close in value in two sand columns. If foam apparent viscosity was higher in the top column, then

surfactant solution and air would be retarded in this column and be diverted to the bottom column, where foam would develop and foam apparent viscosity would increase. Once foam apparent viscosity in the bottom column was higher than the top, vice versa, fluid would be diverted into the top column and foam would further develop in it. In other words, foam apparent viscosity in both columns would catch up with each other.

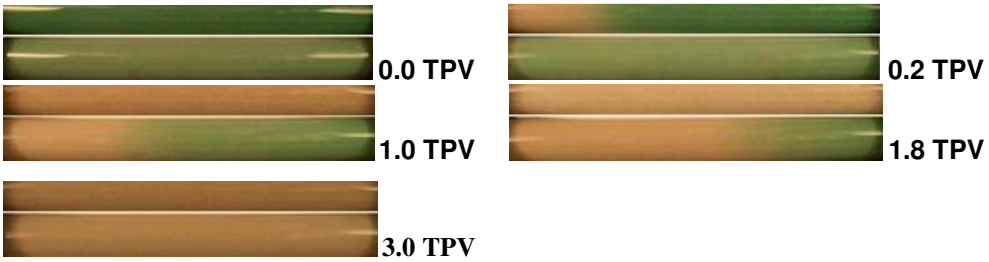

Figure 4-21 Profiles of waterflood. Green water was first swept out in the high permeability column at ~0.6 TPV. Green water was swept out in the low permeability at ~3.0TPV.

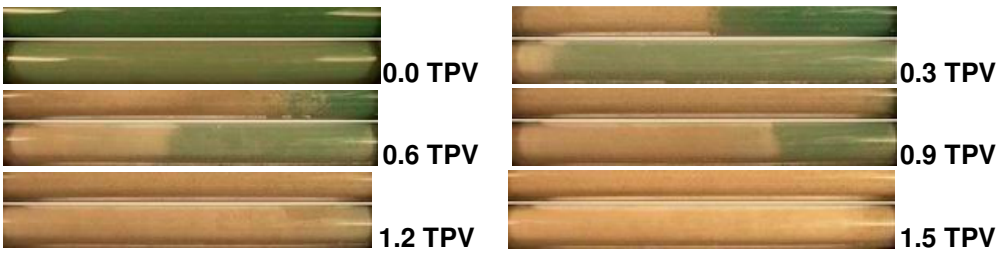

Figure 4-22 Profiles of SAG injection. Green water was first swept out in the high permeability column at ~1.0 TPV. At 1.5 PV, green water in the low permeability was swept.

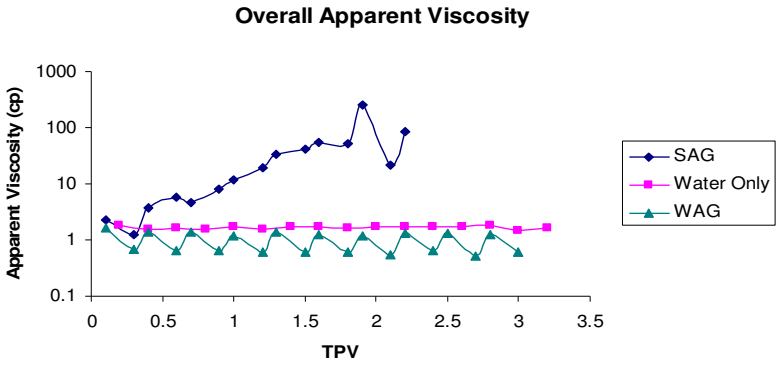

Figure 4-23 Foam apparent viscosity.

4.2.4 2-D Alkaline/Surfactant/Polymer/Foam (ASPF) Process in a Clean Water-Wet Silica Sandpack

The sandpack was purged with 5 cycles of total 18000 mL DI water (~54 PV) through various injection ports located on the side and at the back of the sandpack prior to this experiment. Specifically, each purging cycle was comprised of CO_2 purging (2.5 psig, 30 minutes), and 3600 mL DI water flushing.

Oilflood was carried out by injecting SME crude through various injection ports located at the back of the sandpack. Oil saturation after oilflood is 86.0%. Figure 4-24 shows profiles during oilflood.

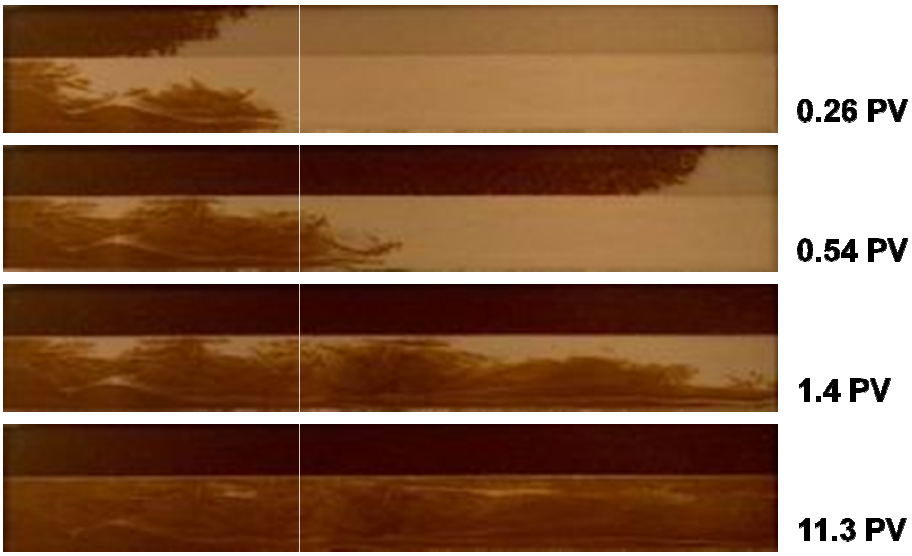

Figure 4-24 Profiles during Oilflood.

Waterflood was carried out 6 days after oilflood by injecting 2% NaCl through a manifold of three injection ports on the left end of the sandpack, as shown in Figure 4-2. Total of 1661 mL (~5 PV) brine was injected. ASPF flood was carried out 224 days later. Immediately before ASPF flooding, 374 mL (~1.1 PV) brine was injected at 5 ft/D. A

total of 140 mL oil was produced from waterflood. Waterflood recovered 49.1% OOIP (original oil-in-place). Figure 4-25 shows profiles during waterflood.

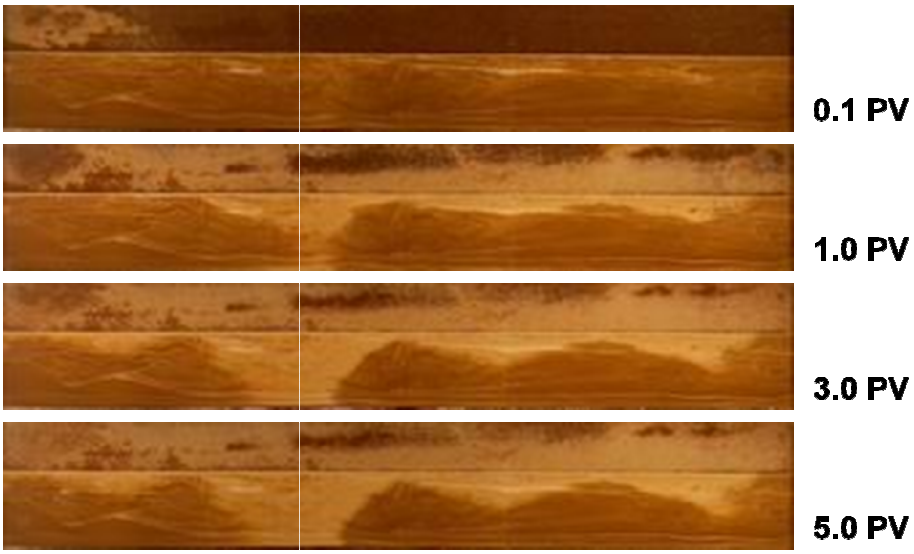

Figure 4-25 Profiles during waterflood.

Chemical slugs of liquid alternating air (SAG) were injected with *fg*=1/3 through a manifold into all three inlets located on the left end of the 2-D model. Injection scheme was as follows: 0.1 PV NIP (NI and polymer)→0.1 PV NIP→0.1PV Air; 0.1 PV NIP→0.1 PV IOS→0.1PV Air; 0.1 PV IOS→0.1 PV IOS→0.1PV Air; 0.1 PV IOS→0.1 PV IOS→0.1PV Air; etc. The first 0.2 PV of NIP was injected at a fixed rate of 5 ft/D and the rest of the slugs were injected at a fixed pressure of 6 psig. 0.1 PV air was at compressed condition of 6 psig. Fixed-rate injection of chemical slugs was carried out by a syringe pump (Harvard Apparatus). Fixed-pressure injection was controlled manually by adjusting the injection rate. Pressure was monitored by a pressure transducer connected to a PC. Figure 4-26 shows profiles during ASPF flood. Figure 4-27 is a picture of effluent samples. Fig. 4-28 is a plot of cumulative recovery. Figure 4-29 shows foam apparent viscosity. Table 4-2 is a summary of this experiment. The oil bank formed

in the upper layer as shown in Figure 4-26 was a result of favorable mobility control by polymer. However, unlike foam that has higher apparent viscosity in high- than in low-permeability layers, polymer does not have such 'biased' viscosity behavior, and its viscosity is uniform in both layers. Therefore, the ASP slug still bypassed the lower layer, and the remaining unrecovered oil saturation in the lower layer was still high after the process.

Figure 4-26 Sweeping profiles during ASPF flooding.

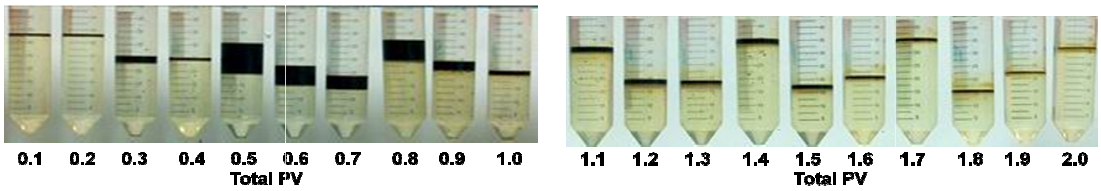

Figure 4-27 Picutres of effluent.

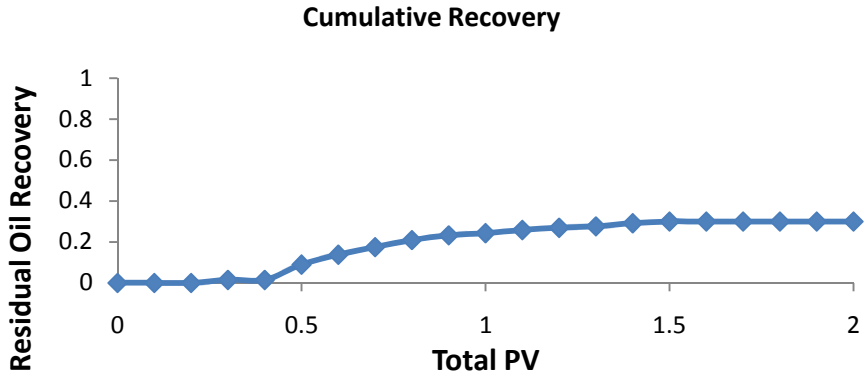

Figure 4-28 Plot of Cumulative Recovery.

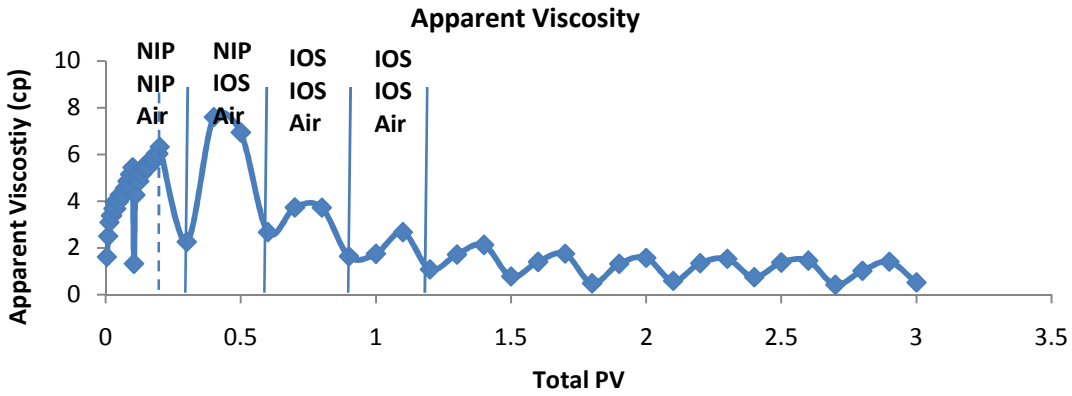

Figure 4-29 Apparent Viscosity.

Table 4-2 Summary of 2-D ASPF in the untreated clean silica sandpack

2-D Sandpack	Silica, coarse sand overlays fine sand; Porosity 0.381; Thickness Ratio 2:3; Permeability Ratio 19:1; Overall permeability 38.5 darcy; Pore Volume: 332.1 mL
Oilflood	11.3 PV oil (2 PV fresh oil, 9.3 PV recycled oil); Oil Saturation before Water Flooding 86%
Waterflood	6.1 PV 2% NaCl; Waterflood remaining oil saturation: 43.8%;
Chemical Slugs	ASP Slug: 1% Na_2CO_3,0.2% NI blend, 2000ppm polymer 2% NaCl; Foam Drive: 1% Na_2CO_3,0.5% IOS15-18, 2% NaCl;
Injection Scheme	0.1 PV NIP (5 ft/D)→0.1 PV NIP (5 ft/D)→0.1PV Air (6 psig); 0.1 PV NIP (6 psig)→0.1 PV IOS (6 psig)→0.1PV Air (6 psig); 0.1 PV IOS (6 psig)→0.1 PV IOS (6 psig)→0.1PV Air (6 psig); etc.
Recovery	30.0% from residual oil; 64.3% from original oil-in-place (OOIP)

Immediately after ASPF process, oil in the lower layer started to move upwards due to gravity and reduced IFT hence reduced capillary pressure. Figure 4-30 shows such phenomenon.

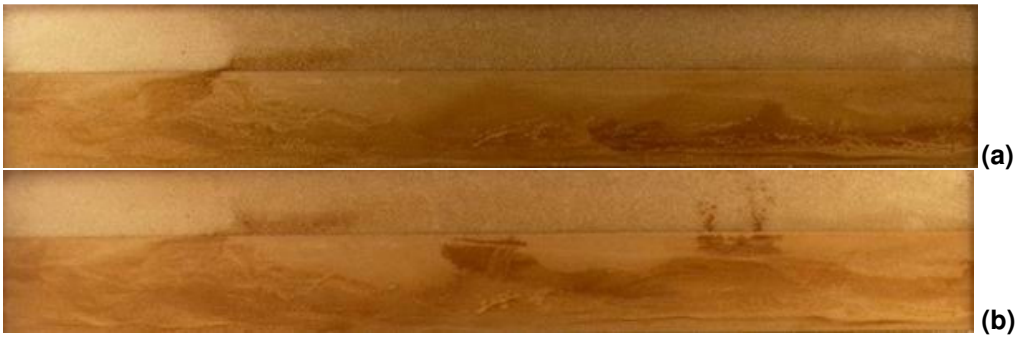

Figure 4-30 (a) is a picture taken at the end of ASPF flooding; (b) is a picture taken 10 days later.

4.2.5 2-D Alkaline/Surfactant/Foam (ASF) Process in a CTAB-Treated Oil-Wet Silica Sandpack

Silica sand was treated to be preferentially oil-wet with CTAB (1/2 CMC). Oilflood was carried out by injecting SME crude through various ports located at the back of the

sandpack. Waterflood was carried out first at low then at high flow rate to demonstrate viscous forces dominating capillary pressure and gravity by injecting brine through a manifold at the inlet. The sandpack was restored to the condition where capillary pressure dominated viscous forces, and lower tight layer remained relatively high oil-saturated by re-doing oilflood followed by waterflood at low flow rate. Alkaline surfactant (NI) was injected for 0.5 PV and the system was then shut in for 42 days to induce gravity (buoyancy) and capillary pressure driven counter-current flow. Foamflood was carried out after thickness of the oil rim accumulated on top of the sandpack stopped growing. SAG injection scheme was adopted with *fg*=1/3, slug size=0.1 PV, at ~2.7 psig. Figure 4-31 is a summary of cumulative recovery. Table 4-3 summarizes this experiment. A detailed description of various aspects of the experiment is given in the following sections.

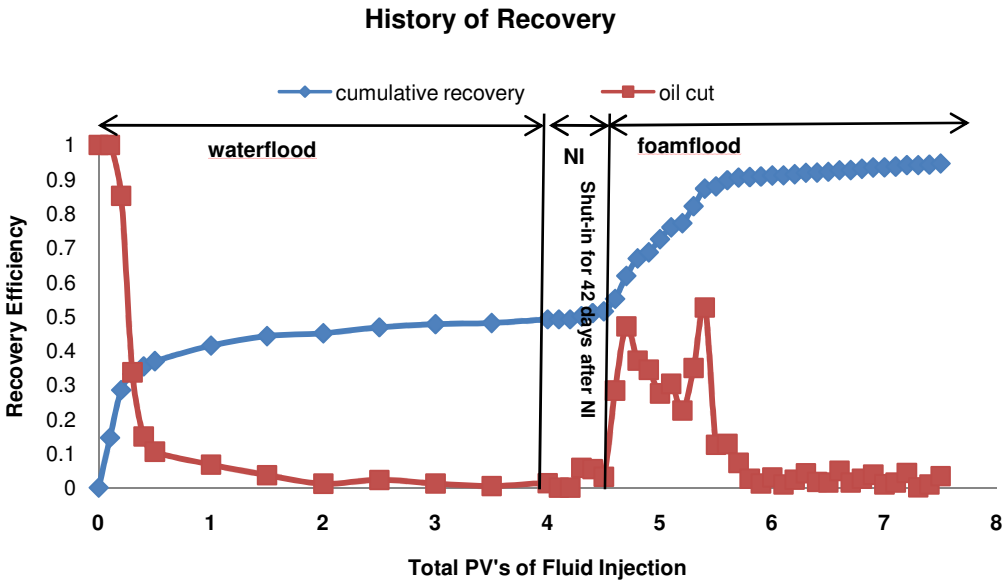

Figure 4-31 Summary of cumulative oil recovery and oil cut. Recovery efficiency was based on oil-in-place after 2nd oilflood.

Table 4-3 Summary of 2-D CTAB-treated SME ASF flood

2-D Sandpack	CTAB-treated silica, coarse sand overlays fine sand; Porosity 0.38; Thickness Ratio 2:3; Permeability Ratio 19:1; Overall permeability 44.0 darcy; Pore Volume: 330.0 mL
1st Oilflood	16.6 PV oil (2 PV fresh oil, 14.6 PV recycled oil); 5 ft/D Oil Saturation: 75.1%
1st Waterflood (2% NaCl)	4 PV (5ft/day ~0.1 psig) Cumulative Recovery: 54.1% OOIP 13.7 PV (2-5 psig, ~140-390 ft/D) Cumulative Recovery: 76.2% OOIP Remaining oil saturation: 17.9%
2nd Oilflood	1.5 PV recycled oil; 5-10 ft/D; Oil Saturation: 62.4%
2nd Waterflood (2% NaCl)	4 PV (5ft/day ~0.1 psig) Cumulative Recovery: 49.1% of oil-in-place based on 2nd oilflood. Remaining oil saturation: 31.8%
Chemical Slugs	NI: 0.2% NI, 1% Na_2CO_3, 2% NaCl; Foam Drive: 0.5% IOS15-18, 1% Na_2CO_3, 2% NaCl;
Injection Scheme	0.5 PV NI (1 ft/D); Cumulative Recovery 51.5% of oil-in-place based on 2nd oilflood. Remaining oil saturation: 30.3% Shut-in for 42 days; 0.1 PV IOS (1 ft/D)→0.1 PV IOS (1 ft/D)→0.1PV Air (2.7 psig); 0.1 PV IOS (2.7 psig)→0.1 PV IOS (2.7 psig)→0.1PV Air (2.7 psig); etc. Cumulative Recovery: 94.6% of oil-in-place based on 2nd oilflood. Remaining oil saturation: 3.4%

4.2.5.1 Surface Treatment with CTAB

CTAB can effectively alter the wettability of clean silica surface from preferentially water-wet to preferentially oil-wet. Furthermore the wettability of CTAB-treated surface can be altered back to preferentially water-wet in the presence of anionic surfactants *e.g.* NI. Zeta potential measurements showed CTAB-treated silica flour surface was positively charged (29.2 mV), compared to negatively charged untreated clean silica surface (-53.9 mV). Figure 4-32 shows water receding and advancing contact angle

measurements on various glass surfaces in 1% NaCl. When $0°<\theta<75°$ a surface is preferentially water-wet, and when $115°<\theta<180°$ it is preferentially oil-wet, where θ is the contact angle measured through the water phase [Morrow 1990]. Figure 4-33 is a microscopic picture of CTAB-treated silica soaked in brine. Water drops can be seen in big pores whereas oil was coating the surface of the sand grain, showing that the CTAB-treated sand was preferentially oil-wet. From these measurements, it is concluded that CTAB was able to effectively change the wettability of glass surface from preferentially water-wet to preferentially oil-wet. Anionic surfactants such as NI could alter the wettability of CTAB-treated glass from preferentially oil-wet back to preferentially water-wet.

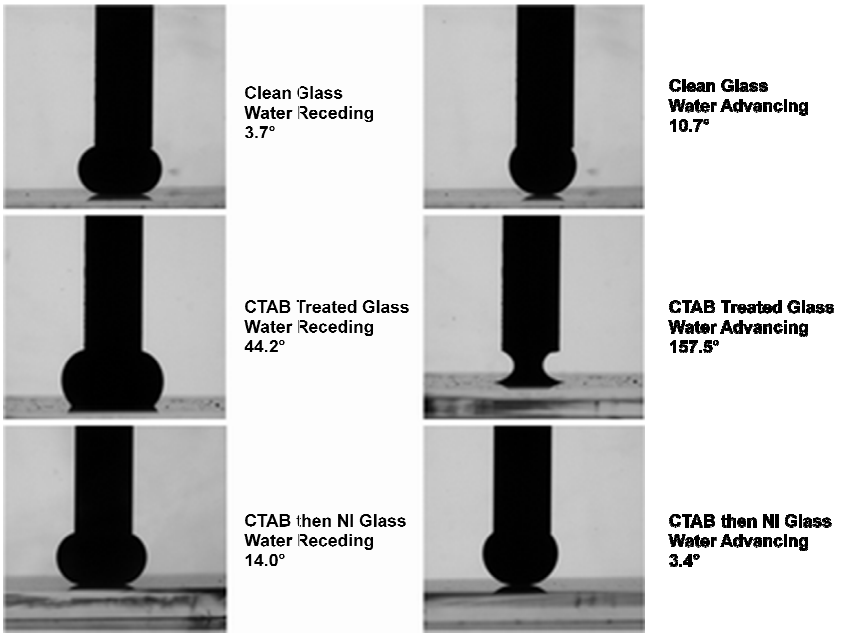

Figure 4-32 Water receding and advancing contact angles with oil on glass.

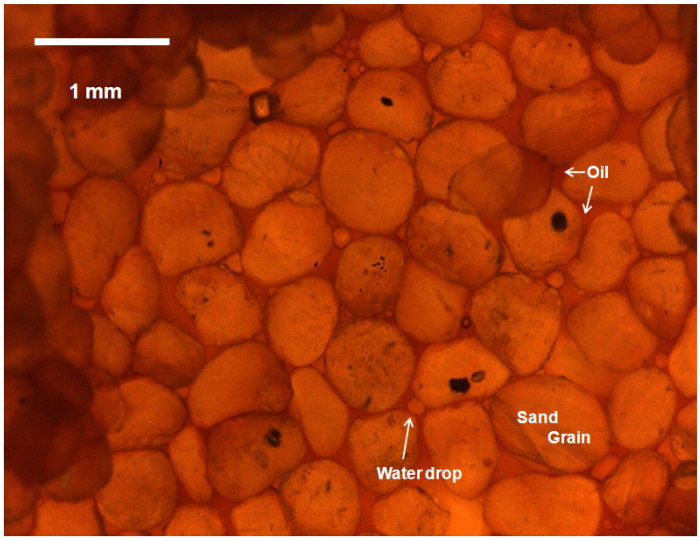

Figure 4-33 Microscopic picture of CTAB-treated silica sand.

4.2.5.2 Oilflood

Oil saturation after the first oilflood was 75.1%. Figure 4-34 shows profiles.

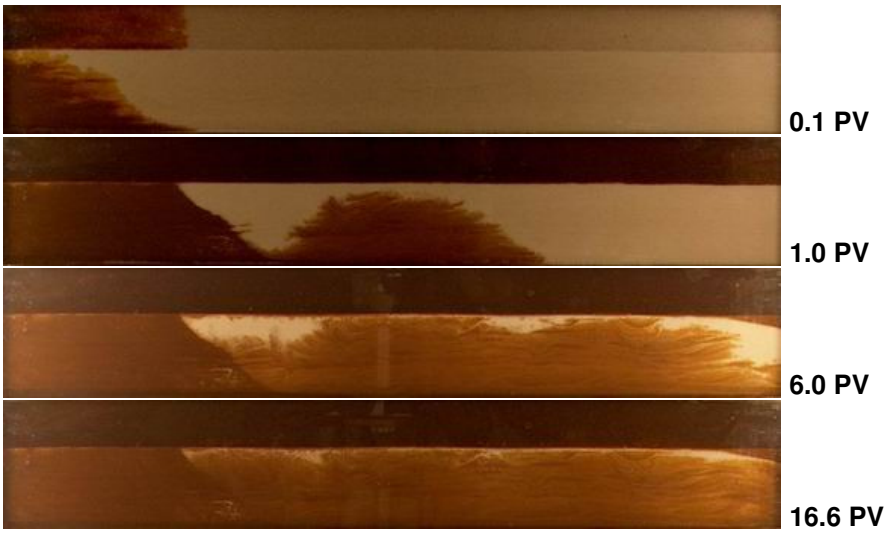

Figure 4-34 Profiles during the first oilflood.

4.2.5.3 Waterflood

At low rate waterflood (5 ft/D ~0.1 psig), capillary pressure dominated viscous forces, and oil saturation remained high in lower tight layer. Cumulative recovery at this

point was 54.1% OOIP. At high rate (2-5 psig, ~140-390 ft/D), oil in the lower tight layer became mobilized because viscous forces dominated capillary pressure. Cumulative oil recovery at this point was 76.2% OOIP. Figure 4-35 shows injection rate and pressure. Figure 4-36 shows profiles during waterflood. Figure 4-37 shows recovery from this waterflood.

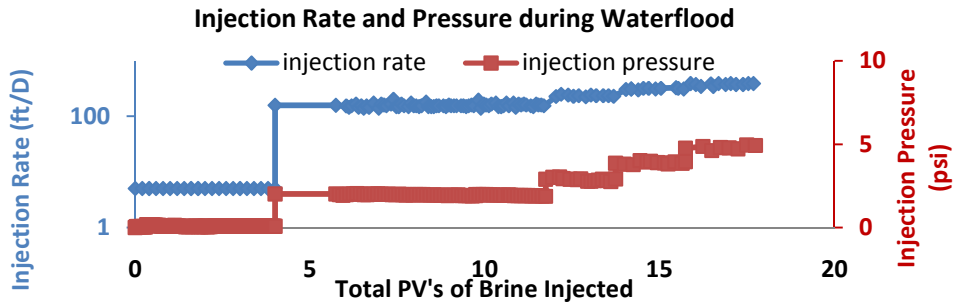

Figure 4-35 Injection rate and pressure during waterflood.

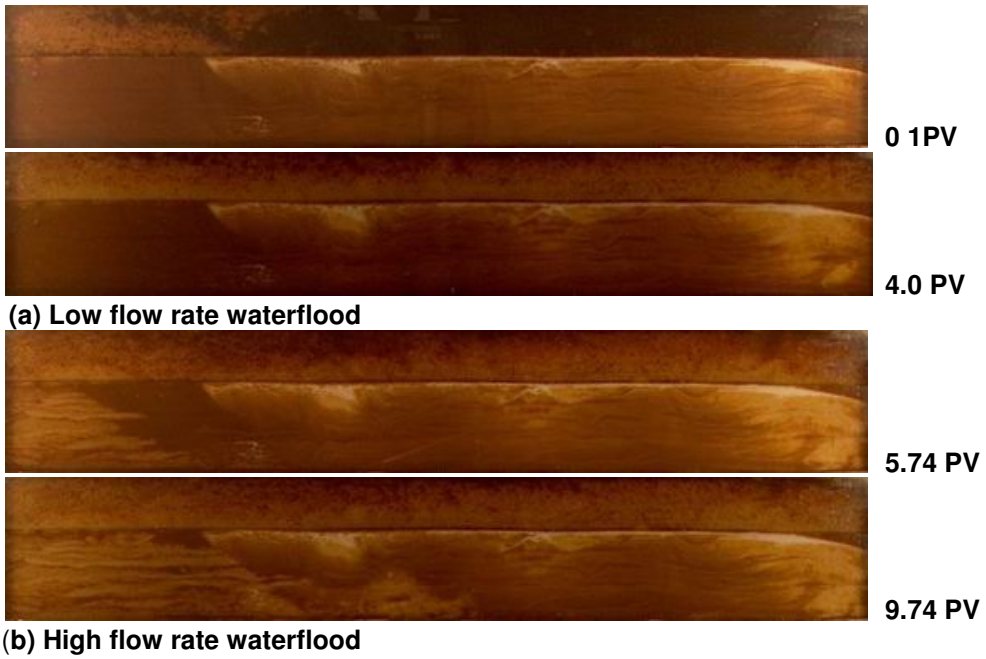

Figure 4-36 Profiles during waterflood. (a) at low flow rate (5 ft/D, ~0.1 psig) injection; (b) at high flow rate injection (2-5 psig, ~140-390 ft/D).

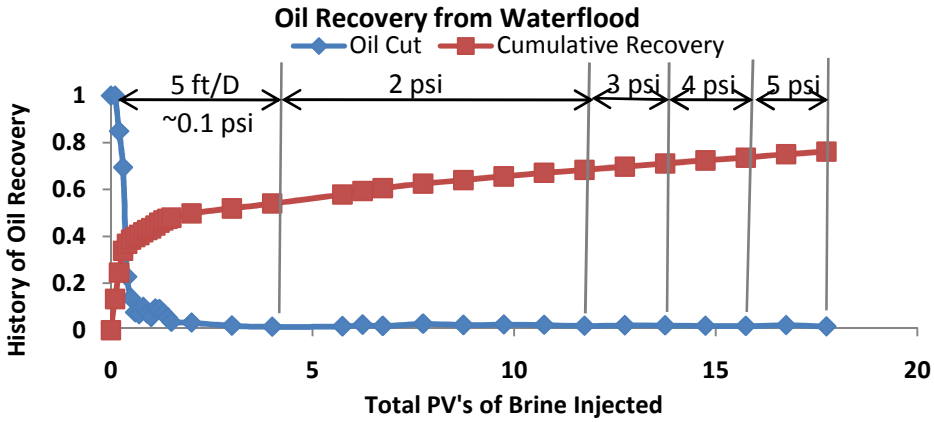

Figure 4-37 Oil recovery during the first waterflood.

4.2.5.4 Restoration

Restoration to Oilflooded Condition. Oil was injected at 5 ft/D, and later 10 ft/D (during 1.2-1.5 PV) for total of 1.5 PV's through various injection ports located at the back of the sandpack. Figure 4-38 (a)-(c) show profiles during oil re-injection. Compared with original oilflood [Figure 4-38 (a), and (c)], although profiles look very similar, recent oilflood yielded a lower oil saturation of 62.4% due to secondary drainage, whereas previous oilflood yielded 75.1%.

(a) Profile after original oilflood. Oil saturation 75.1%

(b) Profile after previous waterflood. Oil saturation 17.8%

(c) Profile after oil re-flood. Oil saturation 62.4%

Figure 4-38 (a)-(c). Profiles during oil re-flood.

Restoration to Previous Low Flow Rate Waterflooded Remaining Condition. Brine was again injected at 5 ft/D to restore the situation where capillary pressure dominated gravity and viscous forces. Figure 4-39 shows profiles during this 2nd waterflood. After 4.0 PV, lower layer still remained highly oil-saturated. This new waterflood recovered 49.1% of oil-in-place based on 2nd oilflood. Oil saturation at this point was 31.8%. Figure 4-40 shows the comparison of recovery efficiency between 1st and 2nd waterflood at low flow rate. Recovery curves almost overlap indicating experiments were reproducible.

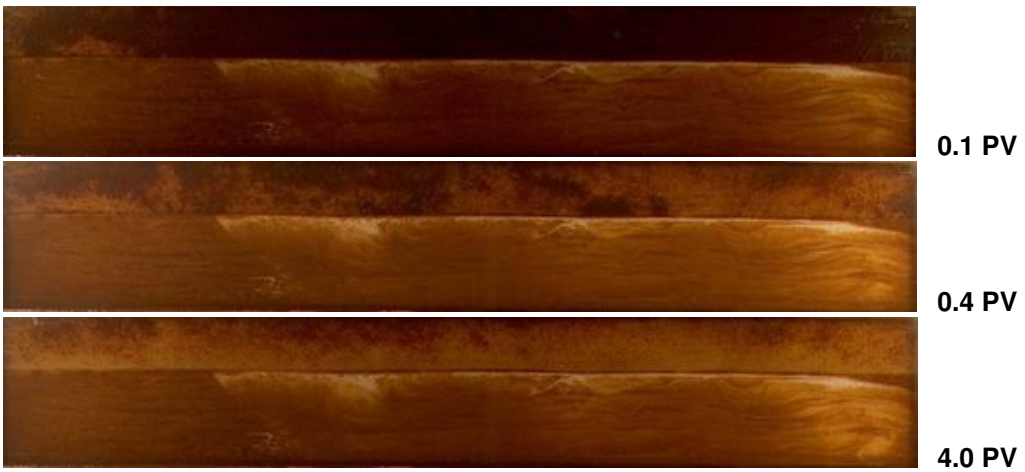

Figure 4-39 Profiles during new waterflood.

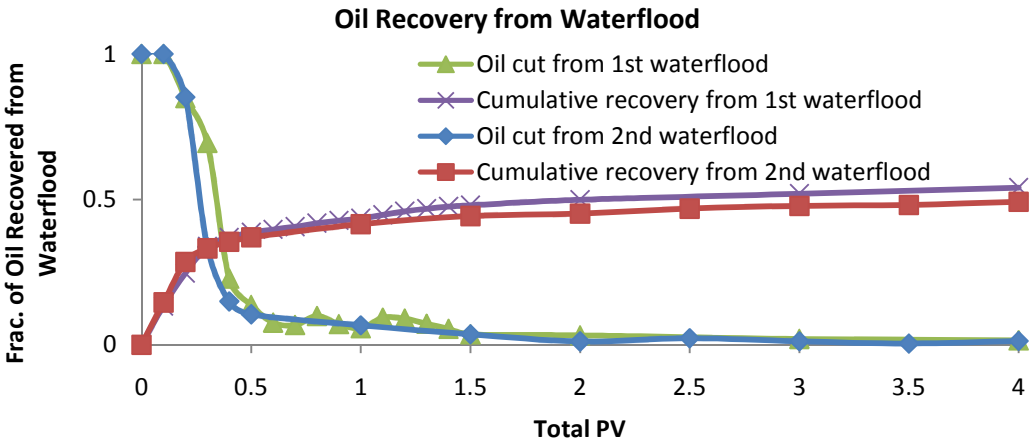

Figure 4-40 Comparison between oil recovery from 1st and 2nd waterflood. Recovery efficiency of the 2nd waterflood was based on oil-in-place after 2nd oilflood.

4.2.5.5 Gravity and Capillary Pressure Driven Counter-current Flow

The measured interfacial tension (IFT) between crude oil and 2% (wt) NaCl brine was 26.5 mN/m. IFT values between SME and 0.2% NI were 0.016 mN/m (2% NaCl, 1% Na_2CO_3), 0.002 mN/m (3.5% NaCl, 1% Na_2CO_3), and 0.001 mN/m (4.15% NaCl, 1% Na_2CO_3) respectively. However when weight concentration of NaCl was greater than 4%, surfactant precipitation occurred. The surfactant formulation of NI in either 2% or 3.5% NaCl, with 1% Na_2CO_3 was a clear single-phase solution.

NI blend was injected at 1 ft/D for 0.5 PV and broke through top layer between 0.4 to 0.5 PV. Sweep profiles are shown in Figure 4-41. Lower layer, however, still remained highly oil-saturated at this point. This process alone recovered 2.3% oil-in-place based on 2nd oilflood. Oil saturation after this process was 30.3%.

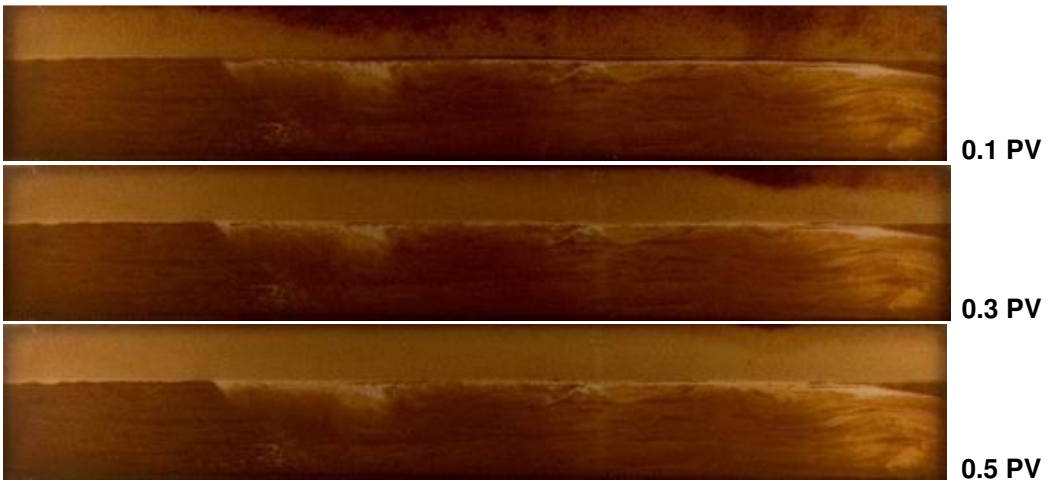

Figure 4-41 Profiles during NI injection. Lower layer stilled remained highly oil-saturated due to unfavorable mobility.

The injected NI blend was expected to lower the IFT between oil and water and therefore reduce the capillary pressure. This would allow untrapped oil to float upwards due to buoyancy. Consequently, surfactant solution would flow downward to replace this oil and would contact additional oil and reduce IFT. The system was shut in after NI

injection to allow gravity and capillary-driven counter-current flow to take place. Streaks of oil were observed immediately in the upper layer upon shut-in. Also, streaks of upward-moving oil were observed on day-5 in the lower layer. A rim of oil had accumulated on top of the sandpack. Figure 4-42 shows pictures of such phenomena. Figure 4-43 shows the rate of oil accumulation at the top of the high permeability layer which floated from the low permeability layer. Note that the patch of oil near the inlet changed slowly compared to other locations in the lower layer. This may have been due to water-in-oil emulsion in some of the injected oil that may have increased the viscosity and density.

Displacement Profiles during System shut-in	t (day)	t_{Dg}	$t_{D,\,Pc}$
	**0**	**0**	**0**
	**2**	**53**	**0.5**
	**6**	**107**	**1.0**
	**10**	**178**	**1.6**
	**42**	**748**	**6.7**

Figure 4-42 Profiles of gravity and capillary pressure driven counter-current flow.

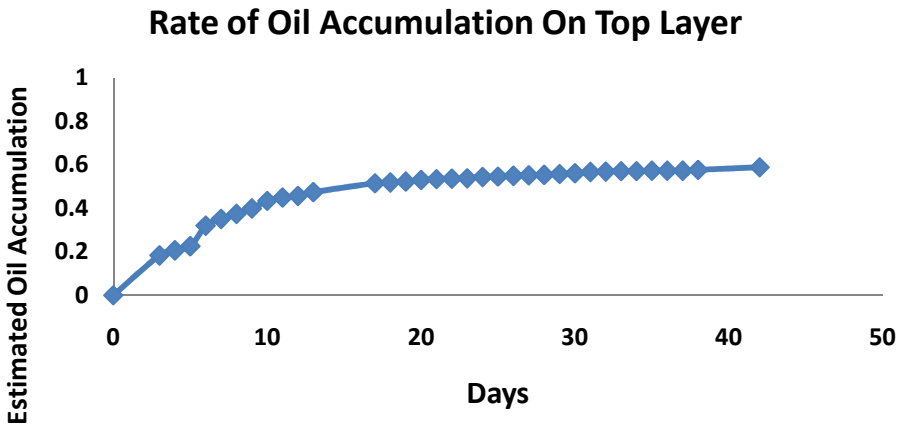

Figure 4-43 Estimation of oil accumulation on top layer that resided originally in the lower tight layer. The fraction of accumulation was based on oil-in-place after 2nd oilflood.

The data were interpreted by evaluating the effects of gravity drainage and capillarity. The dimensionless time for gravity drainage alone assuming zero capillary pressure was defined as follows [Richardson and Blackwell, 1971; Hagoort, 1980]:

$$t_{Dg} = \frac{k k_{ro}^{o} \Delta\rho g t}{(S_{oi} - S_{or}) \emptyset \mu_o L} \qquad \text{Equation 4-3}$$

Relative permeability was estimated by Corey correlation

$$k_{ro=} k_{ro}^{o} S_o^n \qquad \text{Equation 4-4}$$

In this equation, k_{ro}^{o}=0.9, and Corey exponent n=3 were used.

The dimensionless time for capillary imbibition assuming zero gravity was defined as follows [Ma *et al.*, 1997],

$$t_{D,Pc} = t\sqrt{\frac{k}{\emptyset}} \frac{\sigma}{\sqrt{\mu_o \mu_w}} \frac{1}{L_c^2} \qquad \text{Equation 4-5}$$

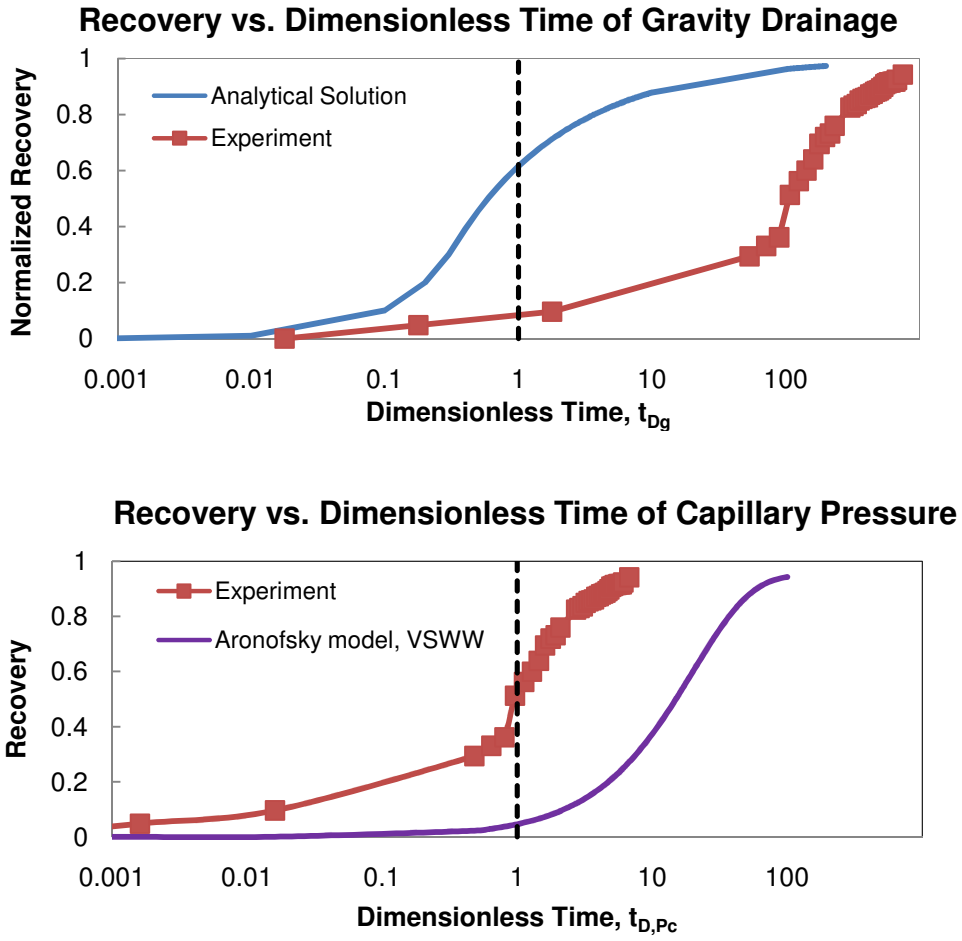

Figure 4-44 Recovery as a function of dimensionless times.

These dimensionless times were indicated in Figure 4-42. Figure 4-44 shows plots of recovery as a function of dimensionless time for gravity t_{Dg}, and for capillary pressure $t_{D,Pc}$. The experiment was compared with the 1-D analytical solution for gravity drainage [Richardson and Blackwell, 1971; Hagoort, 1980].

$$E_R = t_{Dg}, t < t_{BT}; E_R = 1 - \frac{1-\frac{1}{n}}{(nt_{Dg})^{\frac{1}{n-1}}}, t > t_{BT}; \text{breakthrough time}, t_{BT} = \frac{1}{n}, n > 1 \quad \text{Equation 4-6}$$

The experiment recovered much slower than gravity drainage alone (assuming zero capillary pressure). This is because, at the beginning of system shut-in, surfactant was not present in the entire lower layer, and areas where surfactant had not yet reached were still

oil-wet. The adverse capillary pressure dominated gravity and retarded recovery by buoyancy. Once surfactant came in contact with oil, the tension was reduced to ultra low value and the capillarity became negligible compared to gravity. Then buoyancy force became dominant and contributed significantly in displacing oil which had been contacted with surfactant.

As a comparison, if surfactant solution was initially present everywhere, the rate limiting step would be gravity. This has been observed in the spontaneous imbibition test in an Amott cell [Hirasaki and Zhang, 2004]. In that test, the oil-saturated core sample was surrounded by surfactant, and surfactant solution entered from the sides and the bottom and promoted a co-current flow of gravity drainage. The recovery took place around t_{Dg}=1, and agreed fairly well with the analytical solution. Similar surfactant-induced co-current flow processes were also discussed by Gupta and Mohanty (2007).

Although displacement was driven by difference in capillary pressure, this 2-D experiment is different than the spontaneous imbibition process in a very strong water-wet (VSWW) system assuming zero gravity, as shown by the purple curve [Aronofsky *et al.*, 1958] in Figure 4-44. This is because in the 2-D experiment, 1) it was not water-wet bur rather, preferentially oil-wet; and 2) gravity could not be neglected and therefore displacement was faster than as if it were just capillary pressure dominated. In this experiment, P_c was nearly zero where surfactant was present, and P_c was still negative (oil-wet) where surfactant had not reached. Therefore, the rate limiting step of this process was the transport of surfactant solution to the trapped oil, *i.e.* how fast the front of P_c=0 advanced. This phenomenon was evident from the profiles in Figure 4-42, especially day 6 and day 10 after shut-in. Streaks of oil (low tension) floated up by

buoyancy above the front of the surfactant solution displacing remaining oil. Below the front, oil (high tension) was still trapped.

4.2.5.6 Foamflood

Figure 4-45 shows the profile during foamflood. Figure 4-46 shows the foam apparent viscosity. Strong foam was not formed. This may have been due to high oil saturation in the top layer breaking the foam. As soon as IOS was injected (at 1 ft/D), the patch of oil which was difficult to be displaced during shut-in days by gravity and capillary pressure driven counter-current flow, was mobilized during foamflood. Furthermore, it continued moving upwards after foamflood. After foamflood, counter-current flow between oil and aqueous phase immediately happened again. Figure 4-47 shows such a case. The top profile in this figure was 1.5 hours after the end of foamflood; middle was one day after; bottom was 4 days after.

Figure 4-45 Foamflood profiles.

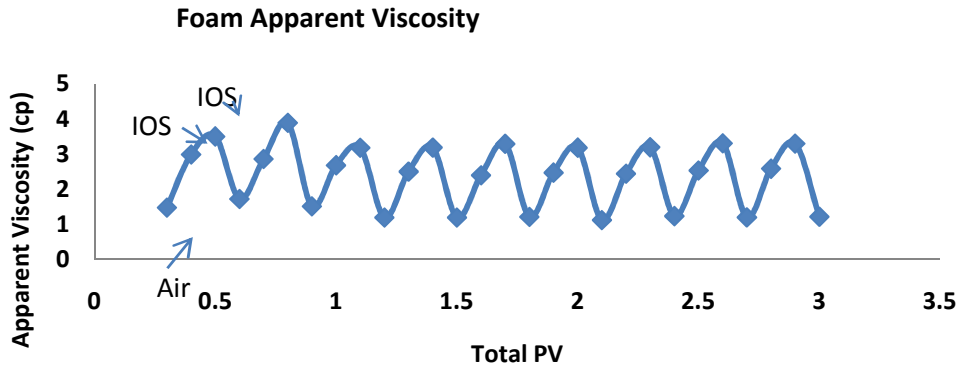

Figure 4-46 Apparent viscosity during foamflood.

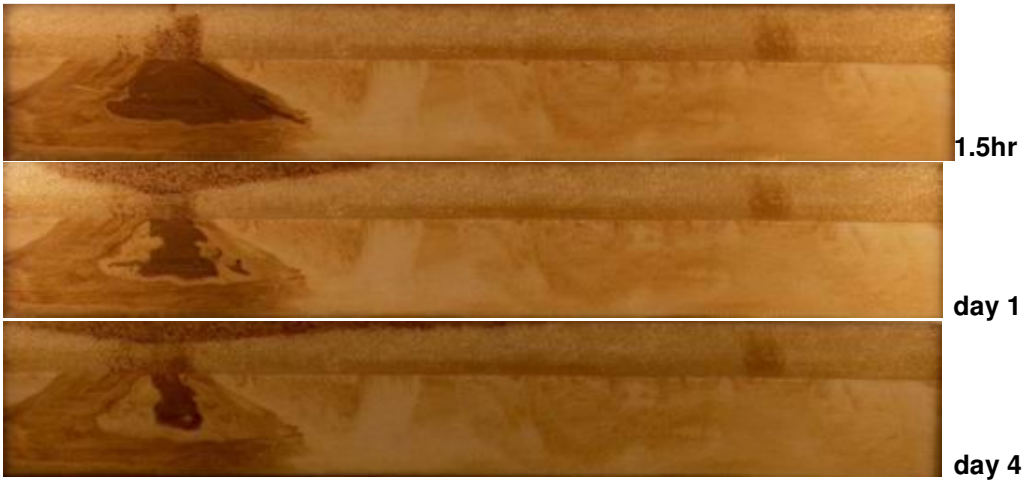

Figure 4-47 Profiles after foamflood. Gravity and capillary pressure driven counter-current flow was observed immediately after foamflood where the system was shut in.

Foamflood in addition to NI flood recovered 89.4% of the waterflood remaining oil. Recovery was high despite that strong foam was not formed. This may have been due to the fact that IFT between oil and water was low and oil was not trapped, and transient gas bubbles displaced oil by local pressure gradient and attrition. Figure 4-48 is a picture of effluent samples from foamflood. Figure 4-49 shows recovery history during foamflood. Overall recovery (waterflood+NI-flood+foamflood) was 94.6% of oil-in-place based on 2nd oilflood. Final oil saturation was 3.4%. Recovery would have been higher and oil saturation lower except for inadvertent injection of emulsion near entrance of the bottom layer. Nevertheless the observed recovery is an improvement from previous 2-D ASPF forced displacement which recovered 30.0% of the waterflood remaining oil and 64.3% OOIP.

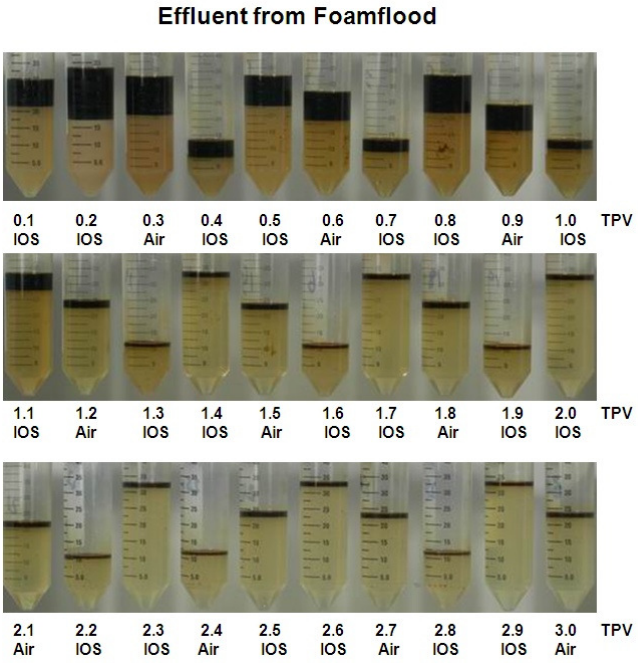

Figure 4-48 Effluent from foamflood.

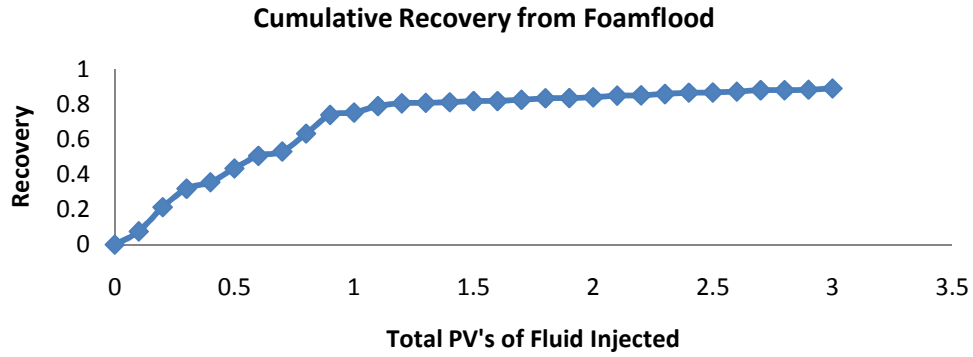

Figure 4-49 Recovery efficiency from remaining oil (after waterflood and NI blend flood) during foamflood.

Table 4-4 lists comparison between clean and CTAB-treated silica sand. On the one hand, oil saturation after oilflood was lower in CTAB-treated sandpack because once oil broke through, it would flow as a continuous phase. This made it difficult to displace the remaining water (as a discontinuous phase), resulting in lower oil saturation. On the other hand, waterflood remaining oil saturation was higher because water, as a non-wetting

phase, resided in large pores or pore bodies whereas oil would stay in small pores or pore throats. The major difference between current and previous 2-D flood is system shut-in and settling enabled gravity and capillary driven counter-current flow to occur. Polymer was used in previous 2-D flood whereas no polymer was used in current 2-D flood.

Table 4-4 Comparison with previous 2-D ASPF flood

	Previous Experiment	Current Experiment
2-D Sandpack	Untreated Silica Sand Porosity 0.38 Thickness Ratio 2:3 Permeability Ratio 19:1 Overall permeability 38.5 darcy Pore Volume: 332.1 mL	CTAB-Treated Silica 0.38 2:3 19:1 44.0 darcy 330.0 mL
Oilflood	Oil Saturation 86.0%	75.1% (1st oilflood) 62.4% (2nd oilflood)
Waterflood	Cumulative Recovery 49.1% OOIP Remaining Oil Saturation 43.8%	49.1% oil-in place based on 2nd oilflood 31.8%
EOR	(Incremental Recovered Oil/ Waterflood Remaining Oil)×100% 30.0%	 89.4%
Cumulative Recovery (Wateflood+EOR)	64.3% OOIP	94.6% oil-in-place based on 2nd oilflood
Remaining Oil Saturation	30.7%	3.4%

4.2.6 Foam Mobility Control in the Presence of Oil in an Oil-Wet Heterogeneous Layered System

NIB alone was evaluated in a layered, CTAB-treated, oil-wet silica column. Results are summarized in Figures. 4-50 to 4-52 and Table 4-5. The vertical stripes in the upper layer are due to packing defects. After waterflood, oil saturation in lower layer remained high, judging from the color in Figure 4-50. This is because capillary pressure was dominating viscous forces and gravity. Instead of shutting in the system after surfactant

injection to let surfactant-induced wettability alteration and gravity drainage take place, we applied foamflood using NIB SAG immediately after waterflood as a viscous force controlling process. Since NI could effectively alter the wettability from preferentially oil-wet to water-wet (Figure 4-32) and since NIB was a good foaming agent in presence of SME, foam was formed and worked effectively as a mobility control agent in displacing remaining oil from the lower, tight layer. The reduction in oil saturation is illustrated in Figure 4-51 by dramatic color change in the lower layer. Cumulative recovery including waterflood and EOR recovered 93.1% OOIP. Figure 4-52 is a plot of foam apparent viscosity. Foam kept building up and its apparent viscosity increased as injection went on.

Figure 4-50 Pictures during waterflood in the oil-wet sand column. Lower layer remained highly oil-saturated because of wettability (oil-wet) and lower permeability.

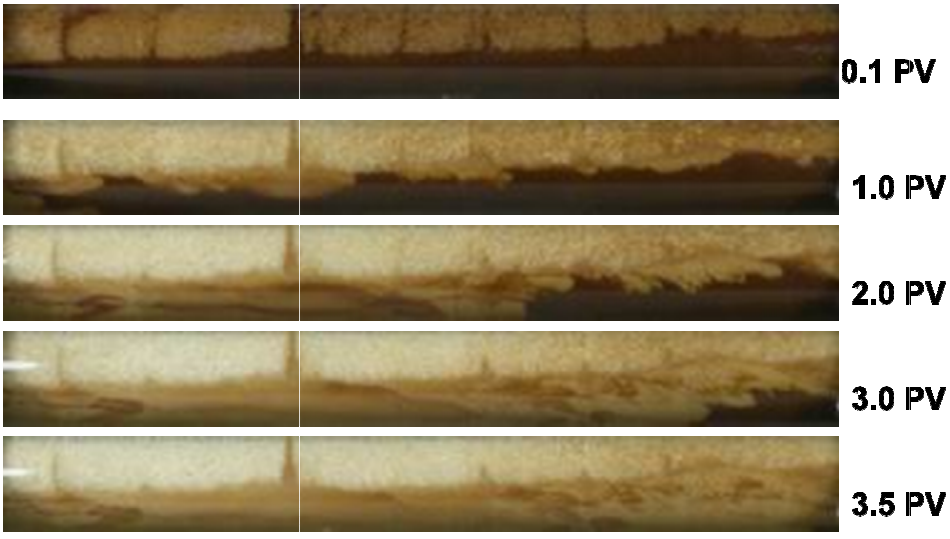

Figure 4-51 Pictures during ASF process in the oil-wet sand column.

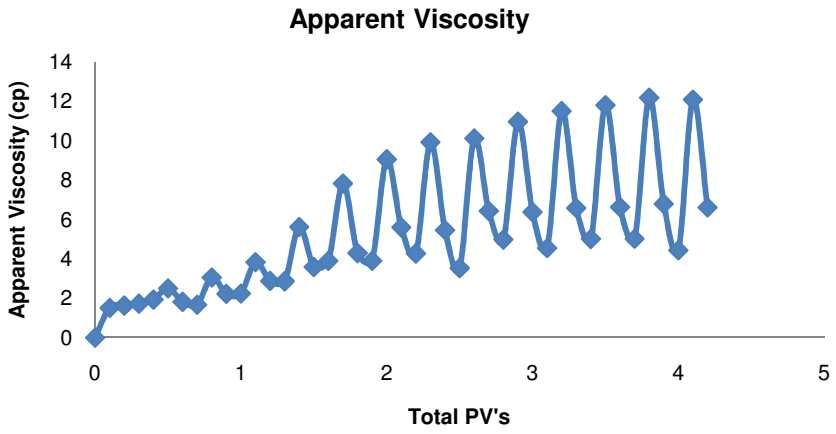

Figure 4-52 A viscosity during an ASF process in the oil-wet sand column.

Table 4-5 Summary of the foam experiment in an oil-wet heterogeneous sand column

	Oil-Wet Column
Sandpack	43 darcy, coarse overlays fine sand
Flow Direction	horizontal
Surfactant Formulation	NIB, 1.18 cp
Salinity	3.5% NaCl, 1% Na_2CO_3
Temperature	25 °C
Oil Viscosity	3.93 cp (25ºC)
Injection Scheme	5 ft/D (0-0.2TPV); 2.5 psi/ft from 0.3 TPV
Slug Size	0.1 PV
Foam Generation	NIB alternating air; *fg*=1/3
Initial Oil Saturation	S_{oi}=1
Waterflood Remaining Oil Saturation	S_{orw}=0.62
(Incremental Recovered Oil by EOR/ Waterflood Remaining Oil)x100%	88.7%
Cumulative Recovery (Waterflood+EOR)	93.1%

4.2.7 2-D ASF Process in an Environmental Room Aged Crushed Limestone Sandpack

2-D carbonate sandpack was packed with crushed limestone N16/20 (219±22 darcy) overlaying N40/120 (29.3±1.3 darcy). The thickness ratio was 2:3, and the permeability ratio was 6.4~8.3:1. The measured pore volume was 350.5 mL. Porosity was 0.439. The porosity was higher than that of a silica sandpack due to micro pores in carbonate sand.

Oilflood was carried out by injecting old SME crude through various injection ports located at the back of the sandpack so as to fill the entire tight layer. Oil saturation was 83.1% at the end of oilflood.

After oilflood, 2-D model was placed in the environmental room at 37°C for two weeks. It was heated by infrared lamps to 42°C, 8 hrs a day for 7 days in an effort to make the sand less water-wet.

Waterflood was carried out by injecting 2% NaCl for 2.5 TPV at 5ft/D. The 2-D model was shut-in for 6 days for gravity driven vertical counter-current flow to take place. Then waterflood resumed for another 0.5 PV at 5 ft/D. After 3.0 PV injection, recovery was 67.2% OOIP.

NI (0.2% NI, 1% Na_2CO_3, 2% NaCl) was injected at 5 ft/D for 0.5 PV. After NI injection cumulative recovery including waterflood was 67.9%. The system was shut-in for 85 days to allow gravity and capillary pressure driven counter-current flow.

Foamflood was carried out using SAG injection (0.5% IOS15-18, 1% Na_2CO_3, 2% NaCl), at 2 psig, fg=1/3 (0.2 PV IOS alternating 0.1 PV air). Cumulative recovery was 75.2%. Remaining oil saturation was 20%. Figure 4-53 is a summary of cumulative recovery. Table 4-6 is a summary of this experiment.

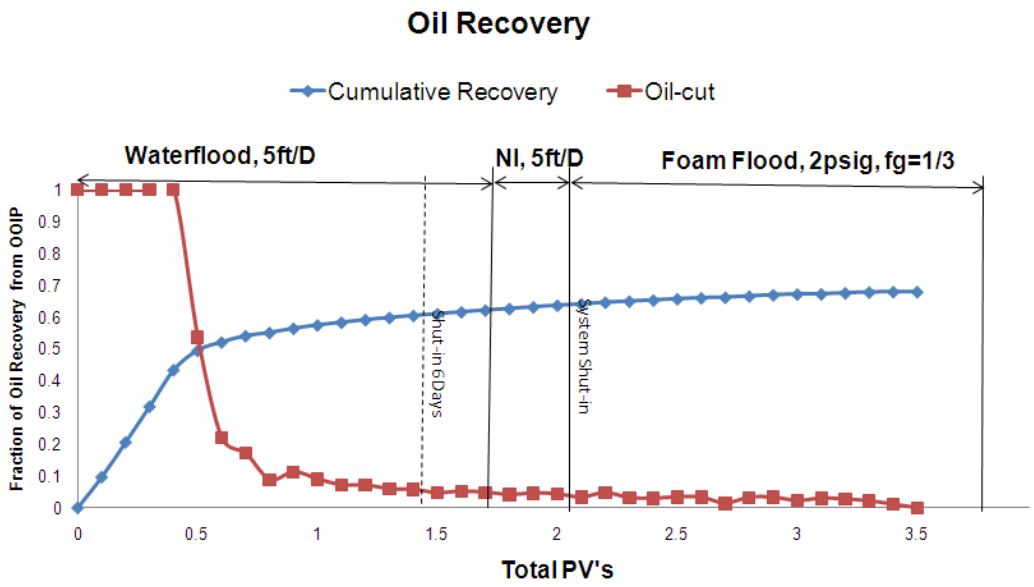

Figure 4-53 Plot of oil recovery.

Figures 4-54 and 4-55 show profiles during oilflood and waterflood respectively. In Figure 4-55, profiles before and after shut-in at 2.5 PV waterflood have noticeable change in saturation. Oil had accumulated on the upper layer due to gravity and capillary pressure after 6 days. This indicates that the sandpack was still water-wet. Aging in the environmental room at this particular condition was not enough to change the wettability to oil-wet. Figure 4-56 shows profiles during NI flooding. The sandpack was kept in a shut-in condition for 85 days after NI injection. Figure 4-57 shows profiles during shut-in. Not much oil was accumulated on the top layer and lower layer saturation did not change noticeably as may be seen by comparing with Figure 4-56 This is another indication that the sandpack was not oil-wet.

Table 4-6 Summary of 2-D carbonate (environmental room aged) SME ASF flood

2-D Sandpack	Crushed Carbonate N16/20 (219 darcy) overlays N40/120 (29.3 darcy). Porosity 0.439; Pore Volume: 350.5 mL; Thickness Ratio 2:3; Permeability Ratio 6.4~8.3:1; Overall permeability 113.7 darcy;
Oilflood on 3/22/2009	1.6 TPV injected at 5 ft/D. Oil saturation: 82.9%
Oilflood continued on 3/25/2009	An incremental of 0.64 PV (2.24 TPV) injected at 10~60 ft/D. Oil Saturation: 83.1%
Waterflood (2% NaCl)	3.0 PV (5ft/day) Cumulative Recovery: 67.2% of oil-in-place Remaining oil saturation 26.8%
Chemical Slugs	NI Blend: 0.2% NI blend, 1% Na_2CO_3, 2% NaCl; Foam Drive: 0.5% IOS15-18, 1% Na_2CO_3, 2% NaCl;
Injection Scheme	0.5 PV NI (5 ft/D); Cumulative Recovery 67.9% of oil-in-place Shut-in for 85 days; 0.1 PV IOS (1 ft/D)→0.1 PV IOS (1 ft/D)→0.1PV Air (2 psig); 0.1 PV IOS (2 psig)→0.1 PV IOS (2 psig)→0.1PV Air (2 psig); etc. Cumulative Recovery: 75.2% of oil-in-place. Remaining oil saturation: 20%

Figure 4-54 Profiles during oilflood.

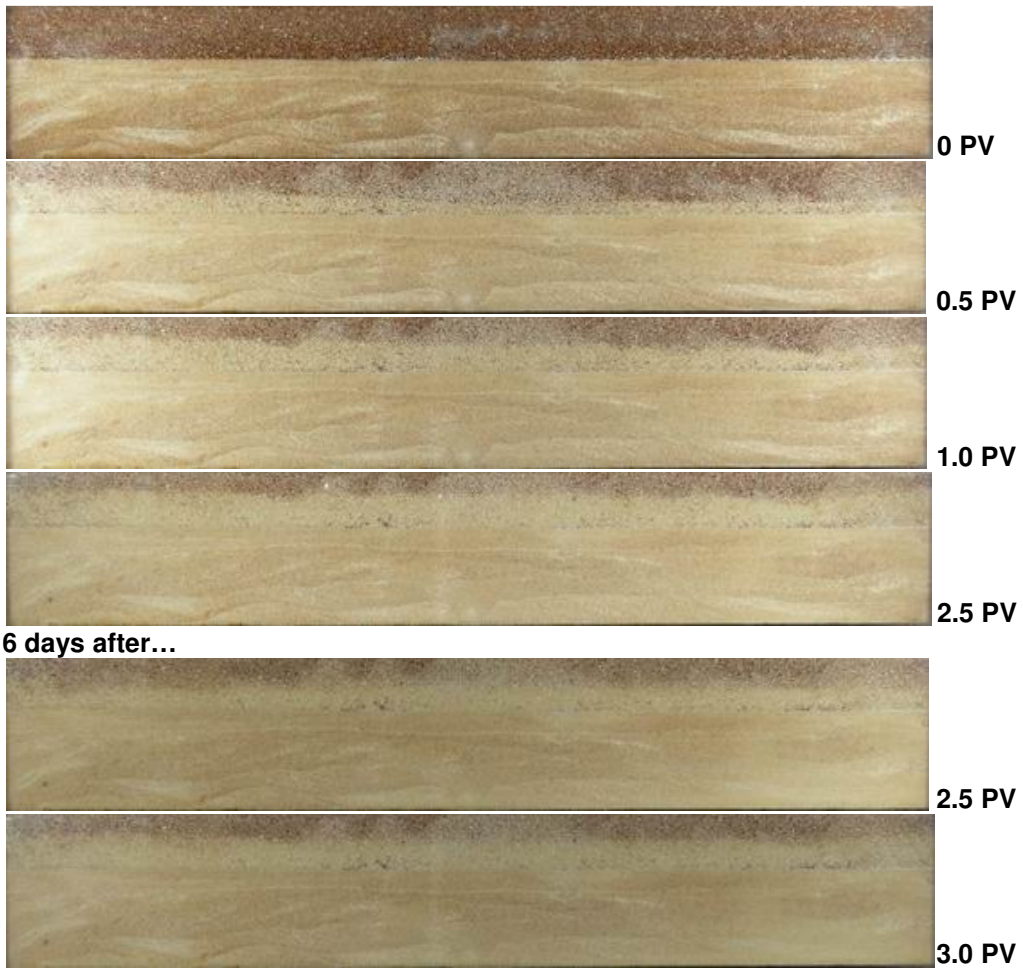

Figure 4-55 Waterflood profiles. 2-D model was shut-it for 6 days after 2.5 PV. Oil in higher permeability layer had a noticeable change in saturation after 6 days.

Figure 4-56 NI-blend flood. 5ft/D; Cumulative recovery including waterflood 67.9%. Surfactant broke through after 0.5 PV. The system was shut-in at this point.

Figure 4-57 Profiles during 85-day shut-in.

Foamflood was carried out using IOS alternating air, *fg*=2/3 at 2 psig. Figure 4-58 shows profiles during foamflood. Figure 4-59 is a picture of effluent. Figure 4-60 shows foam apparent viscosity. Strong foam was not formed due to residual oil breaking the foam, and possibly surfactant adsorption on carbonate surface. Cumulative recovery after foamflood was 75.2% OOIP. Although most of the additional oil which had accumulated in the upper layer was recovered, the recovery was not as high as the experiment in the 2-D CTAB-treated silica sandpack.

Figure 4-58 Profiles during foamflood.

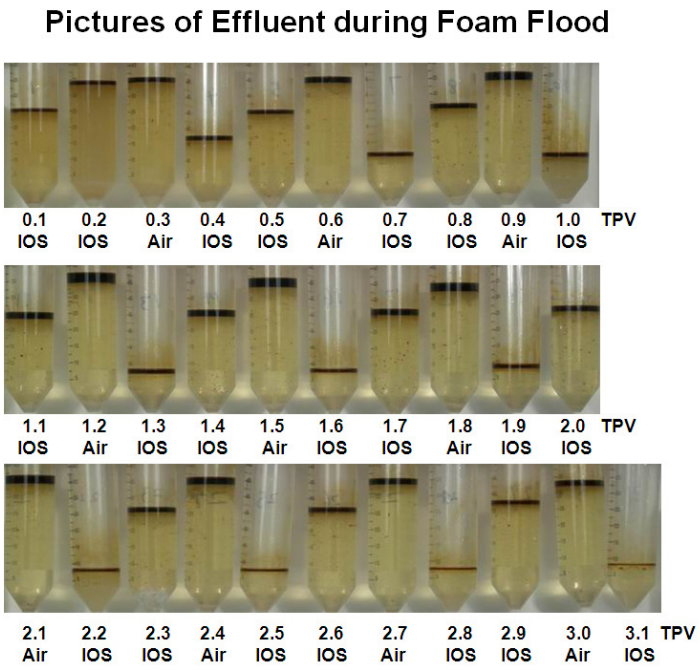

Figure 4-59 Picture of effluents.

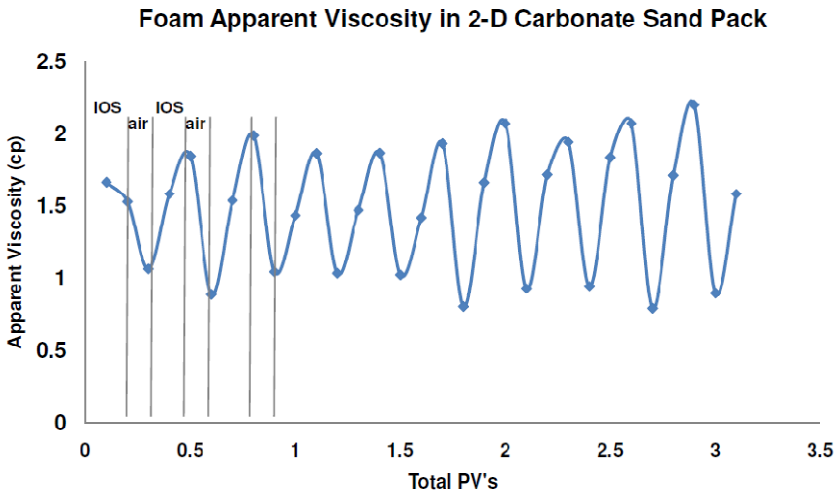

Figure 4-60 Foam apparent viscosity in the 2-D carbonate sandpack.

4.2.8 2-D ASF Process in a Pre-Treated Crushed Limestone Sandpack

In this experiment, cleaned carbonate sand (in which micro pores were saturated with water) was pre-treated by first centrifuging to specific capillary pressure hence specific remaining water saturation, then soaking in SME crude oil and aging in 85°C oven for 11 days. The centrifuging speed was selected based on Equations 4-7 and 4-8.

$$Pc = (\rho_w - \rho_o) \cdot g \cdot (D - D_0) \qquad \text{Equation 4-7}$$

where Pc is the capillary pressure, ρ_w is the density of water, ρ_o is the density of oil, g is the gravitational acceleration constant and $(D\text{-}D_0)$ is the depth from water-oil-contact.

The centrifuging process was to drain water to the specific capillary pressure similar to that in the reservoir with connate water saturation. Therefore in an air and water system,

$$Pc = (\rho_w - \rho_a) \cdot RCF \cdot L \qquad \text{Equation 4-8}$$

where, ρ_w is the density of water, ρ_a is the density of air, *RCF* is the relative centrifuge force, measured in units of gravity (times gravity), *L* is the length of packed sand in the centrifuge tube. Figure 4-61 is a picture of sand in a centrifuge tube with water being separated from micro pores. Although the location of water-oil-contact of SME reservoir is unknown, the thickness of SME reservoir was between 150-170 ft. Hence an average value of $(D\text{-}D_0)$=160 ft was used in Equation 4-7, and calculated *Pc* was 12.89 psig. With this *Pc*, *RCF*=130**g* is required. Actually, *RCF*=200**g* was used because the minimal increase in the machine's setting is 100**g*. With 95% confidence interval, remaining water saturations with upper layer sand N20/40 and lower layer sand N40/120 are $S_{wc(N20/40)}$=0.753±0.057 and $S_{wc(N40/80)}$=0.988±0.141, respectively.

After aging in SME crude oil at 85°C for 11 days, the sandpack was wet-packed with pre-treated carbonate sand. Oilflood was carried out after CO_2 purging. Waterflood was performed by injecting 3.0 TPV 2% NaCl at 5 ft/D. Cumulative recovery after waterflood was 41.5% OOIP. 0.2% IOS15-18 alone in 1% Na_2CO_3 and 2% NaCl was injected at 5 ft/D for 0.5 TPV. The sandpack was then shut-in for 6 days. Foamflood was performed by co-injecting IOS15-18 and air through a foam pre-generator. Injection scheme was as follows: IOS and air co-injection at 20 ft/D for 3.0 TPV; 3.0-5.1 TPV SAG fg=1/3 at 4 psig. Cumulative recovery after foamflood was 66.8% OOIP. Figure 4-62 is the plot of cumulative oil recovery and oil-cut. Table 4-7 lists the summary of this experiment.

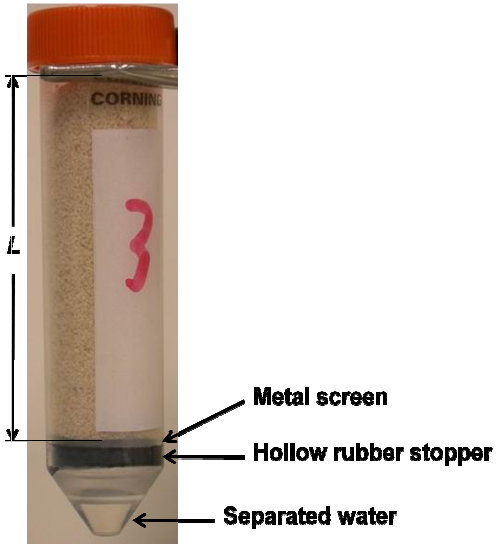

Figure 4-61 Picture showing the end of centrifuging. This is a 50mL Corning centrifuge tube. A No.4 hollow rubber stopper was cut to 1/8" thick from the top and was fitted towards the bottom of the tube. On top of the rubber, there was a metal screen to hold sand grains.

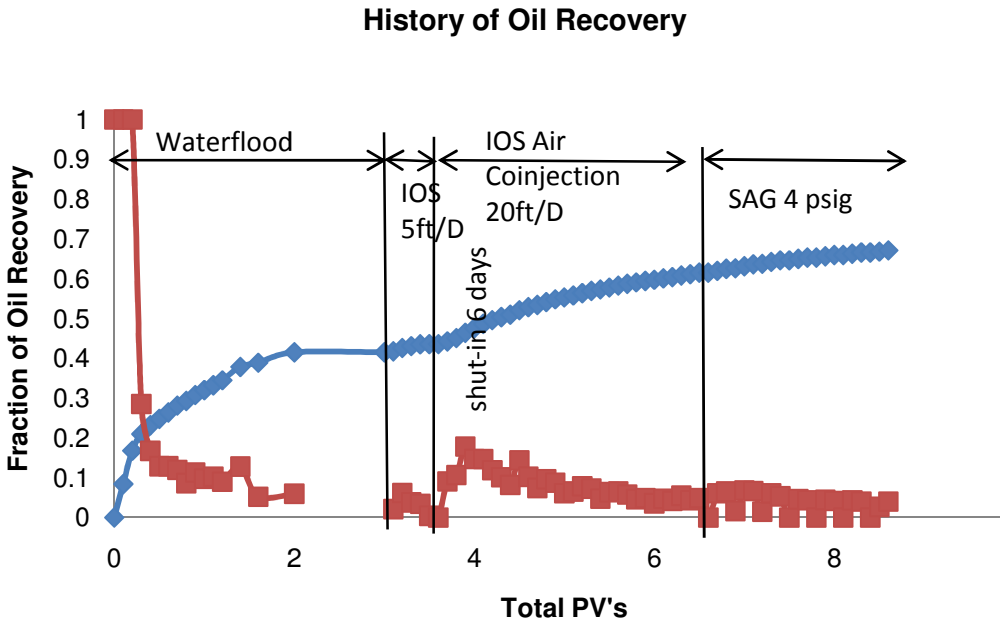

Figure 4-62 Cumulative oil recovery curve (blue line) and oil-cut (red line).

Table 4-7 Summary of 2-D carbonate (pre-treated) SME ASF flood

2-D Sandpack	Crushed limestone N16/20 (219 darcy) overlays N40/120 Connate water saturation $S_{wc(N20/40)}$=0.753 $S_{wc(N40/80)}$=0.988. Sand aged in crude oil in 85°C oven for 11 days before packing
Waterflood	2% NaCl, 3.0 TPV, 5ft/day; Cumulative Recovery: 41.5% OOIP
Chemical Slugs	0.2% IOS15-18, 1% Na_2CO_3, 2% NaCl
Injection Scheme	0.5 PV IOS (5 ft/D); Shut-in for 6 days; 0-3.0 TPV: IOS and air co-injection at 20 ft/D through Foam pregenerater 3.0-5.1 TPV SAG fg=1/3 at 4 psig . Cumulative Recovery: 66.8% OOIP

Figure 4-63 shows profiles during waterflood. Oil in lower layer was noticeably displaced by waterflood at even 5 ft/D indicating that the sand might still have been water-wet or mixed-wet. Figure 4-64 shows profiles during IOS injection. The system was then shut-in for 6 days, and Figure 4-65 shows profiles during shut-in.

Figure 4-63 Profiles during waterflood at 5 ft/D for 3.0 TPV.

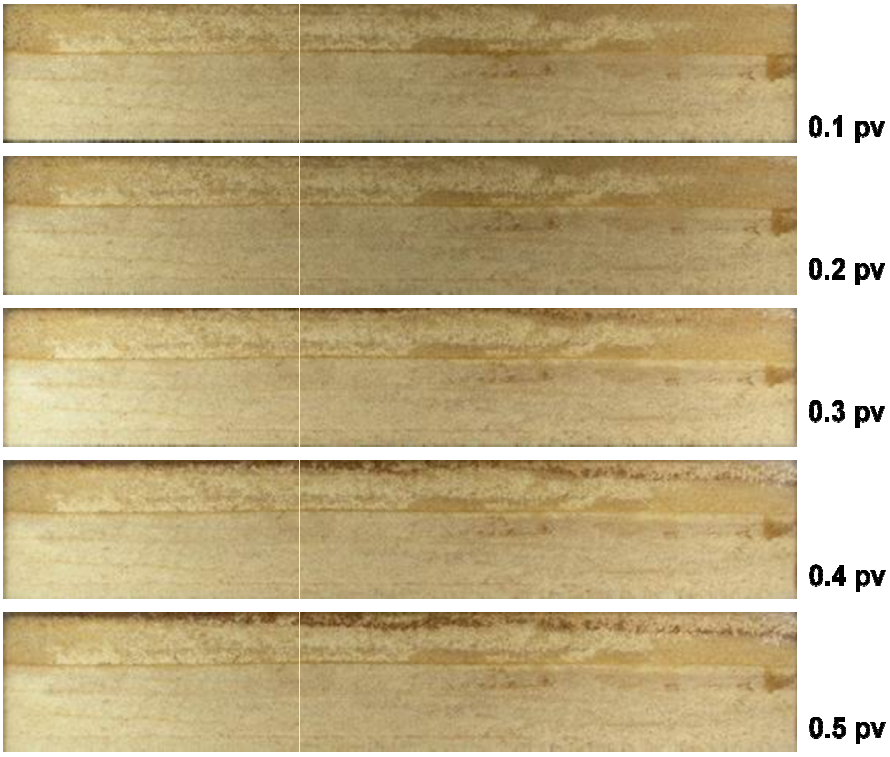

Figure 4-64 0.2% IOS15-18 with 1% Na_2CO_3, 2% NaCl, 5ft/D, 0.5 TPV.

Figure 4-65 Shut-in after Injection of 0.5 TPV IOS15-18.

Pre-generated foam was injected to the sandpack during foamflood for the first 3.0 PV. SAG at 4 psig with *fg*=1/3 was used from 3.0~5.1 PV. Figure 4-66 shows profiles during foamflood. During foamflood, residual oil in the lower layer (Figure 4-66, red circle) was mobilized and cross-flowed upwards to the high permeability layer as described in Figure 4-11. Figure 4-67 shows foam apparent viscosity during co-injection. It was weaker in 2-D than in 1-D.

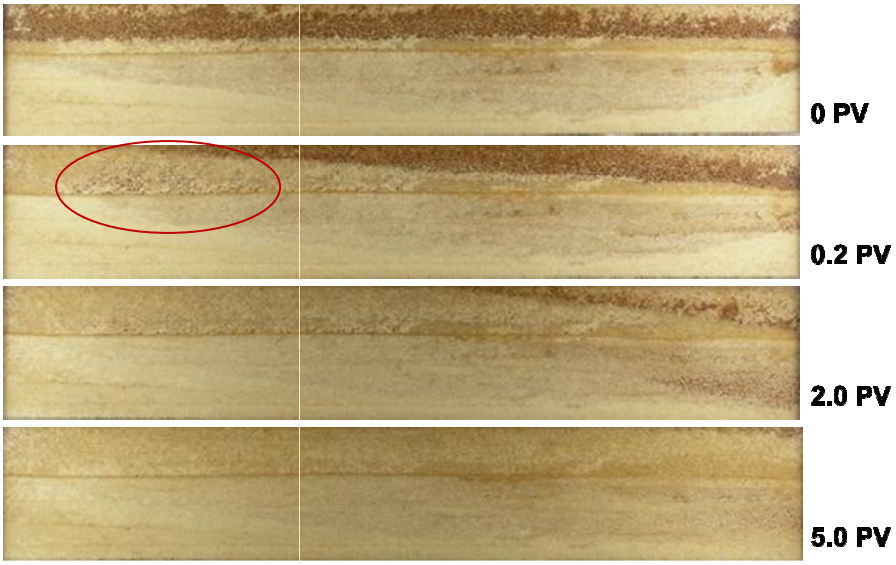

Figure 4-66 Foamflood with 0.2% IOS15-18 in 1% Na_2CO_3, 2% NaCl: 0-3.0 TPV: co-injection through foam pre-generator; 3.0-5.1 TPV SAG fg=1/3 at 4 psig.

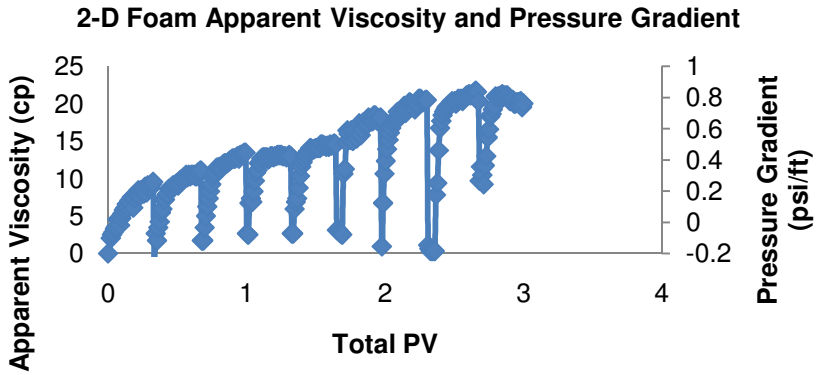

Figure 4-67 Foam apparent viscosity. Drop in the viscosity was due to syringe refill.

4.3 Conclusions

The vertical sweep of a layered sandpack with a 19:1 permeability contrast where capillary communication was allowed, was greatly enhanced with SAG compared to waterflood or WAG. Foam sweep efficiency improved with increased injection pressure or reduced gas fractional flow. To achieve 100% sweep efficiency, it took 1.3 TPV for foam (6 psig, f_g=1/3), but it took 8 TPV for water only (4 psig, f_g=0). For WAG injection, after 6 TPV, there was still over 30% left unswept.

Foam had much higher apparent viscosity than water or WAG in 2-D system and is a promising agent for mobility control. In 2-D foam-aided sweep, there were two types of crossflow across the foam front. Behind the foam front, liquid was diverted from the high permeability layer to the low permeability layer. Ahead of the foam front, liquid was diverted in the opposite direction. Foam generated at 6 psig with f_g=1/3 showed a nearly piston-like displacement of the resident liquid even if the permeability contrast was 19:1. Crossflow resulted from the favorable mobility ratio displacement but the fluid that was diverted to the low-permeability layer was primarily the liquid fraction of the foam.

Surfactant formulations of 0.2% IOS-C15-18 and 0.2% AOS-C1618 worked very similarly in a 2-D foam sweep.

In two parallel 1-D sand columns where capillary communication was not allowed, with water only experiment, it took ~0.6 TPV to sweep out green water in high permeability region and ~3.0 TPV to sweep out the entire system. With WAG, after 1.5 TPV there was still over 80% left unswept in the low permeability region. With SAG, it took ~1.0 TPV to sweep out green water in high permeability region and 1.5 TPV to sweep out the entire system.

CTAB was effective in altering the wettability of clean silica sand from water-wet to preferentially oil-wet. Anionic surfactants such as NI could alter the wettability back to preferentially water-wet.

A 2-D heterogeneous sandpack with 19:1 permeability contrast was made preferentially oil-wet with CTAB. Gravity- and capillary pressure-driven, vertical, counter-current flow occurred after 0.5 PV alkaline/surfactant was injected and the system was shut-in. This displaced most of the oil from lower, low-permeability layer. Foamflood recovered most of the oil accumulated on top of the high-permeability layer. Strong foam was not formed due to crude oil breaking the foam. Foamflood in addition to alkaline surfactant flood recovered 89.4% of the waterflood remaining oil. Overall recovery (waterflood+ASF) was 94.6% OOIP. This was a great improvement compared to the ASPF process in an untreated silica sandpack where shut-in was not allowed and recovery was only 64.3% OOIP.

Carbonate sand should be treated to be preferentially oil-wet with low initial water saturation and at high temperature. Treatment of crushed limestone in the environment room at 37-42 °C did not change the wettability to preferentially oil-wet. Temperature was not high enough in this short period of time and 16.9% water saturation was too high. Centrifuging and pre-treating carbonate sand in SME crude at 85 °C may have been effective but the initial water saturation may still have been too high for effective and robust wettability alteration. The sandpack was still preferentially water-wet. Future experiments should focus on centrifuging to higher capillary pressure hence lower initial water saturation. Empirically, T>85°C and S_w<0.5% are conditions that could effectively treat the core samples and limestone sands to be oil-wet in about two weeks. Since the

carbonate 2-D sandpacks were both water-wet, most remaining oil from lower layer was displaced by spontaneous imbibition during waterflood. Cumulative recovery with 37-42 °C environmental room treated and with 85 °C pre-treated sandpacks was 75.2% and 66.8% respectively. The lower recovery efficiency and weaker foam that was observed with carbonate sand compared with silica sandpacks may have been due to surfactant adsorption on mineral surface and crude oil breaking the foam.

Strong foam was not formed in any of the four forced displacement experiments using 1) untreated silica sand, 2) CTAB-treated silica sand, 3) 37-42 °C environmental room treated carbonate sand, and 4) 85 °C pre-treated carbonate sand. Foam was destabilized by several factors such as crude oil, CTAB, NI, oil-wet mineral surfaces, etc. It is necessary to find a foaming surfactant that can tolerate these factors. While foam mobility control as a viscous dominant process is being studied with SME crude, surfactant induced wettability alteration and gravity drainage worked well in recovering remaining crude oil from the lower low permeability layer. Gravity drainage because of reduced IFT was observed in all cases.

4.4 References

Aronofsky, J.S., Masse, L. and Natanson, S.G., "A model for the mechanism of oil recovery from the porous matrix due to water invasion in fractured reservoirs," Trans. AIME **213**, 17-19, 1958)

Gupta, R. and Mohanty, K.K. 2007. "Temperature effects on Surfactant-Aided Imbibition Into fractured Carbonates," SPE 110204 presented at the SPE ATC&E, Anaheim, CA, 11-14 November.

Hjelmeland, O. and Larrondo, L.E.: "Experimental Investigation of the Effects of Temperature, Pressure, and Crude Oil Composition on Interfacial Properties," *SPERE* (July 1986) 321-328.

Hagoort, J.: "Oil Recovery by Gravity Drainage," *SPEJ* (June 1980) 139.

Hirasaki, G.J., Zhang D.L.: "Surface Chemistry of Oil Recovery From Fractured, Oil-Wet, Carbonate Formations," *SPEJ*., (June 2004) SPE 88365-PA

Li, B., Hirasaki, G.J., and Miller, C.A. 2006. "Upscaling of Foam Mobility Control to Three Dimensions," SPE 99719 presented at the SPE Symposium on Improved Oil Recovery, April 26-29, Tulsa, OK.
Morrow, N.R.: "Wettability and Its Effect on Oil Recovery," *JPT*, (December 1990) 1476-1484.

Ma, S., Morrow, N.R. and Zhang, X., "Generalized scaling of spontaneous imbibition. data for strongly water-wet systems," J. Pet. Sci. & Eng. **18** (1997) 165-178.

Richardson, J.G. and Blackwell, R.J.: "Use of Simple Mathematical Models for Predicting Reservoir Behavior," *JPT* (September 19711145; *Trans.,* AIME, **251.**

Szafranski, R. "Laboratory development of the surfactant/foam process for aquifer remediation," Ph.D. thesis, Rice University, Houston, TX, 1997

Treiber, L.E., Archer, D.L., and Owens, W.W.: "A Laboratory Evaluation of the Wettability of Fifty Oil-Producing Reservoirs," *SPEJ* (December 1972), 531-540.

Yang S.Y, Hirasaki, G.J., Basu, S., Vaidya R.: "Mechanisms for Contact Angle Hysteresis and Advancing Contact Angles," *J of Petro Sci & Eng 24* (1999) 63-73.

Zapata, V.J. and Lake, L.W. 1981. "A Theoretical Analysis of Viscous Crossflow," SPE 1011 presented at the 56th AFTCE of SPE, San Antonio, TX, October 5-7.

Chapter 5

PROCESSES IN A GLASS MICRO MODEL

In this chapter, foam generation mechanisms, foam flow in porous media, alkaline/surfactant enhanced displacement of 266 cp Crude B, and foam stability in presence of SME crude oil will be demonstrated by videos and pictures captured on the pore level in a glass micro model. Videos can be found in the accompanying CD.

5.1 Experiental

5.1.1 Materials

IOS 15-18 (sodium 15-18 internal olefin sulfonate, Shell) in 1% Na_2CO_3, and 2% NaCl was used in oil-free foam generation experiments. The following surfactants and their blends were used in displacement of Crude B, and foam stability in presence of SME experiments. Neodol 67-7PO (ammonium C16-17 7PO sulfate, Stepan); IOS 15-18; lauryl betaine (Rhodia). NI is a blend of 4:1 (wt/wt) Neodol 67-7PO and IOS 15-18. NIB is a blend of 4:1:10 (wt/wt/wt) Neodol 67-7PO, IOS 15-18 and lauryl betaine.

Two crude oils were used. Crude B: moderately viscous oil (266 cp at 25°C, TAN=4.8 mg KOH/g); SME (3.93 cp at 25°C, TAN=0.062 mgKOH/g).

Na_2CO_3 (anhydrous, certified American Chemical Society) and NaCl (biological certified) were both obtained from Fisher Scientific.

Air was used in all gas slugs.

5.1.2 Experimental Setup

The glass micro model (Figure 5-1) was fabricated by infusing two rectangular pieces of glass together. One piece had patterns designed and etched by hydrofluoric acid. The grain size ranged from 400 to 600 microns. There were two channels connecting the porous medium with the flow inlet and outlet.

Figure 5-1 Top view of the glass micro model with waterflood residual oil condition.

An Olympus SZX12 stereo microscope equipped with a video camera was used in taking microscopic pictures on the pore level. Figure 5-2 is a picture of the experimental setup. A syringe pump (Harvard Apparatus) was connected to the micro model for fluid injection.

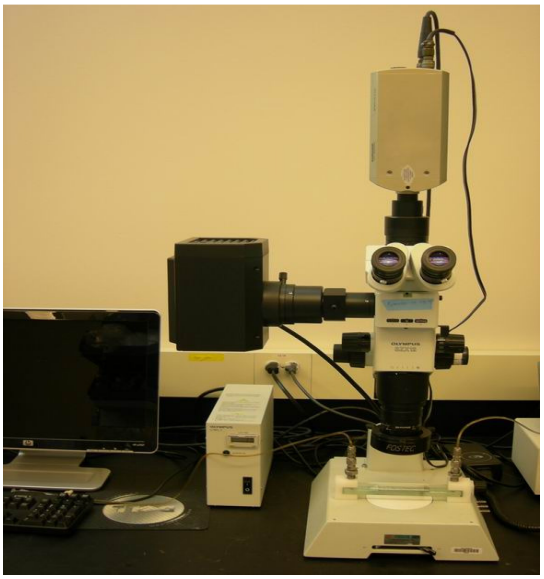

Figure 5-2 Experimental setup.

5.2 Results and Discussion

5.2.1 Foam Flow in Porous Media and Foam Generation Mechanisms

Foam in porous media is defined as "a dispersion of gas in liquid such that the liquid phase is continuous (i.e. connected) and at least some part of the gas phase is made discontinuous by thin liquid films called lamellae [Hirasaki, 1989]." Gas phase is flowing in the continuous phase, but it can be either flowing or trapped in the discontinuous phase Figure 5-3 is a pore level schematic of foam flow in porous media. Video 5-1 is a video clip of foam flow in the glass micro model. Figure 5-4 is a video frame of Video 5-1.

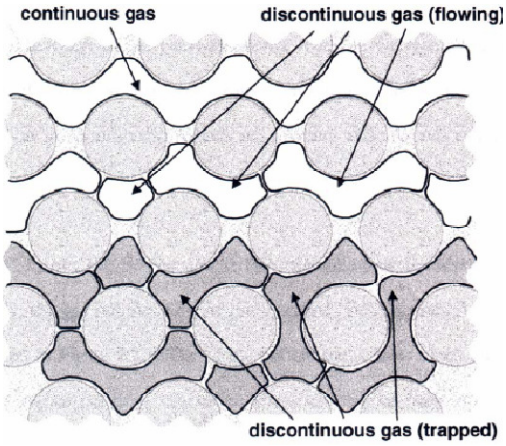

Figure 5-3 Pore level schematic of foam flow in porous media [Radke and Gillis, 1990].

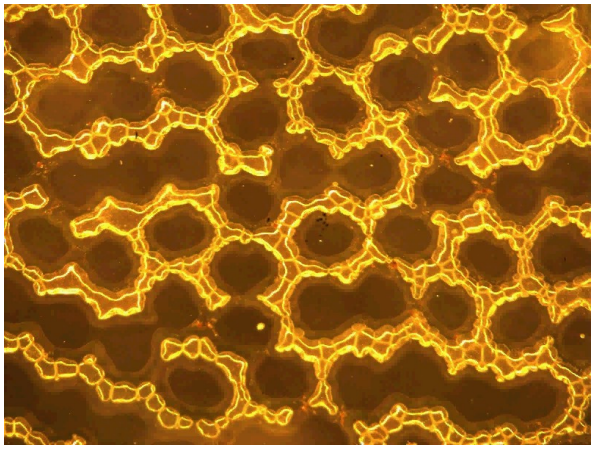

Figure 5-4 Real-life pore level snapshot of foam flow in the glass micro model.

Foam is useful in EOR as a mobility control agent because its resistance to flow is usually significantly higher than that of either phase that makes up the foam. The reduced mobility ($\lambda = k / \mu$) comes from: 1) reduction of gas relative permeability, 2) rise in apparent viscosity. As shown in Figures 5-3 and 5-4, some pore space is occupied by trapped gas, which blocks the gas pathway and reduces the effective gas permeability. Increased viscosity is not only a result from viscous shear stresses in thin films between the pore walls and the gas liquid interface, but also a result of forces required to push lamellae through constricted pore throats [Falls *et al.*, 1989]. It is notable that either trapped or moving gas bubbles exist only in a time-averaged sense. As flow path changes, gas bubbles can switch between moving and blocking as a result of the liquid lamellae mobilization. Furthermore, increased pressure gradient will mobilize trapped gas bubbles and will hence open new flow channels. Foam, therefore, is non-Newtonian and shear thinning [Hirasaki and Lawson, 1985; Falls *et al.*, 1989].

As discussed in Chapter 2, three mechanisms account for foam generation: snap-off (Figure 2-5, Videos 5-2 and 5-3), lamella division (Figures 2-6 and 5-5, Video 5-4), and leave-behind (Figure 2-7). Snap-off and lamella division create strong foam while leave-behind mechanism only leads to weak foam.

Snap-off is a mechanical process. Figure 2-5 in Chapter 2 shows a schematic of such a mechanism. It occurs during multiphase flow in porous media regardless of the presence of surfactant. Snap-off also depends on pore geometry, liquid saturation, and heterogeneity. When gas flows from low permeability zone into a high permeability zone with a permeability contrast at least 4:1, snap-off will occur due to reduced capillary pressure [Tanzil, 2002]. Video 5-2 shows snap-off during foam flow. In this video, the

presence of SME crude oil destabilized foam. One can see bubbles being created at several snap-off triggering points but they collapsed very quickly (due to SME breaking the foam, as will be discussed later in this chapter). Snap-off happened when foam quality was lower than the lamella division case, as will be discussed next. Foam quality is the ratio between gas volume per total volume of foam. Videos also show that snap-off, when triggered, usually generated a series of bubbles (lamellae) rather than creating one single lamella. Video 5-3 shows water drops being snapped off during waterflood of SME. One can clearly see the triggering point in the upper center part in the video.

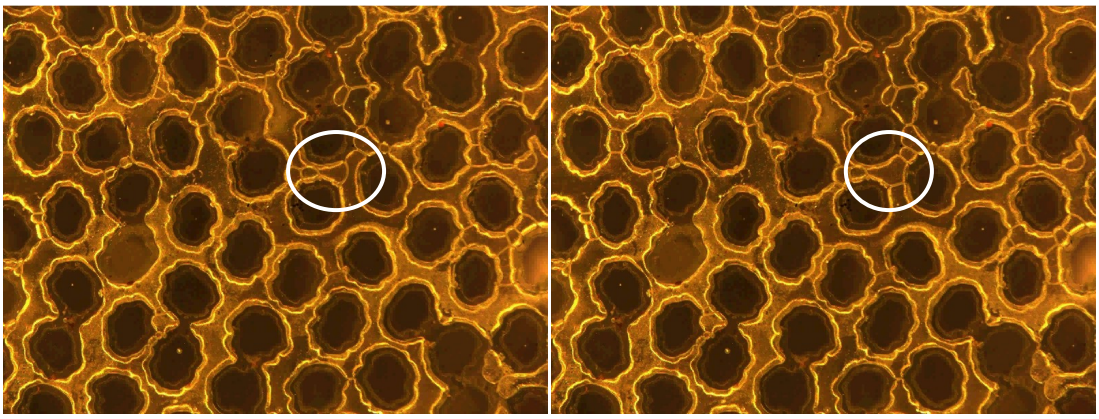

Figure 5-5 Snapshots of lamella division mechanism. White circle on the left picture shows one lamella before division. White circle on the right shows the original lamella split into two lamellae.

Lamella division mechanism was illustrated in Figure 2-6 in Chapter 2. The created lamellae are perpendicular to the flow directions. Therefore, they will block the gas pathway and raise the flow resistance. So lamella division also generates strong foam. Video 5-4 and Figure 5-5 clearly illustrate the lamella division mechanism.

Leave-behind mechanism was illustrated in Figure 2-7. This left-behind lamella is parallel to the flow direction, which does not result in much resistance. Leave-behind mechanism only forms weak foam. Leave-behind mechanism was not observed in the micro model because the pore geometry made it hard for such a phenomenon to occur.

5.2.2 Comparison of WAG and SAG (Foam)

Surfactant alternating gas injection generates foam and hence numerous stable lamellae, while water alternating gas (WAG) does not create stable lamellae. A WAG injection is shown in Videos 5-5 and 5-6. There were few lamellae present in both videos compared to foam cases, as illustrated in Figure 5-6 and Video 5-1. In Video 5-5, a slug of water was being injected into the micro model. Since no surfactant was present, stable lamellae did not form. The absence of substantial resistance to flow resulted in high liquid or gas mobility. Video 5-6 shows a situation when gas slug was being injected into the micro model. The area viewed might seem to be at rest. Fluid, however, was still flowing. Gas broke through the entire system and flowed in continuous channels. Effective gas permeability was not reduced, and the apparent viscosity was not increased. Both resulted in high mobility. Figure 5-7 is a picture taken during SAG (foam) injection. One can see that a substantial amount of lamellae were present. In previous foam videos (Videos 5-1 and 5-4), because of the presence of lamellae, gas flow passages were blocked, and its flow direction was perpendicular to the liquid film resulting in reduced gas relative permeability and increased apparent viscosity. Both effects can greatly reduce the gas mobility.

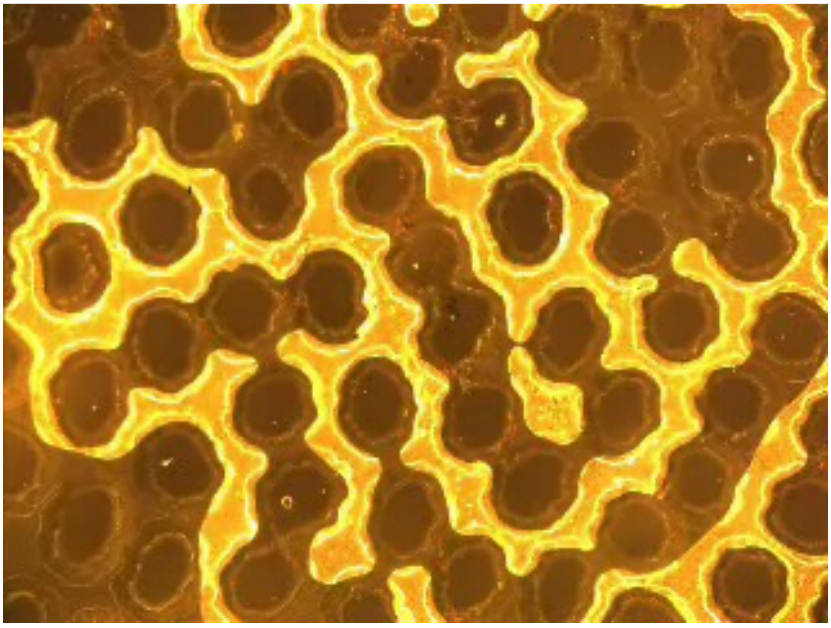

Figure 5-6 Snapshot taken during WAG injection.

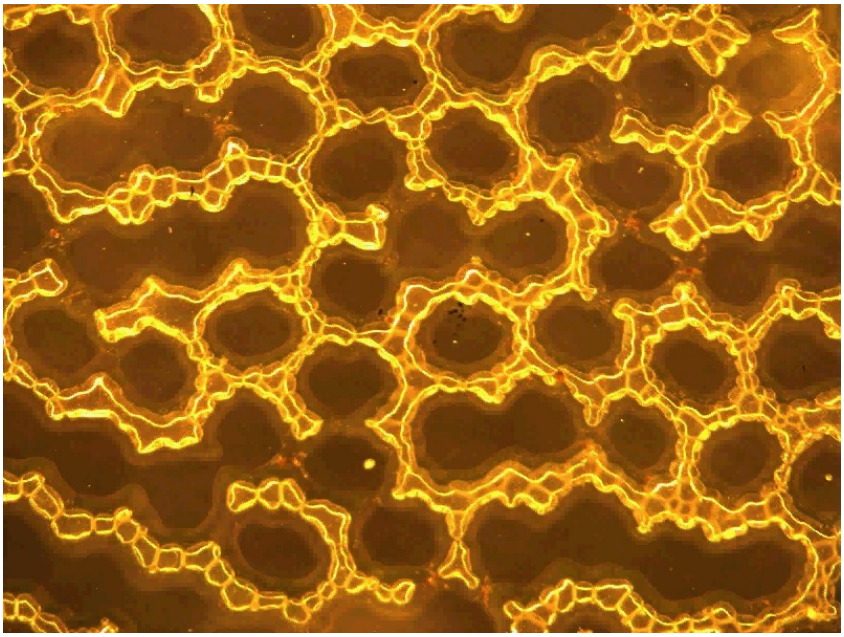

Figure 5-7 Snapshot taken during SAG (foam) injection.

5.2.3 Displacement of Crude B

In Chapter 3, a 1-D ASPF process was shown to have successfully displaced moderately viscous oil: Crude B (266 cp). Its microscopic displacement mechanism was

further investigated in the micro model. The procedure was as follows: oilflood (Video 5-7, Figure 5-8), waterflood (Videos 5-8 to 5-10, Figures 5-9 to 5-11), alkaline/surfactant flood (Video 5-11, Figure 5-12), foamflood (Video 5-12, Figure 5-13).

Video 5-7 was recorded during oilflood. Piston-like displacement front was a result of favorable mobility ratio as shown in Figure 5-8. A closer observation from this video clip shows that when oil drops at the advancing front met from two adjacent pores – on either side of a glass grain, they encompassed a drop of water. The water drop first took the shape of a thread then gradually became rounded. Water-in-oil emulsion was consequently formed. This is in accordance with observation from 1-D column displacement experiment in Chapter 3 where the first produced effluent consisted of water-in-oil emulsion and free gas.

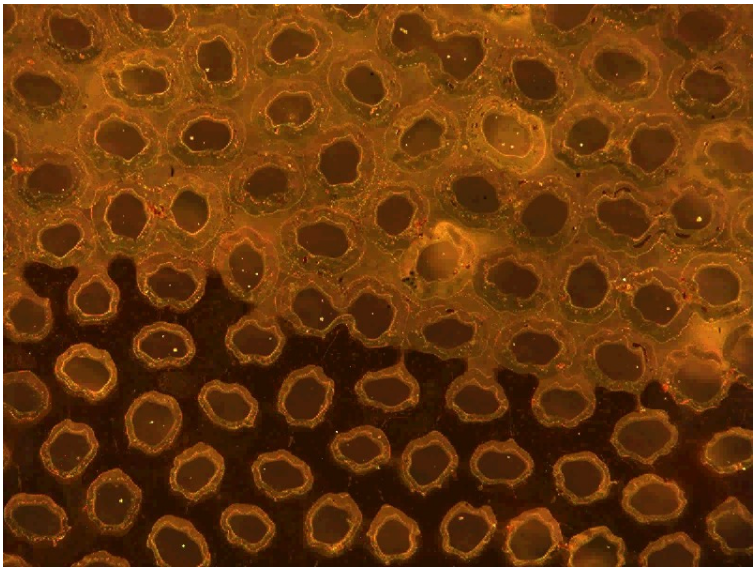

Figure 5-8 Crude B (266 cp) oilflood. Piston-like displacement front was a result of favorable mobility ratio.

Videos 5-8 to 5-10 show waterflood during three different stages: at the beginning, in the middle, and at the end. These stages are also illustrated in Figures 5-9 to 5-11. During early-stage waterflood (Video 5-8, Figure 5-9), when water drops first entered the

porous medium that was initially filled with oil, they fingered through as a result of unfavorable mobility ratio. During middle-stage waterflood (Video 5-9, Figure 5-10), oil saturation was noticeable reduced. Water had already broken through, and flowed as a continuous phase. Oil drops wiggled as water flowed by but was not displaced by it. During late-stage waterflood (Video 5-10, Figure 5-11), oil saturation was further reduced. The video seems stationary, but water was still flowing. These waterflood videos and photos also reveal that oil occupied small pores and coated around the glass grains. This is an indication that the glass model might have been preferentially oil-wet. The production of oil over a long time during waterflood is another indication that the porous medium may be oil-wet.

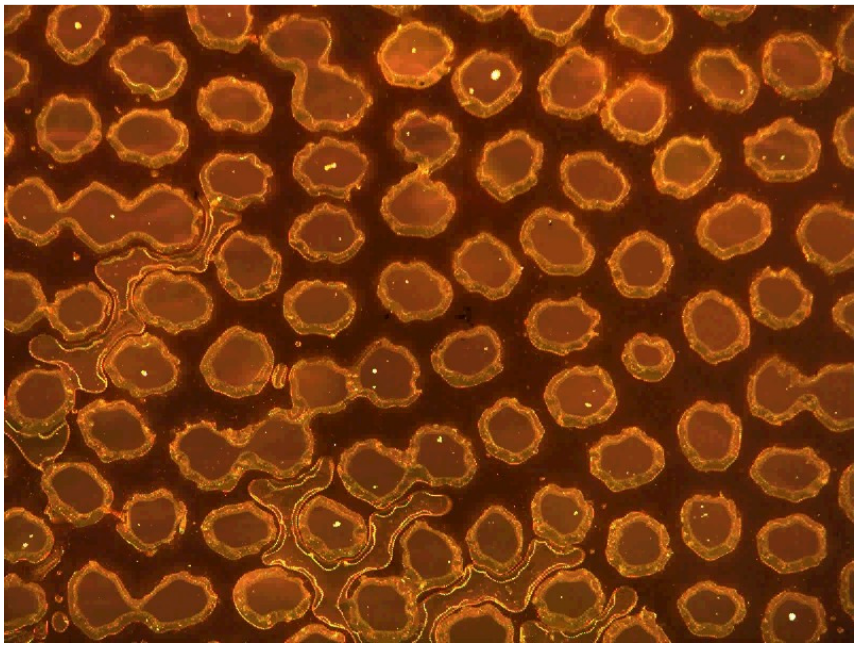

Figure 5-9 Early-stage waterflood of Crude B (266 cp).

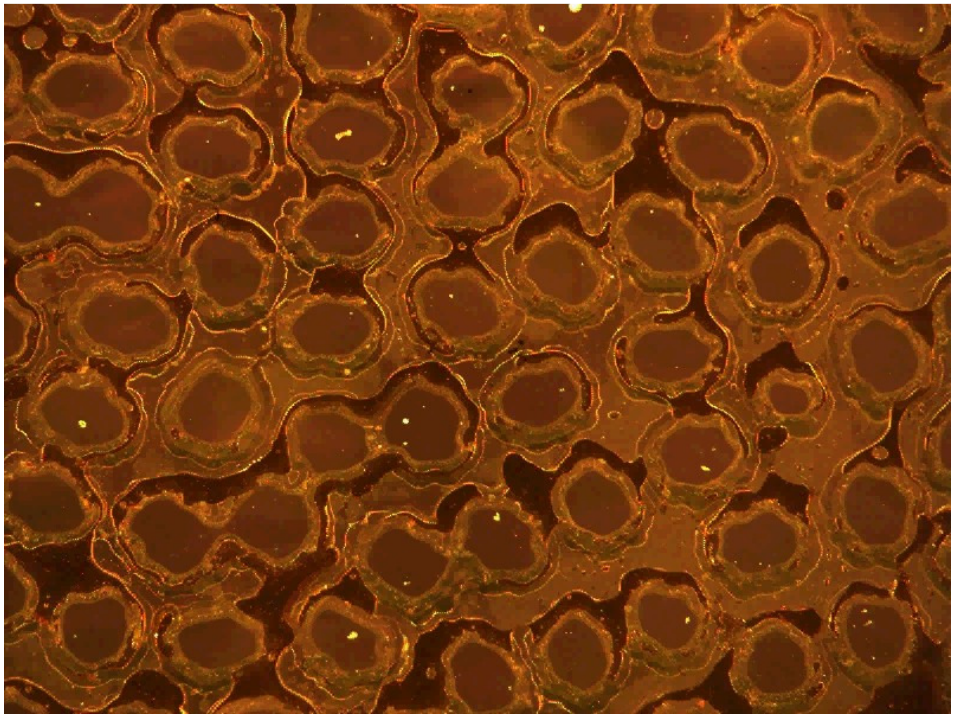

Figure 5-10 Middle-stage waterflood of Crude B (266 cp).

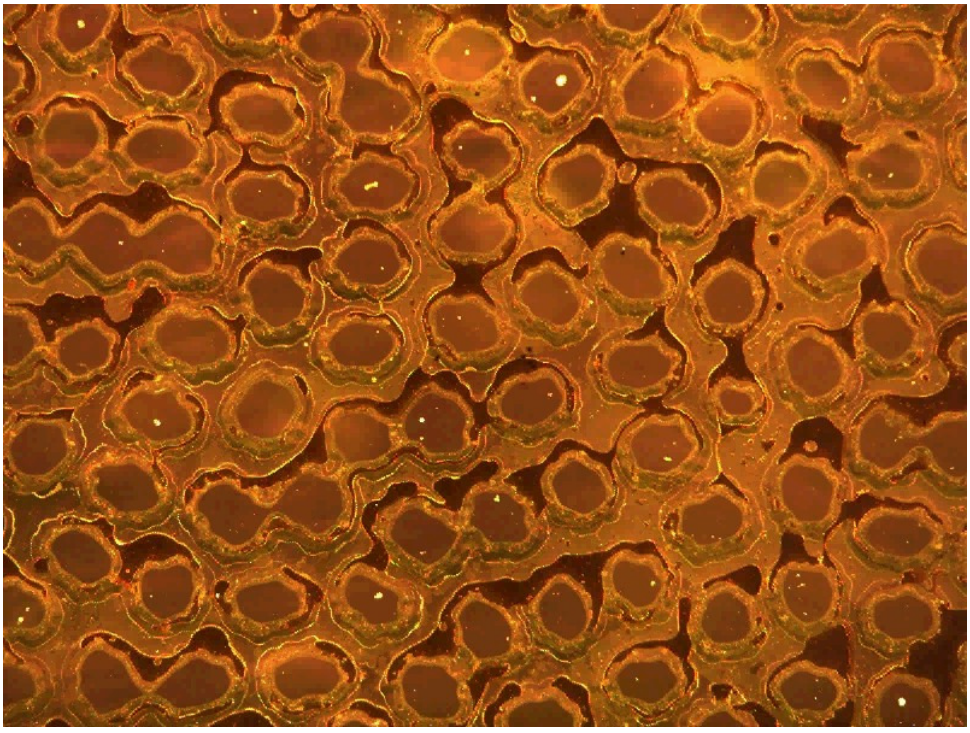

Figure 5-11 Late-stage waterflood of Crude B (266 cp).

Video 5-11 was recorded during alkaline/surfactant flood. The surfactant formulation was 0.5% NI blend, 1% Na_2CO_3, and 1% NaCl. No polymer was added. In this video, one can see that oil drops were emulsified and flowed as smaller drops. The long thin streamlines were actually comprised of very small micro-emulsion droplets, as a result of ultra low IFT. The orange color, lighter than the deep brown color of oil drops, was the color of microemulsion. This is in accordance with, and further supports the observations from the 1-D column experiment in Chapter 3 in which oil was later produced as oil-in-water emulsion whose apparent viscosity was much lower than 266 cp. Figure 5-12 shows comparison before and after the chemical flood. Most of the residual oil was displaced by alkaline/surfactant flood. Un-displaced oil was a result of surfactant slug lacking mobility control.

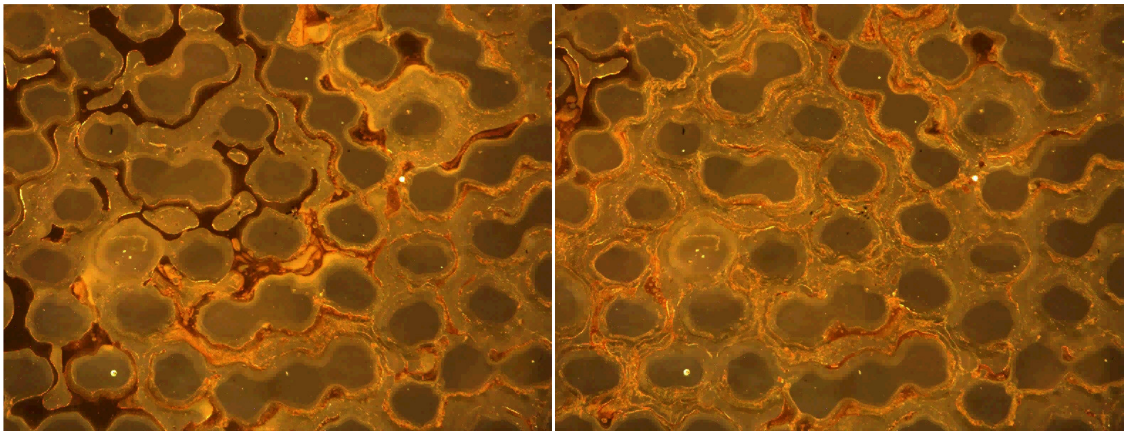

Figure 5-12 Comparison between the beginning and the end of alkaline/surfactant flood.

Video 5-12 and Figure 5-13 show a subsequent foamflood with injected slugs of 0.5% IOS 15-18 followed by air. Judging from few lamellae present in the picture, strong foam was not formed, due to crude oil that broke the foam. However, it is interesting to note that oil drops tended to stick to the gas/water surface, or flowed along the surface. These surfaces would transport the oil drops as they advanced through the porous medium. This

was likely especially when oil/water IFT was ultra low and oil became mobile. This observation may explain why the recovery in the 1-D displacement experiment described in Chapter 3 was high and SAG was successful.

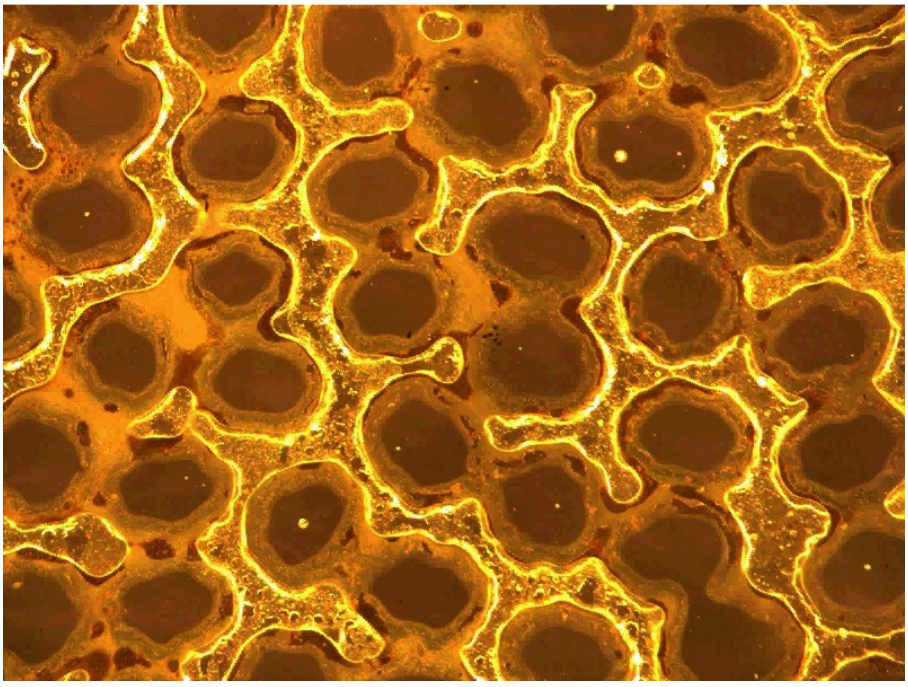

Figure 5-13 Crude B (266 cp) foam flood.

5.2.4 Foam Stability with SME

It is well-known that crude oils often destabilize foam and widely believed that light crude oils are more effective defoaming agents. The mechanisms have been extensively investigated [Garrett 1993; Aveyard 1994; Zhang *et al.* 2003; Schramm 2005]. Garrett summarized three coefficients, namely entry coefficient E, spreading coefficient S, and bridging coefficient B, that are important in interpreting the mechanisms of oil destabilizing foam. Readers may refer to Chapter for the definition of these coefficients. To break a foam lamella, an oil drop must enter the air/water surface, *i.e.* $E>0$. In order to enter the air/water surface, the oil drops must first overcome the repulsive forces caused

by the pseudoemulsion films separating these drops from the air/water interface [Nikolov *et al.* 1986; Manlowe and Radke 1990]. Once an oil drop enters, it may spread at the air/water interface *i.e.* $S \geq 0$, leading to foam lamella rupture. When $S \leq 0$ an oil drop forms a lens on one side of the air/water interface and may reach the other side as the foam film thins, thus forming a bridge. If $B > 0$, the bridge is unstable and the film breaks. By understanding these mechanisms, surfactants that can stabilize foam in presence of oil – foam 'boosters' – can be designed.

The light SME crude (API=41.1°) was extremely detrimental for foam generation. Most surfactant foaming formulations would not work in the presence of SME. These surfactants would otherwise generate very strong foam in oil-free systems. Readers may refer to Chapter 3 for more detailed discussion. As reported there, I found that addition of lauryl betaine to NI at a weight ratio of 1:2 (NI : lauryl betaine) made a new NIB blend, which is a good foaming agent with the presence of the crude oil. The mechanism of stabilizing foam may be due to increasing the critical capillary pressure for the stability of the pseudoemulsion film [Basheva, *et al*., 2000].

Video 5-2 and Figure 5-14 reveal that NI (0.5 wt% in 1% Na_2CO_3, 3.5% NaCl), being a weak foaming agent, did not stabilize foam lamellae in presence of SME. Air flowed in continuous gas channels. Snap-off occurred but transient bubbles broke immediately. However, Videos 5-13 to 5-16, and Figure 5-15 show that NIB (0.75 wt% in 1% Na_2CO_3, 3.5% NaCl) could stabilize foam lamellae. Trapped gas flowed as bubble chains even in the presence of oil, resulting in gas mobility reduction. The dark color on the contour of a bubble or a bubble chain indicates oil was in very close proximity to bubbles but did not break them. Since oil drops did not form lenses or rupture foam

lamellae, it is possible that these drops could not reach the air-water interface through a pseudoemulsion film or could not enter the interface if they did reach it, *i.e., E≤0.*

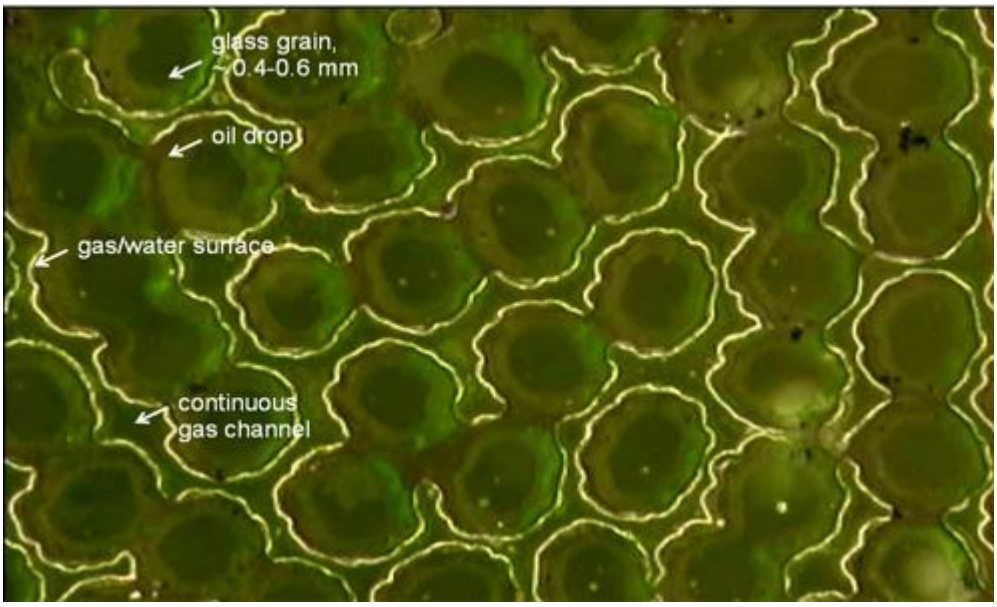

Figure 5-14 NI alone without lauryl betaine in presence of SME in a glass micro model.

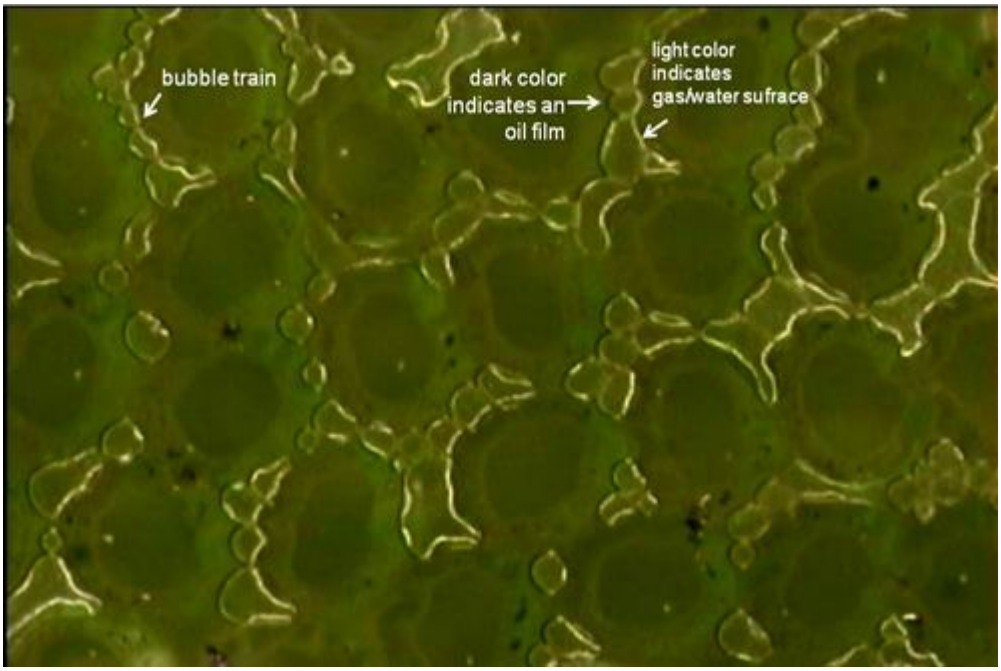

Figure 5-15 NIB (NI:lauryl betaine=1:2) in presence of SME in a glass micro model.

5.3 Conclusions

Gas injected into anionic surfactant solutions created stable lamellae forming strong foam resulting in reduced gas mobility. Gas injected into water, however, formed only continuous gas channels.

A moderately viscous (266 cp) oil was successfully displaced with ASP and SAG in a 1-D sandpack. The apparent viscosity of the displacement process was much less than that of the crude oil. Micro model videos showed that the oil was dispersed as oil-in-water emulsion. When gas was injected, oil drops tended to stick to the gas/liquid interface of gas bubbles and travel with them through the porous media.

SME crude oil was extremely detrimental for foam generation. NI alone was not a good foaming agent. However, the addition of lauryl betaine to NI at a weight ratio of 2:1(betaine: NI) made NIB a strong foaming agent even when SME was present. Micro model videos show oil drops had neither entered nor spread on the gas/water surface. The mechanism of stabilizing foam may be due to increasing the critical capillary pressure for the stability of the pseudoemulsion film.

5.4 References

Aveyard, R., Binks, B.P., Fletcher, P.D.I., Peck, T.G., Rutherford, C.E., *Advanced Colloid Interface Science, 48* (1994) 93.

Basheva, E.S., Ganchev, D., Denov, N.D., Kasuga, K., Satoh, N., Tsujii, K. 2000. "Role of Betaine as Foam Booster in the Presence of Silicone Oil Drops," *Langmuir, Vol. 16*, 1000-1013.

Falls, A.H., Hirasaki, G.J., Patzek, T.W., Gauglitz, D.A., Miller, D.D., and Ratulowski, T. "Development of a Mechanistic Foam simulator: The Population Balance and Generation by Snap-off," *SPE Reservoir Engineering*, August 1988, 884-892.

Falls, A.H., Musters, J.J., and Ratulowski, J. "The Apparent Viscosity of Foams in Homogeneous Bead Packs," *SPE Reservoir Engineering*, May 1989, 155-164.

Garrett, P.R., "The Mode of Action of Antifoams," in *Defoaming: Theory and Industrial Applications*, edited by P.R. Garrett, Marcel Dekker, New York, 1993, p. 14.

Hirasaki, G.J. "The Steam-foam Process," *JPT*, May 1989, 449-456. The full-length article is available as paper SPE 19518, 1989.

Manlowe, D.J. and Radke, C.J. 1990. "A Pore-Level Investigation of Foam/Oil Interactions in Porous Media," *SPE Reservoir Engineering, 5* (4): 495-502.

Nikolov, A.D., Wasan, D.T., Huang, D.W., Edwards, D.A. 1986. "The Effect of Oil on Foam Stability: Mechanisms and Implications for Oil Displacement by Foam in Porous Media," SPE 15443 presented at the SPE ATCE, 5-8 October, New Orleans, Louisiana.

Radke, C.J. and Gillis, J.V. "A Dual Tracer Technique for Determining Trapped Gas Saturation during Steady Foam Flow in Porous Media," paper SPE 20519, 1990.

Schramm, L.L., *Emulsions, Foams, and Suspensions: Fundamentals and Applications*, Wiley-VCH: Weinheim, 2005.

Tanzil, D., Hirasaki, G.J., and Miller, C.A. "Conditions for Foam Generation in Homogeneous Porous Media," paper SPE 75176, 2002.

Zhang, H., Miller, C.A., Garrett, P.R., Raney, K.H., *Journal of Colloid and Interface Science, 263* (2003) 633-644.

Chapter 6

ACID NUMBER MEASUREMENT

In this chapter, acid numbers of nine crude oil samples (Midland Farm 06, MarathonYates labeled 6 and 8, White Castle, Crude B, SMY, SME, PEMEX, CC2) were measured by spiking method. This method was validated by titration of samples with known acid number. Importance of electrode preconditioning was discussed. Effects of oil sample size, titrant volume step and titration dosage rate were evaluated. The benefit of this method was illustrated by an oil titration without spiking.

6.1 Acid Number in Alkali/Surfactant/Polymer (ASP) Flooding

In alkaline/surfactant/polymer/foam (ASPF) flooding, soap (natural surfactant) can be generated by the reaction between alkali and acids in crude oil (usually naphthenic acid). The generated soap will lower oil/water interfacial tension (IFT). The ratio of natural soap to synthetic surfactant determines the optimal salinity in the low IFT range [Liu *et al.* 2008]. Although the particular acids present depend strongly on crude oil type, the number of acid groups present can be characterized by acid number. Acid number is defined as the quantity of base, expressed as milligrams of potassium hydroxide per gram of sample, required to titrate a sample to a specified end point [ASTM, D644-01]. An acid number of 0.5 mgKOH/gOil or greater will be a good candidate for an ASPF process, but acid numbers as low as 0.2 mgKOH/gOil may be candidates since only a small amount of surfactant is required to saturate oil-brine interfaces [Lake, 1989].

6.2 Experimental

ASTM standard procedure requires large amount of sample, 20 g oil sample if acid number is less than 1 mgKOH/gOil. In addition, the titration end point by ASTM is frequently ambiguous. However, measurement of acid numbers measured by spiking method [Fan and Buckley, 2007] not only requires smaller sample, 0.5 to 1.0 g oil, but also yields a clear end point. In this chapter, five crude oil samples were measured following the spiking method.

6.2.1 Materials

6.2.1.1 Crude Oil

Midland Farm labeled 2006 (MF06), Marathon-Yates (MY6 and MY8), White Castle (Q-Sand),Crude B (Crude B), Mars Yellow (SMY), SME, PEMEX, and Chevron CC2 crude oil samples were used. Unless otherwise stated, for each titration 0.5g oil sample was dissolved in 75 mL solvent.

6.2.1.2 Solutions

Organic solvent was comprised of 50% toluene (HPLC grade, Fisher), 49.5% 2-propanol (HPLC grade, Fisher), 0.5% deionized water (18.2 MΩ). Spiking solution was prepared with stearic acid (Aldrich) dissolved in the solvent described above at a concentration of 0.02 M. Blank solution was prepared with 75 mL organic solvent with 1 mL spiking solution. Titrant was prepared by diluting 1.0 M tetrabutylamonium hydroxide (TBAOH) in methanol (Sigma-Aldrich) to 0.05 mol/L in ethanol (200 proof,

Aaper Alcohol and Chemical Co.). Calibration solution was made of 0.002 mol/L potassium hydrogen phthalate (KHP) in deionized water [Fan and Buckley, 2007].

6.2.1.3 Equipment

A titrator (716 DMS Titrino) connected to a computer was used for automatic titration and data collection. A Metrohm Solvotrode glass electrode (6.0229.100) for application in organic solvent was used as sensor. A Metrohm general glass electrode (6.0232.100) and an Orion 8165 combination pH electrode were tested but not used in titration. The electrolyte solution was 0.4 mol/L Tetra Ethyl Ammonium Bromide (TEABr) in ethylene glycol for Metrohm Solvotrode, and 3 mol/L KCl in deionized water for both Metrohm general and Orion.

6.2.2 Method

Electrode time responses in organic and aqueous solvent were tested before titration.

Each oil sample was dissolved in 75 mL organic solvent with 1 mL spiking solution.

The electrode was preconditioned in organic solvent between two titrations.

Unless otherwise stated, titrant was delivered with the volume steps of 0.033 mL. Dosage rate was 0.2 mL/min. Different concentrations of stearic acid were titrated. A control experiment of titrating sample with known acid number (stearic acid dissolved in a mixture of decane and dodecane) was made. Effect of crude oil sample size, volume step and titration rate was examined. Titrant was calibrated by delivering TBAOH to 0.002mol/L KHP. Acid number can be calculated by

$$AN = (V_i - V_b) \cdot M \cdot M_w / W \qquad \text{Equation 6-1}$$

Where

AN : acid number (mgKOH/gOil)

V_i : volume of titrant at the sample inflection point (mL)

V_b : volume of titrant at the blank inflection point (mL)

M : molar concentration of TBAOH (mol/L)

M_w : molecular weight of KOH (56.1 g/mol)

W : weight of the oil sample (g)

6.3 Results and Discussion

6.3.1 Electrode

Three electrodes were tested. Their properties were listed in the table below.

Table 6-1 Properties of tested electrodes

	Metrohm Solvotrode	Metrohm general	Orion 8165
Electrolyte Solution	0.4 mol/L Tetra Ethyl Ammonium Bromide (TEABr) in ethylene glycol	3 mol/L KCl in DI	3 mol/L KCl in DI
Diaphragm	Ground-joint	Ceramic plate	Epoxy body

Metrohm Solvotrode was chosen over the other two electrodes because it has faster and more stable response in organic solvent. For this particular electrode, the filling solution TEABr in ethylene glycol is soluble in the organic solvent. In contrast, Orion and Metrohm general electrodes use nearly saturated KCl as filling solution. This leads to the build-up of KCl precipitate on the diaphragm, which impedes the ion transport (see Figure 6-1). Furthermore, Solvotrode's ground-joint allows inner electrolyte solution to flow out of the aperture covered by the porous glass, which makes it easy to clean.

However the diaphragm in Metrohm general is made of a ceramic plate. When contacted with crude oil, the solid contaminants in oil the may clog the pores in the ceramic plate and damage the electrode.

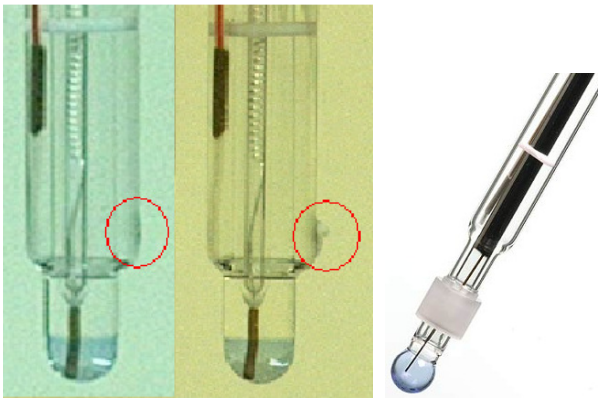

Figure 6-1 Picture of Metrohm general and Metrohm Solvotrode electrode. (Left) Metrohm general: before contact with organic solvent diaphragm is clean of precipitates. (Middle) Metrohm general: after contact with organic solvent KCl precipitates around diaphragm. (Right) Metrohm Solvotrode electrode.

6.3.2 Preconditioning

In order to keep the potential of a glass electrode constant, the ion exchange across the membrane must have reached a stable condition. Conditioning electrode in suitable electrolyte is necessary to ensure an initial solvated layer condition that is as stationary as possible so that the results can be as reproducible as possible. The electrode should be preconditioned in the titration solvent described in **6.2.1.3**, as well as between two successive titrations to restore its response. Preconditioning is important in both non-aqueous and aqueous titration as will be discussed below.

6.3.2.1. Precondition in Organic Solvent for Non-Aqueous Titration

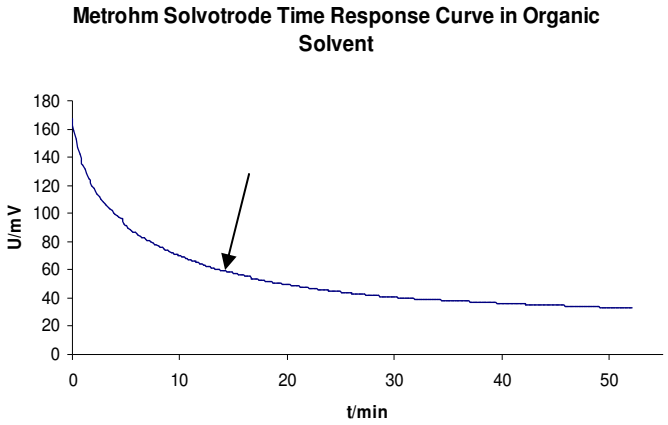

Figure 6-2 Metrohm Solvotrode time response curve in organic solvent. Initial condition: electrode had been soaked in DI water overnight.

The curve in Figure 6-2 is used to determine how long the electrode should be preconditioned. If we want the change in EMF to be less than 5% between two additions of titrant, the rate of change in EMF should be less than $5\%\Delta U / \Delta t$. Here, ΔU is the minimum difference in EMF between two additions of titrant and is about 5 mV from most experiments; Δt is the time interval between two additions of titrant and is about 10 sec. So the rate of EMF change is 1.5 mV/min. This can be satisfied by 14 minutes of preconditioning as shown by the arrow in the above plot. In real cases, however, preconditioning time was usually between 15-30 minutes.

Figure.6-3 shows preconditioning of the electrode in water instead of organic solvent before non-aqueous titration will make a difference.

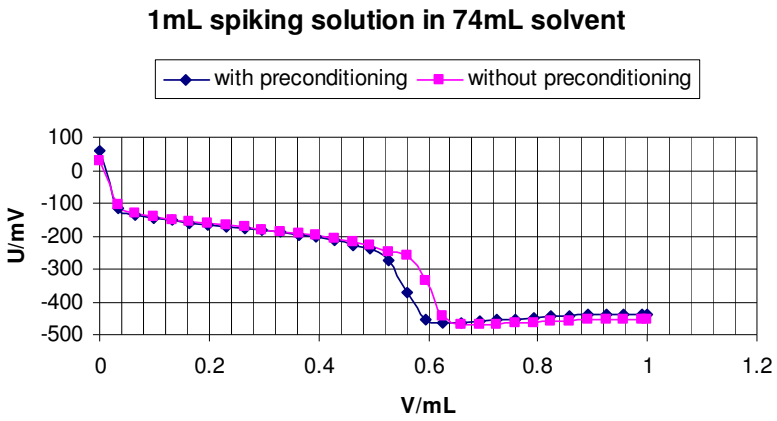

Figure 6-3 Two blank titrations with and without preconditioning. Inflection points V(red)=0.596 mL, V(blue)=0.559 mL. Relative error=6.6%.

6.3.2.2. Precondition in DI Water for Aqueous Titration

TBAOH (prepared to be 0.0500 mol/L) was calibrated by delivering TBAOH to 75 mL 0.00200 mol/L aqueous KHP solution. In Figure 6-4, the plot on left shows that blue curve without preconditioning on day 1 gives C_{TBAOH}=0.0440mol/L. However, black and purple curves preconditioned in DI water for 5 minutes on day 1 and day 2 both give C_{TBAOH} =0.0500 mol/L which is in accordance with the prepared concentration. The electrode time response curve in DI water in Figure 6-4 shows that Metrohm Solvotrode restored very quickly.

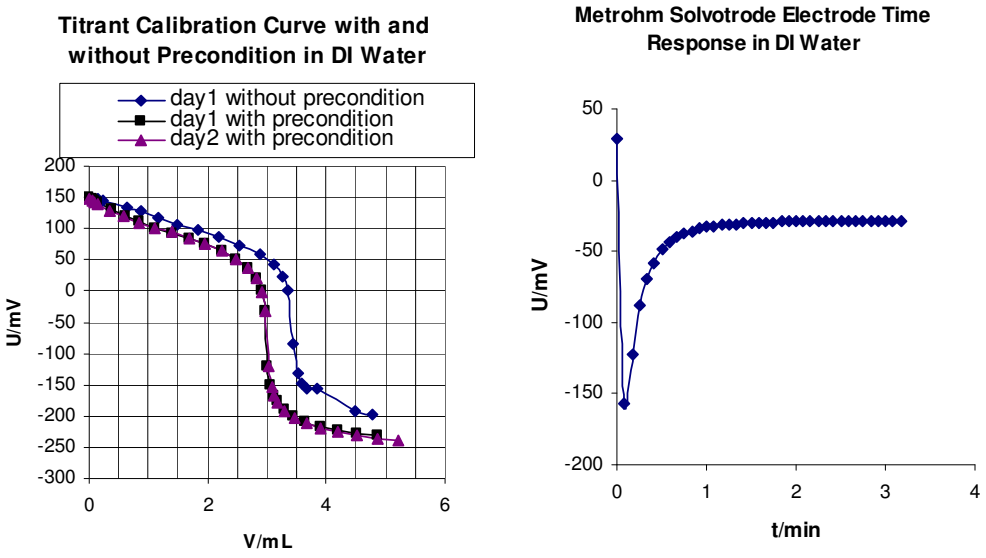

Figure 6-4 Preconditioning shows difference in TBAOH calibration in aqueous solvent. Electrode time response curve (Figure 6-2) provides a criterion in determining preconditioning time. Initial condition: electrode had been soaked in filling solution (TEABr in ethyleneglycol).

6.3.3 Electrode Response with Contact of Crude Oil or Blank Solution

It was reported by New Mexico Tech that whether blank titration was performed before or after oil titration made a dramatic difference [Fan and Buckley, 2007]. Blank titration before oil titration would give $V_b > V_i$, which would result in a negative acid number value. However, if the blank was measured after oil titration, they had $V_b < V_i$. According to them, only if the blank was measured after contact with the crude oil (the electrode response was affected for both measurements in the same manner) could a realistic measure of acid number be obtained. This phenomenon of dramatic change in blank titration curve was not observed in either MY6 or Q-Sand experiments in the present work (Figure 6-5 and 6-6).

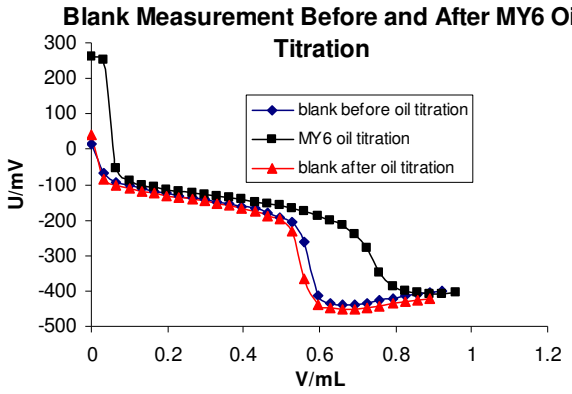

Figure 6-5 Blank measurement before and after MY6 oil titration. Exposure to MY6 crude oil sample does not drastically change the electrode response. V_b (before)=0.566 mL, V_b (after)=0.556 mL.

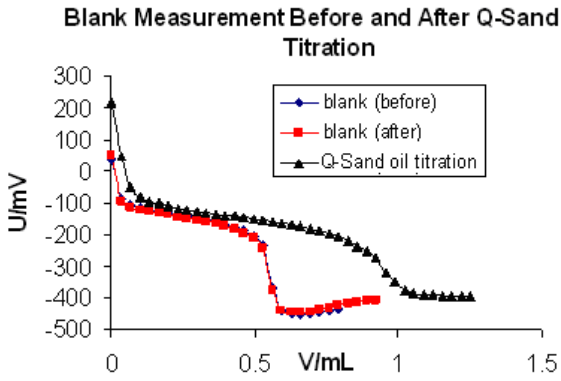

Figure 6-6 Blank measurement before and after Q-sand oil titration. Exposure to Q-Sand crude oil sample does not immediately or drastically change the electrode response either. V_b (before)=0.557 mL, V_b (after)=0.554 mL.

Note that Figure 6-5 shows a difference of 0.01mL (an error of 1.8%) between two blank titrations. This error would be significant if the acid number is low. In this case, oil sample size must be increased.

It is observed that preconditioning in different solutions makes a difference in blank titration provided that other titration parameters remain the same (Figure 6-7).

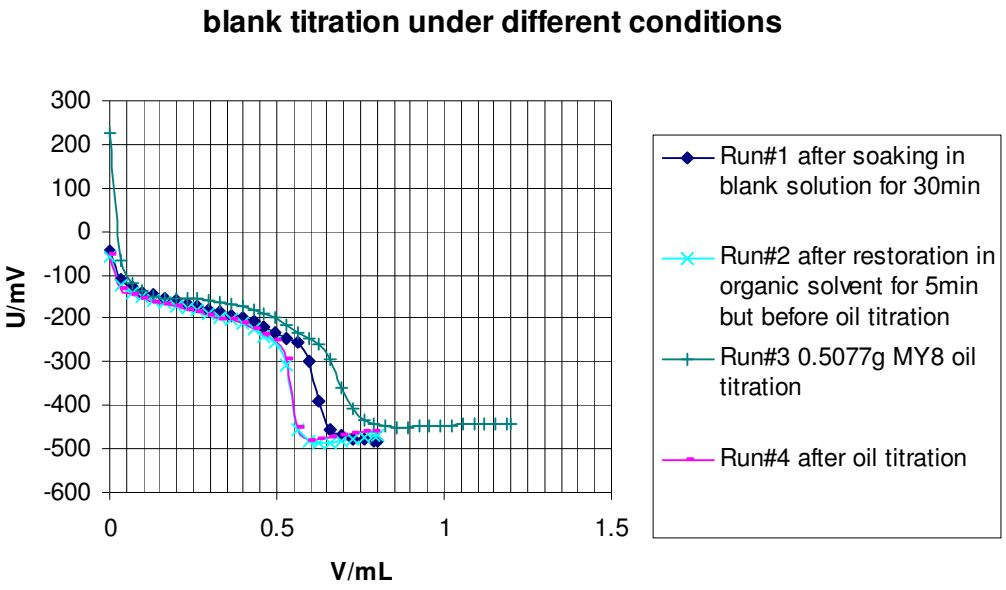

Figure 6-7 Blank titration under different conditions. Run#1 was the first blank titration after the electrode had been soaked in blank solution for 30 minutes, V_{b1} =0.618 mL. Run#2 was the second blank titration, V_{b2} =0.535 mL. Run#3 was the oil titration, V_{i3} =0.687 mL. Run#4 was the third blank titration, V_{b4} =0.538 mL. Between two Runs, the electrode was preconditioned for 5 minutes in organic solvent.

Run#2 and Run#4 curves overlap meaning blank titration before or after oil titration does not make dramatic difference. Run#1 and Run#2 curves do not overlap meaning the electrode response is also affected by blank solution. This is another reason why preconditioning is important. It is also important to establish a standard way of preconditioning, i.e. whether the electrode should be preconditioned in the solvent or the sample. Since preconditioning in organic solvent restores the electrode's original response, and also from Figure 6-7, the difference between Run#2 and Run#4 curves overlap one another, it is suggested that the electrode be preconditioned in the organic solvent before each titration.

6.3.4 Titration

Before oil sample titration, spiking method is validated by two controlled experiments: 1) titration of stearic acid solutions with different concentrations, and 2) titration of an alkane oil sample with known acid number. Both experiments match the measured results with the theoretical values very well, as shown in sections **6.3.4.1** and **6.3.4.2**. The titrant used is TBAOH, which is more stable than KOH [Fan and Buckley, 2007]. Acid numbers for five crude oil samples are presented in section **6.3.4.3** followed in section **6.3.4.4** by a study of method sensitivity.

6.3.4.1 Titration of Spiking Solution

Spiking solution was made to be 0.0200 mol/L stearic acid in organic solvent described in **6.2.1.2**. Stearic acid concentration by this spiking method was measured by titration of various volumes of spiking solution (Figure 6-8 shows the titration curves). If the measured concentration agrees with the prepared concentration, then the spiking method is valid. Measured concentration of stearic acid in spiking solution can be calculated from the slope in Figure 6-9. The concentration of titrant was prepared to be C(TBAOH) =0.0500 mol/L. Calibration of titrant after one week showed this concentration remained unchanged.

$C(stearic) = slope \times C(TBAOH) = 0.3992 \times 0.0500 = 0.0200\ mol/L$. This value was in accordance with prepared concentration (0.0200 M). Therefore, spiking method was valid and controllable.

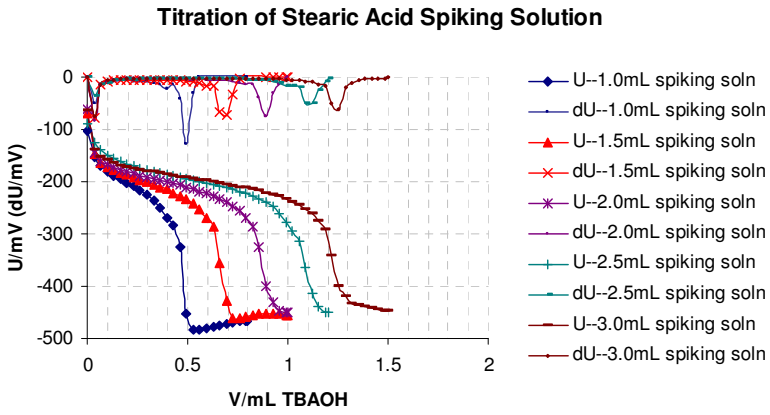

Figure 6-8 Titration curves of spiking solution. Inflection points for 1.0, 1.5, 2.0, 2.5, 3.0 mL spiking solutions were EP(1.0)=0.500 mL, EP(1.5)=0.693 mL, EP(2.0)=0.891mL, EP(2.5)=1.089 mL, EP(3.0)=1.301 mL .

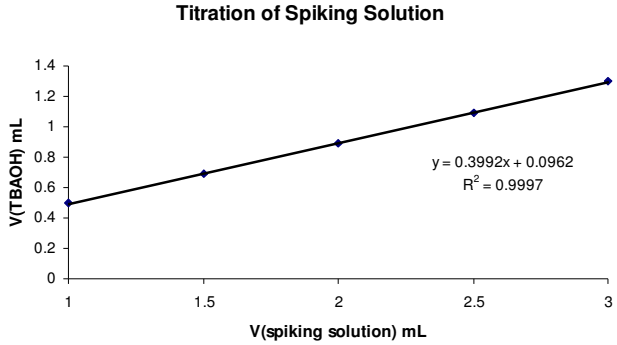

Figure 6-9 Volume of titrant versus volume of spiking solution.

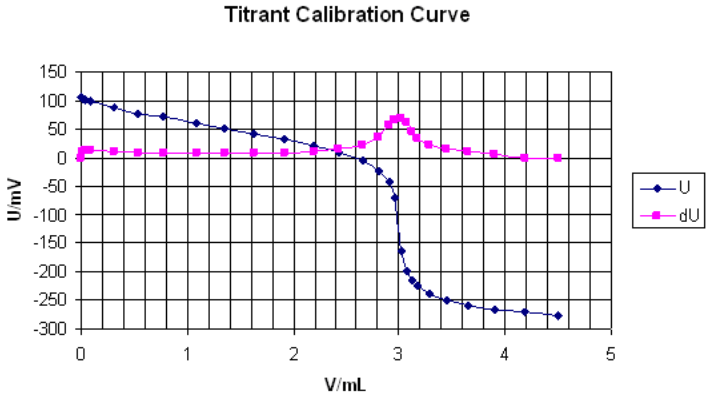

Figure 6-10 Titrant calibration curve. TBAOH was delivered into 75mL 0.002001mol/L KHP. Ending point is at V_{TBOAH}=2.999mL. So C_{TBAOH}=0.0500mol/L.

6.3.4.2 Titration of Oil Sample with Known Acid Number

0.0550g stearic acid was dissolved in a mixture of 10g decane and 10g dodecane. Thus this oil had a known acid number of 0.542 mgKOH/gOil. If measured acid number agrees with this known acid number, the spiking method is valid. Figure 6-11 shows a typical titration curve of this alkane oil sample. The measured acid number values are tabulated in Table 6-2. The error between measured acid number (0.549 mgKOH/gOil) and theoretical value (0.542 mgKOH/gOil) is 1.3%. This error is tolerable and spiking method is valid with alkane oil with known acid number.

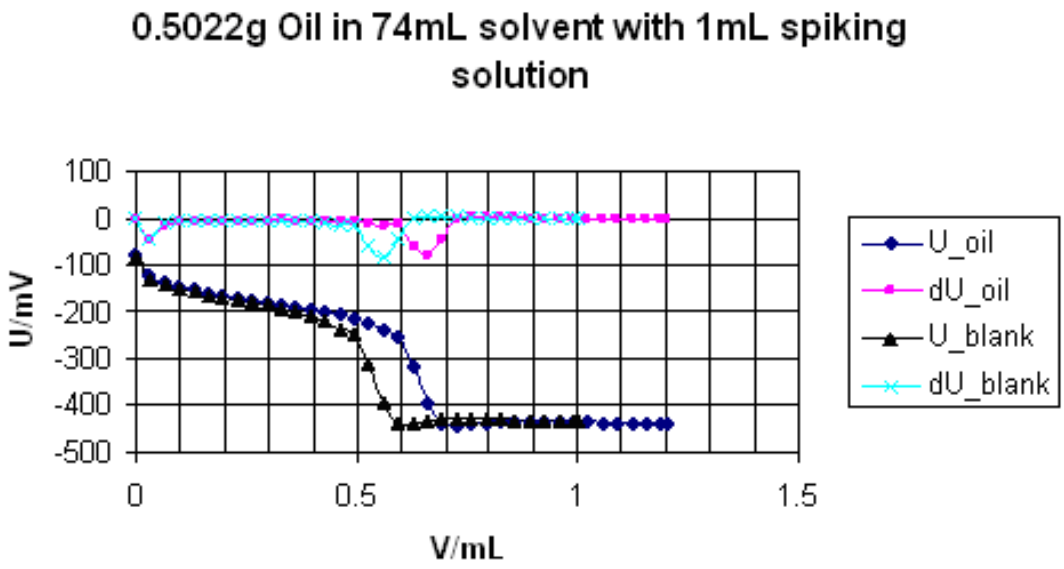

Figure 6-11 Titration of oil with known acid number (stearic acid in decane and dodecane 1:1 w/w). Inflection point at EP(oil)=0.636mL, EP(blank)=0.538mL.

Table 6-2 Samples with known acid number (Mean=0.549; Std=0.010; Error=(0.549-0.542)/0.542=1.3%

)Sample	Vi	Vb	Size	AN
1	0.691	0.596	0.5014	0.544
2	0.636	0.538	0.5022	0.560
3	0.645	0.550	0.5042	0.541

6.3.4.3 Titration of Crude Oil

Table 6-3 Acid number of nine crude oil samples (mgKOH/gOil)

crude oil	MF06	MY6	MY8	Q-Sand	Crude B
TAN	0.343±0.012	0.746±0.019	0.835±0.048	2.22±0.08	4.79±0.03
crude oil	SMY	SME	PEMEX	CC2	
TAN	0.314±0.008	0.062±0.004	0.018±0.019	2.18±0.05	

Table 6-4 Acid number value measured by other institutions (mgKOH/gOil)

	MF06	MY4
New Mexico Tech.	0.69±0.03 0.75±0.06	0.22
Triton Analytics Corp.	--	0.54

Table 6-3 shows the titration results of nine crude oil samples. Figure 6-12 represents a typical crude oil sample titration plot.

Table 6-4 shows that acid number obtained from different laboratories varied from each other. It should be noted that Triton Analytics Corp did not adopt this spiking method. They used standard ASTM method and the choice of inflection point was quite arbitrary. Although New Mexico Tech used the spiking method to measure acid numbers, they used an electrode with KCl as filling solution. Also, they did not precondition their electrode before titration. The disadvantage of KCl in organic solvent and the importance of preconditioning were discussed in previous section of this chapter. Acid numbers could be compared only if the measurements were performed following the same procedures.

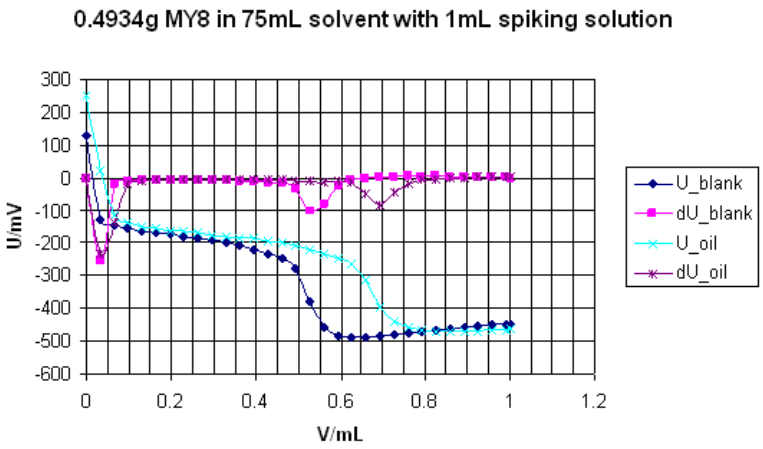

Figure 6-12 Blank and oil titration of Marathon-Yates (MY8) crude oil sample. EP(oil)=0.673mL, EP(blank)=0.525mL; ΔV=0.033mL; titration rate=0.2mL/min.

6.3.4.4 Effect of Sample Size, Volume Step, Titration Rate

From Equation 6-1, with larger sample size or smaller volume step, more accurate acid number value can be obtained. This is evaluated on MY8 crude oil sample by changing the sample size from 0.5 g to 1.0 g and the volume step from 0.02 mL to 0.05 mL. The effect of titration rate was evaluated by changing the dosage rate from 0.1 mL/min to 0.4 mL/min.

Table 6-5 Effect of sample size. ΔV=0.033 mL, titration rate=0.2 mL/min

Vi (mL)	Vb (mL)	Oil Size(g)	AN (mgKOH/gOil)	Mean	Standard Deviation
0.687	0.528	0.5077	0.889	0.834	0.066
0.690	0.555	0.5037	0.761		
0.673	0.525	0.4934	0.852		
0.769	0.528	0.7543	0.907	0.907	0.040
0.735	0.486	0.7471	0.946		
0.724	0.497	0.7441	0.866		
0.798	0.497	1.0006	0.854	0.886	0.039
0.825	0.497	1.0024	0.929		
0.807	0.499	1.0004	0.874		

This table shows that as sample size increased, standard deviation became smaller.

Table 6-6 Effect of volume step. Sample size=0.5 g, titration rate=0.2 mL/min

Vi(mL)	Vb(mL)	Oil Size(g)	ΔV(mL)	AN(mgKOH/gOil)	Mean	Standard Deviation
0.643	0.506	0.4912		0.796	0.835	0.048
0.646	0.504	0.4933	0.020	0.821		
0.660	0.507	0.4915		0.888		
0.687	0.528	0.5077		0.889	0.834	0.066
0.690	0.555	0.5037	0.033	0.761		
0.673	0.525	0.4934		0.852		
0.645	0.500	0.4990		0.829	0.784	0.098
0.642	0.525	0.4971		0.672		
0.648	0.500	0.4960	0.050	0.852		

This table shows that as volume step decreased, standard deviation became smaller.

Table 6-7 Effect of titration rate. Sample size=0.5 g, ΔV=0.033 mL

Vi(mL)	Vb(mL)	Oil Size(g)	Titration rate(mL/min)	AN(mgKOH/gOil)	Mean	Standard Deviation
0.657	0.501	0.5017		0.883	0.875	0.046
0.668	0.502	0.5144	0.1	0.916		
0.662	0.518	0.4948		0.826		
0.687	0.528	0.5077		0.889	0.834	0.066
0.690	0.555	0.5037	0.2	0.930		
0.673	0.525	0.4934		0.852		
0.657	0.499	0.5046		0.889	0.829	0.073
0.645	0.515	0.4935	0.4	0.748		
0.657	0.506	0.5042		0.850		

This table shows that as titration rate decreased, standard deviation became smaller.

Table 6-8 Error analysis by changing the oil size, ΔV=0.033 mL

Sample Size W (g)	0.5	0.75	1.0
Error range	0.093	0.062	0.046
Standard deviation	0.066	0.040	0.039

Table 6-9 Error analysis by changing the volume step, oil size=0.5 g

ΔV(mL)	0.020	0.033	0.050
Error range	0.056	0.093	0.14
Standard deviation	0.048	0.066	0.098

Take ½ ΔV as measuring accuracy, according to equation (6.1), this will change the accuracy in acid number by $1/2\Delta V \cdot M_w \cdot M/W = 1/2\Delta V \times 56.1 \times 0.05/W$. Tables 6-8 and 6-9 show that the standard deviation is smaller than the error range. The volume step and oil size adopted in these measurements satisfied accuracy requirement. Also, standard deviation becomes smaller with larger oil sample size (Table 6-5) and smaller volume step (Table 6-6), as expected. It is also found that accuracy improves with slower titration rate (Table 6-7).

6.3.5 Benefits of Spiking

In ASTM standard procedure, it is sometimes ambiguous to choose the inflection point, especially when a crude oil sample contains different acids with various pKa's. Such samples might give multiple inflection points, or these points offset resulting in no inflection point. Neutralization of multiple acids with only slightly different pKa's could distort the titration curve. Spiking is advantageous in that it allows using smaller oil sample and gives sharper inflection point. Taking MY-6 crude oil, for example, the acid

number is 0.75 mgKOH/gOil. 0.5 g oil sample contains 0.75 mgKOH/gOil)*(0.5 gOil)/(56.1 gKOH/mol)=0.0067 mmol acid (if we consider acid contained in oil to be monoacid). This 0.5 g oil sample was spiked with 1 mL 0.02 mol/L stearic acid (also a monoacid), which is equal to 0.02 mmol acid. So, in the spiked oil sample, the majority is stearic acid (about 75% in this example) and that is why spiking gives sharper end point as shown in Figure 6-12.

Figure 6-13 shows titration without spiking. In this case, the blank is merely comprised of organic solvent in which oil sample will be dissolved. There is not a clear inflection point.

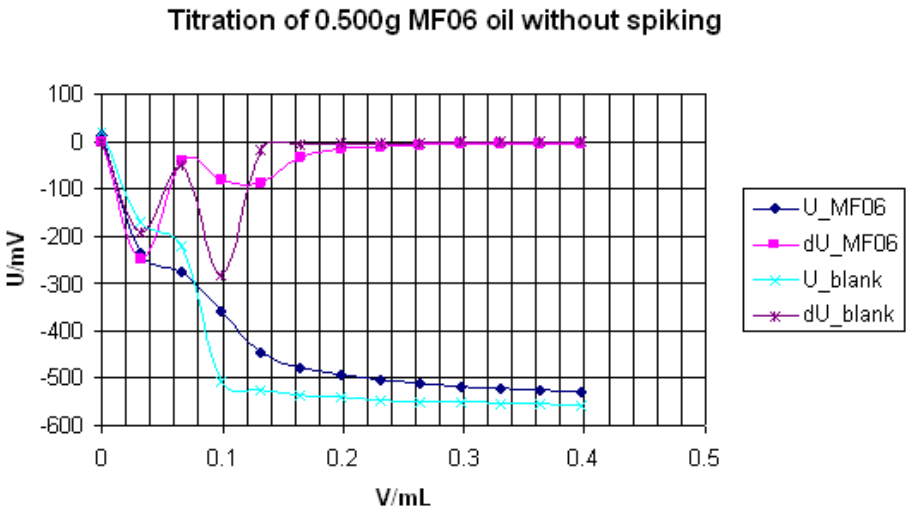

Figure 6-13 Titration of 0.500g MF06 crude oil sample without spiking. Points with maximum magnitude of dU/dV are at 0.033mL and 0.132mL; 0.033mL and 0.099mL for blank curve.

6.4 Conclusions

Metrohm Solvotrode electrode has faster and more stable response in organic solvent.

Preconditioning of electrode is essential in that it restores the electrode behavior in proper solvent. Electrode response changes upon contact with either crude oil or blank

solution. It is therefore important to establish a preconditioning criterion, or to reduce the experimental error (*e.g.* by increasing the sample size). Larger sample size, smaller volume step, and slower titration dosage rate will result in smaller standard deviation and consistent measured values. Spiking is advantageous in that it generates a sharp inflection point.

6.5 References

ASTM Standard Test Method D664-01 "Standard Test Method for Acid Number of Petroleum Products by Potentiometric Titration," Annual Book of ASTM Standards, Sect. 5, Am. Soc. Testing Materials, Philadelphia, 2001

Fan, T. and Buckley, J.S., "Acid Number Measurements Revisited," *SPE J.* 12(4): 496-500, SPE-99884-PA, 2007.

Lake, L.W. *Enhanced Oil recovery*, Prentice Hall, Englewood Cliffs, New Jersey, 1989

Liu, S., Zhang, D.L., Yan, W., Puerto, M., Hirasaki, G.J., and Miller, C.A. 2008. "Favorable Attributes of Alkali-Surfactant-Polymer Flooding," *SPE J.* 13 (1): 5–16. SPE-99744-PA. doi: 10.2118/99744-PA.

Chapter 7

CONCLUSIONS

7.1 Focus/Problem to Be Solved

The focus of this thesis was to conduct laboratory experiments which would help in understanding mechanisms and in actual design of surfactant enhanced oil recovery (EOR) processes in various scenarios close to reservoir conditions such as heterogeneity, effects of crude oil, wettability, viscosity, etc. Two main processes -- surfactant-induced wettability alteration and gravity drainage, as well as application of foam mobility control -- were elucidated by extensive laboratory research.

7.2 Importance

The importance of the subject owes to the unique attributes of foam. Foam has higher apparent viscosity in high- than in low-permeability regions, which makes it a better mobility control agent than polymer in heterogeneous systems. In addition, foam can be applied under many reservoir conditions where the use of polymer is limited. For example polymer will decompose at high temperature; cross-link when divalent or trivalent ions are present; and will not transport in matrix pores whose sizes are smaller than the macromolecules, etc. Last but not the least, less consumption of costly surfactants and/or polymer makes foam an economical candidate in field applications.

The cost is low especially when the gas to be used is available at a pressure high enough that little or no further costly compression is required.

7.3 Methods

Two main methods were systematically established. One method was the surfactant-induced wettability alteration and gravity drainage approach, which was shown to cause exchange of fluids between high- and low-permeability layers and hence greatly improved recovery. The process was demonstrated in a 2-D layered sandpack with various supporting experiments such as acid and soap number determination, phase behavior and salinity scan, IFT and contact angle measurements, etc.

An alternative method was to apply foam mobility control as a robust viscous-dominant process. Foaming surfactant formulations were evaluated in 1-D and 2-D sandpacks first without then with the presence of crude oil. The mechanisms were further investigated at the pore level in a glass micro model. Injection schemes, the sandpack geometry, and surfactant blending ratios, were tested and optimized.

7.4 Context

The context of this research was to find solutions to improve oil recovery in a layered 2-D heterogeneous reservoir with approximately 20 to 1 permeability contrast that was preferentially oil-wet. Recovery by waterflood was low due to injected water flowing through high-permeability zone leaving low permeability zone unswept. Since first introduced more than 30 years ago, foam as a means of mobility control in surfactant

flooding has been widely tested in the field. However it has yet to be commercially applied due to economics, the expense of chemicals, and surfactant adsorption.

7.5 Results

7.5.1 Results from Processes in 1-D Homogeneous Sandpacks

In glass column experiments, in an oil-free system, Triton X-200, AOS16-18, IOS15-18, N25-7EO, N67-9EO were found to be good foaming agents at low salinity (1% Na_2CO_3, 2~3.5% NaCl). N25-7EO was a good foaming agent in high-salinity SME brine. BASF Avanel surfactants, NI, DowFax8390 were not good foaming agents.

Without adding betaine near the optimal ratio, none of the surfactants or their blends would generate strong foam in the presence of residual SME crude oil.

A foam drive with surfactant alternating gas (SAG) can be used as an alternative for polymer drive in an alkaline/surfactant/polymer (ASP) enhanced oil recovery (EOR) process. The apparent viscosity of SAG is a function of pressure gradient, permeability, and gas fraction. A moderately viscous (266 cp) oil was displaced successfully with ASP and SAG. The apparent viscosity of the displacement process was much less than that of the crude oil. The oil may have been dispersed by the foam as oil-in-water emulsion.

In 1-D forced displacement of residual SME crude oil, strong foam was formed in three cases: 1) with polymer, 2) with pre-generated foam, and 3) when betaine was added. Recovery was nearly 100% from residual oil in all three cases, although it took many pore volumes (PV) for the pre-generated foam. NI alone is not a good foaming agent. The addition of lauryl betaine made NIB a strong foaming agent with and without SME crude oil. NIB (NI:B=1:2) worked well in both secondary and tertiary recovery of residual SME

in terms of reducing interfacial tension (IFT) and generating foam for mobility control in silica sandpacks.

NIB (NI:B=1:2) did not work in either water-wet or oil-wet carbonate sandpacks, possibly due to surfactant adsorption.

7.5.2 Results from Processes in 2-D Heterogeneous Sandpacks

The vertical sweep of an oil-free 2-D layered sandpack with a 19:1 permeability contrast was greatly enhanced with SAG compared to waterflood or water alternating gas (WAG) injection. Foam sweep efficiency improved with increased injection pressure or reduced gas fractional flow with respect to total fluid pore volumes injection. To achieve 100% sweep efficiency, it took 1.3 total pore volume (TPV) for foam (6 psig, f_g=1/3), but it took 8 TPV for water only (4 psig, f_g=0). For WAG injection, after 6 TPV, there was still over 30% left unswept.

Foam had much higher apparent viscosity than water or WAG in 2-D system and is a promising agent for mobility control. In 2-D foam-aided sweep, there were two types of crossflow across the foam front. Behind the foam front, liquid was diverted from the high permeability layer to the low permeability layer. Ahead of the foam front, liquid was diverted in the opposite direction. Foam generated at 6 psig with f_g=1/3 showed a nearly piston-like displacement of the resident liquid even if the permeability contrast was 19:1. Crossflow resulted from the favorable mobility ratio displacement but the fluid that was diverted to the low-permeability layer was primarily the liquid fraction of the foam.

Surfactant formulations of 0.2% IOS-C15-18 and 0.2% AOS-C1618 worked very similarly in a 2-D foam sweep.

In two parallel 1-D sand columns where capillary communication was not allowed, with water only experiment, it took ~0.6 TPV to sweep out green water in high permeability region and ~3.0 TPV to sweep out the entire system. With WAG, after 1.5 TPV there was still over 80% left unswept in the low permeability region. With SAG, it took ~1.0 TPV to sweep out green water in high permeability region and 1.5 TPV to sweep out the entire system.

CTAB was effective in altering the wettability of clean silica sand from water-wet to preferentially oil-wet. Anionic surfactants such as NI could alter the wettability back to preferentially water-wet.

A 2-D heterogeneous sandpack with 19:1 permeability contrast was made preferentially oil-wet with CTAB. Gravity- and capillary pressure-driven, vertical, counter-current flow occured after 0.5 PV of an alkaline/surfactant slug was injected and the system was shut-in. The vertical flow displaced most of the oil from lower, low-permeability layer. Foamflood recovered most of the oil accumulated on top of the high-permeability layer. Strong foam was not formed due to crude oil breaking the foam. Foamflood in addition to alkaline surfactant flood recovered 89.4% of the waterflood-remaining oil. Overall recovery (waterflood+ASF) was 94.6% OOIP. This was a great improvement compared to the ASPF process in an untreated silica sandpack where shut-in was not allowed and which recovered only 64.3% OOIP.

Carbonate sand should be treated to be preferentially oil-wet with low initial water saturation and at high temperature. Treatment of crushed limestone in the environment room at 37-42 °C did not change the wettability to preferentially oil-wet. Temperature was not high enough in this short period of time and 16.9% water saturation was too high.

Centrifuging and pre-treating carbonate sand in SME crude at 85 °C may have been effective but the initial water saturation may still have been too high for effective and robust wettability alteration. The sandpack was still preferentially water-wet. Future experiments should focus on centrifuging to higher capillary pressure hence lower initial water saturation. Empirically, T>85°C and S_w<0.5% are conditions that could effectively treat the core samples and limestone sands to be oil-wet in about two weeks. Since the carbonate 2-D sandpacks were both water-wet, most remaining oil from lower layer was displaced by spontaneous imbibition during waterflood. Cumulative recovery with 37-42 °C environmental room treated and with 85 °C pre-treated sandpacks was 75.2% and 66.8% respectively. The lower recovery efficiency and weaker foam that was observed with carbonate sand compared with silica sandpacks may have been due to surfactant adsorption on mineral surface and crude oil breaking the foam.

Strong foam was not formed in any of the four forced displacement experiments using 1) untreated silica sand, 2) CTAB-treated silica sand, 3) 37-42 °C environmental room treated carbonate sand, and 4) 85 °C pre-treated carbonate sand. Foam was destabilized by several factors such as crude oil, CTAB, NI, etc. It is necessary to find a foaming surfactant that can tolerate these factors. While foam mobility control as a viscous-dominant process is being studied with SME crude, surfactant induced wettability alteration and gravity drainage worked well in recovering remaining crude oil from the lower low permeability layer. Gravity drainage because of reduced IFT was observed in all cases.

7.5.3 Results from Processes in a Glass Micro Model

Micro model videos show gas injected into anionic surfactant solutions created stable lamellae forming strong foam resulting in reduced gas mobility. Gas injected into water, however, formed only continuous gas channels.

A moderately viscous (266 cp) oil was successfully displaced with ASP and SAG in a 1-D sandpack. The apparent viscosity of the displacement process was much less than that of the crude oil. Micro model videos showed that the oil was dispersed as oil-in-water emulsion. When gas was injected, oil drops tended to stick on the gas/liquid interface and travel with gas bubbles in the porous media.

SME crude oil was extremely detrimental for foam generation. NI alone was not a good foaming agent. However, the addition of lauryl betaine to NI at a weight ratio of 2:1(betaine: NI) made NIB a strong foaming agent even when SME was present. Micro model videos show oil drops had neither entered nor spread on the gas/water surface. The mechanism of stabilizing foam may be due to increasing the critical capillary pressure for the stability of the pseudoemulsion film.

7.5.4 Results from Acid Number Measurement

In total acid number (TAN) measurements using spiking method, Metrohm Solvotrode electrode had faster and more stable response in organic solvent.

Preconditioning of electrode is essential in that it restores the electrode behavior in proper solvent. Electrode response changes upon contact with either crude oil or blank solution. It is therefore important to establish a preconditioning criterion, or to reduce the experimental error (e.g. by increasing the sample size). Larger sample size, smaller

volume step, and slower titration dosage rate will result in smaller standard deviation and consistent measured values. Spiking is advantageous in that it generates a sharp inflection point.

7.6 Unique Contribution

One unique contribution in this thesis is that one surfactant formulation that can simultaneously reduce IFT and generate strong foam was developed. As a result, microscopic displacement as well as sweep efficiency can be greatly improved from the beginning of the chemical flooding process. Previously, it was commonly observed that for a given surfactant and oil, strong foam is generated at salinities far below optimum but not near the optimum, where IFT is minimized. This leads to a dilemma that a surfactant formulation that can reduce IFT to ultra low values is not a good foaming agent, and vice versa. As a consequence, in such a flooding process, foam is usually injected as a drive after the low-tension surfactant slug. The disadvantage is that the low-tension surfactant slug is lacking mobility control, leading to poor sweep.

Another unique contribution is that wettability alteration induced gravity drainage and capillary pressure driven counter-current flow was experimentally demonstrated to have greatly improved oil recovery (94.6% OOIP) than an ASP process (64.3% OOIP) in a layered heterogeneous system that was preferentially oil-wet.

7.7 Possible Applications

The findings can be applied to improve oil recovery from a heterogeneous oil-wet reservoir that has high remaining oil saturation. This study has also opened a window for

foam to replace polymer as mobility control agent in a tertiary (or even secondary) oil recovery process. This will greatly improve both micro- and macro- displacement efficiency, and will also dramatically reduce the cost of injected chemicals.

7.8 Future Work

Betaine surfactants as foam boosters have their promising applications. However, the mechanisms and betaine adsorptionneed to be further studied.

Optimal salinity of NIB and SME needs to be found by phase behavior study and salinity scan. It will be useful to see whether foam could form at the salinity close to optimum.

Adsorption of NIB, especially lauryl betaine, on carbonate sand surfaces, or on either positively or negatively charged surfaces needs to be measured. Subsequently, chemicals that could reduce adsorption need to be evaluated. Potential adsorption reducing agents may be evaluated include sodium poly acrylate, sodium citrate, Na_4Y (EDTA), Na_2H_2Y, DTPMP (diethylenetriaminepentamethylene phosphonic acid). Equilibrium between dissociation of cationic from zwitterionic including betaine surfactants needs to be further investigated.

Foaming surfactants that are tolerant to light crude oils need to be evaluated also at elevated temperature and high salinity with carbonate formation materials.